INFORMATION TO USERS

This reproduction was made from a copy of a document sent to us for microfilming. While the most advanced technology has been used to photograph and reproduce this document, the quality of the reproduction is heavily dependent upon the quality of the material submitted.

The following explanation of techniques is provided to help clarify markings or notations which may appear on this reproduction.

1. The sign or "target" for pages apparently lacking from the document photographed is "Missing Page(s)". If it was possible to obtain the missing page(s) or section, they are spliced into the film along with adjacent pages. This may have necessitated cutting through an image and duplicating adjacent pages to assure complete continuity.

2. When an image on the film is obliterated with a round black mark, it is an indication of either blurred copy because of movement during exposure, duplicate copy, or copyrighted materials that should not have been filmed. For blurred pages, a good image of the page can be found in the adjacent frame. If copyrighted materials were deleted, a target note will appear listing the pages in the adjacent frame.

3. When a map, drawing or chart, etc., is part of the material being photographed, a definite method of "sectioning" the material has been followed. It is customary to begin filming at the upper left hand corner of a large sheet and to continue from left to right in equal sections with small overlaps. If necessary, sectioning is continued again—beginning below the first row and continuing on until complete.

4. For illustrations that cannot be satisfactorily reproduced by xerographic means, photographic prints can be purchased at additional cost and inserted into your xerographic copy. These prints are available upon request from the Dissertations Customer Services Department.

5. Some pages in any document may have indistinct print. In all cases the best available copy has been filmed.

University
Microfilms
International

300 N. Zeeb Road
Ann Arbor, MI 48106

Thompson, George Andrew

ELECTRON SPIN RESONANCE STUDIES OF MATRIX ISOLATED GROUP I METAL CLUSTERS

City University of New York PH.D. 1985

PLEASE NOTE:

In all cases this material has been filmed in the best possible way from the available copy. Problems encountered with this document have been identified here with a check mark _√_.

1. Glossy photographs or pages _____
2. Colored illustrations, paper or print _____
3. Photographs with dark background _____
4. Illustrations are poor copy _____
5. Pages with black marks, not original copy _____
6. Print shows through as there is text on both sides of page _____
7. Indistinct, broken or small print on several pages ✓
8. Print exceeds margin requirements _____
9. Tightly bound copy with print lost in spine _____
10. Computer printout pages with indistinct print _____
11. Page(s) _____ lacking when material received, and not available from school or author.
12. Page(s) _____ seem to be missing in numbering only as text follows.
13. Two pages numbered _____. Text follows.
14. Curling and wrinkled pages _____
15. Other _____

Electron Spin Resonance Studies of Matrix Isolated Group I Metal Clusters.

by

George A. Thompson

A dissertation submitted to the Graduate Faculty in Chemistry in partial fulfillment of the requirements for the degree of Doctor of Philosophy, The City University of New York.

1985

This manuscript has been read and accepted for the Graduate Faculty in Chemistry in satisfaction of the dissertation requirement for the degree of Doctor of Philosophy.

10/26/84
date

Chairman of Examining Committee

11/7/84
date

Executive Officer

Max Diem

Daniel L. Akins

Supervisory Committee

The City University of New York

Abstract

Electron Spin Resonance Studies of
Matrix Isolated Group I Metal Clusters

by

George A. Thompson

Advisor: Professor Derek Lindsay

Metal clusters of some group I elements, sodium, potassium, silver and gold are synthesized in non-reactive gas matrices and studied by ESR. The experimental apparatus and technique is described in detail. The method for analyzing the spectra is reviewed. Spectra are interpreted with simple molecular orbital theory and the Jahn-Teller effect.

TABLE OF CONTENTS

TABLE OF CONTENTS (continued)

LIST OF TABLES

LIST OF FIGURES

PAGE

LIST OF FIGURES (continued)

PAGE

SECTION IV

LIST OF FIGURES (continued)

I. INTRODUCTION

Metal clusters are broadly defined as molecules or aggregates composed primarily of metal atoms. The size of the cluster provides an approximate means of classification. Small metal clusters with from 3 to 20 atoms are treated as a distinct class. These clusters have received the greatest amount of attention in the literature. The small metal clusters described here contain only metal atoms and are stable in the absence of ligands or other supports. They are electrically neutral molecules which interact only with an unreactive matrix. The spectra observed are believed to represent the ground state properties of the molecule and to be similar to the properties observed in the gas phase.

At the onset of this project the experimental understanding of these molecules consisted of little more than photoionization measurements (1), dissociation energies (2,3), and a number of broad band UV-visible absorption experiments (4,5). Especially noteworthy were the 2-photon ionization experiments which provided some vibrational information (6-8) and a single ESR analysis of Na_3 in an argon matrix (9). With a few exceptions (10-12), most computational efforts were not very sophisticated and predicted a wide range of stabilities, ground states and geometries (13). The more sophisticated *ab initio* calculations did predict reasonable potential surfaces for the alkali trimers (10,11). Most notable is the prediction that internal rearrangment of the nuclei is permitted via low energy (100-300 cm^{-1}) saddle points. This effect, pseudorotation, was to be observed in the ESR experiments.

During the course of this project the state of the art was to improve dramatically. The current status of metal cluster chemistry and spectroscopy has been the subject of a recent review by G. Ozin (14). The more general facets of metal clusters, especially those of economic importance, have been described in a series of articles in Science magazine (15-17).

ESR of matrix isolated metal clusters has several advantages over other techniques. The spectrum is assured of arising from a cold (4-30 K) molecule. Unlike molecular beam work (18), vibrationally excited or metastable states will not be present to affect the spectra. Although matrix effects can be decisive in determining the ground state geometry (19), such effects may be tested by comparing spectra of the molecule obtained in a variety of matrices and at several temperatures. Invariance of the molecular parameters is taken as strong evidence that the spectra represents real, fundamental properties of the molecule rather than matrix effects.

II. EXPERIMENTAL

II. 1. Introduction

Figure 1 shows a block diagram of the experimental apparatus used for these experiments. Each component is discussed in some detail later in this chapter or in the references cited. The molecules of interest are prepared by generating a flux of the precursor atoms from a metal vapor source. This metal flux is co-deposited onto a low temperature substrate with a large excess of an nonreactive gas. The deposition substrate is mounted inside an ESR cavity. Both the substrate and the ESR cavity are maintained near 4K by the liquid helium cryostat. The low temperature results in rapid freezing of the matrix gas, immobilizing the metal atoms and any clusters that may be formed. Samples formed are studied with the commercial spectrometer.

II. 2. The Spectrometer

The spectra contained in this thesis were recorded with commercial ESR spectrometers which had been modified for low temperature matrix isolation experiments. A Japanese Electron Optics Laboratory ME-3X ("Jeolco") was used for all of the work on K_3, Na_5 and Na_7, and preliminary work on Au, Ag and Cu. The Jeolco spectrometer was replaced in September 1983 by an IBM-Bruker ER 200D ESR spectrometer ("Bruker"). The Bruker field control unit was interfaced to the Jeolco electromagnet and power supply by the technical staff at IBM (Danbury, Ct). The Bruker was used for additional work on Ag and Cu. Since a detailed description of these spectrometers is available in the extensive documentation provided by their manufacturers (20,21), only a brief description here is warranted. A more extensive review of the

Fig. II.1 Block Diagram of the Experimental Apparatus

Outline of the experimental system used for the electron spin resonance spectroscopy of matrix isolated metal clusters. A commercial spectrometer is used to detect the spectra of metal clusters isolated in a non-reactive matrix maintained at low temperatures by the liquid helium cryostat.

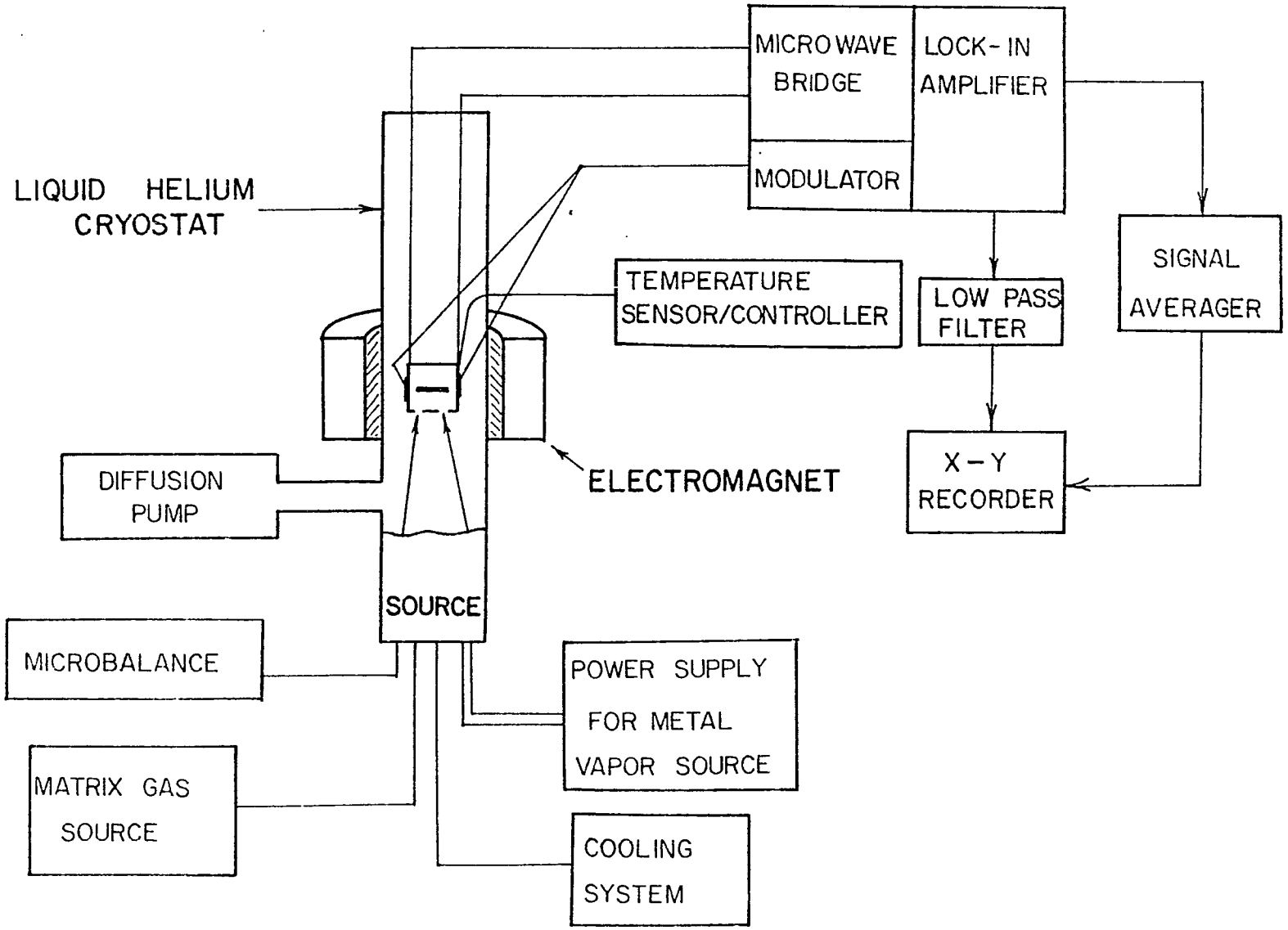
MICRO WAVE BRIDGE
LOCK-IN AMPLIFIER
MODULATOR
LIQUID HELIUM CRYOSTAT
TEMPERATURE SENSOR/CONTROLLER
LOW PASS FILTER
SIGNAL AVERAGER
DIFFUSION PUMP
ELECTROMAGNET
X-Y RECORDER
SOURCE
MICROBALANCE
POWER SUPPLY FOR METAL VAPOR SOURCE
MATRIX GAS SOURCE
COOLING SYSTEM

experimental principles of ESR, along with a detailed review of the various applications, is available in the classic work by Poole (22).

Both spectrometers employed a X-band microwave bridge consisting of a klystron, a reflective type sample cavity, a solid state microwave detector and a reference arm arranged for homodyne detection. Monochromatic microwave radiation (~9.2 GHz) is generated by an AFC stabilized klystron (maximum output ~200 mW), and attenuated and guided to a custom built TE_{102} microwave cavity where a standing wave is established. The quality factor, or Q, of the cavity is between 3500 and 4500 (23). Power densities achieved in this cavity easily suffice to induce allowed transitions between the adjacent zeeman levels of the sample during resonance. Detection of the resonance is achieved by balancing the microwaves reflected from the cavity with those from the reference arm. The deviation from this balanced state caused by the change in Q of the cavity during resonance is detected by the semiconductor diode. In practice the reference arm is adjusted to provide a small bias current.

Proper tuning of the reference arm of the bridge is critical for obtaining maximum signal to noise and resolution. The biasing of the diode is determined by the attenuation level in the reference arm and is necessary for optimum diode response. Overbiasing results in the generation of avoidable Johnson noise in the diode, while underbiasing reduces the output signal. Both underbiasing and overbiasing can result in deviation from the diodes linear response region. Attempts to compensate for improper biasing by changing the output power of the klystron arm of the bridge results in signal loss from

either insufficient power density in the cavity or saturation of the resonance. Higher klystron powers also result in FM sideband generation. This noise source may, under unfavorable circumstances, exceed that of the diode, further degrading signal quality. The phase of the reference arm serves to select only the absorption mode of the resonance for transmission to the detector. The admixture of a dispersion component would distort lineshapes and is highly undesirable, except in special applications.

Careful attention to tuning the microwave bridge was well rewarded by increased spectrometer sensitivity. While on the Bruker spectrometer this tuning procedure is quite simple, the earlier Jeolco instrument was difficult to tune at times. Careful monitoring of the klystron AFC unit with an oscilloscope, in addition to following the manufacturers recommended procedure, was necessary for achieving optimum performance.

In order to detect very small changes in the cavity Q accompanying the resonance condition, the magnetic field was modulated at 100 kHz and the output of the microwave detecting diode was amplified with a 100 kHz band pass amplifier and subsequently phase sensitive detected in a lock-in amplifier. The magnetic field was modulated with custom built low impedance coils mounted directly on the cavity and maintained at cryogenic temperatures. The modulation and phase sensitve detection system was of a standard type used to recover weak signals from noisy backgrounds in many scientific applications (24). The output of the lock-in amplifier was either actively filtered by an "EDC-301" active, low pass filter before being plotted on the spectrometer X-Y recorder, or stored digitally in a signal averager (Tracor Northern #1710-4K,

Tracor Northern Inc., Middleton, Wis.). The sensitivity of this signal detection scheme is on the order of 5×10^{10} spins/gauss (23).

The electromagnet used to tune the zeeman levels into resonance had flat pole caps (300 mm dia) with a 60 mm air gap, mounted on a low impedance water cooled coil which drew 0 to 80 amps to induce magnetic fields from 0 to 10 k gauss. The electromagnet as provided by the factory was unsuitable for these experiments consequently custom made pole caps were used to replace the original Jeolco parts. This change increased the air gap to 90 mm. No significant deterioration of the magnet's performance was observed as evidenced by high resolution spectra of the perylene radical taken before and after modification.

The utlimate resolution was limited by the magnetic field homogeneity of the electromagnet. The system resolution is demonstrated by the spectra of a 10^{-3} mole/liter solution of perylene (Fig. 2) in H_2SO_4 taken on the Bruker in this laboratory. The Jeolco performance specifications include spectra of the same molecule taken at the factory. The superhyperfine (shf) splitting arising from the hydrogen at the #2 carbon (Fig. 3) is clearly resolved. The literature value of this splitting is 0.450 gauss. The spectrum in Figure 4 show peak to peak linewidths on the order of 125 mGauss. This is assumed to be the resolution of the instrument under optimum conditions. For molecules analyzed here, natural linewidths were always much greater than the instrumental resolution.

The magnetic field strength was calibrated as necessary with a proton NMR (Micro-Now, Model 515, Micro-Now Associates, Chicago, Ill. 60646). The accuracy of this calibration technique was confirmed by

Fig. II.2 ESR Spectrum of the Perylene Radical

This ESR spectrum of the perylene radical in H_2SO_4 is 30 gauss wide and centered about g = 2. It was obtained in 2000 seconds using a 200 msec time constant. The magnetic field modulation is 400 mGauss at 100 kHz. The microwave attenuation of 29 dB provides 17 watts of power.

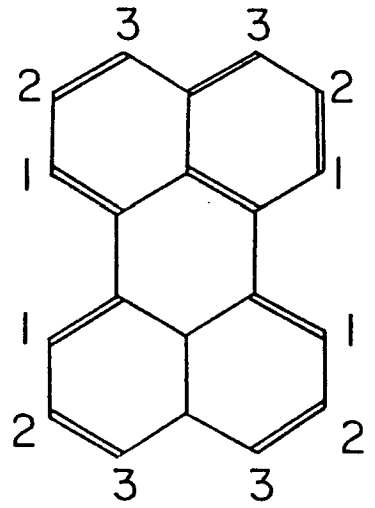

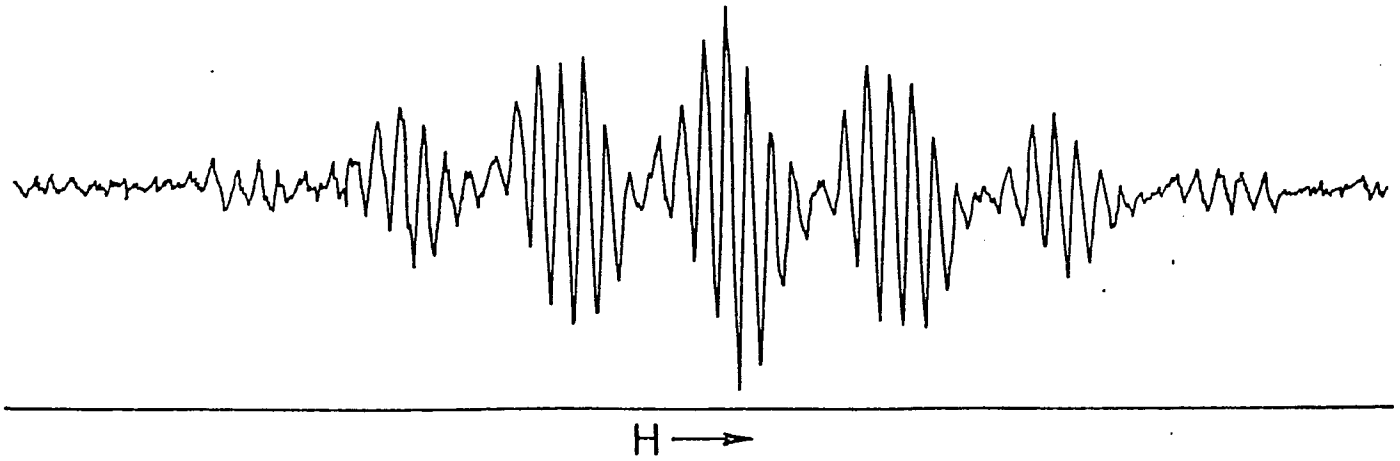

Fig. II.3 High Resolution Spectrum of the Perylene Radical

This ESR spectrum of a single hyperfine group of the perylene radical (Fig. II.2) demonstrates the instrumental resolution of the spectrometer. The 5 gauss spectrum is scanned in 2000 sec wth a time constant of 1000 msec. The magnetic field modulation is 400 mGauss at 12.5 kHz. The microwave attenuation of 25 dB provides 0.63 watts of power.

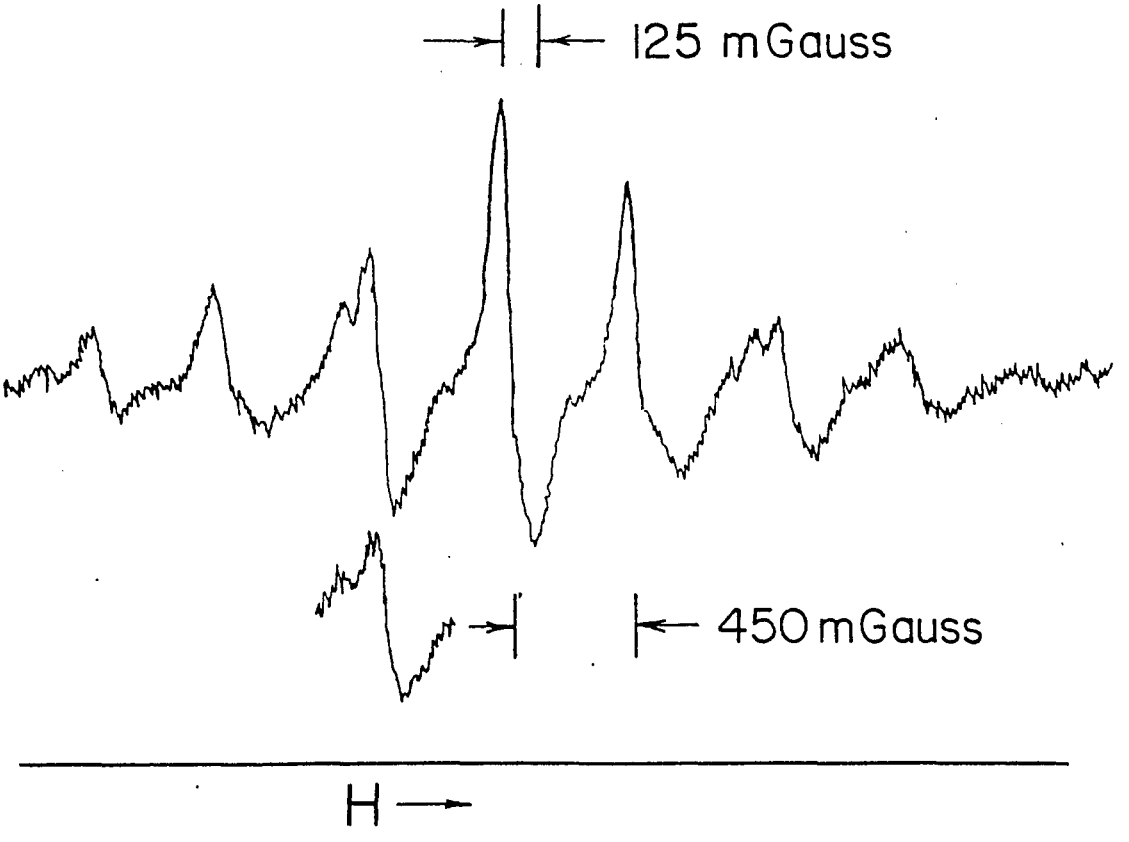

comparing spectra of atomic potassium and KO_2 with literature values (23,25-27). The relative and absolute field values are believed to be accurate to within 0.1 and 2 gauss, respectively.

II. 3. The Dewar

The liquid helium cryostat used in these experiments has been described in detail elsewhere and only a brief description will be given here. The dewar in Figure 4 is a double chambered type capable of maintaining the microwave cavity and deposition substrate at temperatures near 4K for the recording of spectra. The temperature of the sample was monitored by various means over the course of this work. Initially a carbon resister was used. This device was calibrated at 3 fixed points, 4.2 K, 77 K and 300 K and judged to be accurate to 5%. This device and its calibration are described in Ref. 23. This device was later replaced by a calibrated Germanium resistance thermometer (Cryocal Inc., St. Paul, MN 55114). Precision to 0.0005 K was claimed by the manufacturer. The final device used was a Gallium Arsenide diode in conjuction with a Series 5500 Microprocessor Based Temperature Indicator/Controller (Scientific Instruments, Inc., West Palm Beach, Fla. 33407). Precision to ±0.2 K was claimed by the manufacturer. This device was exceptionally convenient to use. After a few minor adjustments it could maintain the cavity at a fixed temperature for extended periods of time with little or no adjustment.

All temperature transducers used were mounted in a similar manner. In the absence of significant heat loads to the cavity, the precision of these measurements should approach the rated precision of the transducer. Large heat loads to the cavity arise from 3 main sources:

Fig. II.4 The Liquid Helium Dewar

Lateral cross sectional view of the liquid helium dewar used for these experiments. The design and construction of the dewar are discussed in detail in Reference 23.

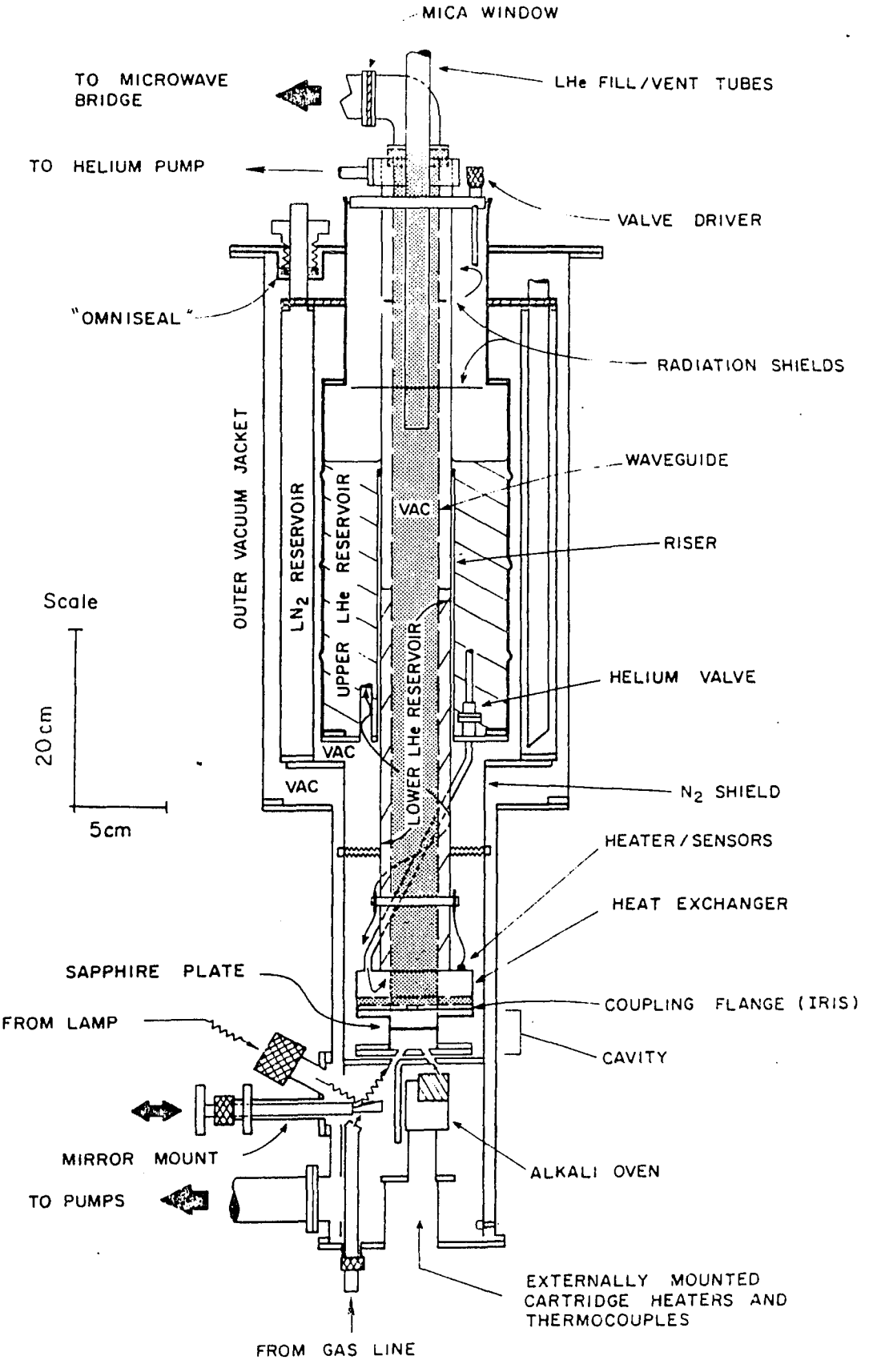
MICA WINDOW
TO MICROWAVE BRIDGE
LHe FILL/VENT TUBES
TO HELIUM PUMP
VALVE DRIVER
"OMNISEAL"
RADIATION SHIELDS
OUTER VACUUM JACKET
LN2 RESERVOIR
UPPER LHe RESERVOIR
VAC
WAVEGUIDE
RISER
Scale
20cm
5cm
HELIUM VALVE
VAC
VAC
LOWER LHe RESERVOIR
N2 SHIELD
HEATER/SENSORS
HEAT EXCHANGER
SAPPHIRE PLATE
COUPLING FLANGE (IRIS)
FROM LAMP
CAVITY
MIRROR MOUNT
ALKALI OVEN
TO PUMPS
EXTERNALLY MOUNTED CARTRIDGE HEATERS AND THERMOCOUPLES
FROM GAS LINE

the deposition system, the modulation coils and microwave power dissipated in the cavity walls. When accurate temperature measurements were needed the deposition system was turned off and both the modulation amplitude and microwave power were kept at a minimum.

II. 4. The Gas Line

A gas handling apparatus was constructed to permit the regulated introduction of high purity gas into the microwave cavity. The gas line in Figure 5 is constructed primarily of stainless steel and is evacuated by a liquid nitrogen trapped oil diffusion pump (Model HVP-150-A, Vactronics Lab Equipment, Inc., East Northport, L.I., N.Y.). Pressures of 1×10^{-6} torr, as measured with an ionization gauge and controller, (Model 6-GC, Vactronics Lab Equipment, Inc., East Northport, L.I., N.Y.) were typical prior to deposition. During experiments, the matrix gas handling section of the gas line is isolated from the diffusion pump and a matrix gas is bled into the microwave cavity through a high pressure, variable leak needle valve (Series 203, Granville-Phillips Co., Boulder, CO, 80301), several feet of vacuum line and a precision cut effusion slit. The gas line pressure is monitored by a sensitive capacitance manometer (Series 200, MKS Industries, Burlington, MA) with 0.001 torr precision. Typical pressures during deposition were 0.700 to 0.800 torr. The effusion slit was 0.020 inch thick and allowed about 10^{15} molecules-sec^{-1} into the cavity, although this figure depends on the particular matrix gas in use and other parameters (23).

Fig. II.5 Block Diagram of the Gas Line

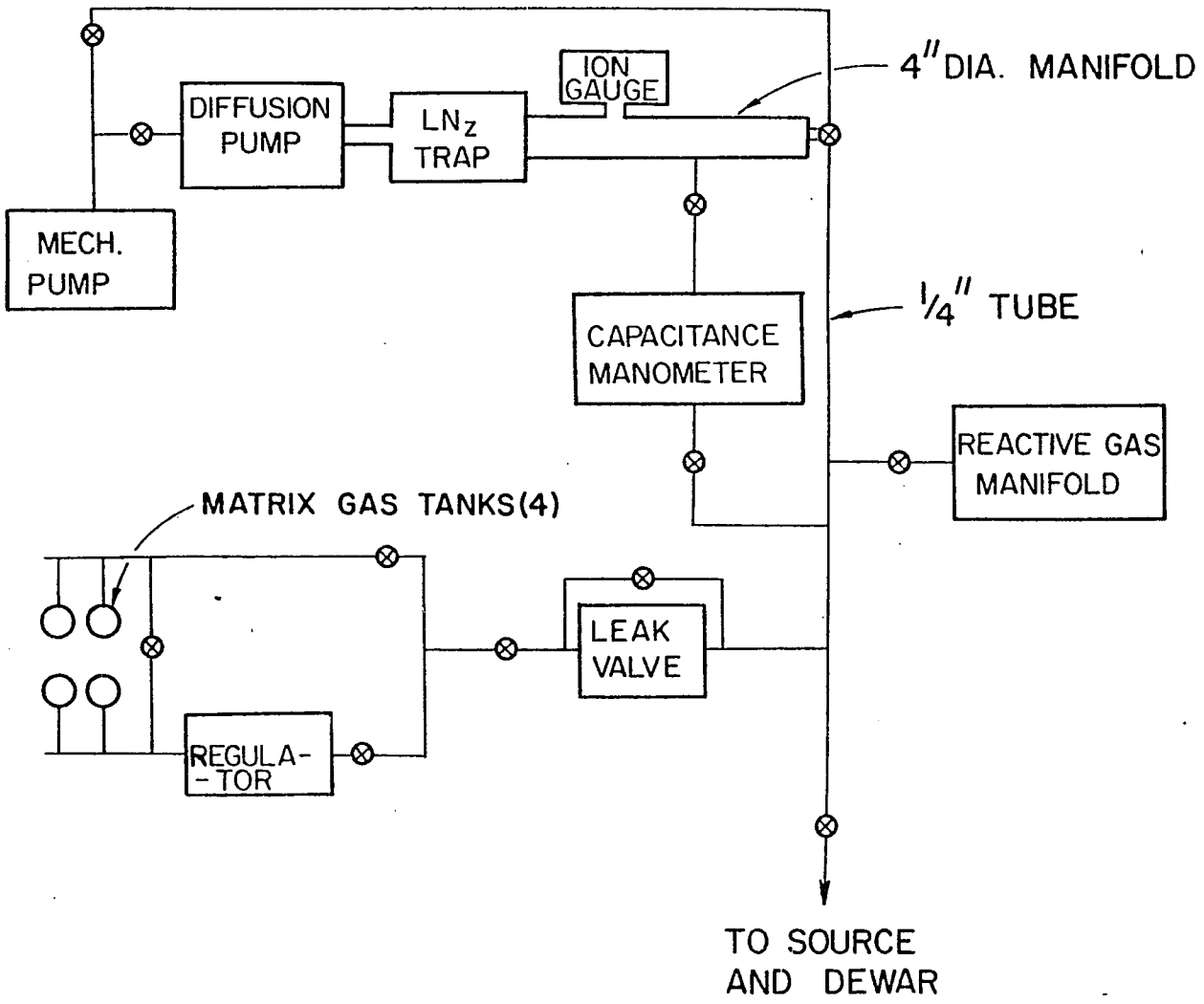

After an experiment, the gas line could be evacuated and outgassed with heating tape prior to the next run. Aside from occasional vacuum trouble, the gas line performed reliably and uneventfully.

II. 5. The Metal Vapor Source

5a. Introduction

As the experiments on the alkalis were in progress using the source described in Ref. 23, the design and constructon of a versatile high temperature metal vapor source was begun. The design needed to meet several demanding requirements. The source had to generate metal fluxes of 10^{14} to 10^{17} atoms-sec^{-1} incident on the deposition substrate for a period of several hours. These fluxes had to be stable, reproducible and directly measured. Fluxes of this magnitude required vapor pressures of metal of up to 100 millitorr, although 1-10 millitorr would suffice for most experiments. For several metals of possible interest, this would require temperatures of about 2500°C (28). Given the prospect of these extreme temperatures, careful attention to heat transfer processes would be required. The maximum acceptable heat input into the liquid helium and liquid nitrogen reservoir is, respectively, 200 mWatts and 20 Watts. The source also had to be interchangeable with the existing low temperature source. This predetermined the beam trajectories for both the metal fluxes and the matrix gas. The space constraints were also severe. The available space inside the vacuum chamber was a cylinder of ∿3" diameter by 6" long.

5b. Methods for Generating Metal Vapor

Of the most common techniques used for heating metal samples to high temperatures, radio frequency induction heating, electron beam

bombardment and high current resistive heating, the latter was chosen due to space constraints in the dewar. Several types of resistively heated sources were considered, some of which are shown in Figure 6. Direct heating of a tungsten filament with the sample wrapped onto the tungsten is shown in Figure 6a. Direct heating of a filament of the metal of interest is also an option (Figure 6b). Other sources contain the molten metal in a crucible heated by a tungsten "basket" heater (Figure 6c), or containment of the metal in a boat of tungsten, tantalum, or molybdenum, which also serves as a heater when current is passed through both the boat and sample (Figures 6d and 6e).

Each of these sources has its advantages and drawbacks. Filament sources have the lowest current requirements and radiate the least amount of heat of the different sources. If the metal has a large enough vapor pressure below its melting point, the sample may be used without a support, eliminating the possiblity of alloying and contamination from contact with a dissimilar metal at very high temperature. Table 1 lists some metals which have a significant vapor pressure below their melting point.

The use of a tungsten filament as a support permits other metals to be studied, though the potential for contamination and alloying are introduced. Tungsten support filaments are advised for very high temperature work when source radiation must be minimized.

Basket heaters in conjunction with a crucible (Fig. 6c) have large surface areas, hence large radiative heat outputs. The crucible material, typically boron nitride, fused quartz or carbon may present a contamination problem. These materials must be carefully outgassed

Fig. II.6 Metal Vapor Sources

Assorted metal vapor sources considered for use. The catalog numbers refer to the R. D. Mathis Co. 1983 catalog.

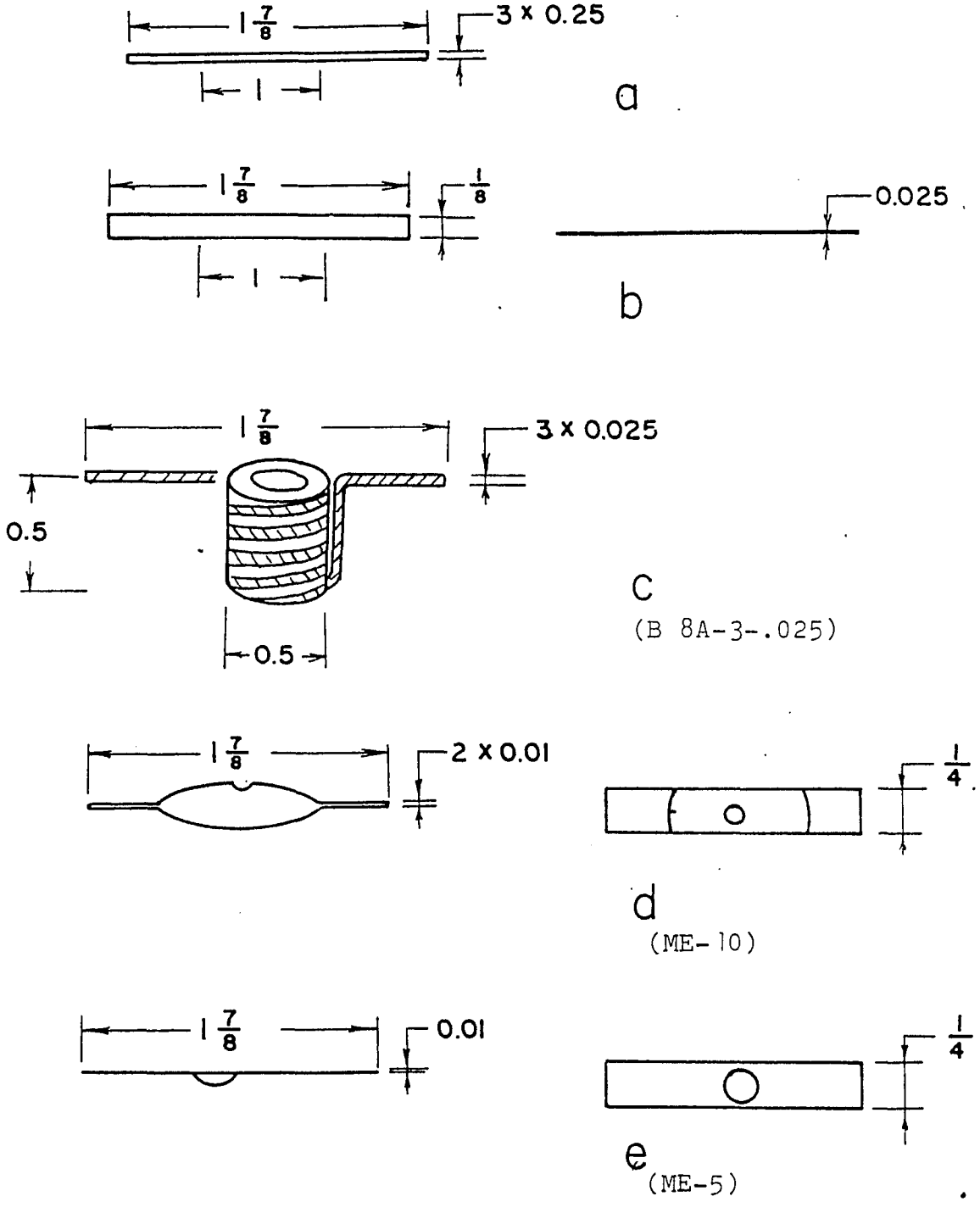

Table II.1 Metals Which May be Used on Filaments Without Support.

Group	Element	Atomic No.	MP (°C)	T_1 [a]	ΔT [b]
IIA	Ba	56	725°C	630°C	105°C
IIIB	Sc	21	1540	1250	290
IVB	Ti	22	1660	1500	160
VB	V	23	1890	1700	190
VIB	Cr	24	1860	1250	610
	Fe	26	1540	1300	240
	Co	27	1500	1100	400
	Ni	28	1450	1000	450
	Pd	46	1550	1400	150
	Pt	78	1770	1300	470

[a] Temperature at which the vapor pressure of the metal is 1 mTorr.

[b] $\Delta T = MP - T_1$, in units of °C.

for a few hours to minimize contamination. They also have a tendency to break, spilling the contents. Their major advantage is that they electrically insulate the sample from the power supply, minimizing changes in source resistively as the sample is consumed. Although the source was designed to accommodate these crucibles, they were never used.

Refractory metal crucibles ("Boats") are a good compromise between filaments and basket heaters with ceramic crucibles. As shown in Fig. 6c, they are small yet capable of holding substantial quantities of sample. These boats were used extensively with generally good results. The covered Moly boats provide faster reloading of the source between boat changes than the uncovered type since the sample will not spill out, circumventing the need for premelting the sample in a test chamber before loading. The covered boats also have a smaller orifice which in theory should provide longer run times. In practice this was offset by small pinholes in the bottom of the boats, spilling the contents. The pinhole problem was partially offset by introducing 8-10 pieces of 25 mil single strand tungsten wire, each about 1/2 cm long in the boat with the sample to provide a large surface area for the sample to wet. In the event of a pinhole in the bottom of the boat, the sample does not flow out as a liquid as most of the liquid metal adheres to the surface of the tunsten wire. The two boats shown in Figs. 6d and 6e (R. D. Mathis Co., Long Beach, CA) were used for most experiments.

5c. Power Supply Design

The power requirement for these sources can be estimated by

balancing the Joule heating in the heater with the power dissipated by conduction and radiation. Each of these power dissipating mechanisms is evaluated for a typical source of each type, a filament, a basket, and a boat. The dimensions of the boats in Figure 6, among other useful quantities are listed in Table 2. The effective length of the source is approximately 1" less than the total length. This compensates for the part of the source which is efficiently cooled by being in good thermal contact with the electrodes. Even when the sources were at high temperatures the sections near the electrodes were cool enough not to radiate in the visible.

Heat Transfer Through a Gas

Heat transfer by conduction through a gas, Q_{gas}, is in general very difficult to estimate a priori. The low pressures within the source chamber greatly simplifies the calculation. Since the mean free path of the gas is large relative to the source chamber and the surface area of the boat is small relative to the radiation shield, a simple model based on the kinetic gas theory is used. The frequency of collisions between matrix gas molecules and the source is calculated by analogy to effusion of a gas through an orifice of the same area. Each collision with the source is assumed to occur with a gas molecule at the temperature of the radiation shield, T_{sink}, and it recoils from the source at a large fraction of the temperature of the source. The fraction of the hot gas molecules is small, hence the collisional frequency is determined by a gas at T_{sink}.

From the kinetic theory of ideal gases, the probability of a collision with a wall segment of unit area is denoted by Z in Eq. 1.

Table II.2 Dimensions of Some Metal Vapor Sources.

Source Type (see Fig. 6)	L[1]	L_h[2]	$L(eff)$[3]	CSA[4]	$CSSA$[5]	SA_h[6]	$SA_h(cm^2)$[7]
Flat Filament	1 7/8	1	7/8	0.0031	0.30	0.30	1.9
Tungsten Filament	1 7/8	1	7/8	0.0015	0.16	0.10[a]	0.68
Basket with Crucible	8.16	8.25	7/8	0.0015	0.16	3.5[b]	22.
Covered Boat	1 7/8	1	7/8	0.0050	0.52	0.52	3.3
Open Boat	1 7/8	1	7/8	0.0025	0.51	0.51	3.3

[a] Contains a factor of 2/3 ($SA_h = 2/3 \times L_h \times CSSA$).

[b] Includes additonal surface are of crucible.

1. Length of source carrying current, in inches.
2. Length of source radiating significantly, in inches.
3. Length of source being significantly cooled by conduction, in inches.
4. Cross sectional area of source, in square inches.
5. Surface area of a cross sectional element, in inches.
6. Total surface area of source radiating significantly, in square inches.

$$Z = \frac{1}{4}\frac{N}{V}\bar{C} \qquad \text{Eq. 1}$$

where N is the number of molecules contained in a volume V. $\bar{C}$ is the mean speed of the molecules.

Substituting the standard expression for $\bar{C}$ yields Eq. 2.

$$Z = \frac{N}{4V}\left(\frac{8RT}{\pi M}\right)^{1/2} \qquad \text{Eq. 2}$$

where R is the gas constant, T is the temperature and M is the molecular weight, in consistent units. Using the deal gas law, N/V can be replaced by PL/RT in Eq. 3.

$$Z = \frac{PL}{4RT}\left(\frac{8RT}{\pi M}\right)^{1/2} \qquad \text{Eq. 3}$$

where P is the pressure and L is Avogradro's number. Eq. 3 gives the frequency of cold molecules colliding with a unit area. For a source with unit area at T_{source}, and a transfer efficiency of α, the rate of heat of dissipation is give by Eq. 4.

$$Z = \frac{\alpha PLkT_{source}}{4RT_{sink}}\left(\frac{8RT_{source}}{\pi M}\right)^{1/2} \qquad \text{Eq. 4}$$

where k is the boltzman's constant.

During deposition pressures in the source chamber of the dewer were approximately 0.010 torr. Assuming a T_{sink} of 300 K, M = 40 for the case of argon, and = 0.7, Eq. 4 is written as:

$$Q_{gas} = 0.031 \text{ mw} \times SA_h \text{ (cm}^2\text{)} \times T_{source} \text{ (K)} \qquad \text{Eq. 5}$$

For the filament in Figure 6b with a 1.68 cm^2 surface area at 1500°C, Eq. 5 predicts that only 80 mw will be dissipated. The basket heater arrangement in Figure 6 with a 28 cm^2 surface area at 1500°C will dissipate approximately 1.3 watts. The boat in Figure 6 with a 3.35 cm^2 surface area will dissipate approximately 0.16 watts at 1500°C. Table 3 summarizes the expected heat transfer at several different temperatures.

Heat Transfer by Conduction

Heat transfer by conduction from the hot region of the source to the water cooled electrodes is estimated using Eq. 6.

$$Q_{cond} = \frac{k \times CSA}{L_h} \times \Delta T \qquad \text{Eq. 6}$$

where k is the conductivity of the metal (29), the cross sectional area, CSA is in cm^2, L_h is the difference between L and L(eff). The use of $L_h = L - L(eff)$ rather than $L_h = L - L(eff)/2$ is offset by omitting a factor of 2 for the two electrode system. $\Delta T = T_{source} - T_{sink}$ where T_{source} = 1500 °C and T_{sink} = 20°C, ΔT = 1480°C.

Strictly speaking, the integral form of Eq. 6 should be used taking into account that k is a function of L. This is not necessary

Table II.3 Heat Transfer Considerations for Various Metal Vapor Sources

Source Type	Temp (°C)	Q_{gas} [1]	Q_{cond} [2]	Q_{rad} [3]	P = A	k [4]	r [5]	V_3 [6]
Flat Filament								
Sc	1000	0.078	0.49	9.9	10	0.950	65	0.28
Cr	1000	0.078	1.87	9.9	12	0.604	57	0.28
	1500	0.090	2.45	50	53	0.526	80	0.75
Co	1000	0.078	1.46	9.9	12	0.472	83	0.36
	1500	0.090	2.00	50	52	0.431	110	1.2
Ni	1000	0.078	2.43	9.9	12	0.78	56	0.29
	1500	0.090	3.84	50	54	0.826	65	0.71
Pt	1000	0.078	2.63	9.9	13	0.848	48	0.28
	1500	0.090	4.47	50	55	0.961	55	0.98
Round Filament								
W	1000	0.027	1.65	3.5	5	1.10	34	0.21
	1500	0.038	2.27	18	20	1.01	50	0.26
	2000	0.048	2.85	55	58	0.950	66	1.0
	2500	0.059	3.56	140	150		84	1.8

Table II.3 (continued)

Source Type	Temp (°C)	Q_{gas} [1]	Q_{cond} [2]	Q_{rad} [3]	P = A	k [4]	r [5]	V_3 [6]
Basket Heater								
W	1000	0.91	0.20	120	120	1.10	34	3.0
	1500	1.63	0.28	580	580	1.01	50	7.9
	2000	1.6	0.35	1800	1800	0.950	66	16
	2500	2.0	0.4	4500	4500		84	29
Boat, ME-9								
Ta	1000	0.14	7.8	17	25	0.614	46	0.45
	1500	0.19	12	87	99	0.634	69	1.0
	2000	0.24	17	270	290	0.650	82	1.9
	2500	0.29	21	670	690	0.666	98	3.3
Boat, ME-5								
W	1000	0.13	14	17	31	1.10	34	0.29
	1500	0.18	19	85	100	1.01	50	0.63
	2000	0.23	24	270	290	0.950	66	1.2
	2500	0.28	30	660	690		84	2.1

Table II.3 (continued)

Source Type	Temp (°C)	Q_{gas} [1]	Q_{cond} [2]	Q_{rad} [3]	P = A	k [4]	r [5]	V_3 [6]
Boat, ME-5								
Ta	1000	0.13	7.8	17	25	0.614	46	0.30
	1500	0.18	12	85	97	0.634	69	0.73
	2000	0.23	17	270	290	0.650	82	1.4
	2500	0.28	21	660	680	0.666	98	2.3
Mo	1000	0.13	13	17	30	1.03	27	0.25
	1500	0.18	18	85	100	9.929	37	0.54
	2000	0.23	22	270	290	0.876	47	1.0
	2500	0.28	27	660	690	0.840	55	1.7

1. Calculated from Equation II.5, in units of watts.
2. Calculated from Equation II.6, in units of watts.
3. Calculated from Equation II.7, in units of watts.
4. From C. Y. Ho, R. W. Powell and P. E. Liley, J. Phys. Chem. Ref. Data 1, 279 (1972). In units of watts-cm/K.
5. Thermophysical Properties of High Temperature Solid Materials, Vol. I: Elements, Y. W. Touloukian (Ed.) 1967, MacMillan. In units of μohm-cm.
6. Calculated from Equation II.9, in units of volts.

at this level of approximation. The water cooled electrode is assumed to be a heat sink of infinite capacity. An average value of the thermal conductivity is used.

For the filament in Fig. 6b, Eq. 6 reduces to Q(cond) = 4.6 k where k = 4 for Cu and 0.60 for Ta. For this arrangement 3-18 watts will be conducted to the electrode.

An analogous calculation for a tungsten basket heater predicts Q_{cond} = 1.4 k = 24 watts and for the tantalum boat in Fig. 6b Q_{cond} = 27 k = 16 watts.

Heat Transfer by Radiation

Radiative heat emitted by a body at temperature T is described by Stephans' law, Eq. 7.

$$Q_{RAD} = \varepsilon \cdot \sigma \cdot SA(T^4_{source} - T^4_{sink}) \qquad \text{Eq. 7}$$

ε is the emittance which can vary between 0 and 1. Metals generally have a value between 0.7 and 1, because this quantity is extremely dependent on characteristics of the surface, especially roughness, oxidation and contamination. Since these are difficult to characterize, ε will be taken as 0.9. σ is Stephans' constant, $5.6 \times 10^{-12} \frac{\text{watt}}{\text{cm} - K}$. For these calculations, $T_{source} >> T_{sink}$ so that T^4_{sink} may be neglected in Eq. 7. The effective surface area of the source is the same as for the problem of convection treated above; again, all quantities are calculated at 1500°C.

For the filament in Fig. 6a

$$Q_{cond} = (.9)(1.68\ cm^2)(5.6 \times 10^{-12}\ \frac{watt}{cm\ -K})(1773K)^4 = 84\ watts$$

For the basket heater arrangement in Fig. 6b

$$Q_{cond} = (.7)(28\ cm^2)(5.6 \times 10^{-12}\ \frac{watt}{cm\ -K})(1773K)^4 = 1400\ watts$$

For the boat in Fig. 6c

$$Q_{cond} = (.7)(3.35\ cm^2)(5.6 \times 10^{-12}\ \frac{watt}{cm\ -K})(1773K)^4 = 170\ watts$$

These calculations were repeated for various temperatures and are summarized in Table 3, along with the total power requirements.

For the design of the power supply, the quantities in Tables 1 and 3 are used. The power, P, dissipated by Joule heating is given by Eq. 8.

$$P = I^2R \qquad \text{Eq. 8}$$

where I is the current through the resistance, R. Substituting V = IR and the expression for resistance, $R = rL_h/CSA$ into Eq. 8 gives the voltage necessary to dissipate a given power P for a source of effective length, L_h, with a cross sectional area of CSA and a resistivity of r.

$$V = \left(\frac{PL_h}{CSA}\, r\right)^{1/2} \qquad \text{Eq. 9}$$

The use of L_h rather than L is justified by the large increase in r between 20°C and 1000°C, a factor of 3. The voltages calculated by Eq. 9 for several sources and temperatures are listed in Table 3. They indicate that voltages from 0 to 50 volts may be needed, though most applicatons will require voltages from 0 to 5 volts. A voltage resolution of 1% was assumed to be necessary.

A power supply was designed and constructed. It consisted of a standard high power variac run off of wall current with an output of 0 to 140 volts. This voltage was applied to the primary stage of a specially constructed transformer (NEW 5258, Newton Engineering, Newton, MA) with a 40 amp primary of 30 turns and no secondary as delivered by the manufacturer. Depending on the particular experiment, the secondary would be wound with n turns of 2-0 cable, n = 1 to 5. The final voltage output for a variac setting of x is xn/30. n was usually 1 so that the power supply could deliver 0-4½ volts with a precision of 3% or better. This was satisfactory for these experiments. Current through this boat was continuously monitored with a commercial current meter.

II. 5d. Radiation Shield Design - Heat transfer considerations.

The calculations in the previous section used elementary heat transfer considerations to establish the power needs of the source. Similar methods are now applied to estimate the heat input to the surrounding experimental apparatus - the liquid helium, liquid nitrogen,

supporting electrodes and radiation shields. For the purposes of these calculations a source at 2000°C radiating 5000 watts into space is assumed. Also assumed is that the electrodes will have to heat sink 1000 watts. Inspection of Table 3 shows the large margin for error implicit in these assumptions.

The heat input into the liquid helium from the high temperature source can be estimated from Stephans' law. Assuming appropriate shielding, the radiant heat transfer to the liquid helium is determined by the 0.124" diameter metal vapor input hole in the liquid nitrogen cooled radiation baffle 2" above the metal vapor source. This configuration permits use of radiation shields which limit the heat input to less than 100 mw-hr^{-1}. This corresponds to a liquid helium loss of less than 0.2 liters-hr^{-1}.

The 3" diameter liquid nitrogen cooled radiation baffle would absorb a considerable amount of radiation. From simple geometric considerations, about 20% of the 5000 watts, 1000 watts would reach the liquid nitrogen in the absence of an additional radiation shield, an unacceptable amount. The heat input was reduced by the "top radiation shield" (Fig. 7). The top slit block opening is 0.0625" x 0.750" and about 1.25" from the metal vapor source. While this does not affect the flow of metal into the cavity, it prevents most of the radiation from reaching the liquid nitrogen. Of the 5000 watts emitted, only about 0.2% of it, 12 watts reach the liquid nitrogen.

The radiation shield is subject to a large heat input and some care was needed in its design. It consists of a solid 0.375" thick plate of oxygen free high conductivity ("OFHC") copper. The slit

opening which permits the metal vapor to reach the cavity was cut as 2 separate plates which were mounted on the main copper plate, which had a large (0.375" x 1.5") opening (Fig. 7). This design allowed for changes in the metal flux trajectory without replacing the main shield. The copper radiation shield was in good thermal contact with a water cooled heat sink. A brief calculation demonstrates the need for this heat sinking. Assuming the boundary of the shield is insulated, only radiative heat transfer would remove heat from the shield. The temperature of the shield under these conditions can be estmated from Stephans' law. The shield will not be able to radiate away 150 watts from a unit area until it reaches about 2000°C, which is considerably above the melting point of copper. Clearly heat sinking of the shield is necessary. The adequacy of heat sinking the shield at the edge is checked by considering the heat flow through a copper bar 3 cm long, this being the distance from the center of the radiation shield to the edge. Equation 10 gives the temperature gradient established in a bar 3 cm in length (L) of cross section A (1 cm^2) of a material of thermal conductivity k (4.1 watt $-°C^{-1} - cm^{-1}$) conducting 450 watts of heat, Q.

$$T = QL/kA \simeq 330°C \qquad \text{Eq. 10}$$

This is a most conservative estimate relying on higher than anticipated radiation fluxes. The geometric arrangement of the radiation shield also provides for greater thermal conductivity than a simple bar of the above dimensions. The worst case temperature of 330°C is still well within the working temperature of copper.

Fig. II.7 Top Radiation Shield

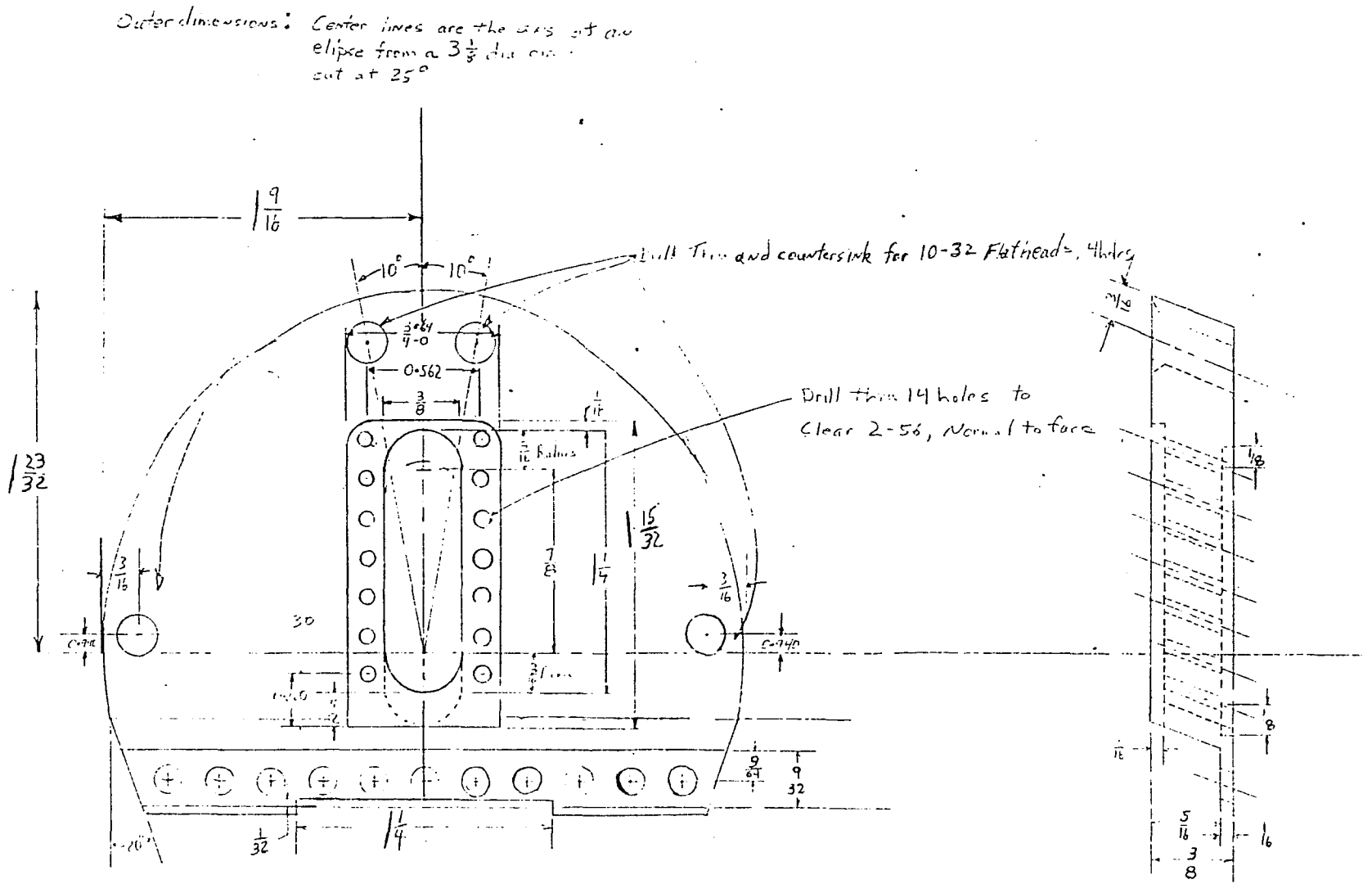

The temperature of the lower slit block is estimated by considering the temperature gradient established in a plate of stainless steel 1 cm x 1 cm x 0.16 cm conducting 150 watts. A thermal gradient of less than 150° is predicted by Eq. 10. The temperature of the plate, being sunk to the copper radiation shield at 330°, should not exceed 480°C. This is well within the working temperature of stainless steel.

The other components of the source which serve as radiation shields, the flat shield and the curved shield (Figs. 8 and 9), are overdesigned. Both shields have extensive water cooling channels. All of the flat shield is within 0.25" of cold, flowing water, while for the curved shield no spot is more than 1" away from cold, flowing water. The upper operating limit of these parts is much greater than the top radiation shield. The pumping gap in the curved shield (Fig. 10) permits a small amount of radiation to reach the stainless steel tail of the dewar. During the most extreme conditions encountered in experiments with this source, a slight warming of the dewar tail was observed. The base of the source was efficiently protected by a 0.25" copper plate. Being 6" from the source relatively little heat is incident on it and direct cooling was not necessary.

The electrodes may be required to conduct a considerable amount of heat away from the source without reaching an excessively high temperature. From the top of the electrodes where the source is attached, to the cold water in the hollow body, is approximately 1 cm. Given the 1 cm diameter of the electrodes and an assumed heat input of 500 watts a thermal gradient of 350°C is calculated by Eq. 10. Although this is acceptable, the actual heat input, hence the thermal gradient, should be a factor of 10 less for most experiments.

Fig. II.8 Flat Radiation Shield and Electrodes

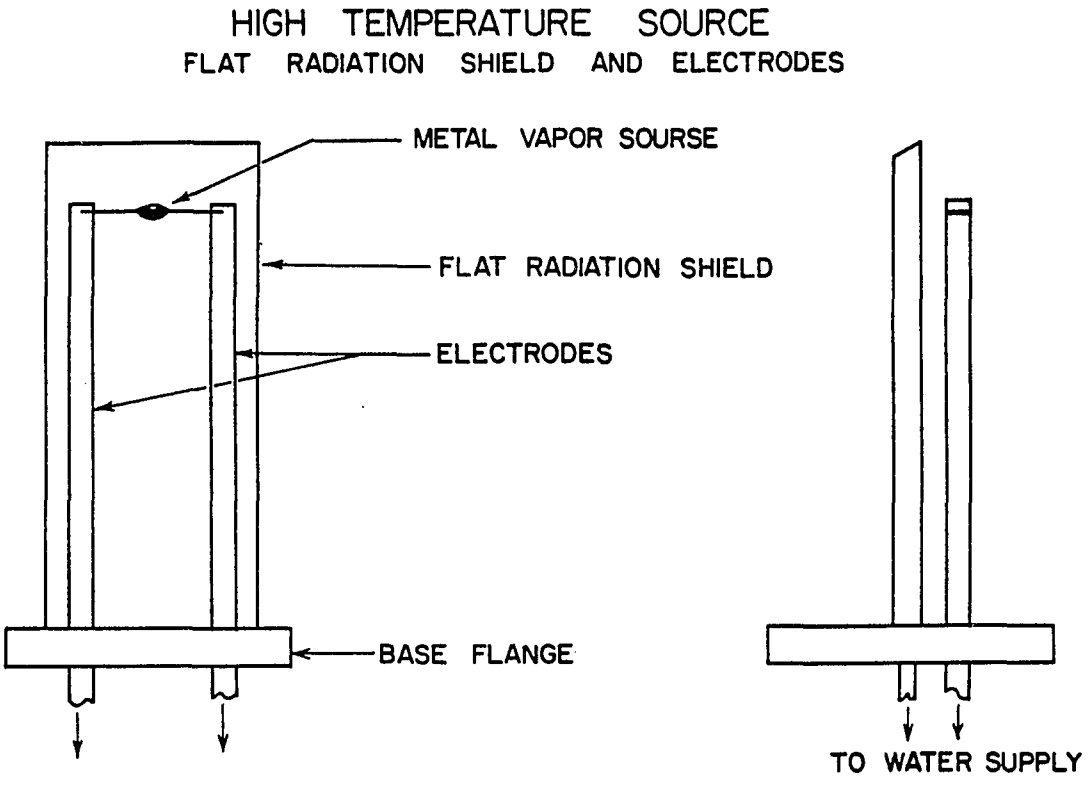

Fig. II.9 Curved Radiation Shield

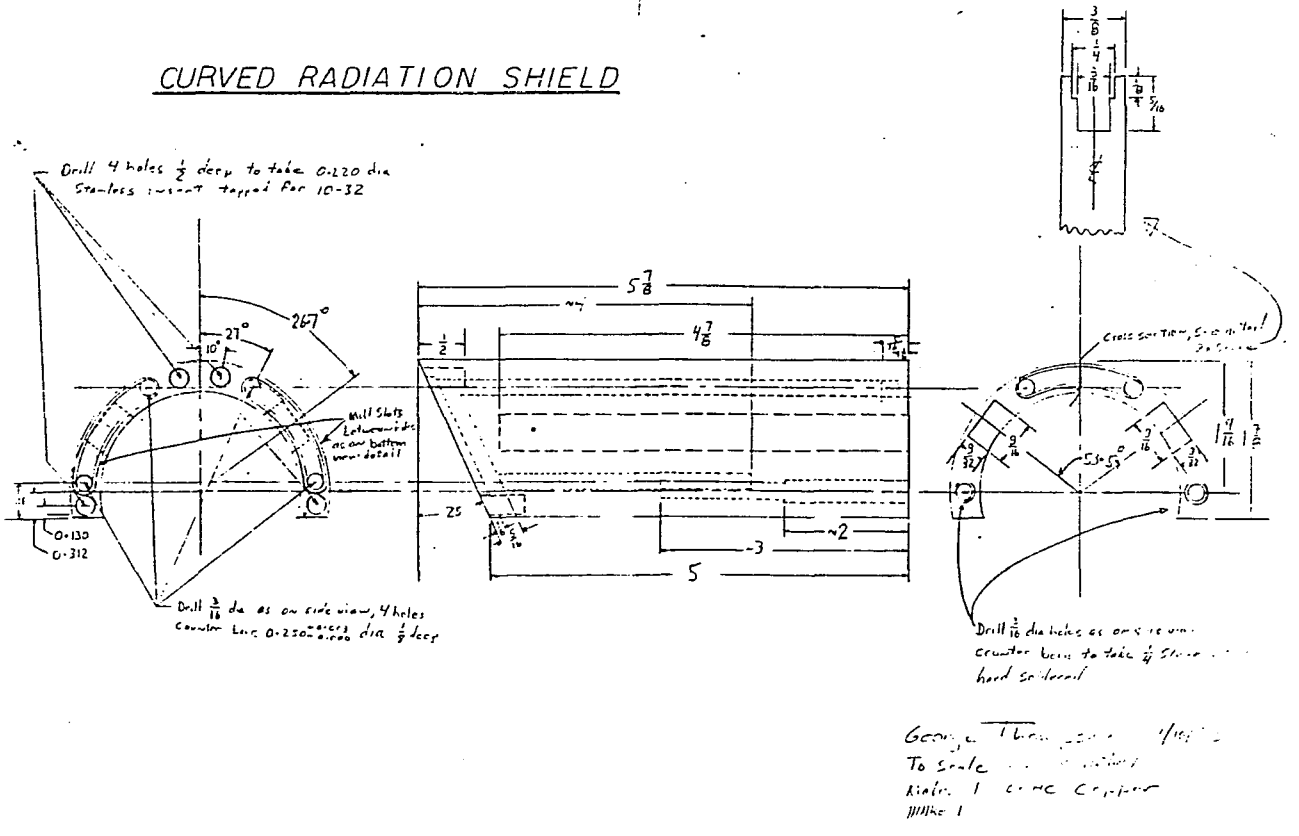

Fig. II.10 Side View of Assembled High Temperature Source

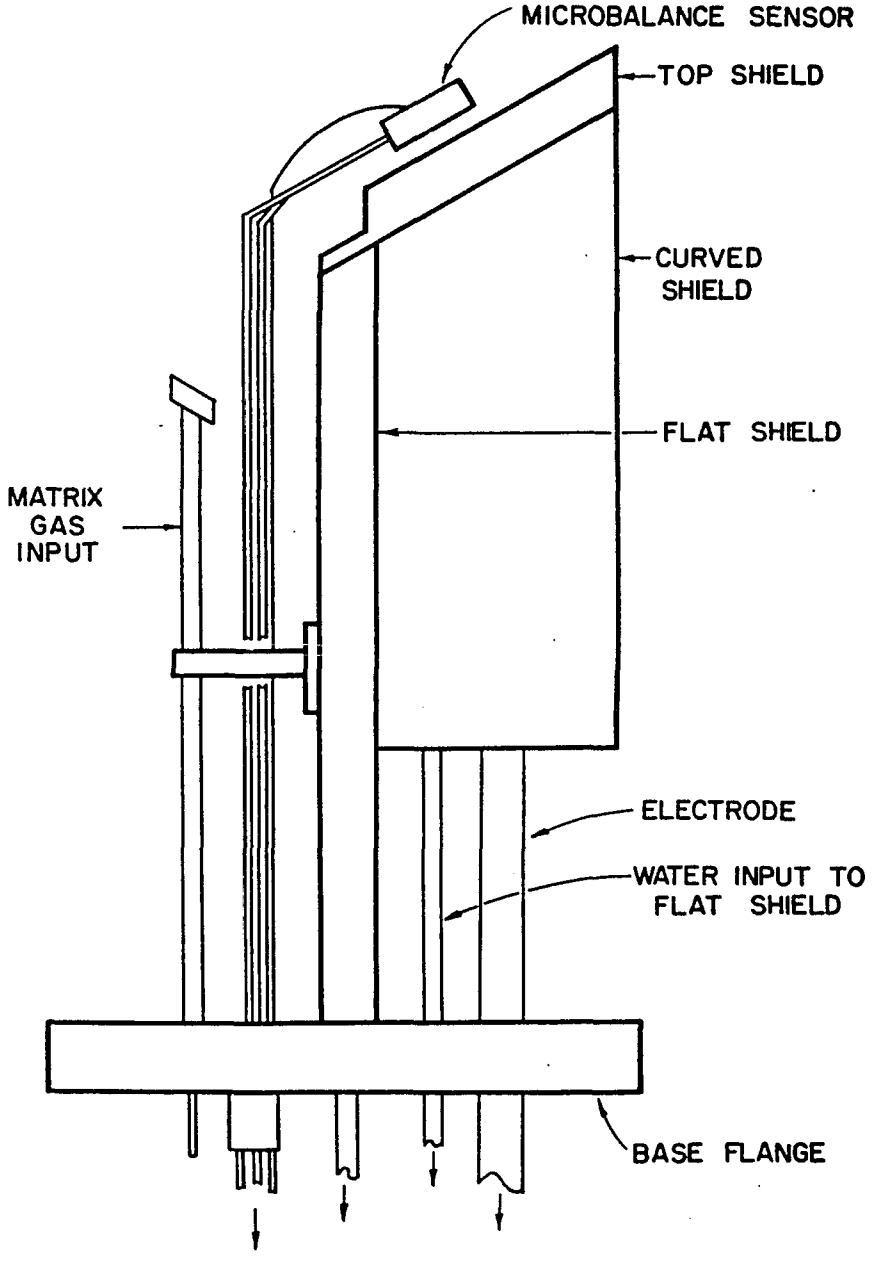

II. 5e. Monitoring Metal Fluxes

Metal fluxes were monitored using a commercial quartz crystal deposition monitor (Model QM-300, Veeco Instruments, Inc., Plainview, LI., N.Y.) with a custom built high temperature sensor head (Fig. 11). The sensor head was similar to the Veeco VTT 300 except that the cooling system was more sophisticated. The microbalance sensor head worked quite well at all temperature ranges encountered.

The microbalance reading can be related to the metal flux incident on the sapphire plate by considering geometric factors and correcting for the density of the metal in use. The geometric factors can be described by Eq. 11.

$$\text{Flux(cavity)} = 0.121 \text{ flux (microbalance)} \qquad \text{Eq. 11}$$

in the unusual units of angstrom per second ($\mathring{A} - S^{-1}$) of aluminum. Converting from $\mathring{A} - S^{-1}$ of aluminum to atoms-sec^{-1} of metal of density, ρ, Equation 11 becomes

$$\text{Flux} = 0.121 \times (\rho g/cm^3) \times N(1/\text{mole}) \times 10^{-8}\ cm/\mathring{A} \times \text{rate}(\mathring{A}/S)/M(g/\text{mole}) \qquad \text{Eq. 12}$$

where the rate is read directly from the instrument in units of $\mathring{A}/S$ and N is Avogadro's number.

The numerical factors can be combined to form Equation 13.

$$\text{Flux} = 7.3 \times 10^{14} \times (\rho/M) \times \text{flux } (\mathring{A}/\text{sec}) \qquad \text{Eq. 13}$$

Fig. II.11 Quartz Crystal Microbalance Sensor Head

Front and side views of the assembled sensor head and vacuum feedthrough.

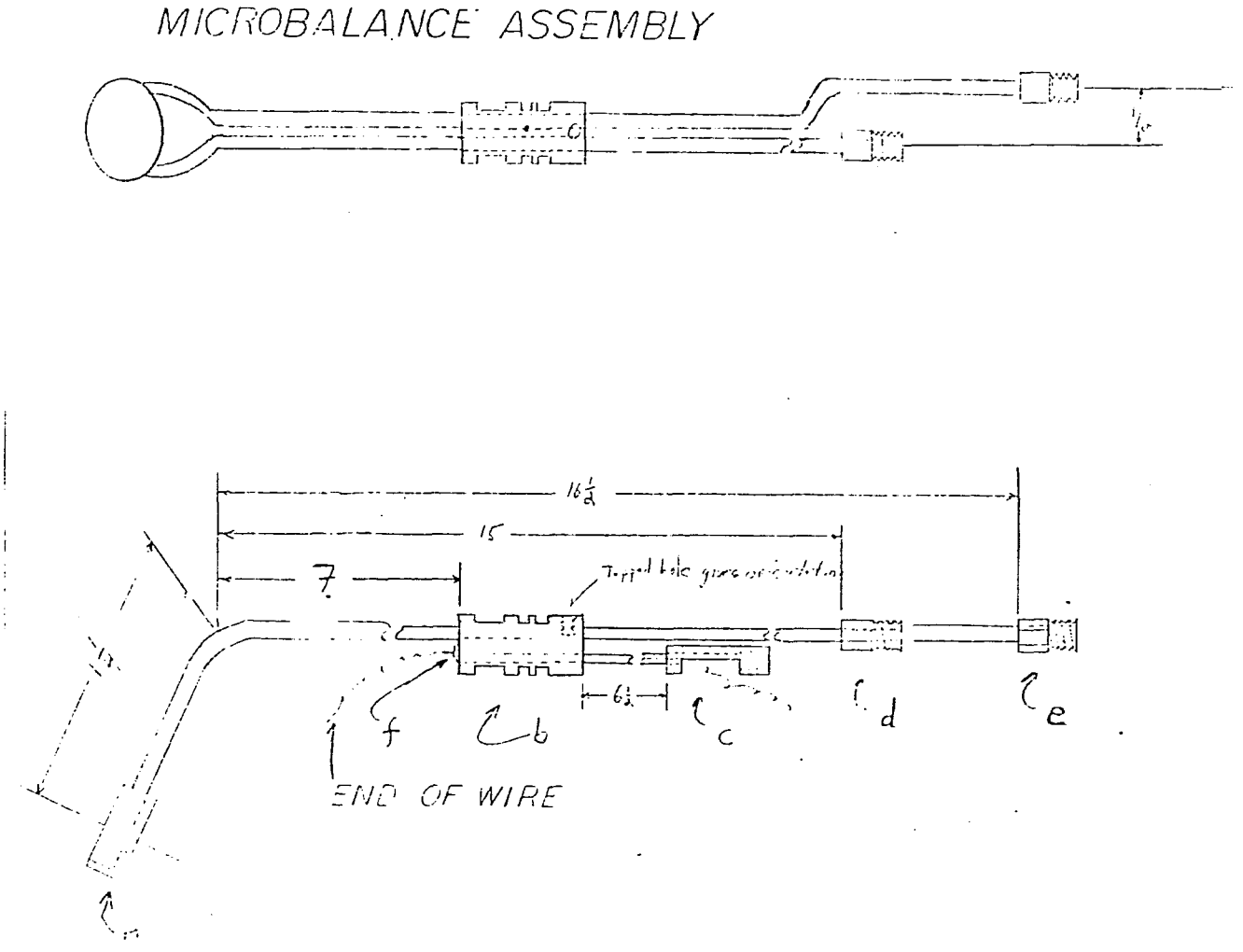

The gas input on the high temperature source is identical to the one on the low temperature source. These fluxes are calculated in Ref. 23 and are given by Eq. 14.

$$\text{Flux(gas)} = 3.4 \times 10^{18} \, (P/M \times T)^{1/2}$$

where P is the pressure in torr of gas behind the input slit, usually 0.75. M, the gram molecular weight is 40 if argon is used and T is 300 K. The dilution factor, D is the ratio of flux(gas)/flux(metal). For copper metal being deposited in argon, D = 230/rate(Å/sec).

This calculation neglects that not every atom incident on the deposition substrate or microbalance crystal adheres to the surface. Also neglected is the effect of aggregation of metal in the matrix. These factors are assumed to be small and the above dilution factor should be of the correct order of magnitude.

In practice, flux rates were chosen to provide the best spectra. For alkali metals, excessively large fluxes resulted in the growth of a large signal centered about g = 2. For the group IB metals, large fluxes resulted in severe instabilities in the spectral baseline.

II. 5f. Operation of the High Temperature Source

The high temperature source is a simple device to use and maintain. Loading of the source with metal is accomplished by first choosing a metal vapor source (Sec II.5) and fitting it to the ends of the electrodes. (Only the top radiation shield need be removed for this.) Each electrode is fitted with a small stainless steel electrode cap which

holds the boat or filament in place. The electrode caps need only be tapped gently to secure the boat in place. After the top radiation shield is attached the source is ready to mount in the dewar. This procedure is quite fast and involves breaking only 2 vacuum seals (source to dewar and source to gas line). As the dewar is being pumped down, the water, electrical power and sensor head connections are made. The source is then warmed up to operating fluxes. During this initial warm-up, dewar pressures are closely monitored to insure a slow rate of outgassing. Typically this takes about 0.5 hour. After the performance of the source has been checked the dewar and source are leak checked with a mass spectrometer helium leak detector (Model MS-9, Veeco Instruments Inc., Plainview, L.I., N.Y.) and precooling of the dewar begins.

The actual experiments follow closely the procedure outlined in Ref. 23. After the dewar is cooled to 4 K, an assortment of background spectra are taken under conditions similar to those anticipated after deposition. These background spectra are quite important for comparison with spectral data, since inevitability important spectral features will be either masked by or confused with these background signals. In an effort to minimize the impact of these background signals the deposition substrate was changed twice. The original substrate was a sapphire plate 0.020" thick. Impurities present give rise to the spectrum in Fig. 12. This plate was satisfactory for the work on the alkalis. It was later changed to a different sapphire plate. This spectrum is shown in Fig. 13. While this strong feature fully obscures the center of the spectrum, it was acceptable for work with copper.

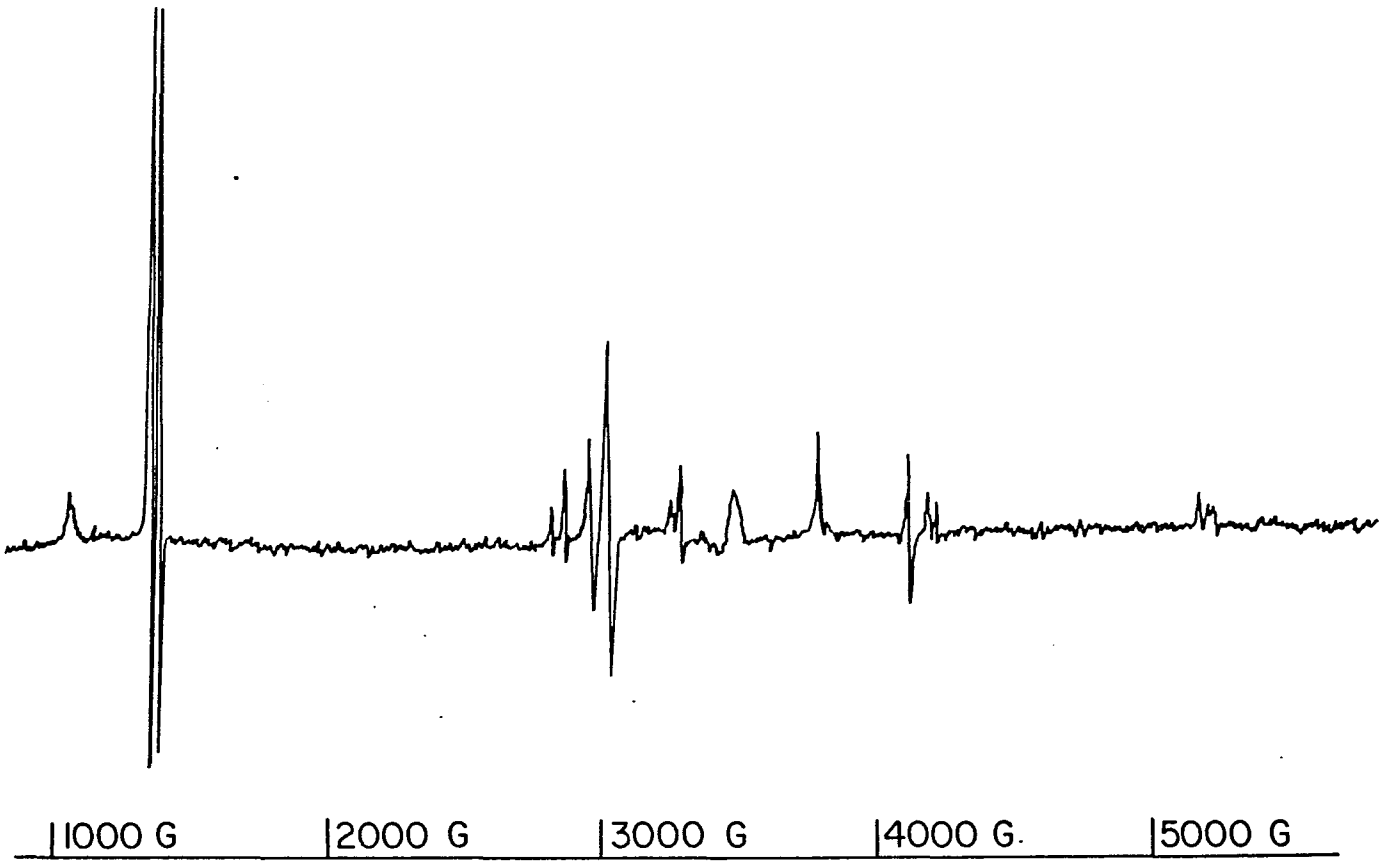

Fig. II.12 Background Spectrum from Deposition Substrate I

ESR spectrum of impurities in a sapphire plate used as a deposition substrate. This sapphire plate was used for all of the experiments with potassium, sodium and the early experiments with gold, copper and silver. The spectrum is 500 gauss wide and centered about g = 2. A 10 min scan time with a 500 msec time constant. The microwave power is 1 mwatt.

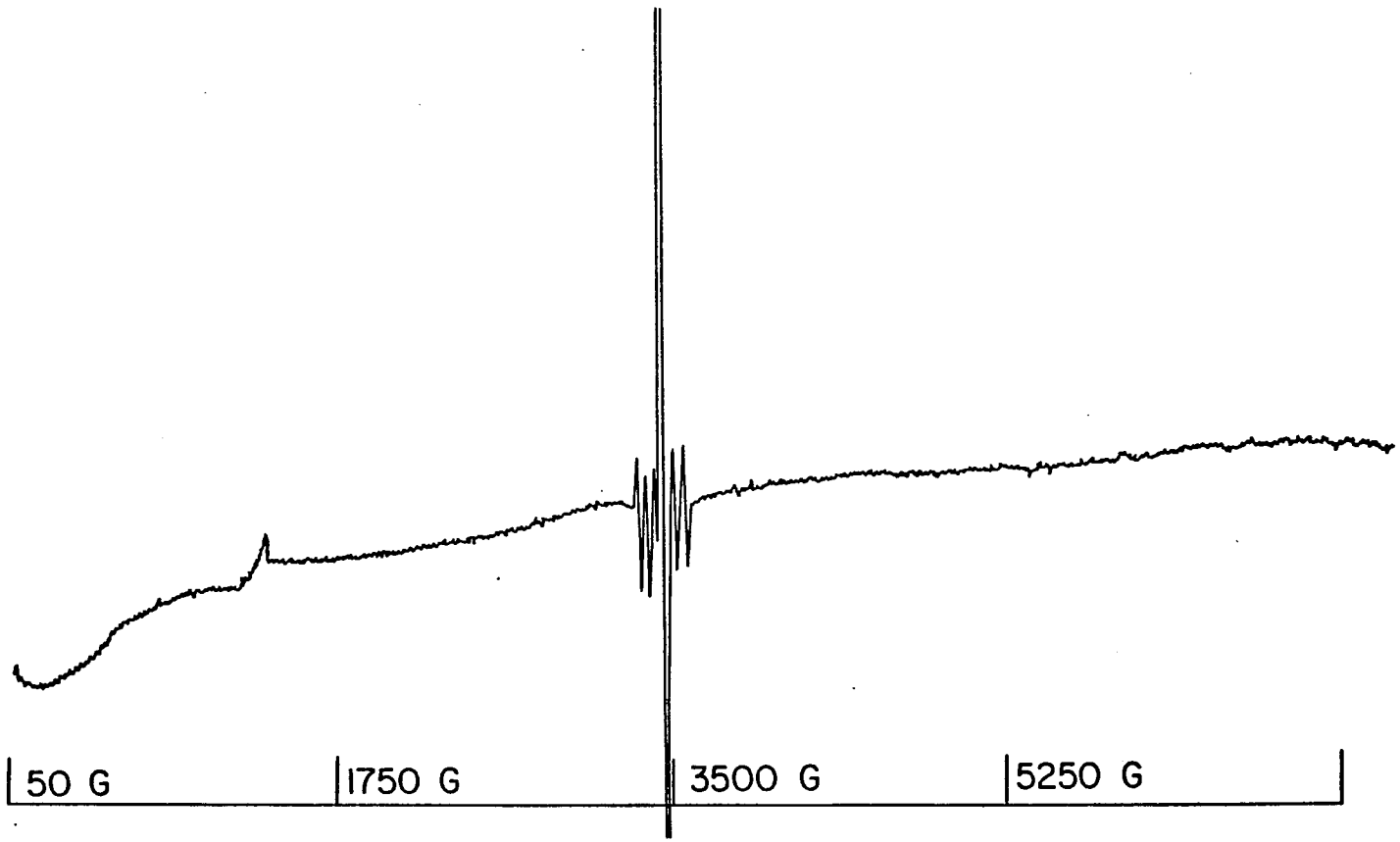

Fig. II.13 Background Spectrum from Deposition Substrate II

ESR spectrum of impurities in a sapphire plate used as a deposition substrate. This sapphire plate was used only for the later experimental attempts to isolate Cu_3. This spectrum is 7000 gauss wide and centered about g = 2.

The final plate, used for the work on silver is a 0.010" thick copper plate. Its spectrum is the least offensive (Fig. 14). This spectrum probably arises from an organic glue used to hold a small quartz window in place.

Before starting the deposition it is imperative that the electromagnet is either shut off or turned to a low (50 gauss) value. The magnetic field can couple to the AC current in the source, throwing the liquid metal out of the boat or even breaking the boat. Needless to say, the water cooling for the radiation shield must also be on. In the absence of water flow, the radiation shield can be destroyed in less than 5 min at moderate power levels. After stabilizing the metal flux and setting the matrix gas flow rate, a process that takes about 20-30 minutes, the deposition can start. The metal flux needs to be checked and if necessary adjusted every 30 to 60 minutes.

Metal flux rates are set according to the type of experiment being done. Four frequently used methods for forming clusters are: 1) forming matrices with a high concentration of metal, 2) forming moderately concentrated matrices and then annealing the matrix to an exceptionally high temperature, 3) forming a less concentrated matrix while the temperature of the substrate is held at an unusually high temperature, and 4) photolyzing the matrix after formation.

Method 1 is the most useful. This technique, at times enhanced by a small heat leak to the substrate, was used to synthesize K_3, Na_3, Ag_3, and Na_7. Method 2 was used for synthesizing $Cu_{3(?)}$. Method 3 was used to form an unidentified gold containing molecule. Method 4 never worked but did enhance the formation of metal-impurity complexes.

Fig. II.14 Background Spectrum from Deposition Substrate III

ESR spectrum of a copper plate used as a deposition substrate for the Ag_3 experiment. The signal probably arises from an optical window or mounting material used for other experiments. This spectrum is 7000 gauss wide and centered about g = 2.

Table 4 provides a summary of the experiments done for this project. The Table includes the deposition conditions, i.e. length of deposition, metal-matrix gas concentration, temperature of the substrate and the supplier and purity of the reagents used.

Table II.4 Summary of Experiments with Potassium, Sodium Copper, Gold, and Silver.

Run #	Metal	Matrix	Time (min)	Ratio	Dep. Temp.
2	K	Ar	2401	100-35	4K
3	K	Ar		53-35	4K
4					
5	K	Ar	2401	23	4K
6	K	Ar	2401	18	
7	K	Ar	2401	18	
8	K	Ar	2401	11	
9	K	Ar	2401	12	
10					
11					
12	K	Ar	2401	31	
13					
14					
15					
16	K	Ar	2401	86-114	
17	K	Ar	2401	93-114	
27	Au	Ar	30	32-40	4
			30	23-54	4
28	Au	Ar	45	5-8	4
29			160	7-24	20
31	Cu	Ar	20	0-46	4

Table II.4 (continued)

Run #	Metal	Matrix	Time (min)	Ratio	Dep. Temp.
34	Cu	Ar	30	12-15	4
			70	18-11	4
35	Cu	Ar	30	6-23	
			30	6-9	
			30	10-	
			30	7-15	
36	Cu	Ar	30	12	25
			30	5-12	20
			30	6-18	15
			30	10-21	10
			60	9-19	10
37	Cu	Ar	20	19-46	21
			15	14-57	14.5
			15	46-77	11-12
			200	46-57	13-14
38	Cu	Ar	60	230	4
			40	46-57	4
			20	0-57	4
39			45	230	4
			80	38	4
			60	22	4

Table II.4 (continued)

Run #	Metal	Matrix	Time (min)	Ratio	Dep. Temp.
40	Cu	Kr	40	115-230	4
			50	33-115	4
			135	29-115	4
			20	77-115	26
41	Cu	Kr	60	82-104	30
			40	77-115	20
			30	85-92	15
			30	57-77	15
			60	38	15
42	Ag	Kr	90	50	4
			60	50	4
			60	50	16
43	Ag	Kr	60	55	4
			30	30	4
44	Ag	Ar	15	60-70	4
			180	40-50	20
			60	46-80	30
45	Ag	N_2	40	322	4
			60	54	4
			180	54	4
47	Cu	Ar	60	203-288	4
			60	265-431	11.6-11.9
			60	276-345	14.0-14.7

Table II.4 (continued)

Run #	Metal	Matrix	Time (min)	Ratio	Dep. Temp.
48	Cu	Ar	60	238-255	16.4-16.7
			60	216-226	15.5-15.6
			60	212-281	14.9-15.3
49			60	234-294	5.4
			60	238-288	17.9-18.1
			60	314-321	18.9-19.1
50			240	223-307	18.9-19.1
51			60	256-265	21.1
			60	197-230	23.0
			60	244-255	25.0
			60	179-265	27.6-28.0
58			60	511-531	4
			60	226	4
			60	115	4
59			60	575	4
			30	282-314	4
			30	87-110	4
			30	53-60	4
			30	30-34	4
60			30	314-345	19.0
			30	1000	19.0

Table II.4 (continued)

Run #	Metal	Matrix	Time (min)	Ratio	Dep. Temp.
61	Cu	Ar	30	406-460	13.1-13.5
			30	194-200	13.3-13.4
			30	106-116	13.2
			30	52-56	13.2
			30	23-47	13.2-13.5
62			60	29-46	4
			60	17-21	4
			60	16	4
			60	16-17	4
63			60	16	4
			60	17-18	4
			60	17-18	9.9
64			60	15-17	15.2
65	Cu	Kr	90	19-10	4
			60	16-10	4
			120	17-19	4
66		N_2	60	13-15	4
			120	13-15	4
67		Xe	60	18	4
			120	16-17	4
68		Kr	240	6-16	4

Table II.4 (continued)

Run #	Metal	Matrix	Time (min)	Ratio	Dep. Temp.
70	^{63}Cu	Ar	60	115-117	4
			80	107-117	4
			90	119-134	4
			75	82-85	4
71	^{63}Cu	N_2	210	73-86	4
72	^{63}Cu	Ar	120	73-86	4
73			120	47-122	4
			120	77-92	4
74	^{63}Cu	N_2	120	69-92	4
75	^{63}Cu	N_2	60	?	4
KK-1	Ag	N_2	240	80	4

Reagents Used

Material	Source
Potassium	Gallery, 99.95%
Sodium	Gallery, 99.95%
Gold	Alpha, 99.9999%
	Cerac, 99.999%
Silver	Alpha, 99.999%
Silver (^{107}Ag)	USDOE, Oak Ridge National Laboratory (99% ^{107}Ag)
Copper	Alpha, 99.99%
	Hookup wire - USDOE, Oak Ridge National Laboratory (99% ^{63}Cu)
Argon	Airco, 99.9998%
Krypton	Alpha, 99.995%
Xenon	Alpha, 99.995%

III. THEORETICAL CONSIDERATIONS

III.1. Introduction

Electron spin resonance spectroscopy depends on the ability to detect the absorption of radiation accompanying the resonance condition of two spin states of an electron. The experimental factors are discussed in Section II.2. This chapter serves only as a brief review of the theory useful for analyzing an ESR spectra. A large number of texts present the theory with varying degrees of depth and rigor (30-35). Each of the major features of an ESR spectrum, e.g. line position, intensity, and lineshape will be briefly discussed in this chapter.

III.2. Line Positions

The resonance condition is observed by inducing transitions between the allowed spin orientations of an unpaired electron in a magnetic field. The allowed energy levels for an isolated electron in a magnetic field can be determined by evaluating Eq. 1.

$$H = g \beta H M_S \qquad (1)$$

where g is the electron free-spin g-factor (2.00232), β is the Bohr magneton (9.27410×10^{-21} erg-Gauss^{-1}) and H is the magnetic field strength responsible for the quantization of the electron spin, S, into the allowed states $M_S = (\pm 1/2)$. The resonance condition is met when the difference between the 2 energy levels, corresponding to $M_S = \pm 1/2$ in Equation 1, coincide with the radiation field of frequency, ν. This condition is described by Equation 2.

$$h\nu = g\beta H \tag{2}$$

where h is Plancks constant and the other quantities are defined earlier. In the experiments described here ν is in the X-band microwave region of the spectrum ($\sim$9.2 GHz) and H is $\sim$3300 Gauss.

An analogous effect occurs for a nuclear spin, I, in a magnetic field and is described by Equation 3.

$$H = g_N \beta_N H M_I \tag{3}$$

where g_N is the nuclear g factor, β_N is the nuclear magneton, (5.05095×10^{-24} erg-Gauss^{-1}), and M_I are the allowed levels of the nuclear spin, I, in the applied magnetic field, H. This term is generally three orders of magnitude smaller than the electronic effect described in Equation 1 and is usually neglected. For the case of an atom or molecule the electronic and nuclear spins may be coupled by the Fermi contact interaction, a, as given by Equation 4.

$$a \vec{I} \cdot \vec{S} \tag{4}$$

Other interactions are well known but not included here as they were not used in interpreting the spectra presented here. A general survey of the different interactions which may need to be considered is available in the literature, Reference 35 being the most comprehensive.

The above terms are collected in Equation 5:

$$H = g\beta HM_S + g_N\beta_N HI_Z + a\vec{I}\cdot\vec{S} \qquad (5)$$

Before evaluating Equation 5, the general features are noted to be a first term giving rise to a single resonance at about 9.2 GHz, corresponding to an "electron spin flip". Variations in g are small for spectra presented here. Only molecules with $M_S = \pm 1/2$ were observed. This term is the largest and serves to define the "center" of the spectrum. The second term is very small and was always neglected in the final analyses of spectra in Section IV. The last term, the Fermi contact interaction couples the nuclear spin to the electron spin, splitting the resonance into several components. For molecules examined, this splitting ranged between 20 and 6000 MHz (7 to 2100 Gauss) and was the greatest source of chemical information.

For the case of an atom, the Hamiltonian in Equation 5 can be evaluated in the $|S,M_S,I,M_I>$ basis. This problem, or a similar one, is treated in most texts on ESR. The original work is due to Breit and Rabi (36). Properly ordering the basis set block diagonalizes the Hamiltonian. In addition to the two pure states, represented by 1 x 1 matrices of the form;

$$<S, \pm M_S, I, \pm M_I \mid \tilde{H} \mid S, \pm M_S, I, \pm M_I>$$

the remainder of the matrix block diagonalizes into 2 x 2 matrices of the form;

	$\lvert S, M_S-1, I, M_I\rangle$	$\lvert S, M_S, I, M_I-1\rangle$
$\langle S, M_S-1, I, M_I\rvert$	$(M_S-1)H-M_Ih+M_IM_Sa$	$\frac{a}{2}\{I(I+1)-M_I(M_I-1)\}^{1/2}$
$\langle S, M_S, I, M_I-1\rvert$	$\frac{a}{2}\{I(I+1)-M_I(M_I-1)\}^{1/2}$	$M_SH-(M_I-1)h+(M_I-1)M_Sa$

Where $H = g\beta H$ and $h = g_N\beta_N H$. When diagonalized and specialized to the case of $M_S = \pm 1/2$ the energy levels are found to be those given by Equations 7 and 8.

$$E(+\tfrac{1}{2}, I, M_I) = -\tfrac{1}{2}(2hM_I + \tfrac{1}{2}a + h) + \tfrac{1}{2}\{(H+h)^2 + 2a(H+h)(M_I+\tfrac{1}{2}) + a^2(I+\tfrac{1}{2})^2\}^{1/2} \quad (7)$$

$$E(-\tfrac{1}{2}, I, M_I) = -\tfrac{1}{2}(2hM_I + \tfrac{1}{2}a - h) - \tfrac{1}{2}\{(H+h)^2 + 2a(H+h)(M_I-\tfrac{1}{2}) + a^2(I+\tfrac{1}{2})^2\}^{1/2} \quad (8)$$

A plot of these equations for I = 3/2 is given in Figure 1. Included in Figure 1 is a labeling of the states in both the $|S,M_S,I,M_I>$ basis and the $|F,M_F>$ basis where F = I + S and M_F = F, F -1 --- -F. The $|F,M_F>$ basis is the most frequently encountered basis set used for problems of this type, including the original work by Breit and Rabi. The $|S,M_S,I,M_I>$ basis is often preferred by ESR spectroscopists, especially when the coupling of I and S is small compared to the coupling of the spins to the external magnetic field. In cases where the nuclear magnetic moment is neglected ($h << H$), h can be set to zero in Equations 7 and 8.

Resonances may be observed when the energy difference between the states described by Equations 7 and 8 coincide with the energy available from the incident radiation field,

$$h\nu = E(+1/2,I,M_I) - E(-1/2,I,M_I) \tag{9}$$

For an experiment where $h\nu$ is held constant and the magnetic field is varied Equation 9 can be rewritten. Substituting Equations 7 and 8 into Equation 9, recognizing the selection rules $M_I = 0$ and $M_S = \pm 1$, changing units and rearranging, Equation 9 is written as Equation 10.

$$\eta(M_I) = -\frac{M_I\,\alpha}{1-\frac{\alpha^2}{4}} \pm \left\{ \frac{M_I^2\alpha^2}{1-\frac{\alpha^2}{4}} + \frac{1 - \alpha^2(I+\frac{1}{2})^2}{1-\frac{\alpha^2}{4}} \right\}^{1/2} \tag{10}$$

where $\eta(M_I)$ is the magnetic field strength of a particular resonance

Fig. III.1 Zeeman Energy Level Diagram

A Zeeman energy level diagram for a ^2S atom with I = 3/2. States are labeled in both the $|S,M_S,I,M_I\rangle$ basis and the $|F,M_F\rangle$ basis.

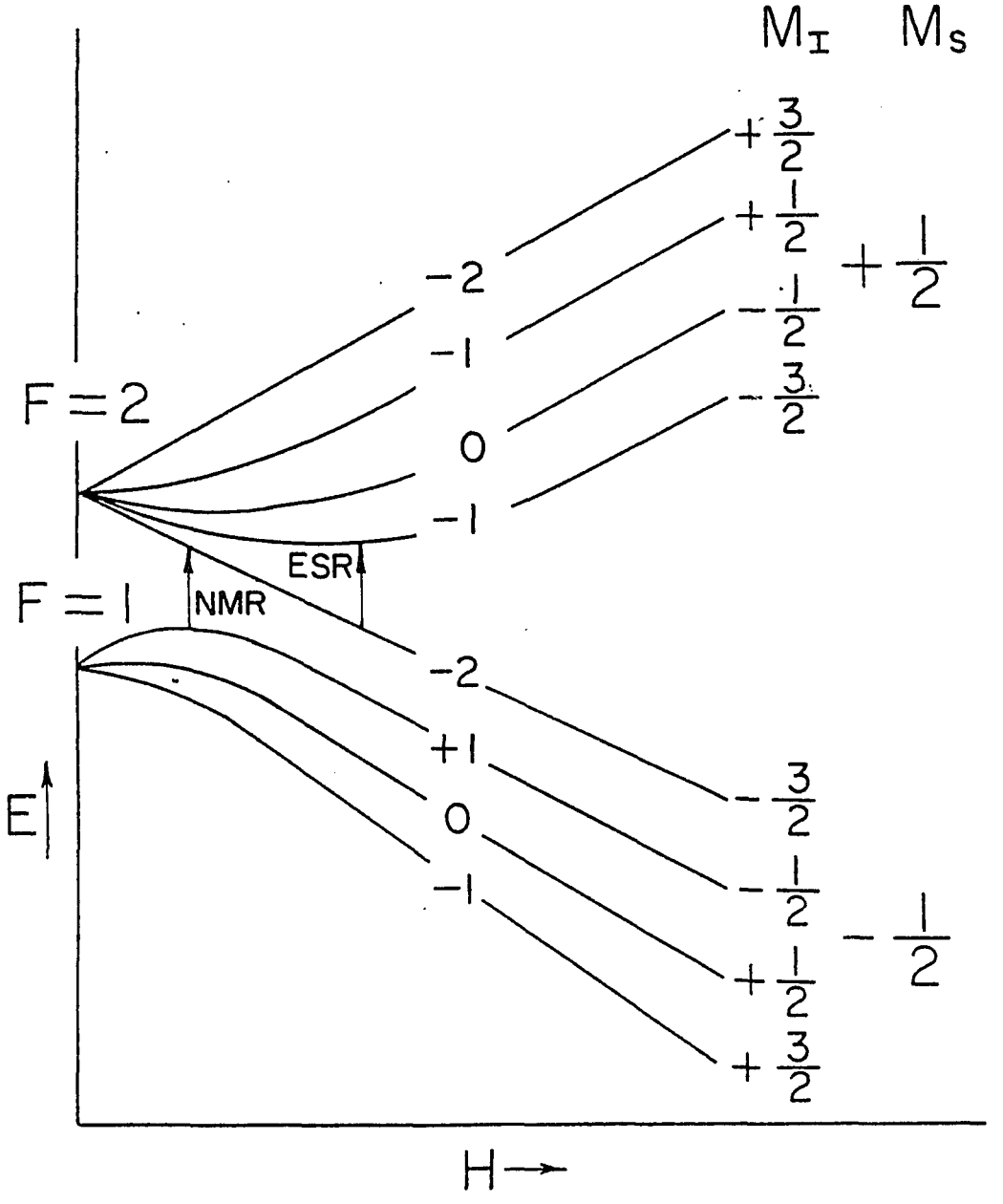

between 2 states with the same M_I value. It is expressed in units of $(H + h)/h\nu$. The hyperfine splitting is given by α in units of $a/h\nu$. The sign preceding the square root is taken to be the same as the sign of M_I. A plot of $\eta(M_I)$ versus α for $I = 3/2$ and $M_I = \pm 3/2, \pm 1/2$ is given in Figure 2. The resonance condition is met at all points on the curves shown. For purposes of discussion the figure is divided into different regions according to the magnitude of the hyperfine interaction.

In the region of a small hyperfine interaction $2I + 1$ transitions are predicted by Equation 10. The magnetic field value that each transition occurs at varies linearly with changes in the hyperfine constant. This case is the well known "high field approximation", described by Equation 11.

$$\eta(M_I) = -M\alpha \tag{11}$$

This equation is equivalent to the neglect of all off-diagonal matrix elements in Equation 6.

Also in Figure 2 is a region labeled "large hyperfine". In this region there are still $2I + 1$ transitions predicted but they are not equally spaced and cannot be described by Equation 11. An exact solution of Equation 10 is required.

For the case of "very large hyperfine" the spectrum has a drastically different appearance. In this region of Figure 2 some transitions require more energy than is available from the radiation field and they are not observed. There will always be at least two

Fig. III.2 Transition Field Diagram

Transition fields for a ^2S atom with I = 3/2 are plotted. The bold lines indicate combinations of the hyperfine value and external magnetic field strength which fulfill the resonance condition.

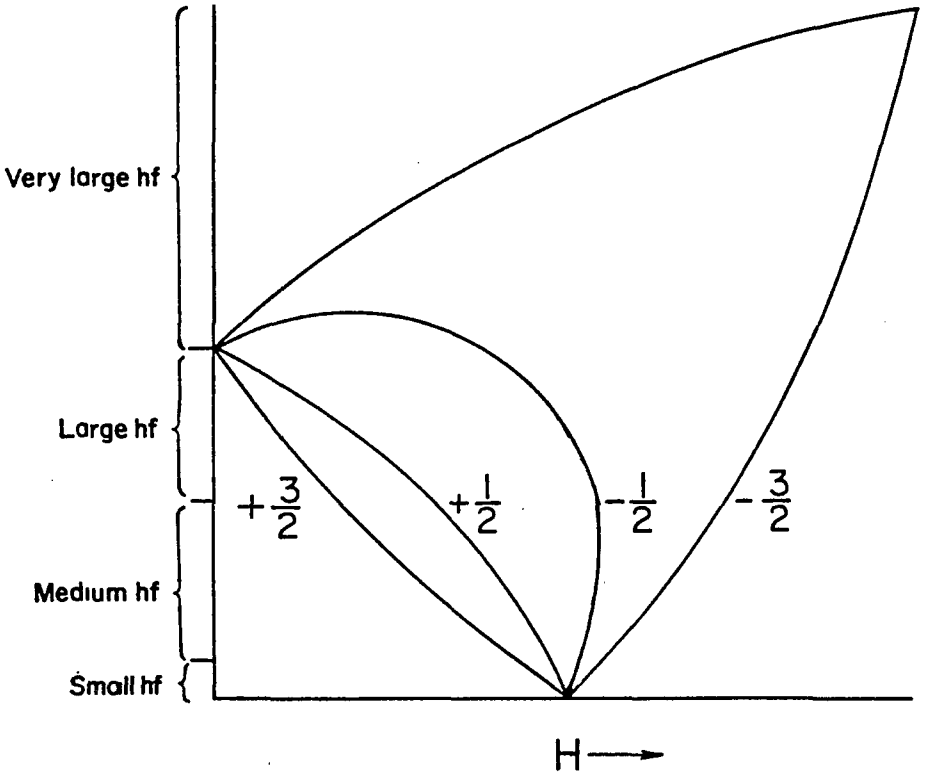

real solution to Equation 10. The first is an ESR transition between states with $M_I = -I$. The second transition will be predicted to occur at a negative magnetic field. It is observed at the absolute value of the predicted field position. This transition is not a true ESR transition but rather an NMR type transition (Fig. 1). The different nature of these transitions is apparent from the phase relation between the ESR and NMR lines in dispersion spectroscopy (Fig. 3). The remaining transitions, if absent, correspond to the case when

$$\frac{M_I^2 \alpha^2}{1 - \frac{\alpha^2}{4}} < \frac{1 - \alpha^2 (I + \frac{1}{2})^2}{1 - \frac{\alpha^2}{4}}$$

and real solutions of Equation 10 do not exist. If the inequality is reversed (for states where $M_I \neq \pm I$) two resonances for a single $M_S = \pm 1$, $M_S = 0$ transition will be observed, often at widely differing magnetic field values. This interesting possibility has been observed with copper atoms in neon (37).

Two limits of Equation 10 are especially useful for analyzing spectra (37). Equation 11 gives the field position for $M_I = \pm I$ transitions

$$\eta(\pm I) = [(2I \pm 1)\alpha - 2]/(2 \pm \alpha) \qquad (11)$$

Fig. III.3 Absorption and Dispersion Spectra of Atomic Copper

ESR spectra of copper atoms isolated in an argon matrix at 4 K with the spectrometer in the: a) absorption mode, b) dispersion mode. Except for the tuning of the microwave bridge instrumental conditions for the two spectra are the same.

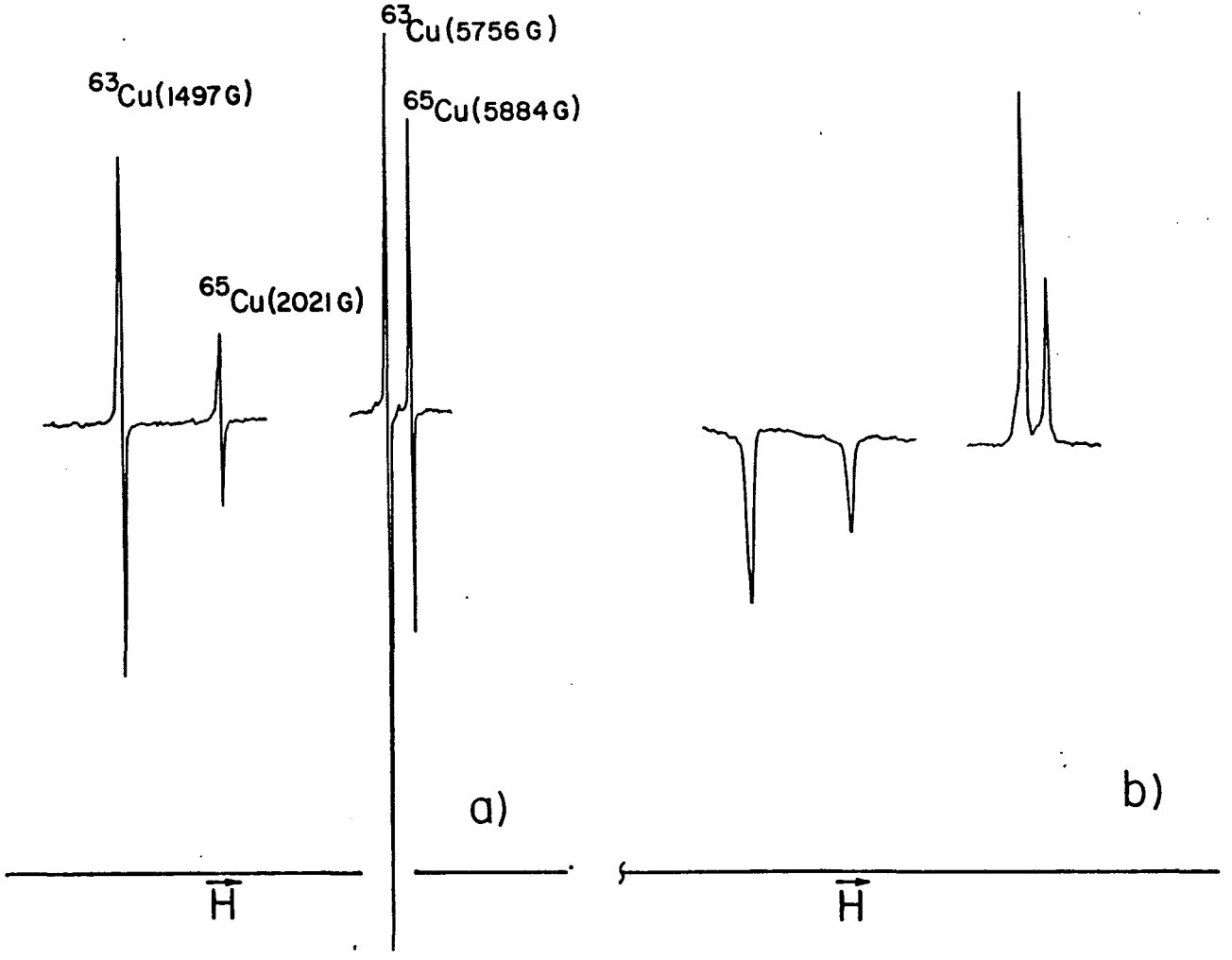

Equation 12 gives the value of α for which "very large hyperfine" behavior is first observed.

$$\alpha = 2/(2I + 1) \tag{12}$$

For cases intermediate between small and large hyperfine splitting, "medium hyperfine", the spectrum retains the qualitative appearance of the high field approximation but no longer can be described quantitatively by Equation 11 to sufficient accuracy. Rather than using an exact solution of the Breit-Rabi formula, a binomial series expansion of the square roots in Equation 7 and 8 may be combined in Equation 9. This results in a power series expression for the resonance condition (Eq. 14).

$$\begin{aligned} \eta(M) = (H + h) + M &+ \frac{\alpha^2}{2(H + h)} [I(I + 1) - M^2] \\ &+ \frac{\alpha^3}{(H + h)^2} [M(M^2 + \frac{1}{2} - I(I + 1))] \\ &+ \frac{\alpha^4}{4(H+h)^3} [(I + \tfrac{1}{2})^4 + (2MI)^2 + 4M^2I - \tfrac{1}{2}M^2 - M^4] \end{aligned} \tag{14}$$

This expression is most frequently given in units of gauss, with the nuclear moment neglected, as in Equation 15.

$$H = \frac{g_e}{g_o} He + \frac{g_e}{g_o} AM + \left(\frac{g_e}{g_o}\right)^2 \frac{A}{H(M)} [I(I + 1) - M^2]$$

$$+ \left(\frac{g_e}{g_o}\right)^3 \frac{A^3}{H(M)^2} [M(M^2 + \tfrac{1}{2} - I(I + 1)] \qquad (15)$$

$$+ \left(\frac{g_e}{g_o}\right)^4 \frac{A}{H(M)^3} [(I + \tfrac{1}{2})^4 + (2MI)^2 + 4M^2I - \tfrac{1}{2} M^2 - M^4]$$

where H_e is the resonant value of the free electron for the cavity and sample used (3312.2 Gauss), g_o is the g value for the electron in the atom and g_e is the g value for a free electron, a is the hyperfine splitting constant in units of gauss and H is the observed line position in gauss. The term in a^4 is rarely used, it being easier to rely on exact solution of the Breit-Rabi formula (Eq. 10). As given in the literature (32,35) the term in a^3 contains an additional factor of 1/2. The expression here appears to be correct. The degree of approximation used when calculating line positions is noted by referring to the order of the hyperfine constant in the final term used.

III. 3. Molecular Breit-Rabi Formula

ESR of molecular systems with large or very large hyperfine splittings is not common. The application of Breit-Rabi type formula to molecular systems has been considered by other workers previously (38,39,40). The formulas used were applied only to molecules with a single large or very large hyperfine interaction on one nuclei, the remaining nuclei responsible for little or no hyperfine interaction. No literature examples of molecules containing two or more nuclei, each with a large or very large hyperfine interaction, are apparent.

Attempts to analyze spectra of molecules with multiple large hyperfine interactions used a modified Breit-Rabi formula. In the coupled basis, where the total nuclear spin vector is defined as $J = I_1 + I_2 + \cdots$, a formula analogous to Eq. 10 is obtained (Eq. 16).

$$(M_I, J) = -\frac{M_I\alpha}{1-\frac{\alpha^2}{4}} \pm \left\{ \frac{M_I^2\alpha^2}{1-\frac{\alpha^2}{4}} + \frac{1-\alpha^2(J+1/2)^2}{1-\frac{\alpha^2}{4}} \right\}^{1/2} \qquad (16)$$

where J may vary as J, J-1 --- M_I and the other quantities have the same meaning as in Eq. 10. Except for the presence of additional states associated with J, Eq. 16 is analogous to Eq. 10 in both appearance and application. The behavior of Eq. 16 for J = 9/2 is illustrated in Fig. 4. At vanishingly small values of either the hyperfine constant or the magnetic field all J values within a given M_J manifold are degenerate. As the degeneracy is lifted each M_J group is split

Fig. III.4 Transition Fields for a Molecule with J = 9/2

Lines indicate the combinations of hyperfine values and external magnetic field strength which fulfills the resonance condition. Large values of the hyperfine interaction or magnetic field are omitted.

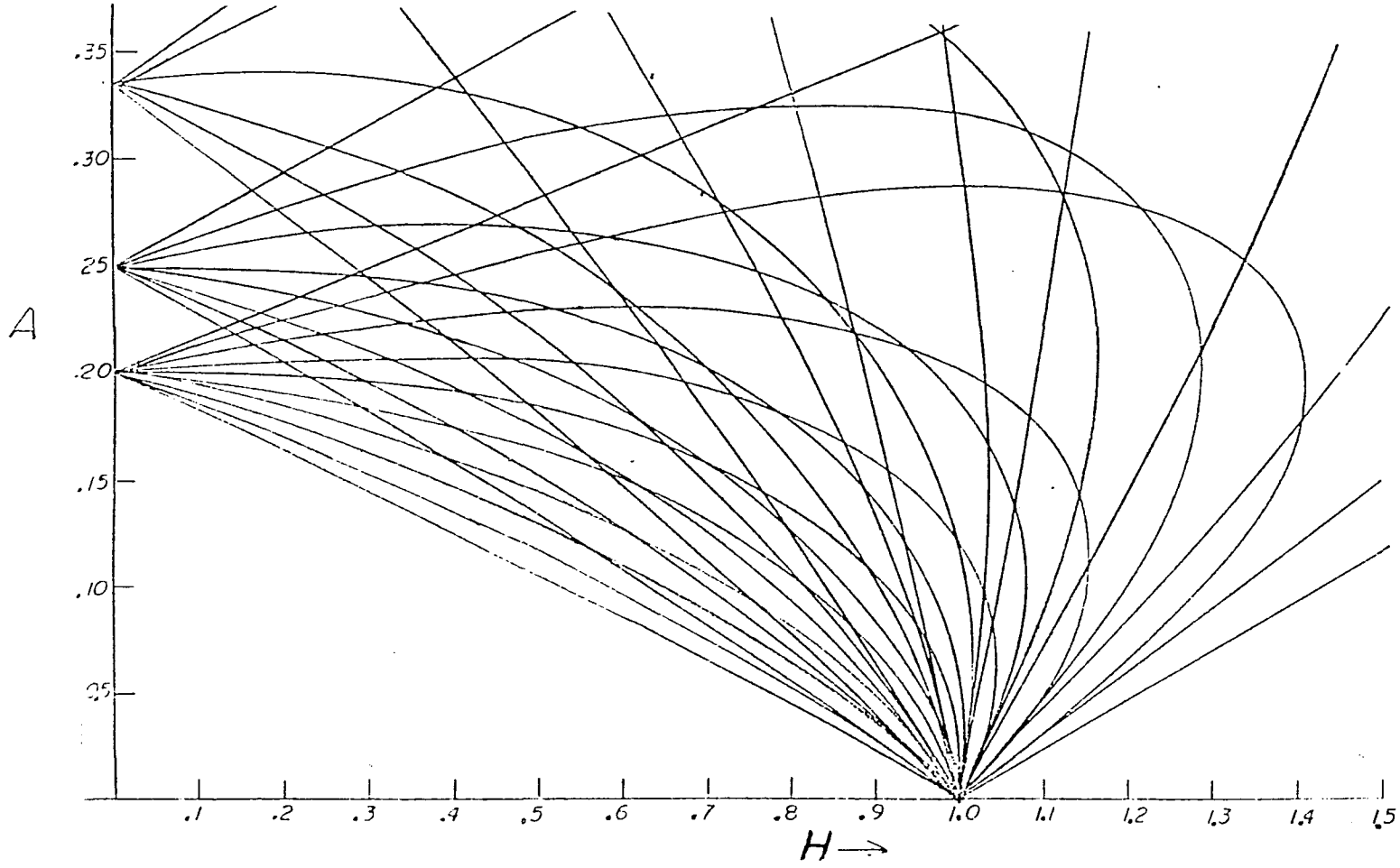

according to its possible J values. For small splittings the transitions are best described by the quantum number M_J, J being treated as a perturbation. As the splitting becomes large J best describes the qualitative behavior of the transitions. Figure 4 shows how the onset of very large hyperfine behavior depends on the quantum number J rather than M_J.

With the exception of Cu_3(?) the hyperfine interactions of the observed metal clusters were of either small or medium magnitude. This permitted analysis of spectra with a power series expansion formula exactly analogous to Eq. 15 with J substituted for I. Many of the clusters observed had spectra which showed well resolved superhyperfine structure. Molecules with groups of magnetically non-equivalent nuclei are described by adding successive hyperfine interactions together. Equation 15 is rewritten for the case of n exactly equivalent groups of nuclei.

$$H = \frac{g_e}{g_o} He + \frac{g_e}{g_o} A_1 M_1 + \cdots + \frac{g_e}{g_o} A_2 M_2 \qquad (17)$$

In this case an 'exactly equivalent' group of nuclei means a group of nuclei characterized by a single time <u>independent</u> hyperfine splitting constant. This equation, truncated to the appropriate degree

of accuracy, will be used in later sections for describing the spectra of static metal clusters.

The line positions of some molecules are dependent on hyperfine constants which are <u>not</u> time independent, and the use of Eq. 17 is incorrect. Time dependent hyperfine constants occur when the molecule, or its environment, undergoes a change which affects the unpaired spin density at a particular nucleus. These molecules are described using a time dependent Hamiltonian which describes the various configurations which the molecule assumes. In cases studied here, the molecules were described by a "Jump" model which considers only the individual metastable conformations of the molecule, each of which can be described by a Hamiltonian, $\hat{\mathcal{H}}_i$. This results in the Hamiltonian

$$\hat{\mathcal{H}} = \frac{1}{n} \sum_{i=1}^{n} \hat{\mathcal{H}}_i \qquad (18)$$

when each state described by $\hat{\mathcal{H}}_i$ has an equal probability of existing at a given instant. $\hat{\mathcal{H}}_i$ is simply Eq. 17 truncated to the necessary degree of accuracy. Equation 18 predicts the resonance of molecules with small hyperfines to occur at the field positions given by the results calculated by Eq. 17 using M, J and a values consistent with n equivalent nuclei. The deviation that the observed lines manifest as higher order effects become significant are known as dynamic frequency shifts. These shifts, most noticeable in pseudo-rotating Na_3 (12) have been described in detail in several references (41-45).

III. 4. Lineshapes and Intensities

In principal the intensities and lineshapes in ESR spectra contain a wealth of information. However, for spectra contained here, severe overlapping, unresolved matrix and anisotropic effects prevented full analysis of the lineshapes. The most valuable information obtained from the lineshapes was qualitative. Symmetric, first derivative-like lineshapes are indicative of isotropic a and g values. a and g values are in general tensors. With the exception of Ag_3, all spectra interpreted were well characterized by isotropic a and g values where $\tilde{a} = a\tilde{1}$ and $\tilde{g} = g\tilde{1}$.

The relative intensity of different lines in an ESR spectra arises from the variable degeneracy of the states giving rise to the transition. For a spectrum with a small hyperfine splitting, where the different J values associated with a single M_J level are degenerate, the intensity distribution among different M_J components is given by the coefficients of the binomial expansion.

Dynamic processes

Exchange or other dynamic process may result in the broadening of some spectral features while leaving others unchanged. These "alternating linewidth effects" are symptomatic of various changes in the molecule's geometry or spin state. The general principles have been well described elsewhere (41-45). The specific cases encountered in this work are discussed later.

IV. SPECTRA AND ANALYSIS

IV.1. K_3

The initial experiments for the thesis were efforts to synthesize the potassium trimer. The previous synthesis and identification of isovalent Na_3 (9) with the available apparatus augered well for success. K_3 was isolated (46) and found to be markedly similar to the previously observed sodium trimer. The analysis of the spectra was straightforward and closely paralleled the analysis of Na_3. Also observed was an isomeric form of K_3, denoted p - K_3. This molecule was the subject of a literature report (46) which is reprinted in Appendix 1.

Matrices yielding predominantly K_3 were formed by codepositing argon and atomic potassium. The argon-metal ratio was approximately 100:1, as determined by comparing the source temperature with the literature values for the vapor pressure of the metal (28). During deposition the spectrometer's modulation coils were on (2-3 Gauss peak to peak, 100 kHz) to enhance clustering, presumably by raising the temperature of the deposition substrate by joule heating from eddy currents (9).

The matrices formed by this technique gave rise to two intense, well resolved ESR spectra, assigned to two forms of K_3, designated s - K_3 and p - K_3, in addition to lesser amounts of atomic potassium. The intensity of these two spectra show a pronounced temperature dependence. The temperature dependence for each isomer is plotted in Figure 1. At 19 K, where s - K_3 is most intense, the spectrum shown in Figure 2 is obtained. A well resolved septet of quartets centered

Fig. IV.1 Temperature Dependence of the s-K_3 and p-K_3 ESR Spectra

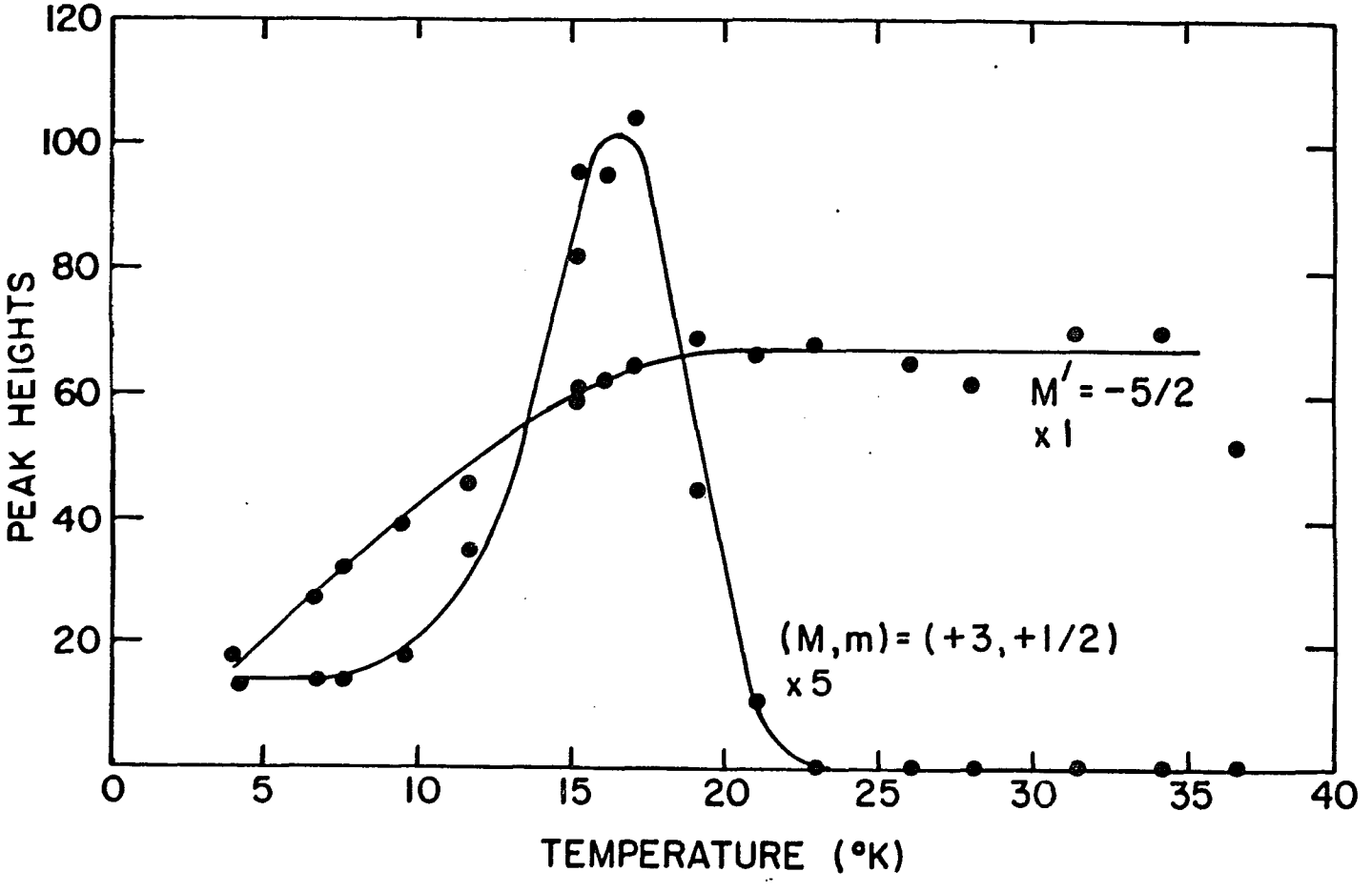

Fig. IV.2 ESR Spectrum of s-K_3

The ESR spectrum of s-K_3 in an argon matrix at 19 K is denoted by the quantum numbers M = +3, +2, ... -3. Also evident are transitions arising from atomic potassium in two sites, m = ±3/2, ±1/2, and from p-K_3 with M' = +9/2, +7/2, ... - 9/2.

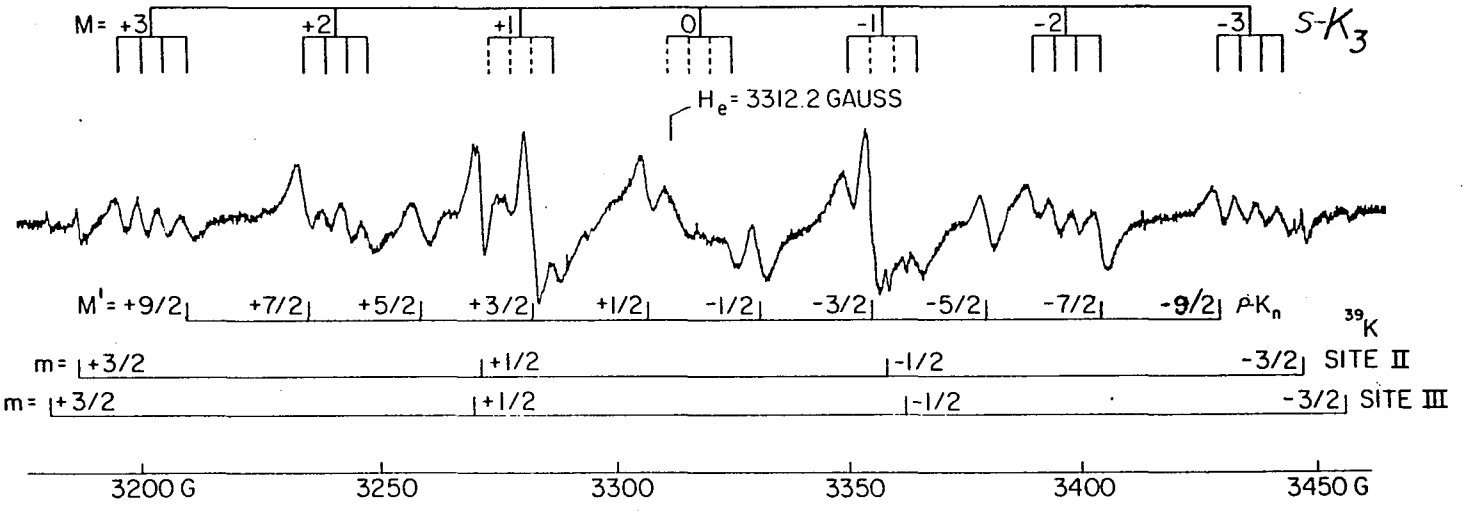

about $g_e = 2$ is apparent. The absence of transitions corresponding to a zero field splitting or changes in the electron spin projection (M_S) other than ±1 implies that the carrier of this spectra has a doublet ground state (5). The first derivative-like line shapes indicate that the g and a tensors are predominantly isotropic (30-35). The septet pattern, split by about 39 gauss, arises from the hyperfine interaction of the unpaired electron with two equivalent potassium nuclei of spin 3/2 ($M = I_1 + I_2 = 3/2 + 3/2$, $M_i = 3,2,.....-3$). The intensity distribution of the septet approximates that expected for two equivalent I = 3/2 nuclei, (1:2:3:4:3:2:1). The quartet pattern, split by about 5 gauss, arises from an additional potassium nuclei ($m = \pm 3/2, \pm 1/2$) with a much smaller hyperfine interaction.

Table 1 lists the observed line positions and their assignment. The line positions calculated from the Breit-Rabi formula, truncated to first order (Sec II, Eq. 17) for both the hyperfine splitting (M) and the superhyperfine splitting (m), are also in Table 1. The difference between the observed and calculated values are small. Possible sources of error include unresolved anisotropic character, matrix effects and calibration uncertainties. Unresolved anisotropies, 2nd order effects partially lifting the degeneracy of J, and matrix effects may be responsible for the observed 2-3 gauss linewidth. The magnitude of the parameters used, and their expected uncertainties are in Table 2.

The spectra of the same matrix at 25 K is shown in Fig. 3. At this temperature, the spectra of s-K_3 is absent and the intensity of the p-K_3 spectra is at a maximum. As for the case of s-K_3, the carrier of

Fig. IV.3 ESR Spectrum of p-K_3

The ESR spectrum of p-K_3 in an argon matrix at 25 K is denoted by the quantum numbers M' = +9/2, +7/2, ... -9/2. Also evident are transitions arising from atomic potassium in two sites (m = ±3/2, ±1/2). The calculated stick spectrum of s-K_3 is also plotted and denoted by the quantum numbers M = +3, +2, ... -3.

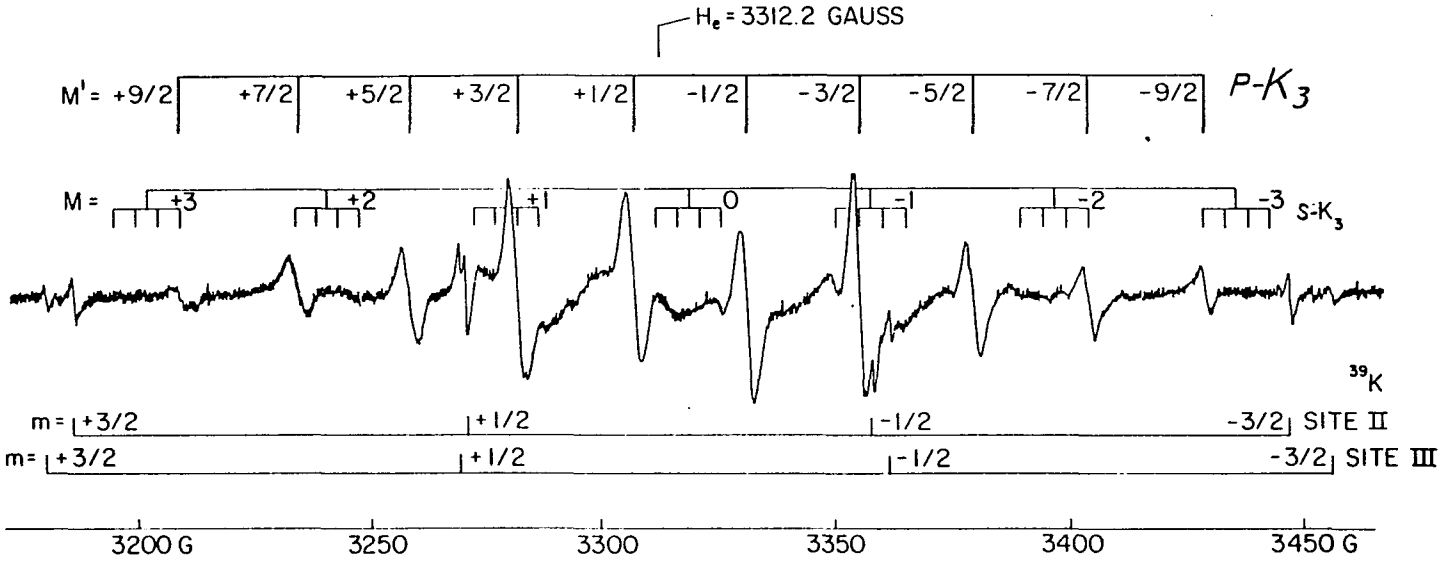

Table IV.1 Comparison Between Measured and Calculated Field Position for s-K_3.

M	m_3	Experimental	Calculated	Differences	Experimental a_3
+3	+3/2	3194.9	3195.0	-0.1	4.7(4)
	+1/2	3199.6	3199.7	-0.1	
	-1/2	3203.9	3204.4	-0.5	
	-3/2	3209.0	3209.1	-0.1	
+2	+3/2	3233.8	3233.9	-0.1	4.6(2)
	+1/2	3238.4	3238.2	+0.2	
	-1/2	3242.9	3242.9	0.0	
	-3/2	3247.3	3247.6	-0.3	
+1	+3/2		3272.4		
	+1/2		3277.1		
	-1/2		3281.8		
	-3/2	3286.7	3286.5	+0.2	
0	+3/2		3311.8		
	+1/2		3316.5		
	-1/2		3321.2		
	-3/2	3325.2	3325.9	-0.7	
-1	+3/2	3350.0	3350.4	-0.4	4.9
	+1/2		3355.1		
	-1/2		3359.8		
	-3/2	3364.9	3364.5	+0.4	
-2	+3/2	3389.7	3389.6	+0.1	4.5(8)
	+1/2	3394.5	3394.3	+0.2	
	-1/2	3398.9	3399.0	-0.1	
	-3/2	3404.2	3403.7	+0.5	
-3	+3/2	3429.0	3429.0	0.0	4.6(2)
	+1/2	3434.0	3433.7	+0.3	
	-1/2	3438.3	3438.4	-0.1	
	-3/2	3443.0	3443.1	-0.1	

Table IV.2 Magnetic Parameters for Alkali Trimers.

	Matrix	g_0	a_1	a_2	1	2
			Gauss			
$Na_3(I)$[a]	Ar	2.0012(12)	149.5(15)	22.6(10)	0.473	0.072
$Na_3(II)$[a]	Ar	2.0012(12)	153.0(15)	20.3(9)	0.484	0.064
s-K_3	Ar	1.9985(5)	39.0(3)	4.7(2)	0.474	0.057
s-K_3	Kr	2.001	38	4.7	0.46	0.06
p-K_3	Ar	1.9990(5)	24.5(7)			

[a] From Reference 9.

Comparison of Parameters for s-M_3 and p-M_3 in Argon.

M	g	$\bar{a}$ (Gauss)	$(a^2)^{1/2}$ (Gauss)
s-Na_3(I)	2.0012(12)	92.1(8) (calc)	122.8(12) (calc)
(II)	2.0012(12)	95.2(8) (calc)	125.5(12) (calc)
(III)	2.0012	93.6 (calc)	123.9 (calc)
s-K_3	1.9985(5)	24.4(7) (calc)	32 (calc)
p-Na_3	2.0012(3)	93.2(2) (obs)	122.0(30) (obs)
	2.0016(3)	95.6(2) (obs)	117.7(30) (obs)
	2.0018(3)	94.7(2) (obs)	121.1(30) (obs)
p-K_3	1.9990	24.5(7) (obs)	----[a]

[a] Not resolved, the $(a^2)^{1/2}$ value of 32 calculated from the s-K_3 spectrum predicts line shifts of less than a gauss.

the p-K_3 spectra is a doublet. The spectrum is well described by isotropic g and a values. The intense 10 line spectrum arises from three potassium nuclei which appear equivalent. The observed transitions are assigned to M = ± 9/2, ±7/2, ±5/2, ±3/2, ±1/2 and listed in Table 3. The positions calculated with the 1st order Breit-Rabi formula are also listed. The parameters used are in Table 2. The intensity ratio is in good agreement with the predicted 1:3:6:10:12:12:10:6:3:1 ratio for three equivalent 3/2 nuclei. The absence of superhyperfine structure on any component strongly, but not absolutely, precludes the possibility of additional nuclei.

The temperature dependence of these spectra differs for different M components. Figure 4 shows the striking difference between the spectra taken at 4 K and 32 K. Only the ±7/2, ±5/2, ±1/2 components show any significant temperature dependence. These components are broadened severely at 4 K while the ±3/2 and ±9/2 components remain unbroadened. This "alternating linewidth effect" has been well documented for the case of organic radicals undergoing exchange (32,42). The details of this alternating linewidth effect have been reported elsewhere (47,48). These reports are reprinted in Appendices 2 and 3.

IV. 2. p-Na_3

The presence of a pseudorotating potassium trimer co-existing with the static trimer prompted further work on the sodium/argon system. Four features, previously unidentified, were found to be well described by an "Extreme Alternating Linewidth Effect" (9). This effect is analogous to the alternating linewidth effect observed in potassium except that the linebroadening of the ±7/2, ±5/2 and ±1/2

Table IV.3 Comparison Between Measured and Calculated Field Position for p-K_3

M	H(meas) Gauss	H(calc) Gauss	Diff.
9/2	3208.7	3208.9	-0.2
7/2	3234.3	3233.2	+1.1
5/2	3258.1	3257.6	+0.5
3/2	3281.8	3282.1	-0.3
1/2	3306.9	3306.6	+0.3
-1/2	3331.0	3331.1	-0.1
-3/2	3354.9	3355.6	-0.7
-5/2	3379.4	3380.1	-0.7
-7/2	3404.1	3404.7	-0.6
-9/2	3429.2	3429.4	-0.2

Fig. IV.4 Temperature Dependence of the p-K_3 ESR Spectrum

The ESR spectrum of p-K_3 in argon at 34.2 K and 4.2 K. The stick spectrum at the bottom of the figure is proportional to the expected intensity distribution for three equivalent I = 3/2 nuclei. Also apparent are transitions from atomic potassium. He = 3312.2 Gauss is the transition field for the free electron.

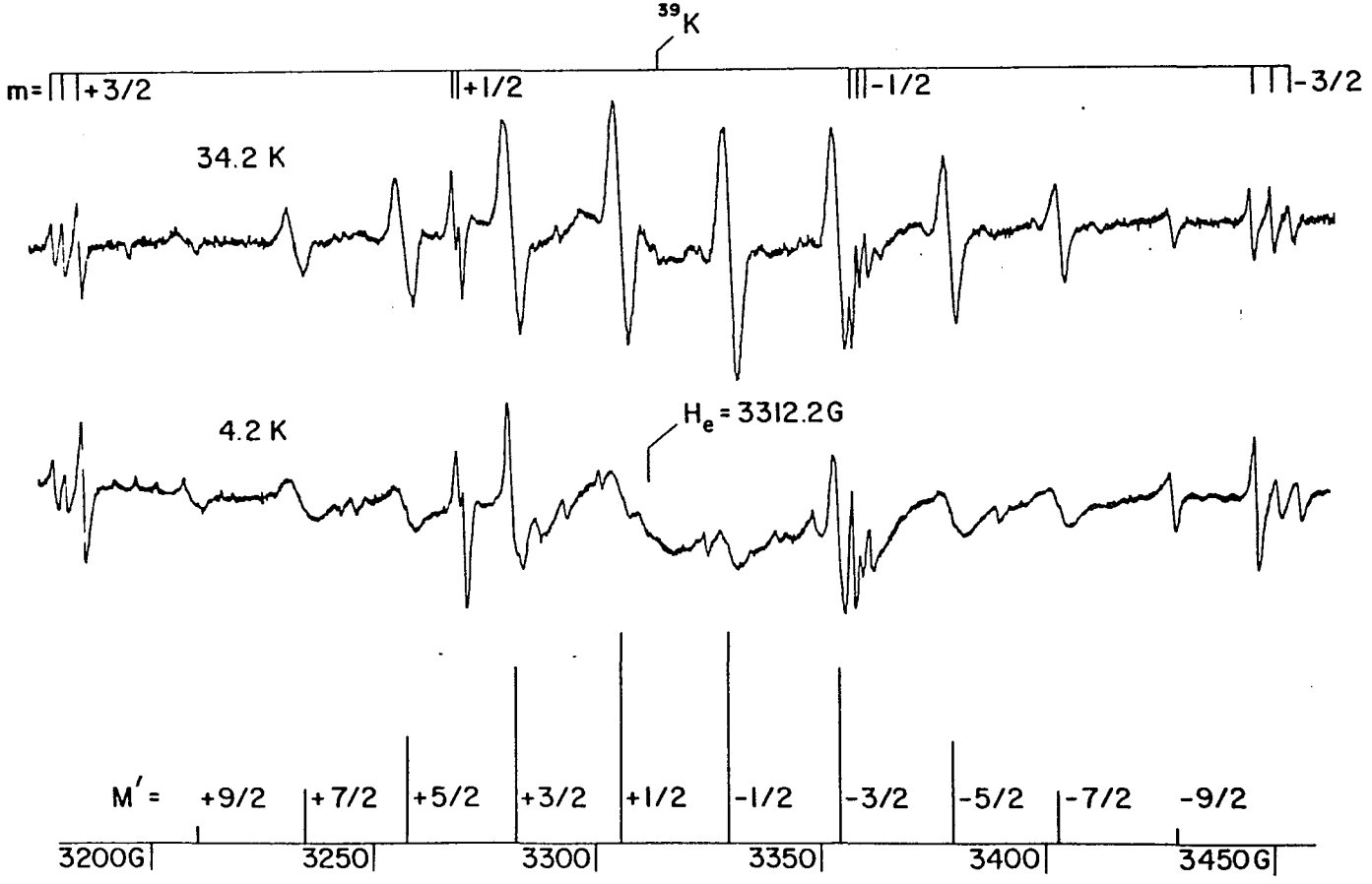

components is extremely severe and broadens these lines beyond recognition over the entire working temperature range of the argon matrix. The observed and calculated line positions are in Table 3. The magnetic parameters used are included in Table 2. A detailed analysis has been reported (9) and is reprinted in Appendix 4.

IV. 3. Na_7

Experiments analogous to the K_3 and Na_3 experiments were conducted using alkali concentrations 3 to 5 times greater (49). For the case of sodium deposited in argon, the spectrum recorded at 30 K is shown in Fig. 5. As in the case of K_3, the spectra arise from a doublet ground state with substantially isotropic $\tilde{g}$ and $\tilde{a}$ tensors. The seven major groups, as for s-K_3, indicates two equivalent sodium nuclei. The observed origins are tabulated in Table 4, as are the values calculated from the Breit-Rabi expression, correct to the 3rd order. The agreement is excellent. The parameters used are listed in Table 5. Not shown in Fig. 5 is the assignment of a 2nd matrix site. The intensity distribution among the major groups approximates that expected for two equivalent spin 3/2 nuclei (1:2:3:4:3:2:1).

Each group shows a further splitting of at least 16 lines from at least five additional nuclei. Figure 6 shows this superhyperfine structure for each component. The above-mentioned site structure is clearly marked. Parameters used to assign these transitions with the first order Breit-Rabi formula are listed in Table 5. Figure 7 shows high signal-to-noise scans of the extrema of the M = ±3 components.

Table IV.4 Comparison Between Measured and Calculated Field Positions for Sodium Clusters, Site I.

M	J	H(meas) Gauss	H(calc) Gauss	Diff.	a
+3	3	2956.6	2956.3	+0.3	6.8(1)
+2	2	3077.0	3076.6	+0.4	6.7(1)
	3	3063.6	3064.0	-0.4	6.6(1)
+1	1	3196.9	3196.8	+0.1	6.7(1)
	2	3188.4	3188.5	-0.1	6.6(2)
	3	3175.3	3175.8	-0.5	6.5(1)
0	0	3317.5	3317.1	+0.4	6.7(1)
	1	3312.5	3312.9	-0.4	6.6(1)
	2	3304.2	3304.5	-0.3	6.6(1)
	3	3290.8	3291.7	-0.9	6.6(1)
-1	1	3433.6	3433.3	+0.3	7.0(1)
	2	3424.9	3424.8	+0.1	6.6(1)
	3	341.7	3412.2	-0.5	6.6(1)
-2	2	3549.6	3549.3	+0.3	6.6(1)
	3	3536.	3536.7	-0.3	6.6(1)

Table IV.5 Magnetic Parameters for Alkali Clusters

	Matrix	g_o	a_1	$\pm a_2$	ρ_1	$\pm\rho_2$
			Gauss			
Na_7	Ar(I)	1.9994(2)	118.2(2)	6.7(1)	0.37	0.021
	Ar(II)	2.0023(4)	116.5(5)			
Na_7	N_2	2.0023(6)	110.7(5)	6.8(1)	0.35	0.022

Fig. IV.5 ESR Spectrum of Na_7

The ESR spectrum of Na_7 in an argon matrix at 32 K. Each of the seven major groups denoted by the quantum number M = +3, +2, ... -3 arises from two equivalent nuclei. The superhyperfine structure from a group of at least five additional nuclei. Also apparent are transitions from atomic sodium, pseudo-rotating Na_3 and background signals from the sapphire deposition surface.

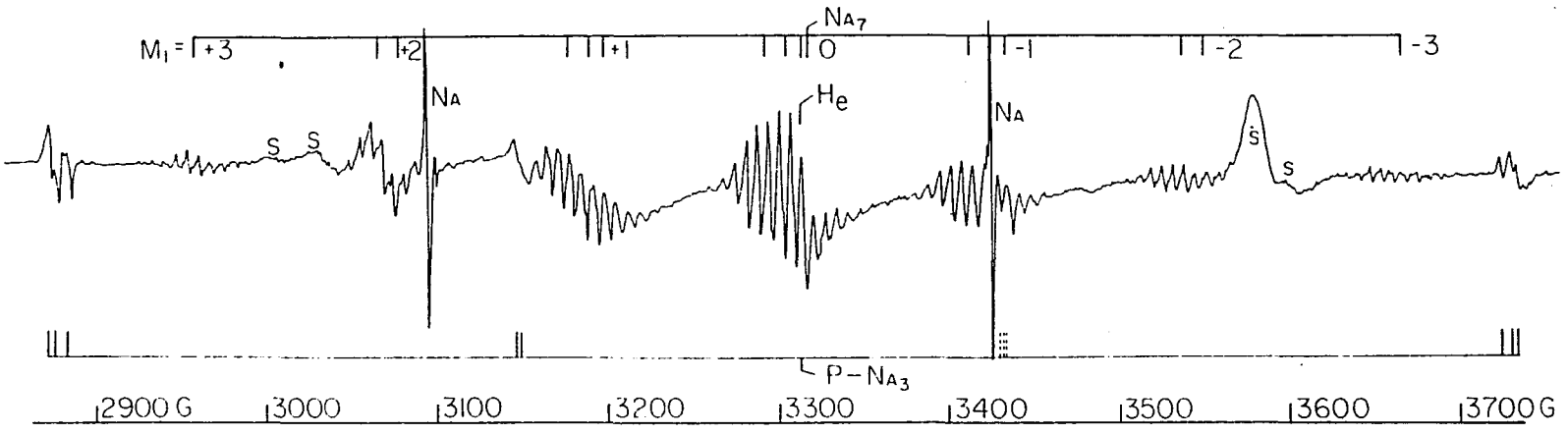

Fig. IV.6 Details of the Major Features of Na_7

High resolution ESR spectra of each major component of Na_7 (Fig. IV.5) showing the detailed structure from higher order effects and multiple sites.

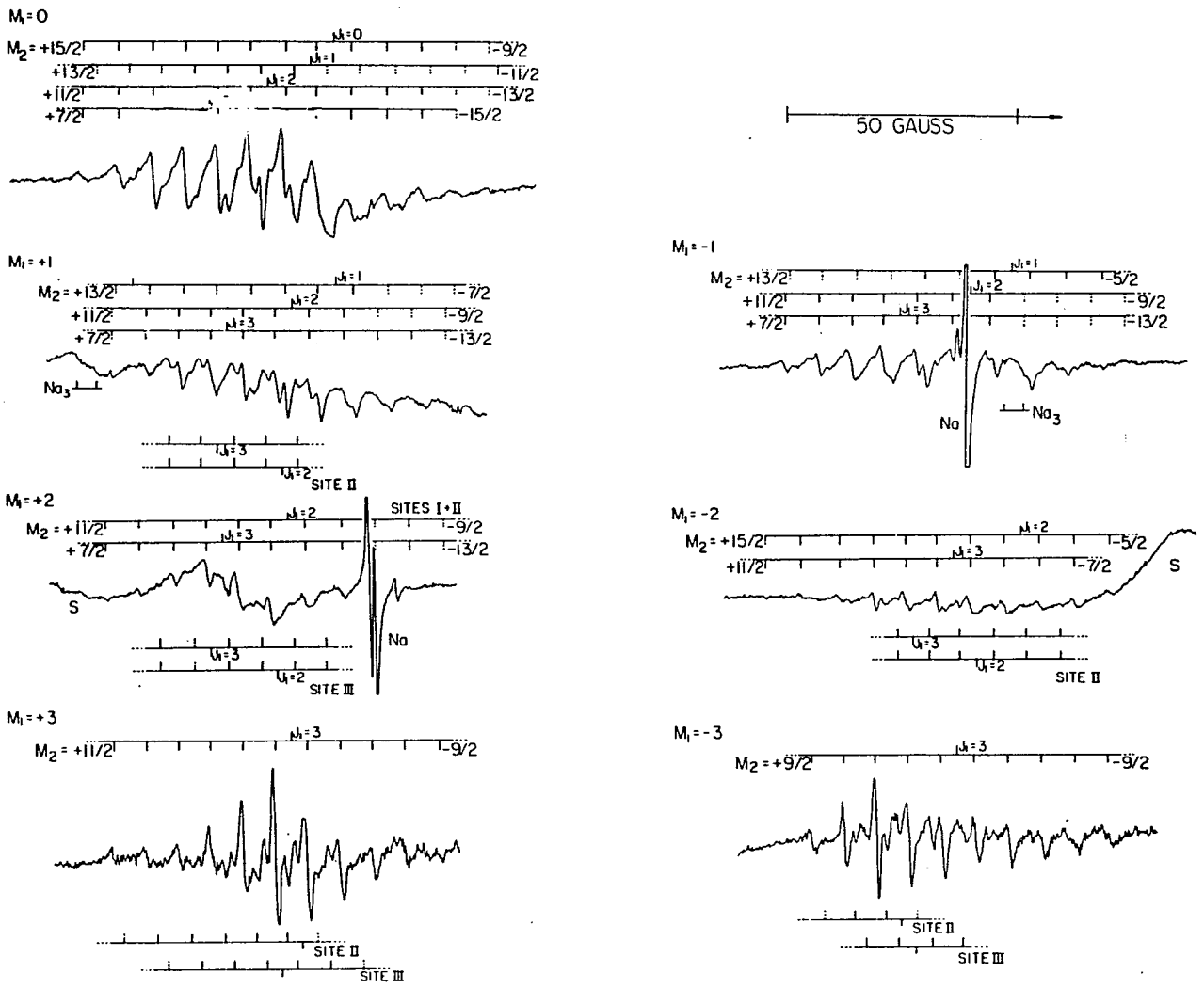
M1 = 0
M2 = +15/2
+13/2
+11/2
+7/2
-9/2
-11/2
-13/2
-15/2
50 GAUSS
M1 = -1
M2 = +13/2
+11/2
+7/2
-5/2
-9/2
-13/2
Na
Na3
M1 = +1
M2 = +13/2
+11/2
+7/2
-7/2
-9/2
-13/2
Na3
SITE II
M1 = -2
M2 = +15/2
+11/2
-5/2
-7/2
S
SITE II
M1 = +2
M2 = +11/2
+7/2
-9/2
-13/2
SITES I + II
S
Na
SITE III
M1 = -3
M2 = +9/2
-9/2
SITE II
SITE III
M1 = +3
M2 = +11/2
-9/2
SITE II
SITE III

Fig. IV.7 High Signal to Noise Spectra of Na_7

High signal to noise spectra of: a) the low field extrema of the M_1= +3 group. b) the high field extrema of the M_1= -3 group.

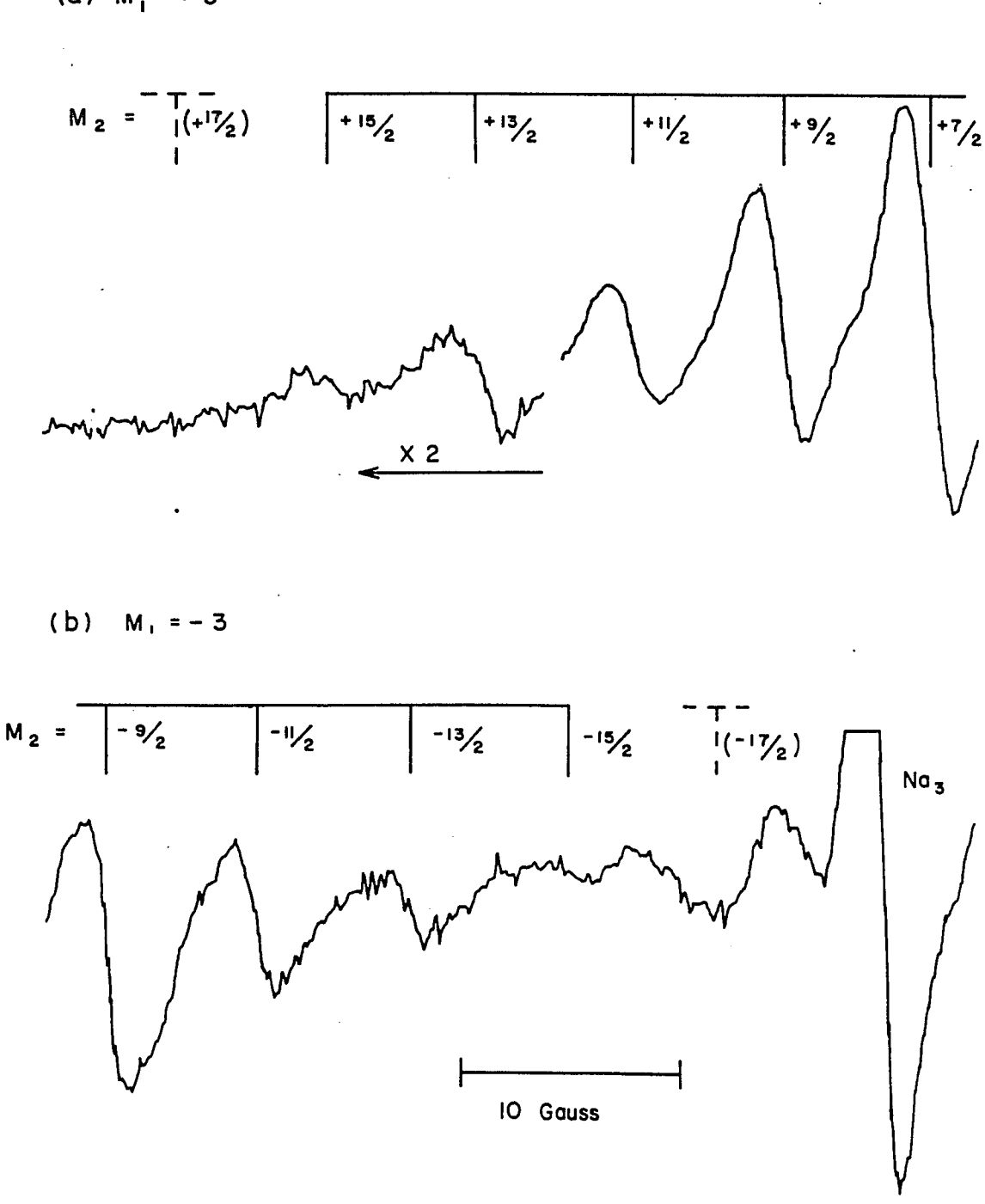

These scans illustrate the uncertainly in determining the number of nuclei contributing to the superhyperfine structure. If more than five nuclei are involved, a ±17/2 component must be present, with an intensity approximately 1/3 that of the M = ±15/2 component. Insufficient signal-to-noise prevented the observation of a ±17/2 line. In Fig. 7b, a previously unobserved line associated with Na_3 obscures the region of interest. Efforts to signal average for longer periods of time were not successful due to "jitter" in the field scan circuitry.

An analysis of the intensity distribution was carried out in an attempt to determine the number of nuclei responsible for the superhyperfine structure. Stick plots of intensities predicted for 3, 5, 7, and 9 nuclei were made and compared with the experimentally determined plots. The envelopes of these plots are shown in Fig. 8 and 9 for the M = +0 and M = +3 components respectively. While these plots do support the assignment of the smallest number of nuclei consistent with the observed Shf, they are sufficiently uncertain to preclude definitive assignment.

The experiment was repeated in a nitrogen matrix with similar results, though complicated by the presence of an additional spectrum. The parameters obtained are listed in Table 5. The literature report of this cluster is reprinted in Appendix 5.

IV. 4. Group IB Metal Atoms

The second stage of these experiments was an effort to synthesize Group IB metal clusters. The design of the necessary metal source is described in detail in Sec. III. 5. ESR spectra of matrix isolated

Fig. IV.8 Observed versus Calculated Intensity Distribution of the M = 0 Component of Na_7

The experimental results are given by the solid curve. See text for an explanation of the calculated values.

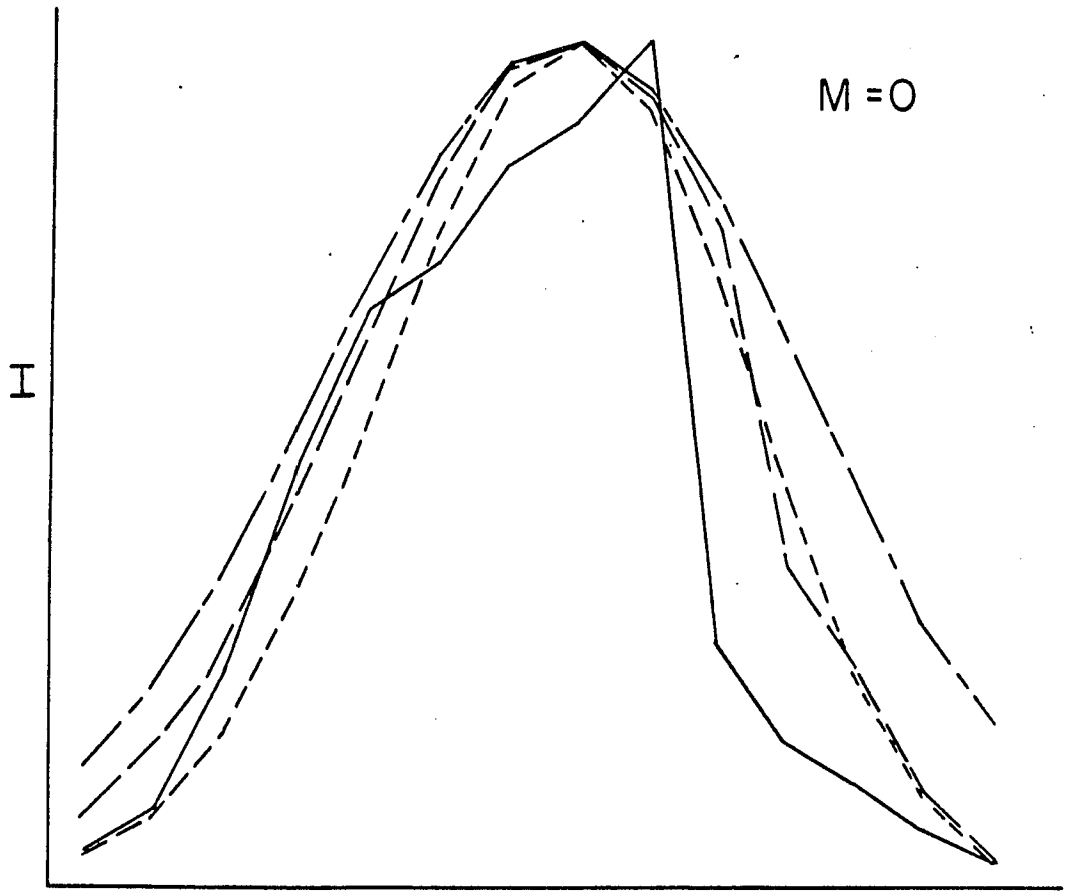

Fig. IV.9 Observed versus Calculated Intensity Distribution of the M = +3 Component of Na_7

The experimental results are given by the solid curve. See text for an explanation of the calculated values.

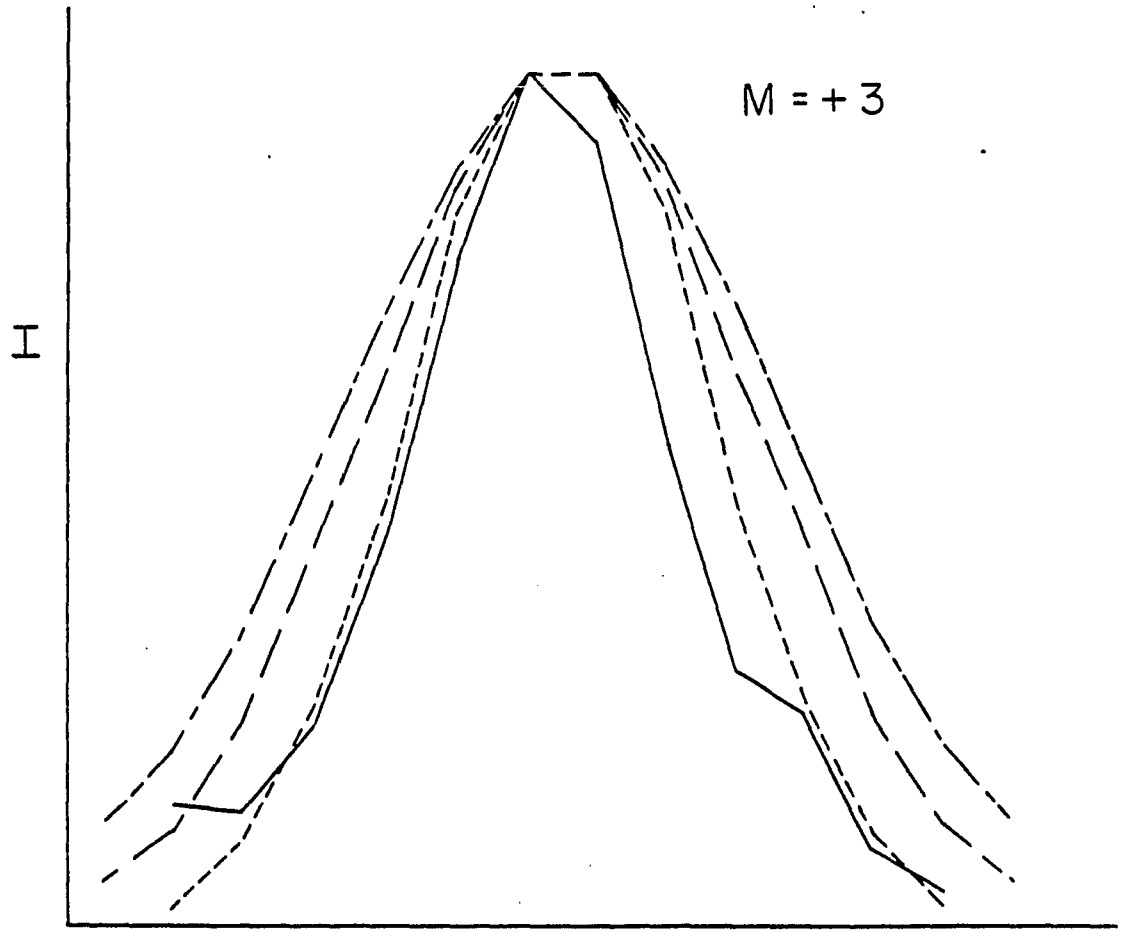

Group IB metal atoms have been reported by Kasai and McLeod (37). This work was reproduced in this laboratory to provide a check of various experimental points.

A deposition of gold in argon (gas-metal ratio ∿100) produced the spectrum in Fig. 10. The four transitions expected from a ^2S atom with nuclear spin 3/2 are clearly evident. The increasing splitting towards the high field side arises from the large higher order effects. The signal-to-noise ratio is excellent, approximately 1000:1, a factor of 10 greater than that commonly encountered for the other metal atoms observed.

A spectrum of silver atoms in argon is in Fig. 11. The high and low field lines are separated by ∿650 Gauss. The two lines from each silver isotope (I = 1/2) are clearly resolved. Also present is a further small splitting of about 3 Gauss. This previously unreported structure is of unknown origin.

Figure 12 shows the ESR spectra of copper in argon after a 200 min deposition at an argon:copper ratio of 500. In addition to the two lines from each isotope, numerous sapphire lines are apparent. (The strong doublet immediately downfield from ^{63}Cu (NMR) is the same as the doublet downfield from M = 3/2 in Fig. 1, the difference in signal-to-noise is quite apparent). Since both isotopes of Cu are ^2S with I = 3/2, the observation of two rather than four transitions for each isotope indicate that two transitions are inaccessible at X band. To confirm that the field lines originate from an NMR type transition rather than an ESR type, a dispersion spectrum was recorded (Fig. 13). The dispersion spectrum, which is sensitive to the sign of the magnetic moment,

Fig. IV.10 ESR Spectrum of Gold Atoms

The ESR spectrum of gold atoms isolated in an argon matrix at 4 K. The overall scan is 5000 Gauss and centerd about g = 2.

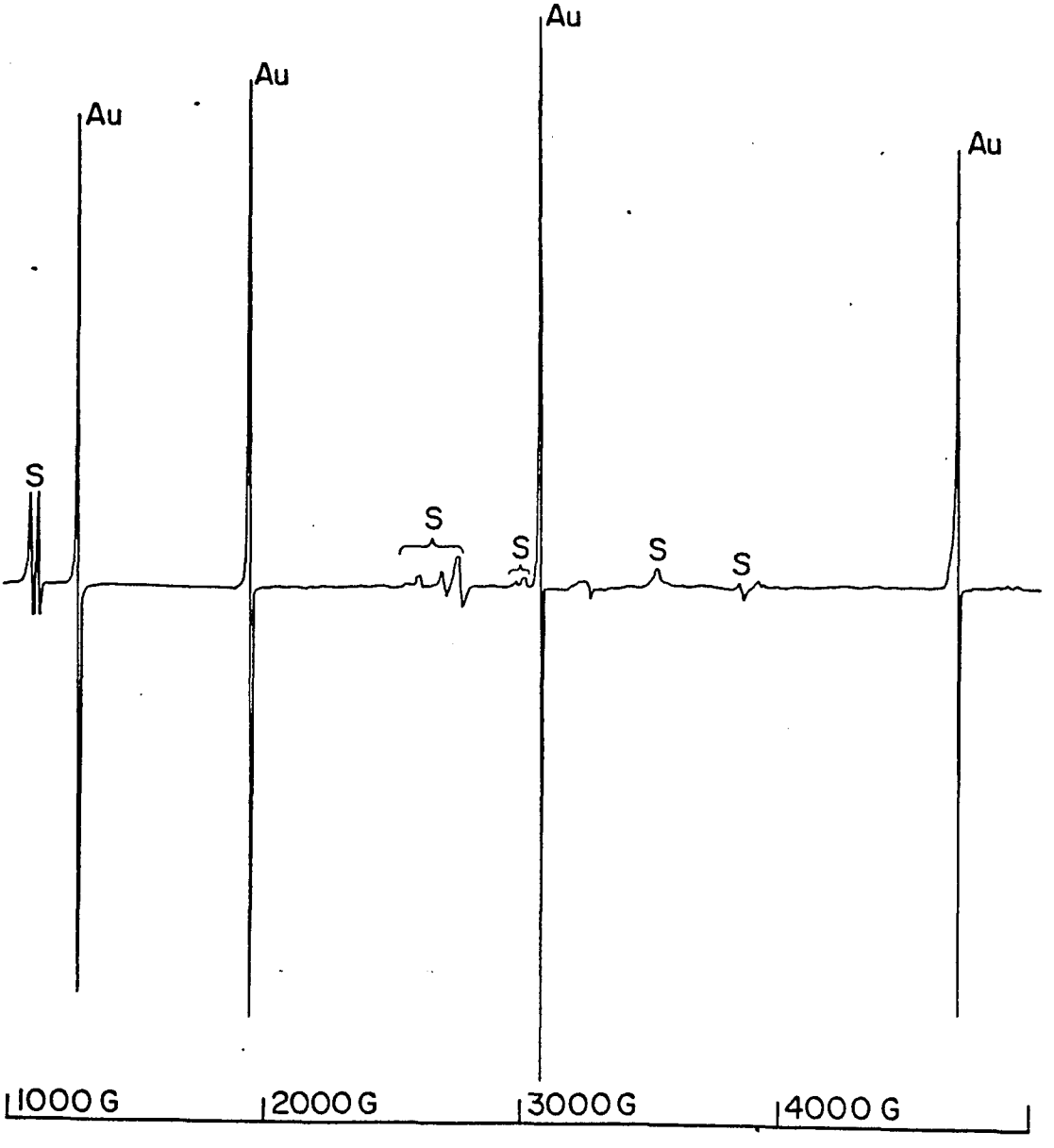

Fig. IV.11 ESR Spectra of Silver Atoms

ESR spectra of silver atoms isolated in argon at 4 K. The high and low field doublets are split by about 650 gauss. Each doublet is due to the presence of two isotopes of silver. The structure apparent on each line is of unknown origin.

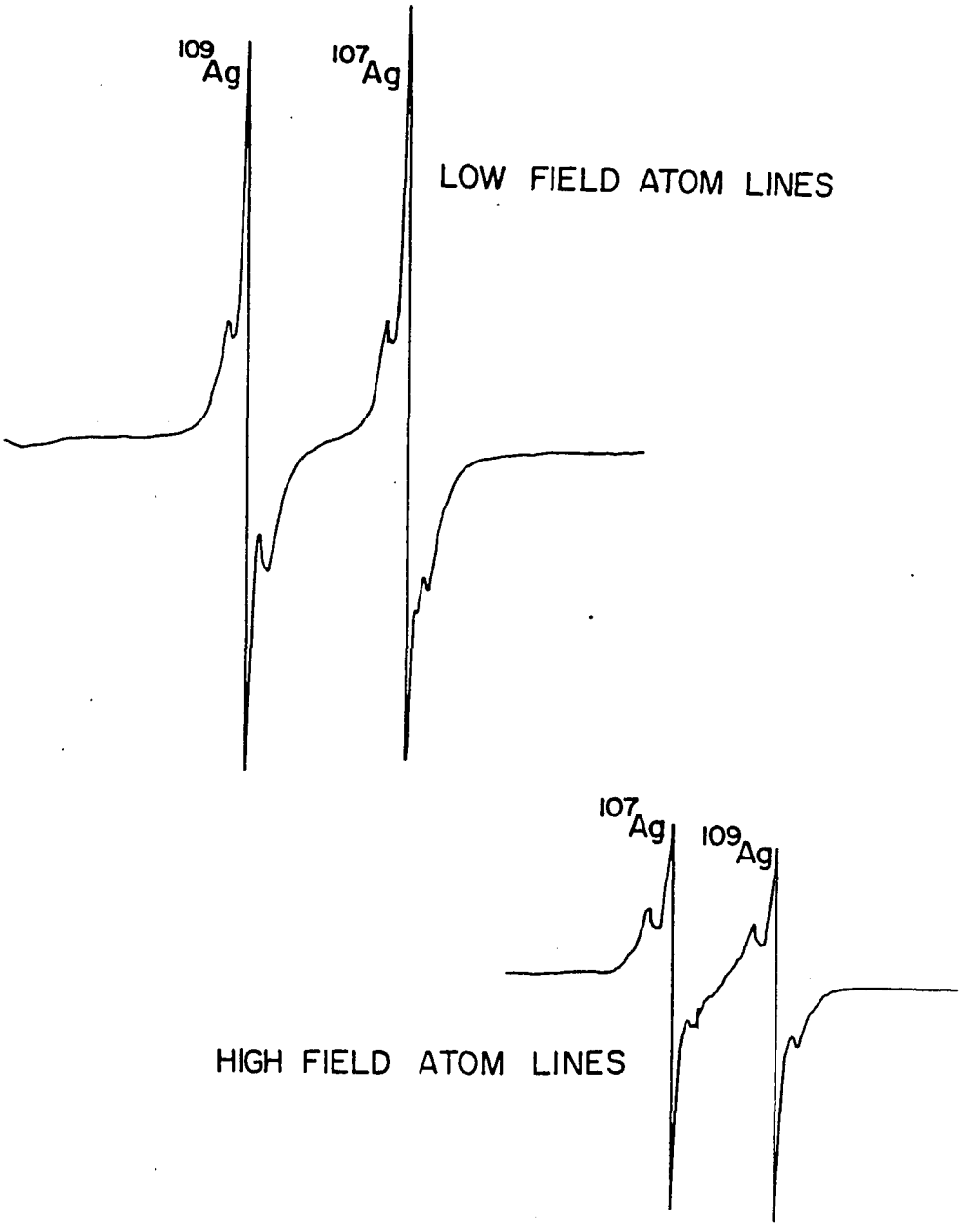

Fig. IV.12 ESR Spectra of Copper Atoms

ESR spectrum of copper atoms isolated in an argon matrix at 4 K. Each doublet is due to the presence of two isotopes of copper. The spectrum is 7000 Gauss wide and centered about g = 2.

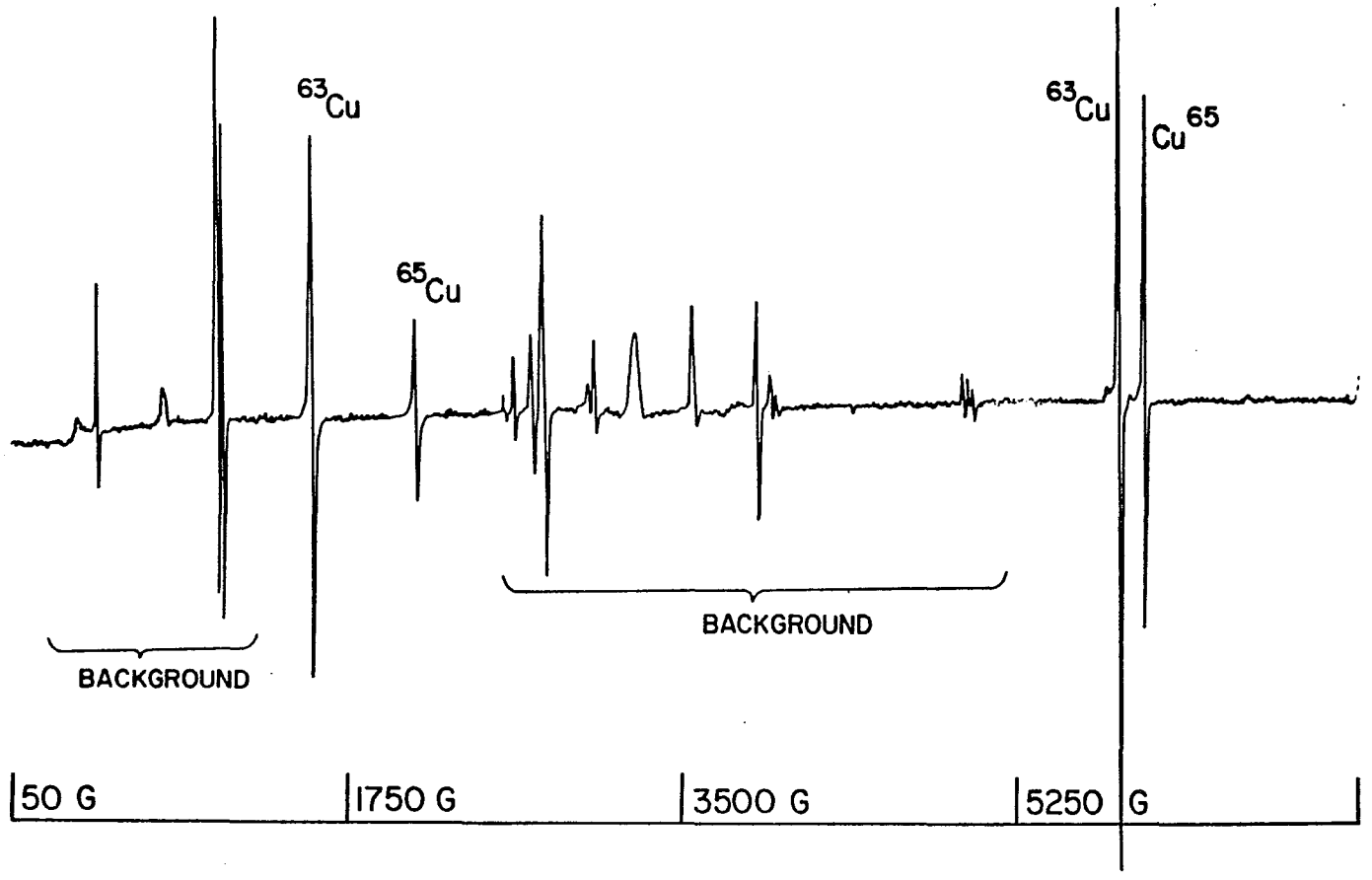

Fig. IV.13 ESR Spectrum of Copper Atoms - Dispersion Mode

ESR spectrum of copper atoms isolated in an argon matrix at 4 K with the microwave bridge tuned to detect the dispersion component of the resonance. The spectrum is 7000 Gauss wide and centered about g = 2.

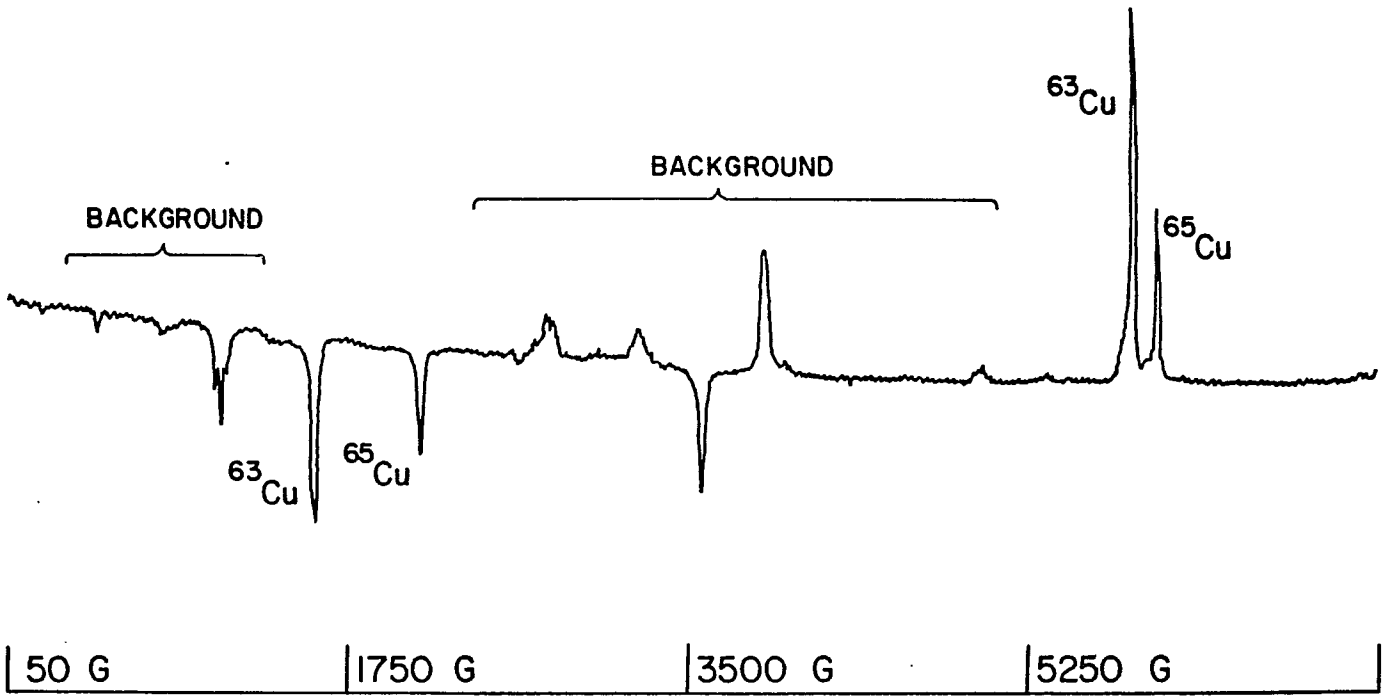

confirms the assignment. Both the absorption and dispersion spectra are the same as those reported by Kasai (37).

IV.5. Ag_3

When silver was deposited in nitrogen matrices for 4 hours with a gas/metal ratio of 200 a weak, poorly resolved spectra is apparent. Annealing of the matrices causes a dramatic improvement in resolution. The spectra in Fig. 14 shows the well-resolved perpendicular features of Ag_3. Also present are the parallel lines characteristic of an anisotropic g and/or a value. A complete analysis will be presented elsewhere (14), only the parallel features will be described here. The spectra is consistent with a trimer containing a single spin 1/2 nulceus carrying most of the unpaired spin. The remaining two equivalent nuclei each carry a smaller amount of the spin. Because silver has a small nuclear spin, the spectra consists of only six lines. This permits the resolution and assignment of the different isotopic combinations, i.e., $^{107}Ag_3$, $^{109}Ag_3$, $^{107}Ag_2{}^{109}Ag$, ------. The intensity distribution is as expected. These experiments were repeated with isotopically pure ^{107}Ag to confirm the assignment and permit resolution of the parallel features. The observed spectra is grossly different than that assigned to Ag_3 in an deuterobenzene matrix (50).

Observed line positions are compared with those calculated from a 2nd order Breit-Rabi formula in Table 6. Parameters used are listed in Table 7. The ratio of the different hyperfine constants assigned to different isotopic combinations is consistent with the difference in the nuclear magnetic moments, as expected. (These spectra differ radically from those previously reported by Howard (50). These spectra,

Fig. IV.14 ESR spectrum of Ag_3

ESR spectrum of Ag_3 isolated in a nitrogen matrix at 4 K. The different isotopic combinations are resolved and are denoted by the notation 107-107-107, 107-107-109, ...

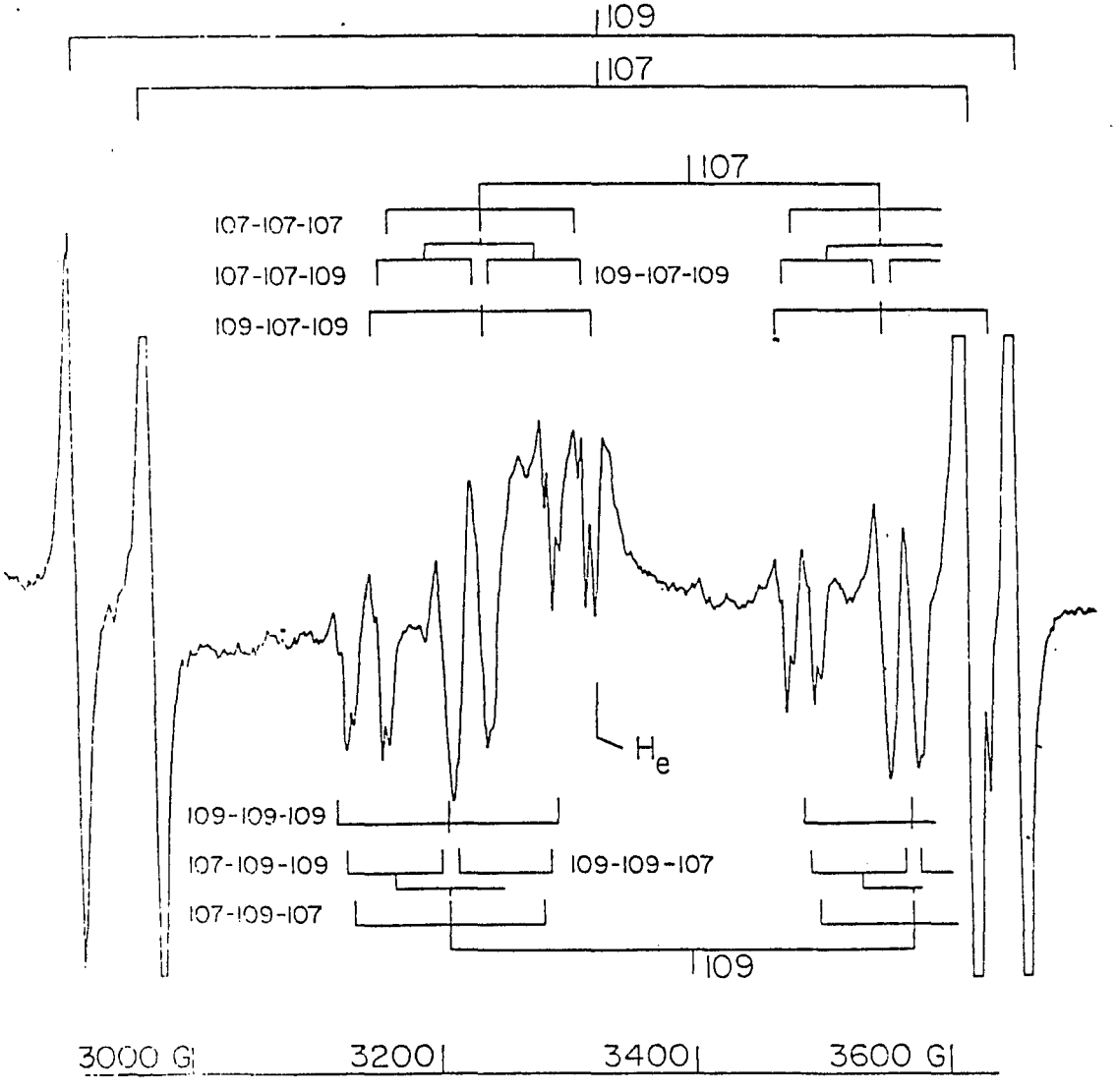

Table IV.6 Observed vs. Calculated for Ag_3[1]

Hyperfine Structure	M	H(obs)	H(calc)
$^{107}AgAg_2$	+1/2	3230.4	3230.5
	-1/2	3564.5	3564.7
$^{109}AgAg_2$	+1/2	3202.6	3202.7
	-1/2	3587.1	3587.1

Superhyperfine Structure (Lowfield Group)	M[2]	H(obs)	H(calc)	Diff.
109-109-109	+1	3116.3	3116.2	0.1
	-1	3291.4	3290.5	-0.1
109-107-109	+1	3144.3	3144.1	+0.2
	-1	3318.5	3318.3	+0.2
109-109-107	+1	3122.2	3122.2	+0.1
	-1	3284.6	3284.8	-0.2
109-107=107	+1	3150.0	3150.0	0
	-1	3312.6	23312.6	0
107-109-107	+1	3129.1	3128.2	0.9
	-1	3278.0	3278.1	-0.1
107-107-107	+1	3157.5	3156.0	1.5
	-1	3306.0	3306.0	0

[1] Calculated using the parameters in Table IV.6.

[2] M = 0 components were not as well resolved as M = ±1 components.

Table IV.7 Magnetic Parameters for Ag_3

	^{107}Ag	^{109}Ag
g	2.0526	2.0526
a_o	317.2 Gauss	364.7 Gauss
a_3	73.3 G	85.0 G

For these experiments, the free electron resonance is at 3322.3 gauss.

obtained in an deuterobenzene matrix imply a different ground state for Ag_3.)

IV. 6. Cu_3 (?)

A large number of experiments with copper in various matrices were conducted. Several copper-containing molecules were synthesized although few were definitively assigned. One species, formed when copper-containing nitrogen matrices are annealed to ∿35 K, clearly consists of more than two copper nuclei, as evidenced by the large number of lines. Figure 15 shows the spectrum attained with isotopically pure ^{63}Cu, the spectrum obtained using the naturally occurring isotope is similar but more complex. The spectrum consists of a large number of groups, most of which show a similar superhyperfine splitting (Fig. 16). Efforts to assign this spectra were unsuccessful.

IV. 7. Copper Adducts or Site Effects

Despite a careful search for Cu_3 in an argon matrix, no strong evidence of copper clusters was found. A wide range of deposition conditions was employed (Fig. 17). One carrier readily synthesized is CuX (Fig. 18). The intensity of this spectrum was greatest in earlier experiments using the first generation high temperature source. In later experiments using the second generation source the spectra assigned to CuX were much less intense. Since the major difference between the two sources was the standard of vacuum integrity, CuX is tentatively assigned to an impurity complex with copper. The nature of X is unknown.

Another spectrum frequently observed in argon matrices is shown in Fig. 19. One possible explanaton of this spectrum is that it is from

Fig. IV.15 ESR Spectrum of a Copper Cluster

ESR spectrum attributed to a copper cluster in a nitrogen matrix at 20 K. Isotopically pure copper is used to simplify the spectrum. The overall spectrum is 8000 Gauss wide.

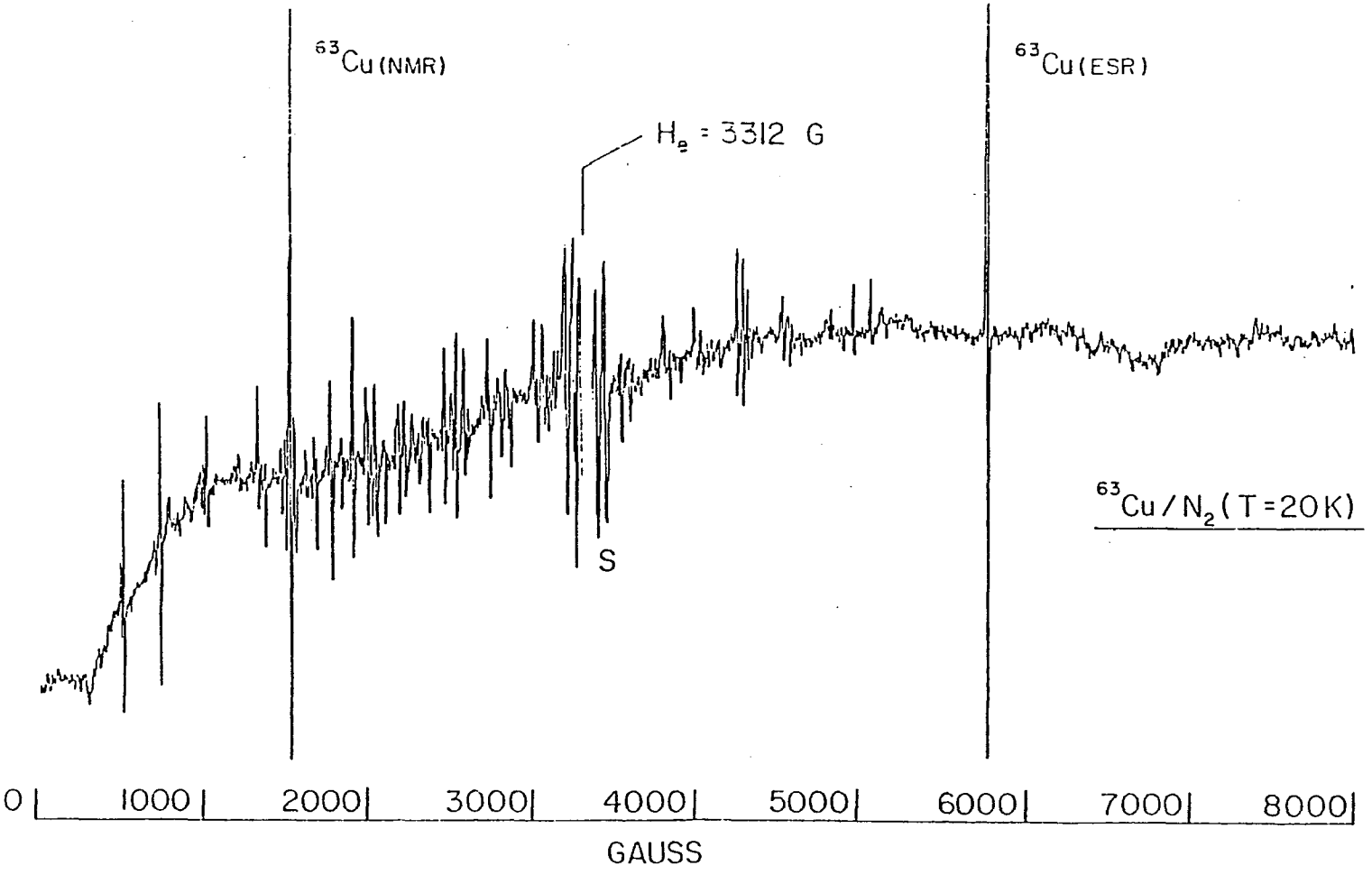

Fig. IV.16 Details of the ESR Spectrum of a Copper Cluster

Portions of Fig. IV.15 enlarged to show the superhyperfine structure. Each section is 1000 Gauss wide.

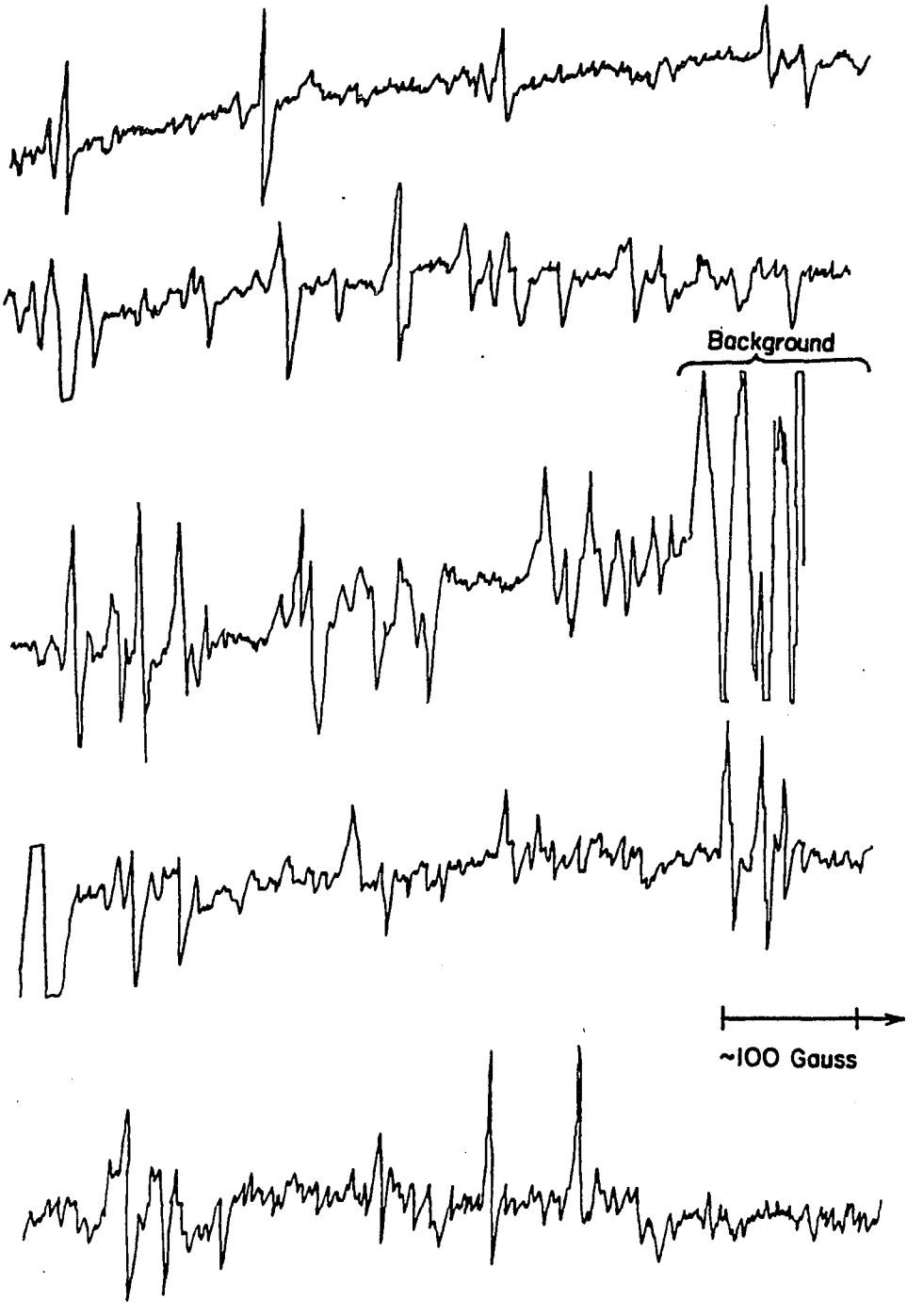

Fig. IV.17 Summary of Deposition Conditions for Copper-Argon Experiment

Deposition conditions used in the attempted synthesis of Cu_3 in argon. The deposition temperature is the temperature of the lower part of the helium dewar and microwave cavity during deposition.

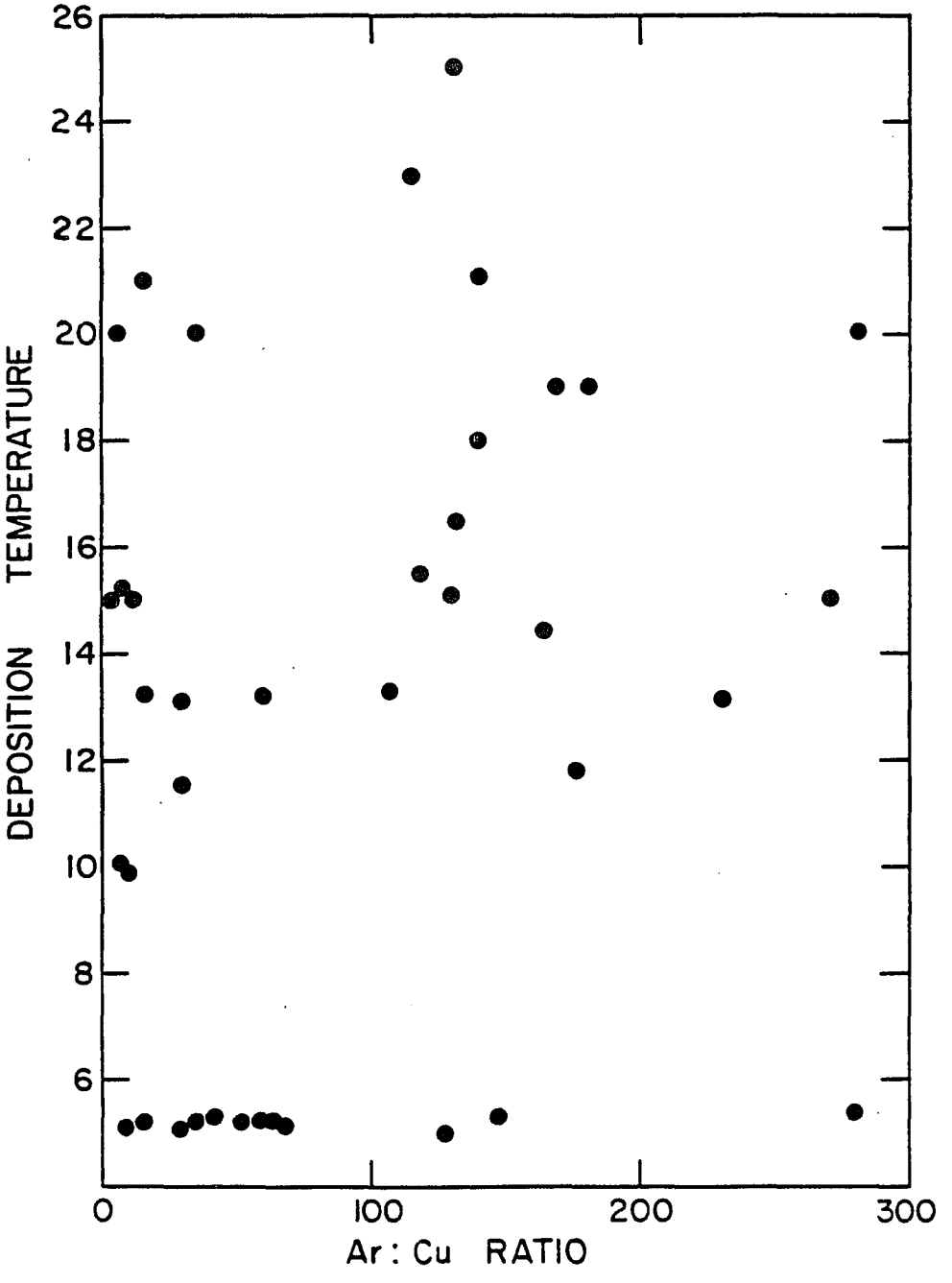

Fig. IV.18 Spectrum of CuX

This ESR spectrum of CuX in argon was most apparent in experiments using the first generation source.

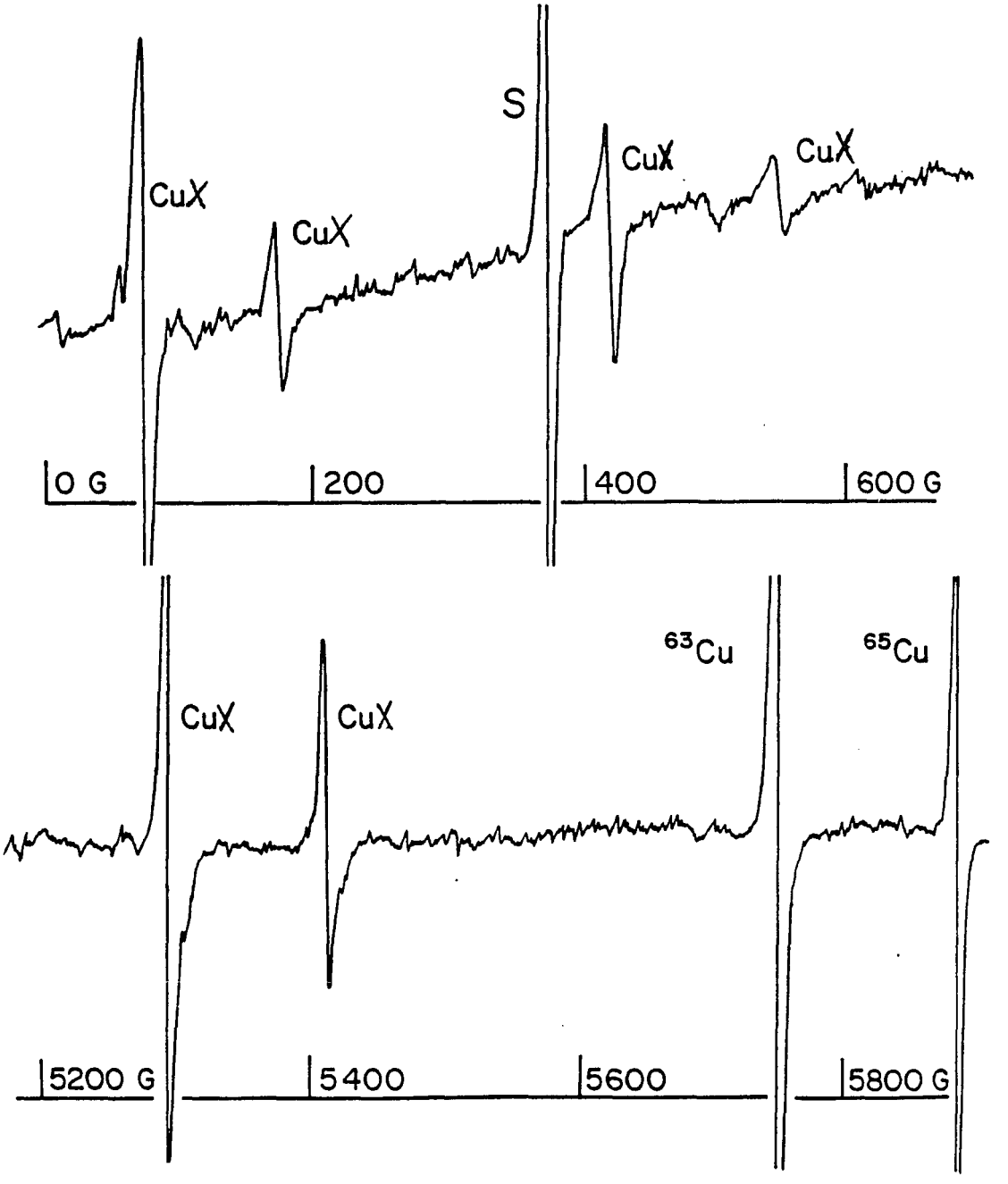

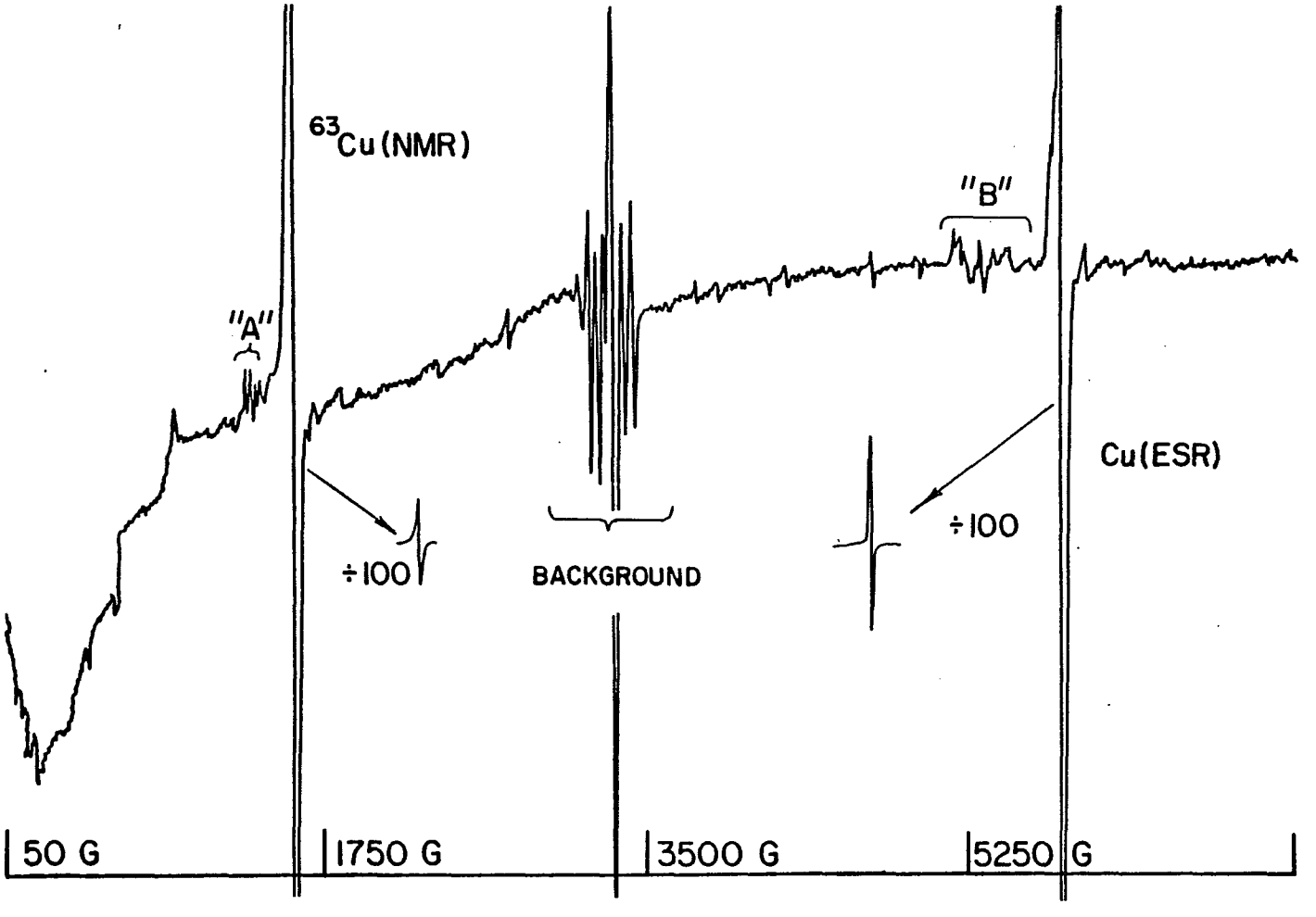

Fig. IV.19 Unassigned Copper Spectrum

The feature marked "A" and "B" were observed when copper was deposited in argon. The inset shows the atom lines with the gain reduced by a factor of 100.

copper atoms trapped in unusual sites, such as the amorphous regions of the argon. Spectra of copper atoms in neon matrices give rise to complex patterns which have been attributed by Kasai (37) to atoms trapped in an amorphous region. This spectrum disappears after the slightest annealing. A similar, though weaker, spectrum of copper in krypton was observed after annealing to 25 K.

IV. 8. Na_5 (?)

During the work on Na_7 in nitrogen matrices an additional spectrum was observed. This spectrum became apparent during annealing at 25-26 K. The 16 groups of transitions have an irregular 45-50 Gauss splitting. While 16 groups are consistent with five spin 3/2 nuclei, the anomalistic pattern prevents assignment.

Fig. IV.20 Spectrum of Na_5 (?)

The ESR spectrum shown is obtained when sodium is deposited in a nitrogen matrix. The number of major features (16) is consistent and may arise from a molecule with five equivalent I = 3/2 nuclei. The irregular pattern is not understood.

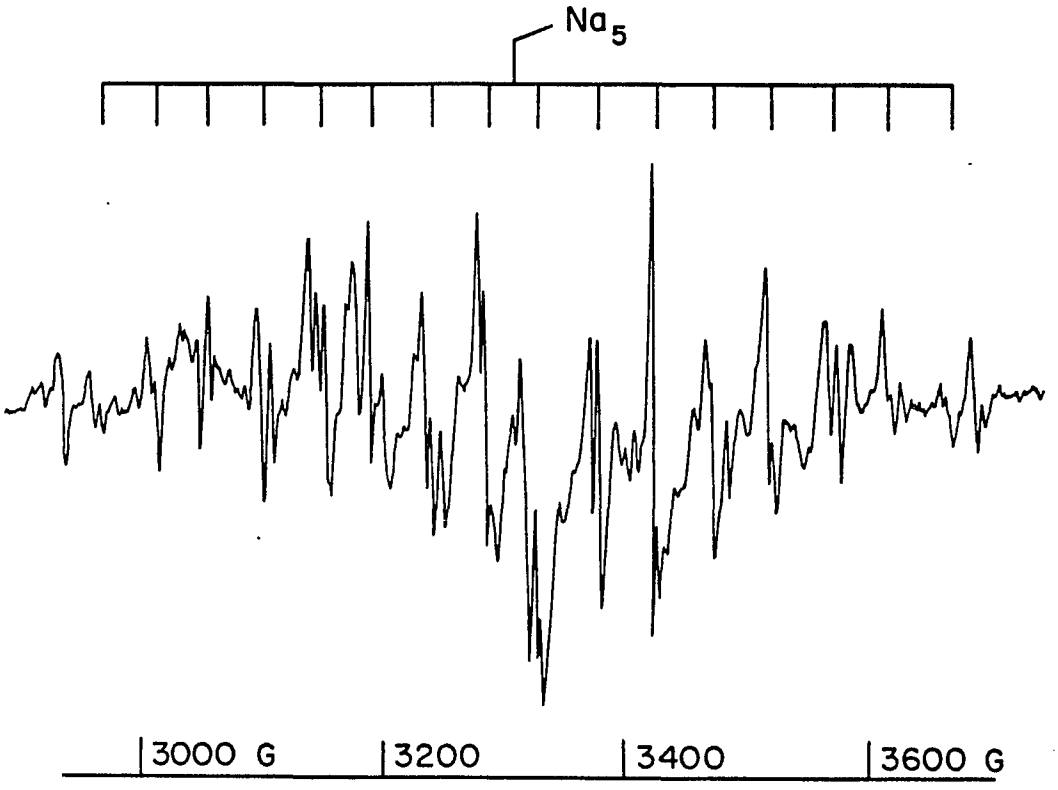

V. INTERPRETATION

V. 1. Introduction

Each spectrum in the previous section is characterized by a unique set of lines. The line positions are determined by the hyperfine constants and the g value. Each line is further characterized by its intensity and lineshape. The information can be used in conjunction with basic chemical and physical principles, such as simple molecular orbital theory and the Jahn-Teller effect to provide an overview of the ground state properties of metal clusters. When possible, conclusions are compared with the results of the most sophisticated calculations available. With the exception of Ag_3, all metal cluster spectra interpreted have isotropic character. The analysis of the anisotropic features of Ag_3 is in preparation.

The hyperfine values obtained from the spectra provide the relative distribution of the unpaired electron over the different nuclei in the molecule. The comparison of hyperfine values of different molecules is done by scaling the observed hyperfine value with that of the atomic gas phase value. The use of the atomic gas phase value to normalize the hyperfine splitting does introduce the potential for error. Orbital contraction, electron correlation and matrix effects all change when the molecule is formed from the precursor atoms. The assumption that these effects are similar for different molecules may not be strictly valid. The use of gas phase data as a scaling factor does provide a reasonably consistent method for comparing the properties of different clusters. Unless otherwise noted, all spin populations here are referenced to gas phase hyperfine splitting. Throughout this

chapter the notation used is that for ρ_1 refers to the spin population on two equivalent nuclei. ρ_2 refers to each of the remaining nuclei. $\bar{\rho}$ is the average spin population on each nuclei. This notation is slightly different from that used in references 41, 46, 47 and 48 (reprinted here as Appendices 1,2,4, and 5) where ρ_o and ρ_3 are used instead of ρ_1 and ρ_2.

The g-values of these molecules, with the exception of Ag_3 which shows significant anisotropies, are very close to the free electron value. These small negative g-shifts increase along the series Li, Na, K for both trimers and septamers and may be indicative of the increase in the spin-orbit coupling constant. Low lying excited states or matrix effects may also be responsible. Since matrix effects of this magnitude are routinely encountered, no attempt to interpet these shifts is made.

This section is arranged into two parts. 1) Metal trimers, 2) Na_7. The spectra of Na_5(?), Cu_3(?) and the Group IB atoms and adducts are not interpreted here.

V. 2. Trimers

Several metal cluster trimers have been observed and interpreted during the course of this project. Two isomers of K_3, s-K_3 and p-K_3 were observed. A previously unreported isomer of Na_3, p-Na_3 was studied. Ag_3 was observed and the major features have been interpreted. Although additional work remains to be done, the spectral parameters obtained are sufficient for determining the ground state.

Summarized in Table I are the isotropic spin populations for several metal trimers in different matrices. The molecules have been organized into three groups; those molecules well characterized by the single parameter, $\bar{\rho}$, molecules with $\rho_1 > \rho_2$, and silver, with $\rho_2 > \rho_1$.

Figure 1 shows the orbital correlation diagram for a triatomic composed of S orbitals. On the left side are the molecular orbitals for a linear or large angled geometry. As this angle is closed the energy of the two upper orbitals, $1a_1$ and $1b_2$ converges and the orbitals become degenerate for the case of an equilateral triangle. Further closure of the angle causes an inversion of the orbitals. Each molecular orbital predicts a unique ESR spectrum, providing a reliable means to determine the crude geometry of a trimer from the ESR spectra. The large angled case with a $^2B_2$ ground state has all of the spin on each of the two equivalent terminal nuclei. If the Jahn-Teller forbidden case were to exist, each nucleus would have the same unpaired spin population. For the small angled $^2A_1$ state 2/3 of the unpaired spin is on the central atom and 1/6 is on each of the remaining atoms.

A typical potential surface for a homonuclear triatomic is in Fig. 2. The Jahn-Teller forbidden D_{3h} structure corresponds to the energy maximum in the center of the surface. Encircling this energy maximum is a low energy pathway. The surface is bounded by an energy barrier corresponding to dissociation. These surfaces are frequently described by the degree of deviation from D_{3h} symmetry. This Jahn-Teller distortion parameter, ρ, gives the difference in energy between the D_{3h} maximum and the geometry of the molecule at the potential minimum. The radial behavior of the molecule on the potential energy surface is given by the pseudorotation parameter, θ. As a result of anharmonicity in the potential function the energy path encircling the conical intersection exhibits three potential minima separated by saddle points.

Fig. V.1 Molecular Orbitals from Three Equivalent Atomic S Orbitals

Molecular orbital scheme for homonuclear triatomics with only S atomic orbitals available.

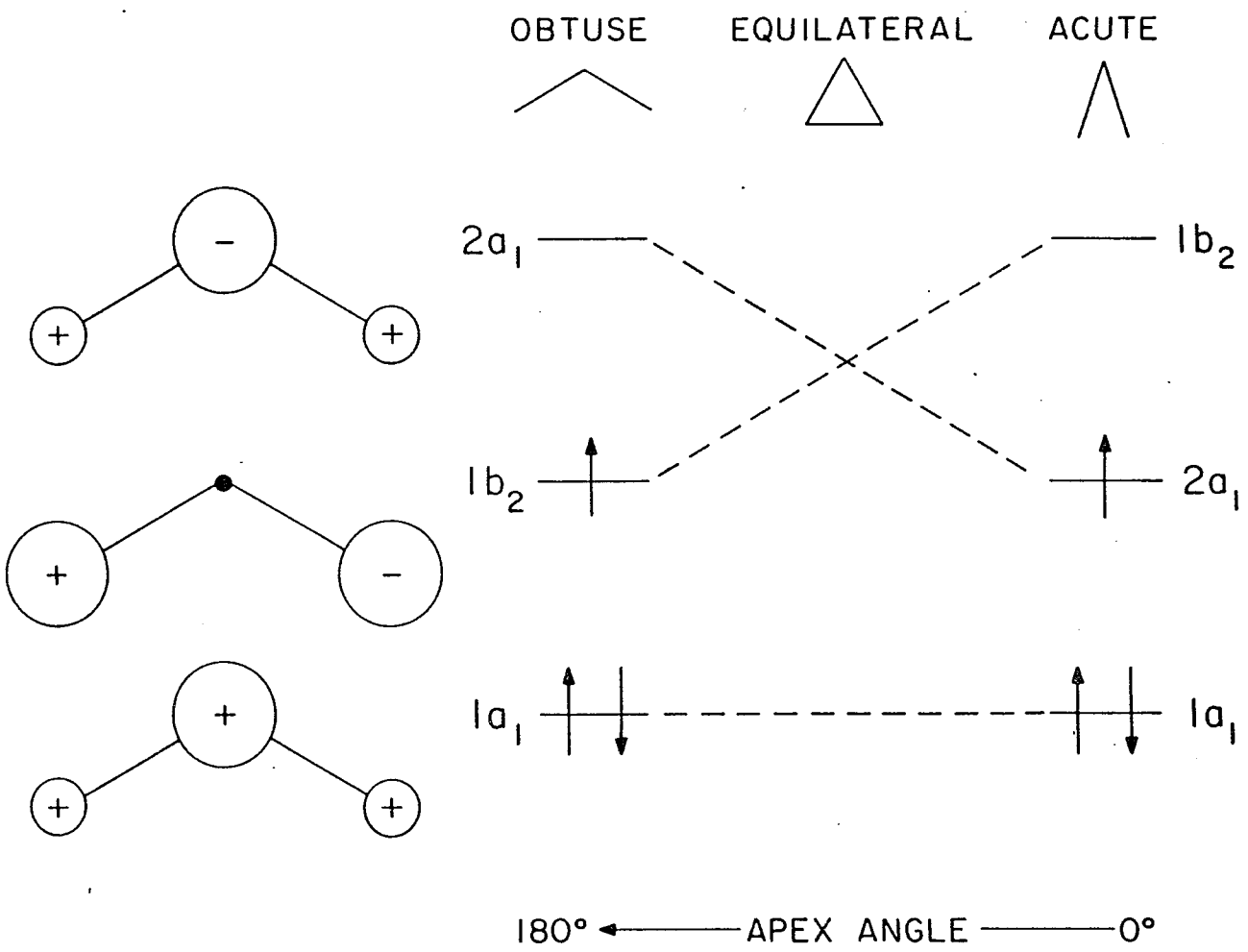

Fig. V.2 Potential Energy Surface for a Triatomic Metal Cluster

a) The top figure shows a "Mexican hat" type potential surface for a molecule subject to a Jahn-Tellr distortion. The peak represents the forbidden high symmetry state.

b) Potential surface for Li_3 calculated by Gerber and Schumacher.

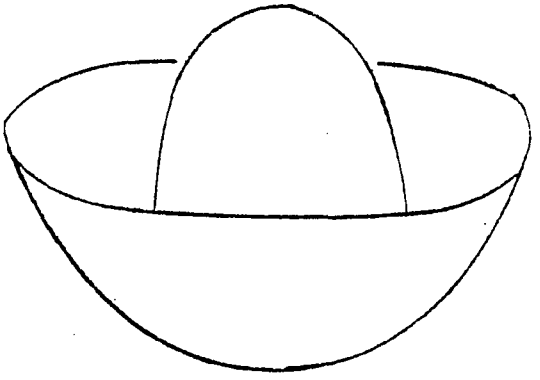

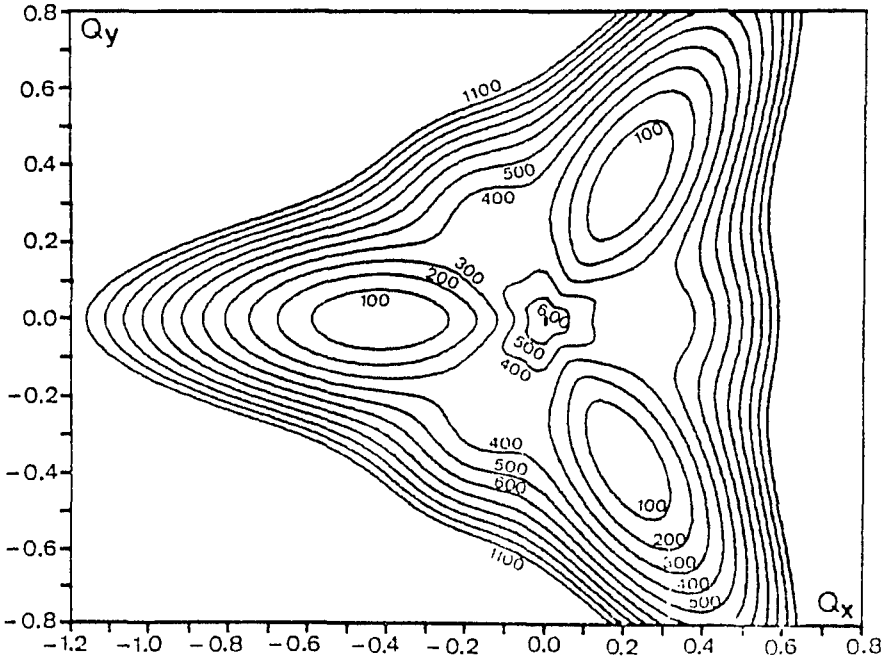

J Chem Phys., Vol 69 [illegible] 4 [illegible] August 1978

The details of these potential surfaces have been investigated for Li_3 and Na_3 by computational techniques. For Li_3 the potential surface was calculated in detail by Gerber and Schumacher (11) using a coupled electron pair approximation (CEPA). This calculation predicts Li_3 to be bound by $\sim$3000 cm^{-1} relative to the $Li_3 \rightarrow Li_2 + Li$ dissociation channel. The saddle points are calculated to be $\sim$250 cm^{-1} above the potential minima. The D_{3h} energy maximum is $\sim$350 cm^{-1} above the saddle points. A more detailed analysis by Gerber (52) indicates that these saddle points are absent. Both reports predict that Li_3 should be able to freely pseudorotate between the three equivalent potential wells. This would preclude isolation of distinct isotopic isomers such as ^6Li-^7Li-^6Li or ^7Li-^6Li-^6Li.

The potential surface of Na_3 was studied by an ab-initio configuration-interaction method with similar results (10). These two calculations are summarized graphically in Fig. 3. The properties of Ag_3 were calculated by Richtsmeier, Eades, Dixon and Gole using the diatomics in molecules technique (51). The Jahn-Teller distortion is predicted to result in a closing of the bond angle. This structure is calculated to be $\sim$200 cm^{-1} more stable than the optimum $^2B_2$ state.

This survey of the gross features of the potential surface for a Jahn-Teller active molecule suggests the possibility of four different ESR spectra. Two types of spectra correspond to a static Jahn-Teller distortion into either the $^2B_2$ or $^2A_1$ states. The dynamic Jahn-Teller effect provides the opportunity to observe spectra corresponding to D_{3h} symmetry. The transition between the static and dynamic case results in an alternating linewidth effect. Each of these cases and their spectra are discussed below.

Fig. V.3 Cross Section of a Potential Energy Surface

A cross sectional cut through a potential surface similar to the one in Fig. V.2. The numbers used are approximate values expected for metal clusters.

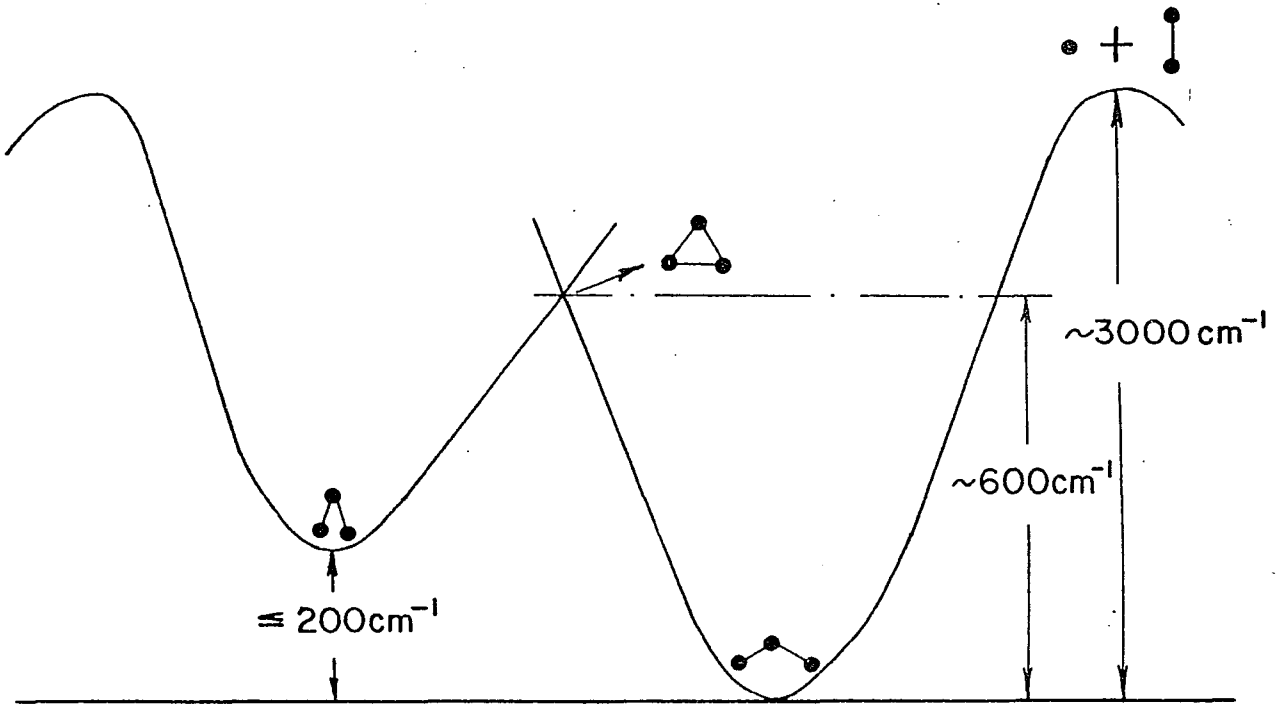

Case 1

If the $^2B_2$ state is more stable than the $^2A_1$ state the molecule is predicted to have all of the unpaired spin localized on two equivalent terminal nuclei. The nodal nucleus, while having zero spin density at the simple Huckel level of approximation, would be expected to have a small spin density induced by polarization effects. For a triatomic composed of spin 3/2 nuclei the spectrum is expected to be split into seven groups by a hyperfine interaction about 1/2 that of the free atom ($\rho_1 \tilde{-} 0.5$). Each group is expected to be further split into a quartet by a small hyperfine interaction. In addition to the results of simple molecular orbital theory there are available a few sophisticated computational results. The CEPA calculation of Li_3 predicts $\rho_1 = 0.48$ and $\rho_2 = 0.03$ after the author's normalization of the spin densities to unity. (While normalizing the total isotropic spin population to unity is incorrect, a correct treatment will not drastically change this value.) Martin and Davison's calculation on Na_3 predict $\rho_0 = 0.43$ and $\rho_3 = 0.047$. E. R. Dietz's $x\alpha$ scattered-wave study of the magnetic properties of the potassium trimer, while not able to predict reliably the optimum geometry, calculates ρ_1 and ρ_2 for a large number of assumed geometries (13). For bond angles from 75° to 180° $\rho_1 = 0.41$ to 0.36 and $\rho_2 = -0.10$ to -0.13.

Both qualitative bonding concepts and detailed calculations are in agreement with the major features of the spectrum of s-K_3 in Sec. IV. The earlier reported spectrum of s-Na_3 by Lindsay et al. is very similar. Garland has observed a transient ESR spectrum of s-$^7Li_3$ which may be similar in nature (51).

Case 2

If the $^2A_1$ state of the molecule is more stable the major hyperfine splitting is expected to be about 2/3 that of the free atom and centered on a single nucleus. Each of these groups will be further split by a smaller hyperfine of 1/6 that of the free atom centered on each of two equivalent nuclei. For a triatomic composed of nuclear spins with I = 3/2 this case predicts a quartet with a large hyperfine with each group showing a septet superhyperfine structure. No alkali cluster spectra have been observed with this pattern. For Ag, with I = 1/2 the $^2A_1$ state of the trimer should consist of a doublet split by a large hyperfine interaction. Each line should be further split into a triplet by a smaller hyperfine interaction. This is the dominate feature of the spectra assigned to Ag_3. The magnitude of the parameters obtained for Ag_3, $\rho_1 = 0.12$ and $\rho_2 = 0.53$ are in good agreement with those predicted by simple molecular orbital theory.

Case 3

Ab-initio calculations suggest that rapid interconversion between equivalent geometries ('pseudorotation') is predicted to be energetically feasible. This results in a dynamic Jahn-Teller effect where the distortion averages out to zero over the time scale of the experiment. Given the slow time scale of the ESR experiment ($\sim 1 \times 10^{-10}$ sec) relative to optical experiments (10^{-13} - 10^{-15}) the possibility of observing these effects must be considered. A spectrum of a molecule appearing to be in the $^2E_1$ state of a triatomic would consist of lines from three equivalent nuclei with each carrying the hyperfine interaction of 1/3 the free atom ($\rho_1 = \rho_2 = 1/3$). For nuclear spins of I = 3/2

this gives a ten line spectrum. At high temperatures (≳ 32 K) this is the spectra observed for p-K_3. Garland has observed similar spectra for both p-$^6Li_3$ and p$^7Li_3$ (53).

Case 4

Intermediate between Cases 1 or 2 and 3 is the possibility of pseudorotation at a rate comparable to the time scale of the experiment. While line positions are identical to Case 3, line broadening occurs for all states except those where $M_1 = M_2 = M_3$. These "alternating linewidth effects" are explained with the aid of Fig. 4, a partial correlation diagram showing the effect of pseudorotation on the nuclear spin configuration. Of the ten different nuclear spin states only four have a component which does not change during pseudorotation. All other states will undergo some broadening during the transition from Cases 1 or 2 to Case 3. The extent of the broadening can be predicted and has been shown to depend on $(a_1 - a_2)^2$ (41-45).

Another spectrum which exhibits an alternating linewidth effect is due to p-Na_3. Because of the large value of $(a_1 - a_2)^2$ all lines susceptible to broadening are broadened beyond recognition over the entire working temperature of the argon matrix (41).

In addition to providing interesting applications for linewidth theories, Case 3 molecules provide strong evidence the p-M_3 and s-M_3 are different isomers of the same molecule. The difference between a static and dynamic Jahn-Teller is often only one of experimental time scale and not a difference in molecular parameters. The parameters used to describe s-M_3, a_1 and a_2 can be related to those which describe p-M_3, as shown in equations 1 and 2 (41).

Fig. V.4 Partial Correlation Diagram of Nuclear Spin States for Three I = 3/2 Nuclei

Only those molecular states comprised of nuclei in identical spin states are unaffected by pseudorotation.

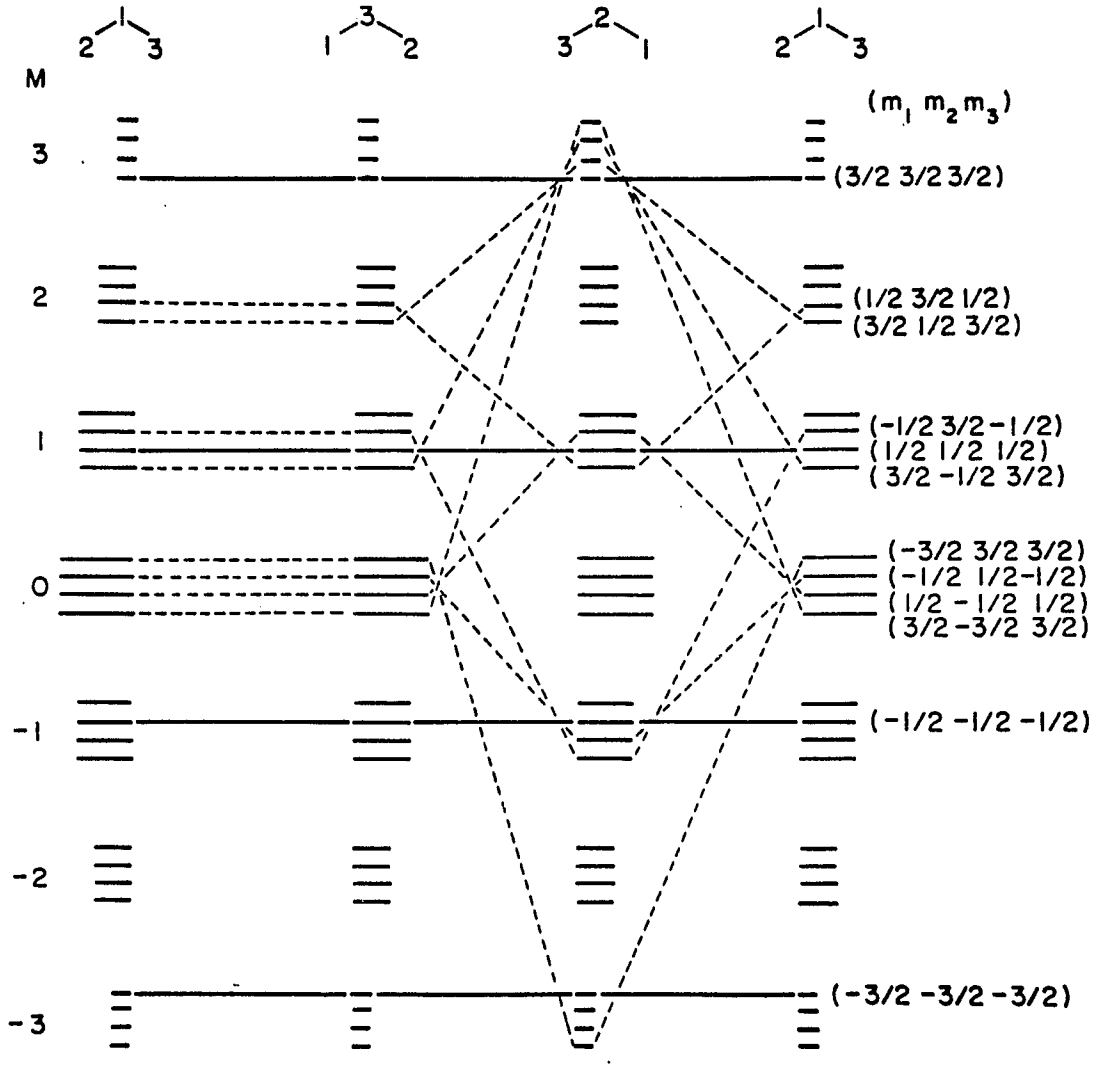

$$\bar{a} = 1/3(2a_1 + a_3) \quad (1)$$

$$\overline{a^2} = 1/3(2a_1^2 + a_3^2) \quad (2)$$

Table IV.2 lists the experimentally determined values of a_0, a_3, $\bar{a}$ and $(a^2)^{\frac{1}{2}}$ along with those calculated by Eqs. 1 and 2. Also listed are the g values of the molecules. The close correspondence between the parameters describing the different spectra strongly implies that the carriers of the different spectra are either the same molecules or closely related isomers.

V. 3. $\underline{Na_7}$

The spectra assigned to the sodium septamer provide information on the symmetry of the valence electron. As for the case of the alkali trimers, the total isotropic spin population is close to unity. The ~36% p character of the bonding does not appear to have a significant influence on the spectra. The spectra are interpreted with molecular orbital theory at the simple Huckel level of approximation. The simple Huckel method, while not very sophisticated, has the advantage of providing a practical method of performing a large number of calculations for clusters of different sizes and symmetry. Over 60 geometries were calculated for an assortment of clusters containing less than 20 atoms. Since a doublet ground state is indicated by the spectra, only odd-numbered clusters were investigated. The molecular orbital schemes generated by this method permit comparison with the experimentally determined unpaired spin distribution.

Given the radical assumptions made in deriving the simple Huckel method, no effort was made to parameterize the calculations to the energy levels of sodium. The utility of the calculations for predicting trends in energy was estimated by comparing the stability of several pentamer geometries with those calculated by Gole et al. using the diatomics in molecules method. The pentamers were chosen for comparison because these are the largest clusters for which a number of geometries have been investigated by the same computational technique. The comparison is given in Fig. 5. The stability of the trigonal bipyramid (D_{3h}), chain ($D_{\infty h}$), branched chain (C_{2v}) and tetrahedral geometries (T_D) are compared. The simple Huckel method does not distinguish between different bond angles or bond lengths, only the assumed bonding between nuclei. In spite of the inability to distinguish between $D_{\infty h}$ linear and "zig-zag" chains, or planar and puckered rings, the order of energies for the different geometries are exactly the same by both methods, $(D_{3h} \tilde{-} C_{4v}) < D_{5h} < (D_{\infty h} \tilde{-} C_{2v}) < T_D$.

Because of the uncertainty of the superhyperfine assignment, the larger clusters, Na_9, Na_{11} and Na_{13} were investigated. A few geometries of particular interest were calculated for Na_{15}, Na_{17} and Na_{19}. Some general properties of metal clusters, at the simple Huckel level of approximation are apparent. For the clusters considered, compact, three-dimensional geometries appear to be most likely responsible for the observed spectra. Most other geometries considered, including chains and rings, predict unpaired spin distributions in gross disagreement with the spectra. For Na_7, Na_9 and Na_{11} bipyramidal geometries have molecular orbitals consistent with the observed spectra. (This assumes

Fig. V.5 Comparison of Simple Huckel (SH) and Diatomics in Molecules (DIM) Methods

Relative stabilities predicted for Na_5 by the Simple Huckel Method and the Diatomics in Molecules method for several geometries. The vertical axis represents increasing stability in arbitrary units.

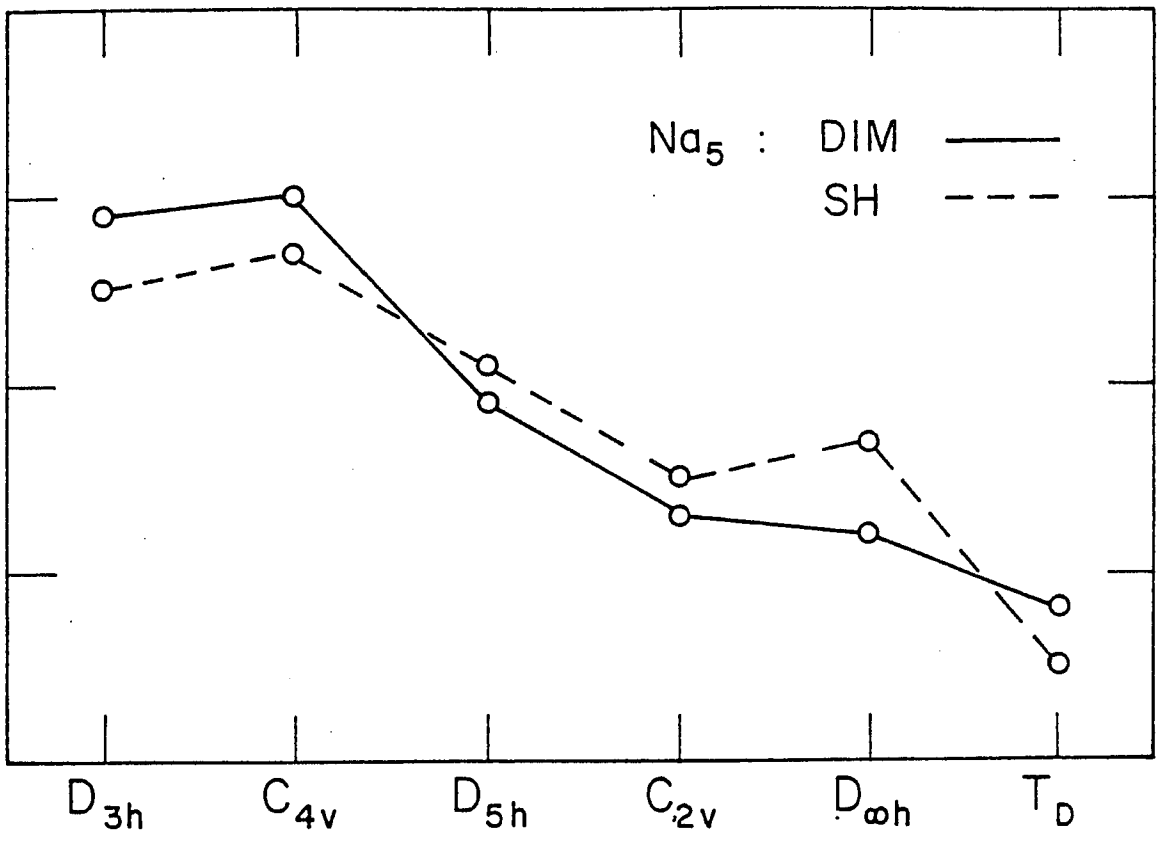

that polarization effects not considered at the Simple Huckel level are capable of inducing small spin densities at nuclei which otherwise have a zero unpaired spin population.) Figure 6 illustrates the molecular orbitals predicted by the simple Huckel method for a pentagonal bipyramid. The valence M.O., ψ_4, has a spin distribution consistent with the observed spectrum. In Fig. 7 the molecular orbitals of a square bipyramid shows the three-fold degeneracy of the valence state. When the degeneracy is lifted by a Jahn-Teller distortion, each of the resulting orbitals are consistent with the observed spectrum. Both of these geometries are predicted to be relatively stable for Na_7 by the simple Huckel calculations. Similar structures for Na_5 are predicted to be the most stable by both the simple Huckel method and the calculations of Gole et al.

A few other geometries found to have molecular orbitals consistent with the observed spectra are given in Fig. 8. The "T" shaped geometry has a valence M.O. consistent with the spectra to a first approximation. In a "real" molecule the five nodal atoms would not experience identical polarization effects. Such a geometry would most likely not have the five nodal atoms exactly equivalent. The ESR spectra are sensitive to these variations. At the simple Huckel level, and diatomic in molecule level, chain type structures are found to be significantly ($\sim$30%) less stable than the close-packed, three-dimensional arrangements. The trigonal arrangements (Fig. 8b) are also predicted to have M.O.'s consistent with the spectra. These are predicted to be slightly less stable than the most favored geometries. Figure 8c shows the valence M.O. for the only Na_9 geometry aside from

Fiv. V.6 Molecular Orbital Scheme for Bipyramidal Na_7

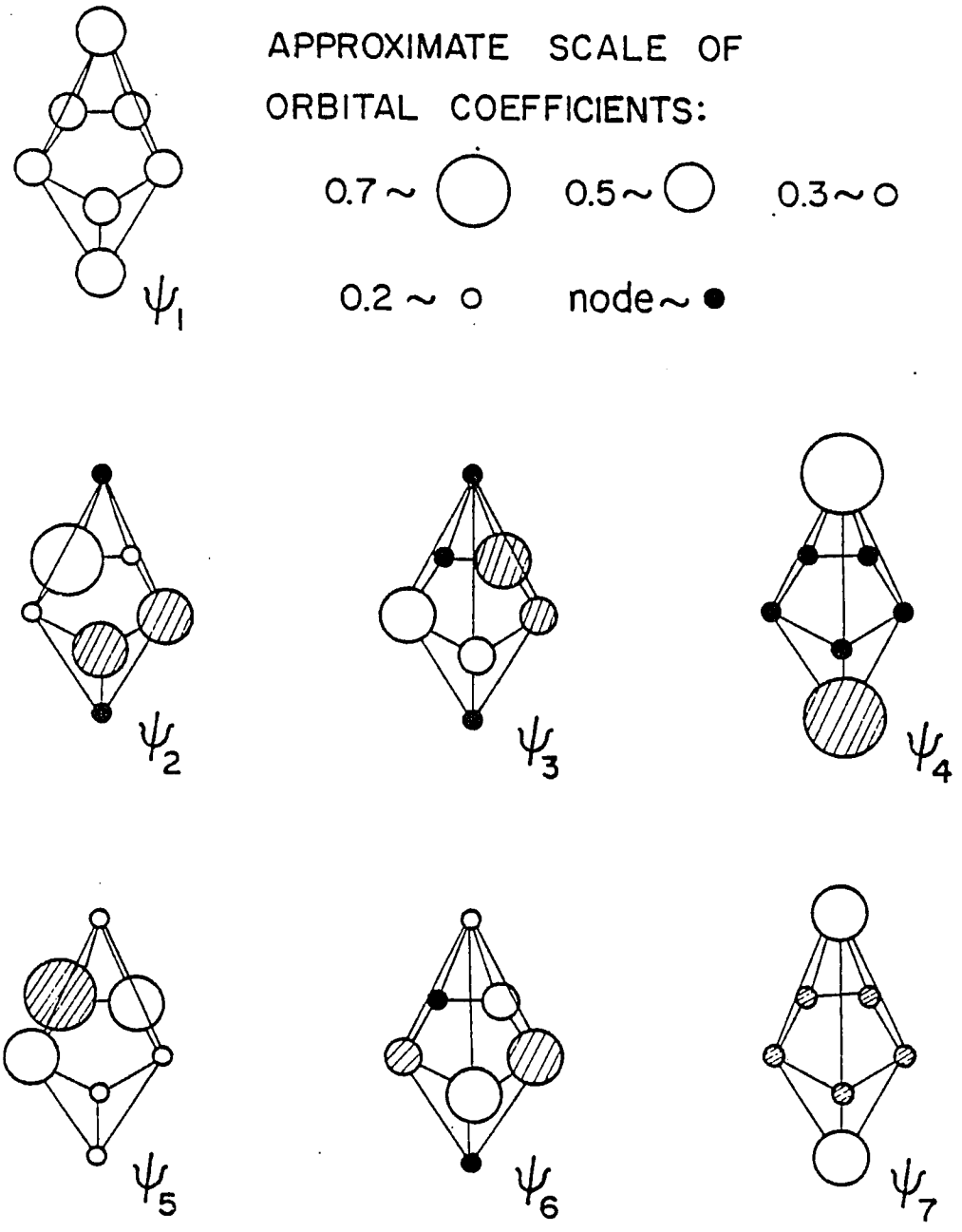

Fig. V.7 Molecular Orbital Scheme for a Square Bipyramidal Na_7

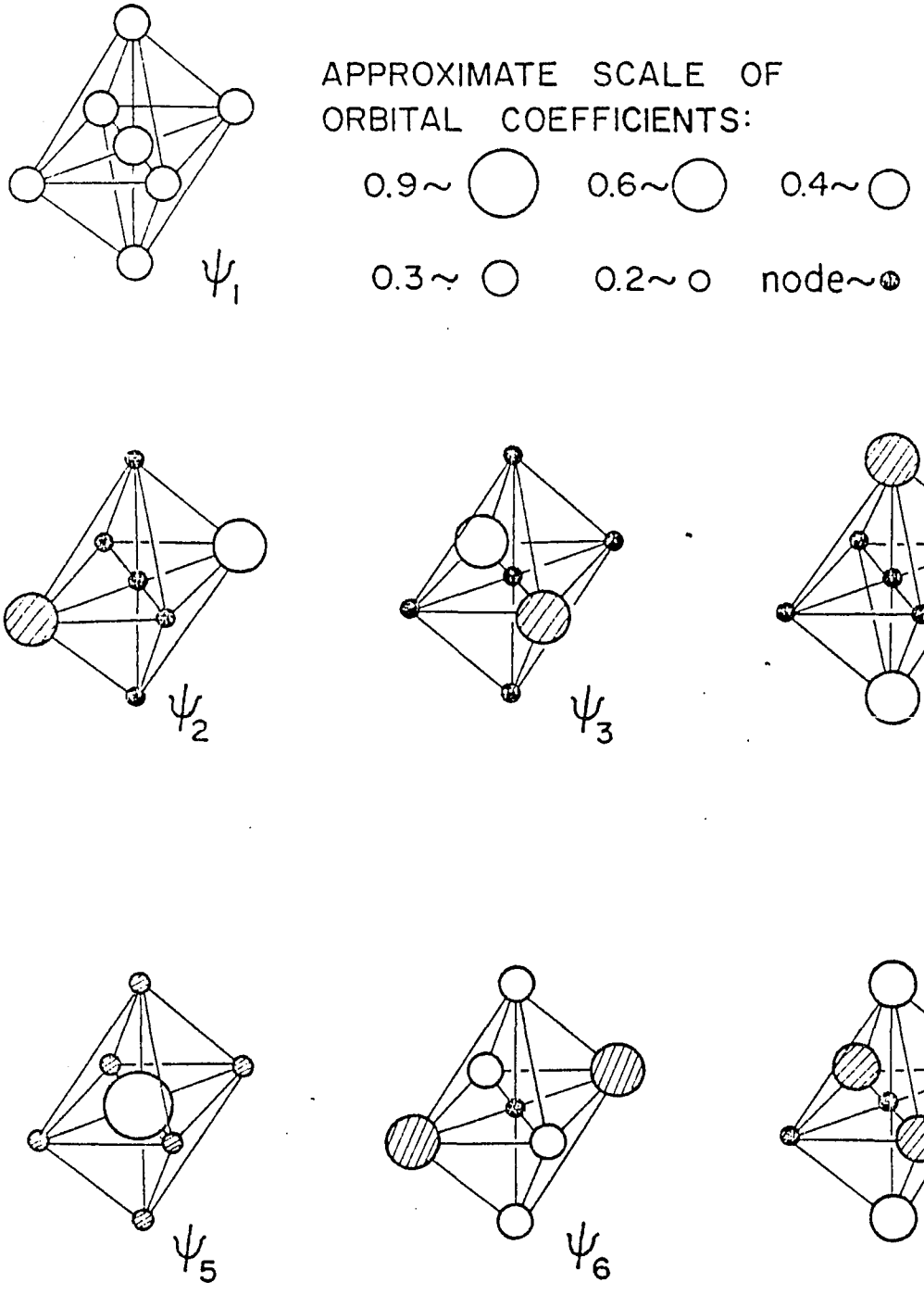

Fig. V.8 Valence Molecular Orbitals for Three Possible Na_7 Geometries

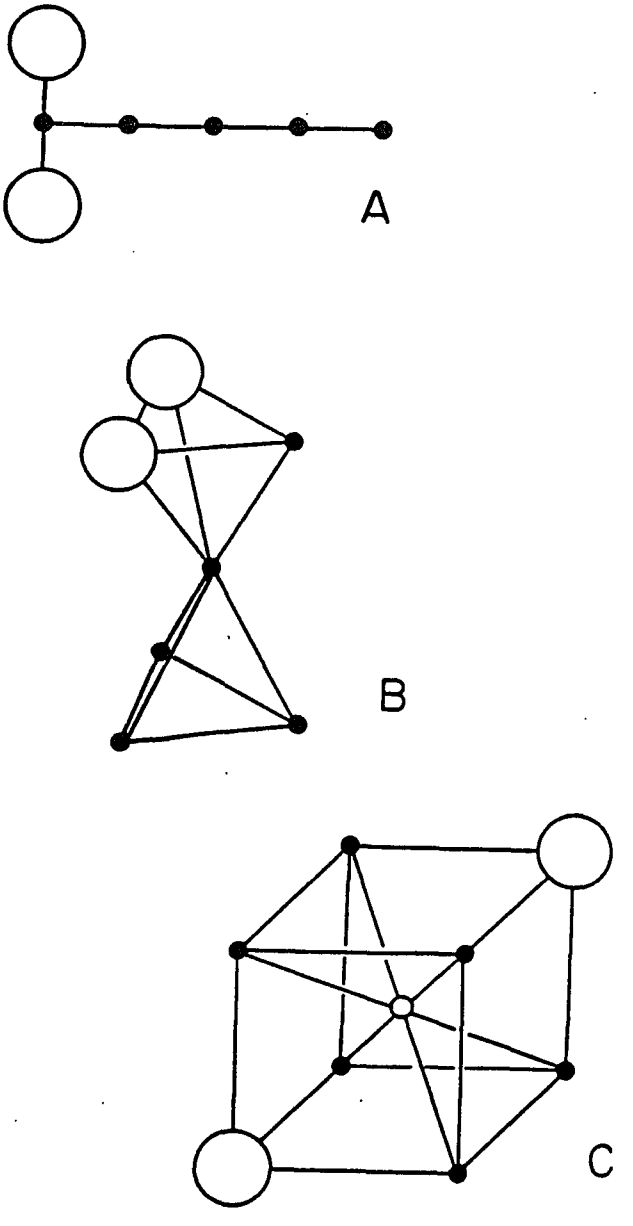

bipyramids which may be consistent with the spectra. The difference between the calculated spin populations is reasonably small. This geometry is intriguing because of the BCC structure of bulk sodium.

Appendix A.1

ESR spectra of matrix isolated potassium atom clusters

G. A. Thompson and D. M. Lindsay

Department of Chemistry, City University of New York, City College, New York, New York 10031
(Received 21 August 1980; accepted 1 October 1980)

ESR spectra assigned to the previously unobserved $^{39}K_3$ molecule have been obtained by co-depositing atomic potassium with argon under conditions favorable to cluster formation. The ESR spectra show that the trimer is chemically bound, with predominantly *s* rather than *p* character. Approximately 95% of the 4*s* spin population resides equally on two ^{39}K nuclei with less than 6% on the third atom. The trimer is assigned a symmetric linear or "obtuse angled" isosceles geometry with ground state symmetry $^2\Sigma_u^+$ or $^2B_2$. A second ESR spectrum, a pattern of 10 equally spaced hyperfine components centered close to the free electron *g* value, is indicative of a radical species containing three equivalent ^{39}K nuclei each having an isotropic spin population of slightly less than 1/3. Plausible candidates for the carrier of this spectrum are K_5 with a linear or "zig-zag" geometry, or a "pseudorotating" isomer of K_5. ESR intensities show a pronounced temperature dependence. K_3 spectra are significantly enhanced by warming to $T \sim 19$ K, but almost completely disappear at $T \sim 25$ K, where the 10 line spectrum is most intense.

I. INTRODUCTION

Small metal clusters represent a relatively new class of compounds whose properties have been receiving increasing attention.[1,2] Recent interest has largely been stimulated by the unifying role that metal clusters may play in a wide range of catalytic events.[3–7] Further areas of application include metal–metal bonding in polynuclear organometallic compounds,[8] nucleation phenomena,[9] atom–dimer reactions,[10] and the transition from the atomic and molecular regime to the solid state.[11] Despite a considerable theoretical and experimental effort, however, metal clusters remain an imperfectly understood area of research whose potential applications remain somewhat speculative at present. Historically, the first studies of note are the photoionization measurements of Foster, Leckenby, and Robbins[12] on alkali clusters containing up to eight atoms. More recently, Schumacher and co-workers have developed an elegant two-photon ionization method of observing discrete transitions from individual cluster species.[13] Other gas-phase techniques include laser fluorescence in supersonic nozzle expansions,[14] Stern–Gerlach deflection in molecular beams,[15] and mass spectrometric measurements of dissociation energies.[16,17] The majority of reported experiments have employed the matrix isolation technique, most commonly in conjunction with UV-visible absorption spectroscopy.[18] With several noticeable exceptions,[19] relatively little structural information has been deduced from this work. A growing number of molecular structure calculations have ranged from detailed *ab initio* studies on alkali trimers[20–22] to a much more ambitious modelling of large clusters containing transition metal elements.[23] While potentially of great practical importance, the properties of this latter extremum remain uncertain in the absence of confirming experimental evidence.

This paper reports the first spectroscopic analysis of potassium trimer molecules. Atomic potassium and diluent argon were codeposited on a sapphire surface loosely coupled to a liquid helium reservoir. The sapphire surface was warmed during deposition in order to promote aggregation before the free atoms are frozen into the argon matrix. Electron spin resonance (ESR) spectra show that three species, atomic potassium in several matrix sites, K_3 and a polymer designated K_n, are formed during deposition, with relative intensities ($T = 4$ K), $K < K_3 > K_n$. Matrices containing potassium clusters show a pronounced, and to some extent reversible, temperature dependence. K_3 spectra are significantly enhanced by warming to $T \sim 19$ K, but almost completely disappear at $T \sim 25$ K, where K_n spectra are most intense.

The ESR spectra show K_3 molecules to be chemically bound with a distribution of unpaired spin distinctly different from precursor atom and dimer moieties. The magnetic parameters for K_3, markedly similar to those of the isovalent sodium trimer,[24,25] suggest a symmetric linear or "obtuse angled" geometry with ground state $^2\Sigma_u^+$ or $^2B_2$, respectively. As a first approximation, the simple Huckel picture provides a good description of the bonding in K_3, which is of predominantly *s*- rather than *p*- character. The unpaired electron resides in a nonbonding orbital having equal spin density on two ^{39}K nuclei and a node at the third atom. Polarization effects induce a small, approximately 6% spin density at the central or apical position.

The second radical species, designated K_n, has an ESR spectrum distinctly different in character from that of the trimer. This spectrum, a pattern of ten equally spaced hyperfine components centered near the free electron *g* value, suggests a polymer containing three magnetically equivalent ^{39}K nuclei, each having an isotropic spin population of slightly less than one third. Plausible carriers of the ten line spectrum are the next highest paramagnetic polymer K_5, or an isomeric form of the trimer. The simple Huckel method was used to predict spin density distributions for a large range of possible pentamer geometries. Only for a linear ($^2\Sigma_g^+$) or "zigzag" ($^2A_1$) structure was approximate agreement between theory and experiment obtained. Recent *ab initio* calculations on Li_5[21] and Na_5[22] suggest an alternative assignment for the ten line spectrum. The trimer is treated as a dynamic Jahn–Teller molecule whose potential surface, resembling a "mexican hat," has a central peak surrounded by a trough

 0021-9606/81/020959-10$01.00

containing three potential wells each corresponding to an obtuse angled geometry. A relatively low barrier to "pseudorotation" about the central peak is calculated. Thus, if pseudorotation is fast compared to the ESR time scale, an averaged trimer spectrum is expected. The predicted result is shown to be in excellent qualitative and quantitative agreement with the measured spectral data for K_n. Possible mechanisms for the temperature dependent intensities are outlined and future experimental studies are suggested.

II. EXPERIMENTAL

The matrix isolation apparatus is similar in design to that described previously.[24] Cluster species were formed by codeposition of atomic potassium (Gallery, 99.95%) and argon (Airco, 99.9998%) on a sapphire surface mounted inside a TE_{102} X-band ESR cavity. The ratio of argon to potassium was approximately 100:1 for the spectra presented here. The cavity was attached to the lower reservoir of a double chamber, variable temperature liquid helium cryostat. All spectra were recorded on a Japanese Electron Optics Laboratory, ME-3X ESR spectrometer using 100 kHz magnetic field modulation and phase sensitive detection. The resonant frequency of the cavity plus sapphire plate and argon matrix was 9.2824(2) GHz over the temperature range 4–25 K. Individual spectra were calibrated with a proton magnetometer (Micronow, Model 515). The accuracy of this method was checked by comparing measured and known transitions from atomic potassium[26–28] and KO_2.[26,29] Relative and absolute magnetic field positions are judged accurate to ±0.2 and ±1 G, respectively.

As in the analogous sodium experiments,[24] clustering took place *during* deposition and not by subsequent warming of the matrix. Cluster formation is, presumably, a surface diffusion phenomenon which occurs at the quasiliquid interface characteristic of a matrix surface during deposition.[18,24] Clustering may be partially controlled by warming the sapphire substrate above the nominal deposition temperature of 4 K. Because of a substantial thermal resistance between the sapphire surface and the liquid helium reservoir, Joule heating by the 100 kHz eddy currents circulating in the cavity walls[24] conveniently provided an appropriate temperature gradient for cluster formation. For the experiments reported here, clusters were formed with little or no magnetic field modulation, indicating a thermal gradient of unknown origin. This is in contrast to earlier experiments[24] utilizing sodium and potassium in argon matrices and presumably relates to subtle differences in the two experimental stations. Preliminary results for cluster formation in krypton matrices show only atomic potassium transitions with no modulation during deposition, but some features attributable to K_3 in matrices formed with large magnetic field modulation. As temperatures were measured close to the liquid helium reservoir and not at the matrix itself, exact deposition conditions were not determined. In experiments where local heating was clearly absent, only the known[26–28] spectrum of atomic potassium was observed. All temperature measurements were made with a carbon resistor calibrated at three fixed points, 4.2 K, 77 K, and room temperature.[24,26] The accuracy of this calibration is approximately 5% between 4.2 and 77 K. Except during deposition, measured temperatures are estimated to be quite close to those of the matrix sample itself.

III. SPECTRA AND ANALYSIS

Three distinct paramagnetic species are evident in the ESR spectrum of matrices formed by codeposition of potassium atoms with argon under conditions favorable to cluster formation. The absence of features corresponding to a zero-field splitting or to changes of greater than unity in the electron spin projection ($\Delta M_s > \pm 1$) implies that all spectra arise from species having doublet ground states. The spectrum of atomic potassium in several distinct matrix sites is readily identified by its sharp features and known spectral parameters.[26–28] A second spectrum is assigned to a bent ($^2B_2$) or linear ($^2\Sigma_u^+$) potassium trimer, $^{39}K_3$. A third, distinctly different, spectrum is most apparent at elevated temperatures. While the identity of the carrier, designated $^{39}K_n$, has not been uniquely determined, plausible candidates are the potassium pentamer with a chain ($^2A_1$ or $^2\Sigma_t^+$) geometry, or a pseudorotating isomer of K_3.

At 4 K in freshly deposited matrices, all three species are observed with relative spectral intensities $K < K_3 > K_n$. However the spectra of K_3 and K_n show a pronounced temperature dependence. Experiments now in progress show that, after an initial annealing, spectral intensities are reproducible, reversible, and dependent only upon the matrix temperature. K_3 spectra are most intense in the temperature range $T \sim 13$–19 K, relatively weak at low temperatures and absent above $T \sim 24$ K. K_n spectra decrease monotonically in intensity as $T \to 4.2$ K, where some component transitions become noticeably broadened. Transitions from atomic potassium show little intensity change with temperature. A more detailed discussion of these effects will be reported elsewhere.[30] Similar, but as yet less well studied, phenomena have been observed in matrices containing sodium polymers.[24] Measured transition fields for K, K_3, and K_n correspond to temperatures 4, 19, and 25 K, respectively. In the several instances where a comparison was possible, spectral parameters measured at one temperature were, within experimental error, identical to those at any other temperature.

A. K_3 spectra

Figure 1 shows the ESR spectrum observed when previously deposited matrices were warmed to 19 K. The spectrum attributed to K_3 consists of seven equally spaced quartets of first derivative transitions whose center falls close to the resonance field $H_e = 3312.2$ G, of the free electron. The separation between adjacent quartets is approximately half that of the atomic hyperfine splitting (hfs) constant, $a(^{39}K) = 82.4$ G.[1] The (substantially smaller) quartet splitting is, within experimental error, constant over the entire spectral region.

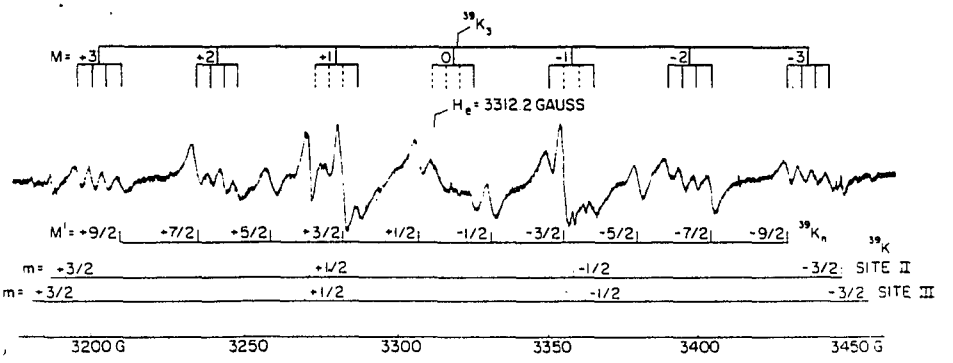

FIG. 1. ESR spectrum of potassium trimers $^{39}K_3$ in an argon matrix at 19 K. $H_e = 3312.2$ G is the resonance field of a free electron for a cavity frequency of 9.2824 GHz. Transitions from atomic potassium in two matrix sites and a species labeled $^{39}K_n$ (see Fig. 2) are also indicated. For the trimer spectrum, M designates the z component of the total nuclear spin angular momentum of two magnetically equivalent ^{39}K nuclei.

The spectral assignment of K_3 closely follows that of the isovalent sodium trimer.[24] The septet pattern in Fig. 1 may be attributed to spin density on two magnetically equivalent potassium nuclei, the quartet structure arising from a third, nonequivalent, nucleus. To a good approximation the magnetic field positions of the trimer spectrum are described by

$$H_1(M, m_3) = (g_e/g_0)\left[H_e - \sum_{i=1}^{3} a_i m_i\right]$$
$$= (g_e/g_0)[H_e - a_0 M - a_3 m_3]. \quad (1)$$

This expression[32,33] pertains to the powder spectrum for the case of an isotropic g tensor ($\mathbf{g} = g_0 \mathbf{1}$) and an isotropic hyperfine interaction ($\mathbf{A} = a\mathbf{1}$). Here m_1 and m_2 are magnetic quantum numbers for two identical ^{39}K nuclei ($a_1 = a_2 = a_0$). The corresponding parameters for the third nucleus are designated m_3 and a_3. The hyperfine pattern depends on m_1 and m_2 only through their sum, $m_1 + m_2 = M$. For $I_1 = I_2 = I_3 = 3/2$, a total of seven equally spaced quartets is expected, corresponding to $M = +3, +2, +1, 0, -1, -2, -3$ and $m_3 = +3/2, +1/2, -1/2, -3/2$. In fast scans recorded at 4.2 K, relative intensities for the unresolved septet features correspond approximately to the expected distribution, 1:2:3:4:3:2:1.

The second-order hyperfine interaction for two magnetically equivalent ^{39}K nuclei adds to Eq. (1) a term given by[34-37]

$$H_2(J, M) = -\tfrac{1}{2}(g_e/g_0)^2 [J(J+1) - M^2]/H(J, M). \quad (2)$$

Here J denotes the total nuclear spin angular momentum of the two equivalent ^{39}K nuclei and $M = m_1 + m_2$ is the total z component. $H(J, M)$ is the magnetic field at the particular line. Since $J \geq |M|$ and the "triangle condition" requires $I_1 + I_2 \geq J \geq |I_1 - I_2|$, each transition with a given M is split into components with J ranging from $|M|$ to $I_1 + I_2 = 3$ in integer steps. The second-order interaction both removes the M degeneracy associated with the first-order results and shifts all lines to lower magnetic field. In contrast to the situation observed for Na_3,[24] Eq. (2) has only a minor influence on the potassium trimer spectrum. The lifting of the M degeneracy is not resolved and line shifts amount to ~1 G.

Superimposed on the trimer spectrum, Fig. 1, are transitions arising from atomic potassium in several matrix sites[26-28] and a ten line spectrum labelled $^{39}K_n$. Although the quartet splitting of the $M = \pm 3$ and ± 2 components is well resolved, spectral overlap noticeably obscures the $M = \pm 1$ transitions. Poor resolution in the $M = 0$ region, expected to be relatively unaffected by either ^{39}K or $^{39}K_n$, may arise from the presence of much larger potassium clusters. ESR spectra of increasingly larger clusters should approach those reported for colloidal potassium,[38] an approximately 30 G wide resonance centered near $H = 3320$ G. For the trimer spectrum of Fig. 1, full lines represent measured field positions whereas broken lines pertain to those calculated as described below.

Table I compares the observed line positions for $^{39}K_3$ (full lines, Fig. 1) with those calculated using Eqs. (1) and (2) and the best fit parameters g_0, a_0, and a_3 given in Table II. Estimated uncertainties in measured parameters are given in parentheses. Also shown in Table I are average quartet splittings, $\langle a_3 \rangle$, for individual M components. The a_3 constant reported in Table II is the mean of the $\langle a_3 \rangle$ values, with an uncertainty of one standard deviation in this average. The error in a_0 arises from a similar analysis, but that in g_0 is largely dependent upon uncertainties in the absolute field calibration. A small correction to g_e is not included in Table I. Since individual (J, M) components are not resolved, second-order contributions to the hyperfine interaction were estimated using a weighted average for each M value. This correction reduced g_0 by approximately 6×10^{-4} but, within experimental uncertainty, had no effect on the hfs constant a_0. For comparison, Table II also contains measured parameters for atomic potassium in several matrix sites.[39]

TABLE I. Comparison between experimental and calculated line positions for $^{39}K_3$. Transition fields H_1 and H_2 are defined in Eqs. (1) and (2). The experimental $\langle a_3 \rangle$ represents the average spacing of the quartets shown in Fig. 1. Experimental uncertainties (see text) are given in parentheses. All units are gauss.

M	m_3	Experimental $H(M,m_3)$	Calculated H_1+H_2	Differences	Experimental $\langle a_3 \rangle$
+3	+3/2	3194.9	3195.0	−0.1	4.7(4)
	+1/2	3199.6	3199.7	−0.1	
	−1/2	3203.9	3204.4	−0.5	
	−3/2	3209.0	3209.1	−0.1	
+2	+3/2	3233.8	3233.9	−0.1	4.6(2)
	+1/2	3238.4	3238.2	+0.2	
	−1/2	3242.9	3242.9	0.0	
	−3/2	3247.3	3247.6	−0.3	
+1	+3/2		3272.4		
	+1/2		3277.1		
	−1/2		3281.8		
	−3/2	3286.7	3286.5	+0.2	
0	+3/2		3311.8		
	+1/2		3316.5		
	−1/2		3321.2		
	−3/2	3325.2	3325.9	−0.7	
−1	+3/2	3350.0	3350.4	−0.4	4.9
	+1/2		3355.1		
	−1/2		3359.8		
	−3/2	3364.9	3364.5	+0.4	
−2	+3/2	3389.7	3389.6	+0.1	4.5(8)
	+1/2	3394.5	3394.3	+0.2	
	−1/2	3398.9	3399.0	−0.1	
	−3/2	3404.2	3403.7	+0.5	
−3	+3/2	3429.0	3429.0	0.0	4.6(2)
	+1/2	3434.0	3433.7	+0.3	
	−1/2	3438.3	3438.4	−0.1	
	−3/2	3443.0	3443.1	−0.1	

The discrepancies between the observed and calculated line position, column 5 of Table I, are mostly within ±0.3 G. This is considered satisfactory in view of the overlapping noted above and the rather large widths, $\Delta H \sim 2\frac{1}{2}$ G, of individual transitions. Trimer (and $^{39}K_n$) linewidths are not instrumentally limited in the spectra presented here (those of atomic potassium are). Possible sources of line broadening in the trimer spectrum include unresolved matrix, second-order and anisotropic effects. For $^{23}Na_3$ in argon at least two distinct trapping sites are observed with magnetic parameter a_0 and a_3 differing by approximately 2% and 10% respectively.[24] Assuming an analogous situation for the potassium trimer, transitions arising from individual matrix sites would differ by at most 3–4 G. This effect should be most apparent in the $M=\pm3$ regions. As noted earlier, individual (J, M) components are not resolved for $^{39}K_3$. Second-order effects are largest in the $M=\pm1$ and 0 transitions, where $H_2(J, M)$ is approximately 2–3 G. Consistent with the first derivative appearance of the line shape, the analysis of the trimer ESR spectrum assumes a powder spectrum with substantially isotropic g and A tensors. Arising almost exclusively from p character in the wave function of the unpaired electron, small anisotropic contributions are expected, however.[40] The s–p hybridization in the neutral dimer K_2 amounts to about 5%–10%.[41] For the $4p$ valence orbital of potassium, the mean inverse cube radius, $\langle r^{-3} \rangle \sim 3$ Å^{-3}.[42] Thus an approximately 10% admixture of $4p$ character will contribute a hyperfine anisotropy of the order of 1 G. Dependent in part upon the trimer excited states, expected anisotropies in the g tensor are more difficult to predict. The measured g shift, $\Delta g_0 = -0.0038$, is consistent with a small hybridization in the ground state and spin–orbit coupling to empty orbitals of predominantly p rather than s character. The absence of transitions having an absorptionlike profile may not imply a near coincidence of the three principal g tensor elements. Rather, these generally weaker features[32,33] may be present but with insufficient intensity to be observed. However Δg for the trimer is also similar in

TABLE II. Magnetic parameters for ESR spectra of potassium species in argon matrices. Experimental uncertainties (see text) are given in parentheses.

	g_0	a_0 (G)	a_3	ρ_0^2
$^{39}K_3$	1.9985(5)	39.0(3)	±4.7(2)	0.474(3)
$^{39}K_n$	1.9990(5)	24.5(7)		0.298(8)
$^{39}K(I)^a$	2.0009(5)	81.7(2)		0.992(2)
$^{39}K(II)^a$	1.9993(5)	86.8(2)		1.054(2)
$^{39}K(III)^a$	1.9984(5)	91.6(3)		1.112(3)
$^{39}K(GP)^a$	2.00231	82.35		

[a] Roman numerals in parentheses denote different matrix sites; GP pertains to gas phase data from Ref. 31.

[b] Unpaired spin populations ρ_0 and ρ_3 are ratios of a_0 and a_3 to the atomic isotropic hfs constant $a(^{39}K) = 82.4$ G, from Ref. 31.

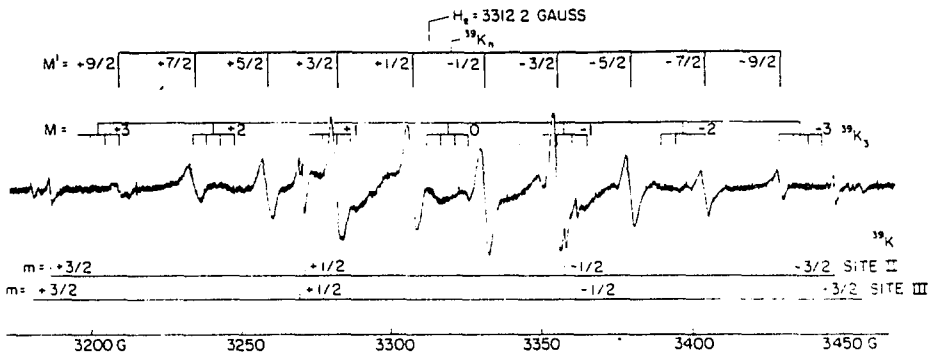

FIG. 2. Ten line ESR spectrum of a radical $^{39}K_n$ in an argon matrix at 25 K. M' denotes the nuclear spin quantum number for three magnetically equivalent ^{39}K nuclei. The "stick spectrum" labelled $^{39}K_3$ pertains to trimer transitions assigned in Fig. 1. Also indicated are potassium atom resonances for two matrix sites. $H_e = 3312.2$ G is the resonance field of a free electron for a cavity frequency of 9.2824 GHz.

sign and magnitude to that for atomic potassium in argon, Table II and Refs. 27 and 28. Consequently, anisotropies in the g tensor, not related to matrix effects, may be small, again contributing only to the trimer linewidth.

Table II also includes spin populations ρ_0 and ρ_3 derived by comparing the values of a_0 and a_3 with the isotropic hfs constant for atomic potassium, $a(^{39}K) = 82.4$ G.[31] Since the ESR spectrum gives only the absolute magnitude of the hyperfine parameters, the signs of the spin densities are not determined. Because of its large magnitude, ρ_0 may reasonably be assumed to be positive. However ρ_3 is small and may be either positive or negative.

B. K_n spectra

Figure 2 shows the result of raising the matrix temperature from 19 to 25 K. Figures 1 and 2 pertain to the same matrix sample with ESR spectra recorded under identical instrumental conditions. At $T \sim 25$ K, the trimer spectrum is almost unrecognizable, a "stick spectrum" having been assigned by reference to Fig. 1 and Table I. Clearly evident in Fig. 2 is a pattern of 10 equally spaced first derivative transitions whose component intensities increase from the wings toward the center. The same spectrum is also evident in Fig. 1 but is overlapped in several regions by features attributed to K_3. The carrier of the 10-line spectrum, labelled K_n, has not been uniquely identified. As discussed in the following section, plausible candidates are K_5 or an isomer of K_3. As in the trimer case, K_n spectral intensities show a pronounced temperature dependence between 19 and 25 K. On average, intensities in Fig. 2 are approximately double those in Fig. 1. However, individual components increase by differing amounts. Transitions arising from atomic potassium change little if any between 19 and 25 K. These observations are reminiscent of the ESR behavior of organic radicals undergoing exchange and similar effects in solution.[32,33,43–45]

Component transition fields for the ten line spectrum of Fig. 2 are well described by the first-order expression,

$$H(M') = (g_e/g_0)[H_e - a_0 M']. \tag{3}$$

The previously defined constants g_e and H_e pertain to the free electron; g_0 and a_0 parametrize the powder spectrum for a species having an isotropic g tensor and hyperfine interaction. Here, however, $M' = m_1 + m_2 + m_3$ denotes the spin projection quantum number for *three* magnetically equivalent ^{39}K nuclei ($a_1 = a_2 = a_3 = a_0$). For $I = 3/2$, Eq. (3) predicts 10 equally spaced components with M' ranging from $+9/2$ to $-9/2$ in integral steps. Relative intensities in Fig. 2 correspond in part to the predicted[37] distribution, 1 : 3 : 6 : 10 : 12 : 12 : 10 : 6 : 3 : 1, for three equivalent ^{39}K nuclei. Significant exceptions most likely arise from dynamic effects which, as noted earlier, appear to be important in these matrix samples. Table II gives the best fit parameters g_0 and a_0 obtained from Eq. (3) using measured transition fields from Fig. 1. The average discrepancy between observed and calculated line positions is ± 0.4 G. The spectral fit was not noticeably improved by inclusion of an estimated second-order hyperfine correction. Unresolved matrix site, second-order hyperfine and anisotropic effects probably contribute to a degree comparable to that discussed above for K_3. The experimental uncertainty in a_0 represents one standard deviation in the average separation of adjacent M' components. As in the trimer measurements, calibration errors contribute the major uncertainty in g_0. Table II also gives the spin population ρ_0 representing the isotropic spin density on each of the three magnetically equivalent ^{39}K nuclei.

IV. DISCUSSION

The measured spin populations in K_3, $\rho_0 = 0.47$ and $\rho_3 = \pm 0.06$, are distinctly different from the corresponding parameters for possible parent species: three non interacting atoms, each with unit spin population.

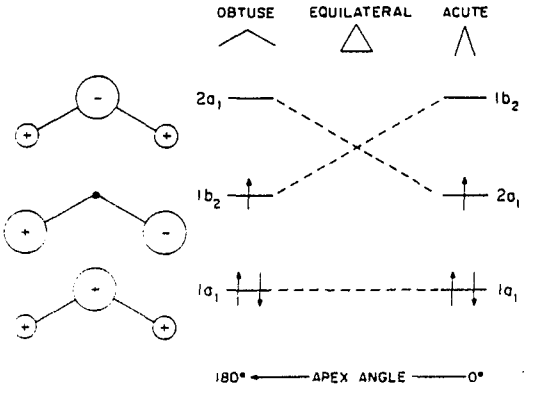

FIG. 3. Molecular orbital scheme for alkali trimer molecules.

or a single atom plus diamagnetic dimer having $\rho_0 = 0$ and $\rho_3 = 1$. The presence of two magnetically equivalent ^{39}K nuclei indicates that the trimer has a symmetric linear ($D_{\infty h}$) or bent isosceles (C_{2v}) geometry. The spin populations for K_3 are remarkably similar to those measured for the isovalent Na_3 complex, $\rho_0 = 0.47$ and $\rho_3 = \pm 0.07$.[24] Thus the ESR results show that alkali trimers in their ground states are chemically bound molecules. This situation may be contrasted with that found for H_3, which is unstable towards dissociation in its ground state.[46,47]

Figure 3 shows a molecular orbital (MO) scheme for the potassium trimer at the simple Huckel level. The figure is analogous to the bonding scheme in the well-known allyl radical,[32,48] with carbon $2p$ basis functions replaced by valence $4s$-orbitals of atomic potassium. For an "obtuse angled" isosceles geometry (apical angle $> 60°$[49]), the expected orbital configuration for the trimer is $\cdots 1a_1^2 1b_2$, giving a ground state symmetry $^2B_2$. For a symmetric, linear trimer of $D_{\infty h}$ symmetry, the relative order of the MO's should remain the same giving a $\cdots \sigma_g^2 \sigma_u$ configuration of symmetry $^2\Sigma_u^+$. Thus, the predicted spin populations for either $^2B_2$ or $^2\Sigma_u^+$ symmetry, $\rho_0 = 0.50$ and $\rho_3 = 0$, are very similar to the values measured for K_3, $\rho_0 = 0.47$ with $\rho_3 = \pm 0.06$. As in the allyl example,[32,48] spin polarization effects, not included in the simple Huckel model, would be expected to induce a small (usually negative) spin density at the central ^{39}K nucleus. Figure 3 also includes a Walsh-type correlation diagram[50] for the bending coordinate in K_3. As the apical angle is decreased from 180°, the $1b_2$ orbital is destabilized by an antibonding overlap between the terminal atoms, 1 and 2. The corresponding bonding interaction lowers the energy of the $2a_1$ orbital. For an "acute angled" geometry (apical angle $< 60°$[49]) the expected configuration is $\cdots 1a_1^2 2a_1$ leading to a $^2A_1$ ground state. For this situation, the predicted spin populations $\rho_0 = 1/4$, $\rho_3 = 1/2$ are in marked contradistinction to those observed. Likewise, the ESR data rule out an equilateral triangle for which $\rho_0 = \rho_3 = 1/3$ on each atom. For an apical angle of 60°, the potassium trimer will have an orbitally degenerate ground state of $^2E'$ symmetry and should, therefore, suffer a static Jahn–Teller distortion to either an obtuse angled or an acute angled geometry. The ESR spectra for both K_3 and Na_3 show that the $^2B_2$ component lies lower in energy.

An alternative model for both K_3 and Na_3 envisions trimer formation by an "electron jump" mechanism,[51] $M_2 + M \rightarrow M_2^+M^-$ or $M_2^-M^+$. The approximate atom–dimer separation at which charge transfer should occur can be estimated from the curve crossing relationship,[51] $r_c = 14.4/(I - E)$ Å, where I and E are, respectively, the ionization potential of the donor and the electron affinity of the acceptor (energies in eV). For $K + K_2$,[52] $r_c \sim 3.8$–4.1 Å, a value comparable in magnitude to the average trimer bond distance $r_e \sim 4.3$ Å.[53] Consequently the trimer ground state might be expected to possess significant ionic character, with isoceles geometry being favored electrostatically. In the strictly ionic limit, predicted spin populations for both $M_2^+M^-$ and $M_2^-M^+$ are $\rho_0 = 1/2$, $\rho_3 = 0$ in qualitative agreement with those measured.

The simple bonding ideas of Fig. 3 are also in accord with several recent *ab initio* calculations on both Li_3[21,54,55] and Na_3.[20] The comparison between observed and calculated spin populations has recently been reviewed.[25] Briefly, there is qualitative and sometimes quantitative agreement for trimer species of either $^2B_2$ or $^2\Sigma_u^+$ symmetry. In most cases an obtuse isosceles geometry is predicted to be most stable although a flat potential surface with multiple minima is also indicated. While none of these calculations gives any indication of an extensive ionic contribution to the trimer electronic structure, a theoretical study of isovalent Li_2H indicates an isosceles $^2A_1$ ground state with 50% ionic character.[56,57] Most noteworthy are the calculations by Gerber and Schumacher[21] on Li_3 and by Martin and Davidson[20] on Na_3. Both studies treat the trimer as a *dynamic* Jahn–Teller molecule. As discussed in more detail below, the previously invoked static distortion may, in some situations, be too naive a model for these molecules.

As noted earlier, the presence of a moderate p character in the wave function for the unpaired electron will not produce directly measurable effects in the ESR spectrum of K_3. Consistent with the 5%–10% and 20%–30% hybridization in K_2[41] and Na_3,[20] respectively, an order of magnitude 10% p character might be expected. Indeed, a more extended basis set may account for the stability found for alkali trimer molecules but not for H_3. Consequently, the isotropic spin populations, $\rho_1 = \rho_2 = 0.474(3)$ and $\rho_3 = 0.057(2)$, should not sum to unity. The ESR measurements leave an ambiguity, not resolved by molecular structure calculations,[25] as to the sign of ρ_3, however. If $\rho_3 > 0$, $\sum\rho = 1.005(5)$ corresponding to little or no p character, whereas for $\rho < 0$, $\sum\rho = 0.891(5)$. If the 10-line spectrum of K_3 (Fig. 2) arises from a pseudorotating isomer of $K_3(^2B_2)$ then, as shown below, $\rho_3 < 0$. For this situation the spin population data indicate an 11% p orbital participation. A number of complications may alter this estimate, however. These include orbital contraction or expansion

upon molecule formation[20,24] and matrix interactions. The latter give rise to a significant spread in the measured hfs constant for atomic potassium (Table II) and produce at least two distinct trapping sites for Na_3 in argon.[24] Likewise, both the sign and magnitude of the measured g shift $\Delta g = -0.0038$, are consistent with either matrix site effects comparable to those of atomic potassium or with p-orbital participation in the unpaired electron wavefunction. For a 10% hybridization and spin–orbit coupling to empty orbitals of dominant p character, a rough g shift may be estimated from,[48] $\Delta g \sim -2(0.10)\lambda_K/\Delta$ where $\lambda_K = 38$ cm^{-1} is the spin–orbit coupling constant for the $4p$ orbital of atomic potassium[58] and Δ is the energy gap between the ground and excited state. Substitution of the observed g shift gives $\Delta \sim 2000$ cm^{-1}, which seems unreasonably small.[60] Most likely hybridization and matrix effects contribute comparably to the g shift in these molecules.[59]

An interpretation of the spectrum shown in Fig. 2 is not as clear cut as in the trimer analysis. Although this spectrum is most apparent at elevated temperatures, it does appear to be present in freshly deposited matrices at 4 K. Here, however, most M' components are overlapped by the much stronger K_3 spectrum and with transitions from atomic potassium in several matrix sites. A somewhat analogous, but not as well documented, phenomenon has been observed in experiments utilizing sodium instead of potassium.[24] In the temperature range $T \sim 25$–30 K, the ESR spectrum of Na_3 is entirely suppressed and a weak underlying spectrum becomes evident. This consists of at least six sets of first derivative transitions, whose intensities fall off towards the wings. The (most intense) central set is closest to the resonance field of the free electron. The spacing between the major features is ~ 110 G and the superhyperfine splitting is ~ 6 G. For the potassium experiments, the ten line hyperfine pattern shows that the carrier contains three magnetically equivalent ^{39}K nuclei, each having an isotropic spin population of slightly less than one third. This situation could arise in one of two ways. Either the spectrum originates from a polymeric species other than the trimer or, alternatively, it might belong to an isomer of K_3 in which all nuclei have become equivalent.

In view of the significantly greater signal intensity of the trimer in comparison with atomic potassium, the presence in these matrices of still larger aggregates is quite plausible. Since, for smaller cluster sizes at least, only odd numbered species are expected to be paramagnetic, the most likely candidate is the potassium pentamer K_5. As in the trimer example above, the simple Huckel method was used to predict spin density distributions for varying K_5 geometries. Assumed structures included the chain, ring, square pyramid, trigonal bipyramid and tetrahedral arrangements, plus several others of still lower symmetry. In four cases (ring, tetrahedron, square pyramid, and trigonal bipyramid) an orbitally degenerate ground state was predicted, but this was assumed to be unstable towards a static Jahn–Teller distortion. Of the > 10 geometries investigated, only the chain (linear or "zigzag") structure gave approximate agreement with the experimental spectra. Figure 4 shows the predicted MO scheme for a linear or bent pentamer molecule. The unpaired electron is seen to occupy an orbital of a_1 symmetry (σ_g if linear) for which $\rho_0 = 1/3$ on three ^{39}K nuclei in approximate agreement with the measured value $\rho_0 = 0.30$.[61] As in the potassium trimer, the total isotropic spin density, $3\rho_0 = 0.89$, does not sum to unity, possibly indicating some p character in the wave function for the unpaired electron. In this context, it is interesting that the total isotropic spin densities, $\rho_0 = 1.00$, $2\rho_0 = 0.95$, $3\rho_0 = 0.89$, for clusters K, K_3, K_5, respectively, decrease monotonically towards the value $\xi_F \sim 0.7$ for the corresponding parameter in bulk potassium.[62]

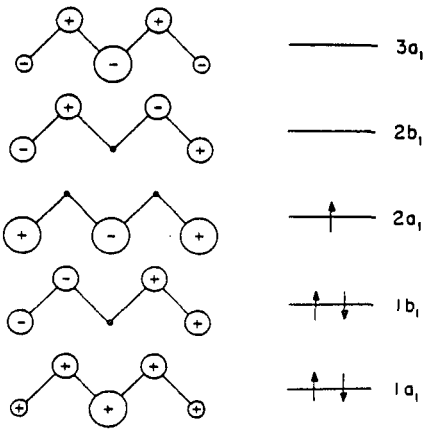

FIG. 4. Molecular orbital scheme for an alkali pentamer with linear or "zigzag" geometry.

At the simple Huckel level, the a_1 wave function for the chain pentamer structure, Fig. 4, has a node at two potassium nuclei. However, as in the case of K_3, higher order effects would be expected to induce a small polarization spin density at these positions. For the trimer this gives rise to the quartet superhyperfine structure characterized by $a_3 \sim 5$ G. The corresponding interaction in the pentamer should produce a septet superhyperfine pattern about each of the ten M' components of Fig. 2. The clear absence of this effect might indicate a superhyperfine splitting considerably smaller than the trimer value. In this situation, an upper bound to the pentamer superhyperfine splitting constant may be estimated from measured linewidths,[63] and is found to be approximately 1 G. As mentioned earlier, ESR spectra of matrices doped with sodium show evidence for a cluster (other than Na_3) whose superhyperfine splitting ~ 6 G. A similar potassium species would have a predicted[64] splitting of ~ 1 G, in good agreement with the value estimated from the observed linewidth data. Semiempirical calculations[35] predict a variety of stable geometries for alkali pentamer molecules, including a chain structure. Since these studies are not as detailed as in the trimer case, it is difficult to make a fair comparison between theory and experiment at this time.

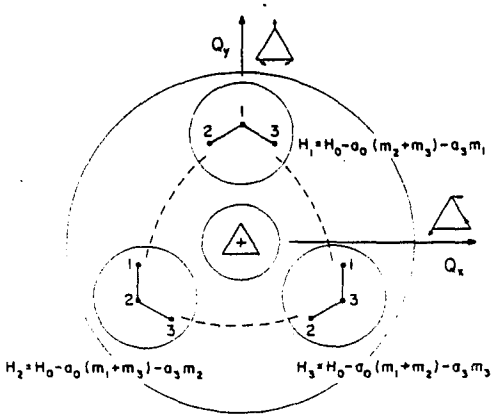

FIG. 5. Normal coordinate and real space description of pseudorotating K_3 with circles representing energy contours for the trimer potential surface.

An alternative interpretation of the ten line hyperfine pattern is suggested by the results of recent theoretical studies on Li_3[21] and Na_3,[20] which treat the trimer as a dynamic Jahn–Teller molecule. In D_{3h} symmetry there are three normal modes of vibration one of which is totally symmetric while the other two comprise a doubly degenerate pair. The trimer potential energy surface is usually described in terms of the two doubly degenerate coordinates Q_x and Q_y.[66,67] The Jahn–Teller interaction gives rise to a continuous, double potential surface, formed by two overlapping paraboloids of revolution, with upper and lower sheets joined at a conical intersection.

Figure 5 is a schematic illustration of the lower potential sheet, whose essential features are a central peak surrounded by a trough containing three potential wells. The central peak, corresponding to a true equilateral geometry, is energetically remote from the trough region. The three minima correspond to obtuse isosceles geometry ($^2B_2$ symmetry), and are indistinguishable except for different occupancies of the apical position, as indicated by the numbering in Fig. 5. Each well is separated from its neighbors by a saddle point of acute isosceles geometry. The broken line in Fig. 5 represents a relatively low-energy path between adjacent minima, intraconverting one obtuse triangular form into another. This "pseudorotation" is accomplished by deforming the trimer in both the Q_x and Q_y directions. The totally symmetric coordinate is not involved in this motion.

Figure 5 also gives magnetic field positions H_1, H_2, and H_3 for the ESR transitions from each obtuse angled structure. These expressions are the same as Eq. (1) and are discussed in Sec. III. If trimer molecules are "locked" into their respective minima, ESR does not distinguish among the three geometries and the resultant spectrum is a superimposition of individual obtuse angled species, i.e., a septet of quartets as observed in Fig. 1. However, for pseudorotation faster than the ESR time scale, only an average spectrum will be observed,

$$\langle H\rangle = \tfrac{1}{3}(H_1 + H_2 + H_3) = H_0 - M' \cdot \tfrac{1}{3}(2a_0 + a_3). \qquad (4)$$

This expression, in which $M' = m_1 + m_2 + m_3$, is similar to Eq. (3) but with an effective hfs constant, $a_{eff} = \frac{1}{3}(2a_0 + a_3)$. Together with the data of Table II, $a_0 = 39.0(3)$ G and $a_3 = \pm 4.7(2)$ G, Eq. (4) predicts a 10-line ESR spectrum for which $a_{eff} = 27.6(3)$ G if $a_3 > 0$ or $a_{eff} = 24.4(3)$ G if $a_3 < 0$. The predicted value with $a_3 < 0$, $a_{eff} = 24.4(3)$ G, is remarkably close to the measured hfs constant for K_n, $a_0 = 24.5(7)$ G from Table II. In addition, Eq. (4) predicts the same g value for both K_3 and K_n. Within experimental error, the data of Table II show this to be the case.[38]

A pseudorotation mechanism is also appealing as it suggests a possible origin of the temperature dependent intensities observed in these matrix samples. For the sodium trimer, Martin and Davidson[20] estimate a vibrational frequency of approximately 85 cm^{-1} for the doubly degenerate normal mode, with a barrier to pseudorotation close to 200 cm^{-1}. Consequently they conclude that "the $^2B_2$ well should support 2 or 3 vibrational levels." More precisely, the ground state for the trimer is a vibronic doublet of E' symmetry with a $^2A_2'$ state lying slightly higher in energy.[17,39,70] In the absence of barrier penetration, all three states have the same energy. This three fold degeneracy, arising from the three indistinguishable obtuse angled configurations of the trimer (Fig. 5), is lifted by quantum mechanical tunneling which raises $^2A_2'$ above $^2E'$. This example is analogous to the more familiar case of inversion doubling in the ammonia molecule.[71,72] For Na_3, a rather crude estimate gives an order of magnitude 1–10 cm^{-1} inversion splitting corresponding to a tunneling frequency in the 10–100 GHz range.[73] If a similar situation pertains to K_3 then it is plausible that at low temperatures the trimer is trapped in its zero point energy level within the $^2B_2$ wells. The tunneling rate might well be less than the 10–100 GHz estimate for Na_3, so that little or no pseudorotating isomer is detected on an ESR timescale. As the temperature is raised above 4 K, several effects may come into play. The matrix, which should be particularly important in systems with a markedly flat potential surface, might "lock" the trimer into an obtuse angled geometry near 4 K but could become sufficiently fluid at higher temperatures to allow pseudorotation. Alternatively, or in addition, higher energy levels of the trimer might become thermally accessible. This could (i) increase the rate of pseudorotation either by thermal population of excited energy levels in the $^2B_2$ wells or by indirect coupling of the three wells through a much higher state as in the Orbach mechanism for spin lattice relaxation, (ii) give rise to the spectrum of a "vibronic singlet" state,[73] for which unresolved anisotropies would be absent, leading to narrower lines and a more intense spectrum as observed at $T \sim 19$ K and (iii) decrease spin lattice relaxation time sufficiently for the obtuse angled trimer spectrum to be broadened beyond detection,[74] as observed at $T \sim 25$ K.

While these explanations for the temperature

intensity changes are qualitative and, consequently, somewhat speculative, additional experiments may provide further guidance and, in addition, allow a definitive assignment of the carrier of the 10-line spectrum. Included are intensity measurements over a finer temperature grid, the use of matrices other than argon and temperature dependent studies using lithium and sodium rather than potassium. The results of these experiments will be reported in later communications.

ACKNOWLEDGMENTS

We thank Professor Alvin Kwiram and Professor Stewart Novick for stimulating discussions, Professor Neil McKelvie for help with the simple Huckel calculations and Mr. Michael Butler for invaluable assistance in the early stages of these experiments. This research was supported in part by The City University of New York PSC–BHE Research Award Program and by The National Science Foundation under grant number CHE 79-13260. Acknowledgment is made to the Donors of The Petroleum Research Fund, administered by the American Chemical Society, for partial support of the research.

[1]*First International Meeting on The Small Particles and Inorganic Clusters*, J. Phys. (Paris) C 2 (1977).
[2]*Size and Symmetry*, Nature (London) **274**, 17 (1978).
[3]T. E. Fischer, Phys. Today **27**, 23 (1974).
[4]K. H. Johnson and R. P. Messmer, J. Vac. Sci. Technol. **11**, 236 (1974).
[5]A. L. Robinson, Science **185**, 772 (1974); **194**, 1150 (1970).
[6]H. F. Schaeffer, Acc. Chem. Res. **10**, 287 (1977).
[7]J. F. Hamilton and R. C. Baetzold, Science **205**, 1213 (1979).
[8]E. L. Muetterties, Bull. Soc. Chim. Belg. **84**, 959 (1975); **85**, 451 (1976).
[9]H. J. Freund and S. H. Bauer, J. Phys. Chem. **81**, 994 (1977); D. J. Frurip and S. H. Bauer, *ibid.* **81**, 1001, 1007 (1977); S. H. Bauer and D. J. Frurip, *ibid.* **81**, 1015 (1977).
[10]J. C. Whitehead and R. Grice, Mol. Phys. **26**, 267 (1973); J. C. Whitehead, *ibid.* **31**, 549 (1976); D. J. Mascord, P. A. Gorry, and R. Grice, Faraday Discuss. Chem. Soc. **62**, 255 (1977).
[11]M. Moskovits and J. E. Hulse, J. Chem. Phys. **67**, 4271 (1977); A. B. Anderson, J. Chem. Phys. **68**, 1744 (1978).
[12]P. J. Foster, R. E. Leckenby, and E. J. Robbins, J. Phys. B **2**, 478 (1969). See also, E. J. Robbins, R. E. Leckenby, and D. Willis, Adv. Phys. **16**, 739 (1967).
[13]A. Herrmann, E. Schumacher and L. Woste, J. Chem. Phys. **68**, 2327 (1978). A. Herrmann, S. Leutwyler, and E. Schumacher, Helv. Chim. Acta **61**, 453 (1978); A. Herrmann, M. Hofmann, S. Leutwyler, E. Schumacher, and L. Woste, Chem. Phys. Lett. **62**, 216 (1979).
[14]J. L. Gole has recently obtained laser induced fluorescence from atomic sodium produced by photodissociation of Na_3 in a supersonic expansion. The observed "fluctuation bands" show evidence of bound-free transitions in the trimer. See also D. R. Preuss, S. A. Pace, and J. L. Gole, J. Chem. Phys. **71**, 3553 (1979).
[15]W. D. Knight, R. Monot, E. R. Dietz, and A. R. George, Phys. Rev. Lett. **40**, 1324 (1978).
[16]K. A. Gingerich, D. L. Cocke, and F. Miller, J. Chem. Phys. **64**, 4027 (1976).
[17]C. H. Wu, J. Chem. Phys. **66**, 3181 (1976).
[18]Notable is the work of Ozin *et al.* See, for example, G. A. Ozin, Catal. Rev.-Sci. Eng. **16**, 191 (1977), and references therein.
[19]See, for example, M. Moskovits and D. P. DiLella, J. Chem. Phys. **72**, 2267 (1980); V. E. Bondybey and J. H. English, J. Chem. Phys. **73**, 42 (1980).
[20]R. L. Martin and E. R. Davidson, Mol. Phys. **36**, 1713 (1978).
[21]W. H. Gerber and E. Schumacher, J. Chem. Phys. **69**, 1692 (1978).
[22]J. L. Gole, R. H. Childs, D. A. Dixon, and R. A. Eades, J. Chem. Phys. **72**, 6368 (1980).
[23]For example: R. C. Baetzold, and R. E. Mack, J. Chem. Phys. **62**, 1513 (1975); R. P. Messmer, S. K. Knudson, K. H. Johnson, J. B. Diamond, and C. Y. Yang, Phys. Rev. B **4**, 1396 (1976).
[24]D. M. Lindsay, D. R. Herschbach, and A. L. Kwiram, Mol. Phys. **32**, 1199 (1976).
[25]D. M. Lindsay, D. R. Herschbach, and A. L. Kwiram, Mol. Phys. **39**, 529 (1980).
[26]D. M. Lindsay, Ph.D. thesis, Harvard University (1974).
[27]J. P. Goldsborough and T. R. Koehler, Phys. Rev. **133**, A 135 (1964).
[28]C. K. Jen, V. A. Bowers, E. L. Cochran, and S. N. Foner, Phys. Rev. **126**, 1749 (1962).
[29]D. M. Lindsay, D. R. Herschbach, and A. L. Kwiram, Chem. Phys. Lett. **35**, 175 (1974).
[30]See, for example: G. A. Thompson, Frances Tischler, Denise Garland, and D. M. Lindsay, "Temperature dependence in the ESR intensities of matrix isolated potassium clusters", *Second International Meeting on the Small Particles and Inorganic Clusters*, Lausanne, Switzerland, 1980, to be published in Surf. Sci.
[31]P. Kusch and V. W. Hughes, *Handbuch der Physik*, edited by S. Flugge (Springer, Berlin, 1959).
[32]J. E. Wertz and J. R. Bolton, *Electron Spin Resonance* (McGraw-Hill, New York, 1972).
[33]N. M. Atherton, *Electron Spin Resonance* (Wiley, New York, 1973).
[34]E. de Boer and E. L. Mackor, Molec. Phys. **5**, 393 (1962).
[35]R. W. Fessenden, J. Chem. Phys. **37**, 747 (1962).
[36]R. W. Fessenden and R. H. Schuler, J. Chem. Phys. **43**, 2704 (1965).
[37]J. E. Harriman, *Theoretical Foundations of Electron Spin Resonance* (Academic, New York, 1978).
[38]R. C. McMillan, J. Phys. Chem. Sol. **25**, 773 (1964).
[39]Only matrix sites II and III are indicated in Figs. 1 and 2. Matrix site I contributes the dominant atomic resonance in freshly deposited samples, but is absent after annealing. Matrix site III is not observed prior to annealing.
[40]Other contributions, such as nuclear quadrupole effects and the interaction of spin density on one nucleus with the magnetic moment of an adjacent nucleus are estimated to be vanishingly small.
[41]L. Pauling, Proc. R. Soc. London, Ser. A **196**, 343 (1949).
[42]R. G. Barnes and W. V. Smith, Phys. Rev. **93**, 95 (1954).
[43]J. H. Freed and G. F. Fraenkel, J. Chem. Phys. **39**, 326 (1963); G. F. Franekel, J. Phys. Chem. **71**, 139 (1967); M. C. R. Symons, J. Phys. Chem. **71**, 172 (1967).
[44]H. M. McConnell and A. D. McLachlan, J. Chem. Phys. **34**, 1 (1960); H. J. Silverstone, D. E. Wood, and H. M. McConnell, J. Chem. Phys. **41**, 2311 (1964).
[45]J. H. Freed, J. Chem. Phys. **43**, 1477 (1965); R. G. Kooser, W. V. Volland and J. H. Freed, J. Chem. Phys. **50**, 5243 (1969).
[46]R. N. Porter, R. M. Stevens, and M. Karplus, J. Chem. Phys. **49**, 5163 (1968).
[47]Bound, excited Rydberg states of H_3 have been observed, however. See: G. Herzberg, J. Chem. Phys. **70**, 4806 (1979).
[48]A. Carrington and A. D. McLachlan, *Introduction to Magnetic Resonance* (Harper and Row, New York, 1967).
[49]Strictly speaking the terms obtuse and acute pertain to distortions from an apical angle of 90°. Their use in relation to 60° is customary for M_3 species; however, see Refs. 20, 21, and 24.

[50]A. D. Walsh, J. Chem. Soc. **3**, 2260 *et seq.* (1953).
[51]D. R. Herschbach, Adv. Chem. Phys. **10**, 319 (1966).
[52]Ionization potentials $I = 4.3$ and 4.0 eV for K and K_2, respectively, from Ref. 12. The electron affinity for atomic potassium is $E = 0.50$ eV, see: J. Slater, F. H. Read, S. E. Novick, and W. C. Lineberger, Phys. Rev. A **17**, 201 (1978). The electron affinity for the dimer was assumed to be approximately 0.5 eV, comparable to the value $E = 0.45$ eV calculated for Li_2: see, D. A. Dixon, J. L. Gole, and K. D. Jordan, J. Chem. Phys. **68**, 567 (1977).
[53]G. A. Hart and P. L. Goodfriend, Mol. Phys. **29**, 1109 (1975).
[54]D. W. Davies and G. del Conde, Faraday Discuss. Chem. Soc. **55**, 369 (1973); Chem. Phys. **12**, 45 (1976); P. S. Bagus, G. del Conde and D. W. Davies, Faraday Discuss. Chem. Soc. **62**, 321 (1977); D. W. Davies and G. del Conde, Mol. Phys. **33**, 1813 (1977). See also Ref. 25.
[55]I. H. Hillier, Faraday Discuss. Chem. Soc. **62**, 321 (1977); J. Kendrick and I. H. Hillier, Mol. Phys. **33**, 635 (1978); J. Kendrick Mol. Phys. **35**, 593 (1978).
[56]P. Siegbahn and H. F. Schaeffer, J. Chem. Phys. **62**, 3488 (1975).
[57]W. B. England, N. H. Sabelli, and A. C. Wahl, J. Chem. Phys. **63**, 4596 (1975); W. B. England, N. H. Sabelli, A. C. Wahl, and A. Karo, J. Phys. Chem. **81**, 772 (1977).
[58]C. E. Moore, *Atomic Energy Levels*, Natl. Bur. Stand. (U.S.) Circ. **467** (1952).
[59]It is interesting to note that the ratio of the experimental g shifts for K_3 and Na_3, $0.0038/0.0011 = 3.5$, is in excellent agreement with the corresponding ratio of atomic spin–orbit coupling constants, $38/11 = 3.5$.
[60]The s–p band gap in bulk potassium gives an approximate lower bound for the energy gap Δ. From the optical conductivity data of N. V. Smith, Phys. Rev. **183**, 634 (1969), this value is $\Delta \sim 4000$ cm^{-1}. An alternative estimate for Δ may be obtained by scaling the lowest excited orbital of predominantly p character in Na_3 by the relative ns–np excitations in the free atoms, $\Delta(K)/\Delta(Na) = 0.76$ from Ref. 58. Using $\Delta(Na_3) = 1.3$ eV from Ref. 20 gives $\Delta(K_3) \sim 8000$ cm^{-1}.
[61]For C_{2v} or $D_{\infty h}$ geometry, symmetry requires that the two terminal atoms, but not necessarily the central atom, be equivalent. Accordingly, higher-order effects might give rise to a hfs constant for the central atom which is slightly different from that of the two end atoms. It is assumed that such effects, if they occur, are not resolved in the ESR spectrum.
[62]The parameter, $\xi_F = |\psi_F(0)|^2/|\psi_K(0)|^2$, is the ratio of the square of the wave function at the nucleus for an electron on the Fermi surface of the metal, $|\psi_F(0)|^2$, to the corresponding entity in the free atom, $|\psi_K(0)|^2 = 7.46 \times 10^{24}$ cm^{-3} from Ref. 42. The quantity $|\psi_F(0)|^2$ can be estimated by combining the Pauli spin susceptibility (χ_p) with the measured Knight shift for potassium, $K = 0.265\%$: see, C. Kittel, *Introduction to Solid State Physics* (John Wiley, New York, 1976) and R. T. Schumacher, *Introduction to Magnetic Resonance* (Benjamin, New York, 1970). Although χ_p for potassium is not well known, a probably reliable value is $\chi_p = 1.7\ \chi_0$, where χ_0 is the paramagnetic susceptibility of a Fermi gas of conduction electrons: see, L. Wilk, A. H. MacDonald, and S. H. Vosko, Can. J. Phys. **57**, 1065 (1979).
[63]A. F. Kip, C. Kittel, R. A. Levy, and A. M. Portis, Phys. Rev. **91**, 1066 (1953).
[64]As estimated using the ratio of nuclear g factors, $g(^{39}K)/g(^{23}Na) = 0.18$, from: E. R. Andrew, *Nuclear Magnetic Resonance* (Cambridge University, London, 1969), Appendix 2.
[65]R. C. Baetzold and R. E. Mack, Inorg. Chem. **14**, 686 (1975); A. Gelb, K. D. Jordan, and R. Silbey, Chem. Phys. **9**, 175 (1975); J. Flad, H. Stoll, and H. Preuss, J. Chem. Phys. **71**, 3042 (1979).
[66]C. Herzberg, *Electronic Spectra of Polyatomic Molecules* (Van-Nostrand Reinhold, New York, 1966).
[67]These are close analogies between the Jahn–Teller effect in the equilateral triangle and the more extensively investigated examples in certain transition metal compounds. See, for example: M. D. Sturge, Sol. State Phys. **20**, 91 (1967); F. S. Ham in *Electron Paramagnetic Resonance*, edited by S. Geschwind (Plenum, New York, 1972); R. Englman, *The Jahn–Teller Effect in Molecules and Crystals* (Wiley, New York, 1972).
[68]The same model does not appear to apply to Na_4 and the second sodium species mentioned earlier. While the agreement for the hyperfine data of the two species is satisfactory, the two radicals have markedly different g values.
[69]R. S. Berry, Rev. Mod. Phys. **32**, 447 (1960).
[70]E. B. Wilson, Jr., J. C. Decius, and P. C. Cross, *Molecular Vibrations* (McGraw-Hill, New York, 1955).
[71]C. H. Townes and A. L. Schawlow, *Microwave Spectroscopy* (McGraw-Hill, New York, 1955).
[72]Using the data of Ref. 20 and methods described in Ref. 71, but assuming a triangular potential along the pseudorotation coordinate. Slightly lower values are obtained using a cosine potential as described by M. D. Sturge, *op. cit.*, Ref. 67.
[73]The transition between the spectrum of a "vibronic doublet" and that of a "vibronic singlet" need not imply direct population of $^2A_2'$, see Ref. 67.
[74]An Orbach type mechanism has been invoked in order to explain similar temperature dependent effects in dynamic Jahn–Teller octahedral complexes. See, K. A. Muller in *Magnetic Resonance and Relaxation*, Colloq. Ampere XIV (North-Holland, Amsterdam, 1967).

Appendix A.2

Dynamic frequency shifts in pseudorotating Na_3

D. M. Lindsay and G. A. Thompson

Department of Chemistry, City University of New York, The City College, New York, New York 10031
(Received 29 March 1982; accepted 15 April 1982)

ESR spectra assigned to pseudorotating Na_3 molecules have been obtained by clustering atomic sodium in an argon matrix. Both a pseudorotating spectrum and the previously reported "stationary" spectrum are observed. As in the analogous potassium case, the pseudorotating spectrum is attributed to a rapid exchange between the three equivalent potential wells of a Jahn–Teller distorted trimer. The ESR spectra show an extreme alternating linewidth effect. Even at $T \gtrsim 30$ K, only those four hyperfine (hf) components which do not broaden are observed. The relaxation matrix formalism is applied to pseudorotating Na_3 and derived expressions give a good fit to the measured line positions. These show 5–10G "dynamic frequency shifts," much larger in magnitude than normally encountered in exchanging radicals. The measured g value and hf constants for pseudorotating Na_3 are in close correspondence with those predicted from the stationary trimer parameters. Together the two spectra determine the sign of the hf coupling in Na_3.

I. INTRODUCTION

In previous work,[1] electron spin resonance (ESR) spectra were reported for sodium trimers trapped in solid argon at 4.2 K. The spectra show an isotropic hyperfine (hf) structure arising from the Fermi contact interaction of a single unpaired electron and three ^{23}Na nuclei. Two nuclei are magnetically equivalent and have hf constants (a_0) approximately half that of the free atom. The hf coupling to the third nucleus ($\pm a_3$) is much smaller. Subsequent studies[2] have identified an analogous spectrum for K_3.

Both trimer spectra have been interpreted as arising from the $^2B_2$ ground state of an "obtuse isosceles" isomer. The unpaired electron is localized almost entirely in valence s orbitals on the two base atoms. Polarization effects induce a small (positive or negative) spin density at the unique apical position. The trimer ground state may be viewed as the stable partner of a Jahn–Teller distorted equilateral triangle.[1–4] The orbital degeneracy of the D_{3h} trimer is lifted by an increase in the apical angle and since no particular atom is preferred this leads to three equivalent potential wells each of $^2B_2$ symmetry. Trimer molecules are equally distributed among the three wells which, if sufficiently deep, give rise to the "stationary spectrum" observed.[1,2]

For potassium in argon, a further ESR spectrum consists of ten equally spaced hf components as would be expected of a radical containing *three* equivalent ^{39}K nuclei.[2,5,6] This spectrum was attributed to a pseudorotating trimer in which all three atoms are made equivalent by rapid exchange between adjacent $^2B_2$ minima. As evidence for this interpretation, the hf splitting constant of pseudorotating K_3 is found to be in excellent agreement with the appropriate average, $\langle a \rangle = 1/3(2a_0 + a_3)$, of the stationary trimer constants, if a_3 is assumed negative.[2] In addition, both spectra have the same g value. Confirming evidence is provided by the striking alternating linewidth effect shown by the pseudorotating spectrum.[5,6] At high temperatures, component ESR intensities approach the predicted ratio for three equivalent ^{39}K nuclei. With decreasing temperature, however, all but *four* hf components become noticeably broadened. This behavior was shown to be both qualitatively[5] and quantitatively[6] in accord with the pseudorotation hypothesis.

In this paper we report ESR spectra for the pseudorotating *sodium* trimer. As is well known from the study of certain organic radicals,[7–11] dynamic behavior may be manifested by both line broadening and frequency shifts. These two effects depend upon the mean-square deviation in the hf splitting $\langle \delta a^2 \rangle$, where,[6] for alkali trimer molecules, $\langle \delta a^2 \rangle = 2/9(a_0 - a_3)$.[2] Because $\langle \delta a^2 \rangle$ for Na_3 is very large (over an order of magnitude greater than in K_3), there are pronounced consequences for the ESR spectrum. Only those four hf components whose linewidths are immune to exchange can be observed (an extreme alternating linewidth effect) and these show large (5–10G) dynamic frequency shifts. As in the potassium case,[2] the magnetic parameters for pseudorotating Na_3 are in good agreement with those predicted from the stationary spectra[1] when a_3 is assumed negative.

II. EXPERIMENTAL

The experimental details have been reported elsewhere.[1,2] Matrices are formed by codeposition of excess argon (Airco, 99.9998%) with atomic sodium (Gallery, 99.95%) on a sapphire plate bonded to the inside of an ESR cavity mounted on a variable temperature liquid helium Dewar. Cluster formation occurs during deposition and is accomplished by warming the sapphire surface above a nominal temperature of 4.2 K. Spectral resolution was considerably enhanced by a subsequent annealing of the matrix sample. Temperature measurements are made with a calibrated carbon resistor and are judged accurate to within ± 5%. The resonance frequency of the cavity plus sapphire plate and argon matrix was 9.2824(2) GHz over the temperature range of these experiments. ESR spectra were recorded on a JEOL ME-3X spectrometer and were individually calibrated with a proton magnetometer (Micronow, model 515).

III. THEORY

Trimer spectra may be described by the isotropic spin Hamiltonian

$$\mathcal{H}(t) = \mathcal{H}_0 + \mathcal{H}_1(t) \ ,$$

 0021-9606/82/151114-04$02.10

where

$$\mathcal{H}_0 = g_0\beta_e S_z H + \bar{a} S_z \sum_q I_{qz} + \tfrac{1}{2}\bar{a}\sum_q (S_+ I_{q-} + S_- I_{q+}) \quad (1)$$

is a time independent part, and

$$\mathcal{H}_1(t) = \sum_q h_q(t) S_z I_{qz} + \frac{1}{2}\sum_q h_q(t)(S_+ I_{q-} + S_- I_{q+}) \quad (2)$$

is a random, fluctuating term which describes the dynamics. In these expressions, g_0 is the trimer g value. β_e is the Bohr magneton, and $\bar{a} \equiv \langle a_q(t)\rangle = 1/3(2a_0 + a_3)$ is the average hf coupling constant for nuclei $q = 1$, 2, or 3. The electron spin operators S_z, S_+ and nuclear spin operators I_{qz}, I_{q+} have their usual meaning but are specialized to $S = 1/2$ and $I = 3/2$. The $h_q(t)$ represent instantaneous deviations from the mean hf,

$$h_q(t) = a_q(t) - \bar{a} , \quad (3)$$

which can take one of two values depending upon whether $a_q(t) = a_0$ or a_3.

A. Static problem

To second order in $\bar{a}/H$, the eigenvalues of the static Hamiltonian ($\mathcal{H}_0$) give, with the selection rules $\Delta m_s = \pm 1$, $\Delta m_q = 0$, transition fields (the units are Gauss)

$$H_0 = \frac{g_e H_e}{g_0} - \bar{a}M - \frac{\bar{a}^2}{2H}\left[3I(I+1) - \sum_q m_q^2\right] , \quad (4)$$

where g_e, H_e are the g value and resonance field for a free electron, $m_q = \pm 3/2$, $\pm 1/2$ is an eigenvalue of I_{qz} and $M = \sum_q m_q$. Assumed in the derivation of Eq. (4) are first order basis functions

$$|\alpha\rangle = |m_s\rangle \prod_q |m_q\rangle , \quad (5)$$

where $|m_s\rangle$ and $|m_q\rangle$ are eigenfunctions of S_z and I_{qz}, respectively. The product representation of Eq. (5) recognizes a choice of uncoupled nuclear eigenfunctions for a pseudorotating trimer.[12] *No nuclei are "completely equivalent" in the sense that $a_q(t) \neq a_{q'}(t)$ at all times t,* and the criterion[7,8] $|a_0 - a_3| \gg a_0^2/2H$, $a_3^2/2H$ is easily met by both Na_3 and K_3. For pseudorotating K_3, the last term in Eq. (4), the "static frequency shift," is small and the spectrum is adequately described using first order theory alone.[2] For the sodium trimer, however, all three terms are insufficient and an additional "dynamic frequency shift," arising from $\mathcal{H}_1(t)$, must be included.

B. Dynamic problem

The first term in Eq. (2), which cannot connect different spin states $m_s = \pm 1/2$, gives rise to a secular broadening of the trimer hf spectrum. In Ref. 6 the secular contribution to the trimer linewidth is shown to be

$$\Gamma(M,k) = 2/9(a_0 - a_3)^2[M^2 - 3(m_1m_2 + m_1m_3 + m_2m_3)]\tau_c , \quad (6)$$

where τ_c is a (temperature dependent) correlation time. The symbol k recognizes that the function in parentheses can, for certain M, take on several values depending upon the particular combination of m_1, m_2, and m_3. Of importance here are $(m_1, m_2, m_3) = (\pm 3/2, \pm 3/2, \pm 3/2)$ and $(\pm 1/2, \pm 1/2, \pm 1/2)$, corresponding to $M = \pm 9/2$ and one component of $\pm 3/2$. For these $\Gamma(M,k) = 0$ and, in the limit of an extreme alternating linewidth effect, only four hf transitions may be detected.

Effects arising from the second term in Eq. (2) are elegantly handled by the perturbation theory of Redfield *et al.* Valid whenever $\langle \delta a^2\rangle^{1/2}\tau_c \ll 1$, the general formulation is well described elsewhere[7,8,11,13,14] and need not be restated here. However, each application requires a computation of the elements of a relaxation matrix $R = R^r + iR^i$, whose real and imaginary parts give rise to a nonsecular linebroadening and the dynamic frequency shift, respectively. Although the two are closely related, only the latter is of importance for pseudorotating Na_3. For the isotropic Hamiltonian [Eq. (2)] a straightforward application of the general theory[7,8,11,13,14] gives a frequency shift

$$R^i_{\alpha\alpha',\alpha\alpha'} = -1/2\, k_{qq}(\omega_0)\left[3I(I+1) - \sum_q m_q^2\right] , \quad (7)$$

where the α, α' subscripts ($m_s = +1/2$ and $-1/2$, respectively) pertain to basis functions of the type (5), ω_0 is the Larmor frequency and

$$k_{qq}(\omega_0) = \int_0^\infty G_{qq}(\tau)\sin\omega_0\tau\, d\tau .$$

The correlation function

$$G_{qq}(\tau) = \overline{h_q(0)h_q(\tau)}$$

is the ensemble average of the expressions (3). The appearance in Eq. (7) of a single spectral density function is a consequence of: (1) the zero matrix elements which multiply $k_{qq'}(\omega_0)$ for $q \neq q'$, and (2) the equality $k_{11}(\omega_0) = k_{22}(\omega_0) = k_{33}(\omega_0)$, but $k_{qq}(\omega_0) = -2k_{qq'}(\omega_0)$, as is easily verified from the results of the next paragraph.

For a stationary, Markov process, in which trimer molecules undergo a random exchange between adjacent $^2B_2$ wells ($i, j = 1$, 2, or 3)

$$G_{qq}(\tau) = \sum_{i,j=1}^{3} h_{qi}(0)\, h_{qj}(\tau)\, P_i(0)\, P_{ij}(\tau) ,$$

where the $P_{ij}(\tau)$ are conditional probabilities relating the occupancy of wells i and j at times $\tau = 0$ and $\tau = \tau$, respectively, and $P_i(0) = 1/3$. A very similar expression, in which the $h(\tau)$ have a slightly different meaning is evaluated in Ref. 6. For pseudorotating alkali trimer molecules

$$G_{qq}(\tau) = \langle \delta a^2\rangle e^{-\tau/\tau_c}$$

giving

$$R^i_{\alpha\alpha',\alpha\alpha'} = -\tfrac{1}{2}\langle \delta a^2\rangle \frac{\omega_0\tau_c^2}{1+\omega_0^2\tau_c^2}\left[3I(I+1) - \sum_q m_q^2\right] .$$

where

$$\langle \delta a^2\rangle = 2/9\,(a_0 - a_3)^2 .$$

For $\omega_0^2\tau_c^2 \gg 1$ and units of Gauss, the dynamic frequency shift is

$$H_1 = -\frac{\langle \delta a^2\rangle}{2H}\left[3I(I+1) - \sum_q m_q^2\right] . \quad (8)$$

TABLE I. Measured line positions (units are Gauss) for pseudorotating Na_3 in an argon matrix at 33 K. Uncertainties are ±0.5 G.

M	(m_1, m_2, m_3)	Site A	Site B	Site C
+9/2	(+3/2, +3/2, +3/2)	2883.0	2872.1	2875.3
+3/2	(+1/2, +1/2, +1/2)	3149.3	3146.5[a]	3146.5[a]
−3/2[b]	(−1/2, −1/2, −1/2)	(3431.0)	(3435.2)	(3432.7)
−9/2	(−3/2, −3/2, −3/2)	3724.6	3734.6	3730.6

[a]For $M=+3/2$, sites B and C are not resolved.
[b]All $M=-3/2$ transitions are overlapped by an additional spectrum. (See the text.) Values in parentheses are calculated using Eq. (9) and the data in Table II.

Combining Eqs. (4) and (8), the complete (to second order) description of the trimer spectrum becomes

$$H = H_0 + H_1 = \frac{g_e H_e}{g_0} - \bar{a}M - \frac{\overline{a^2}}{2H}\left[3I(I+1) - \sum_q m_q^2\right], \quad (9)$$

where

$$\overline{a^2} = \bar{a}^2 + \langle \delta a^2 \rangle = 1/3(2a_0^2 + a_3^2) \ . \quad (10)$$

This last expression suggests a complementary derivation of the result (9). In each $^2B_2$ well ($i=1$, 2, or 3) transitions fields, correct to second order in a/H using the basis set (5), are given by

$$H_i = \frac{g_e H_e}{g_0} - \sum_q a_{qi} m_q - \sum_q \frac{a_{qi}^2}{2H}\left[I(I+1) - m_q^2\right] ,$$

where $a_{qi} = a_3$ if, in well i, nucleus q is apical and $a_{qi} = a_0$, othewise. The average over all three wells $H = 1/3\sum_i H_i$ is identical to Eq. (9).

IV. RESULTS AND DISCUSSION

Table I gives ESR transition fields assigned to pseudo rotating Na_3 in three matrix sites. The relative uncertainty in these measurements is estimated to be $\lesssim 0.5$ G, although the absolute error may be slightly greater. While Table I pertains to ESR spectra recorded at $T = 33$ K, trimer line positions are not noticeably affected by temperature. Below $T \sim 20$ K, the pseudorotating spectrum is strongly overlapped by transitions from the stationary spectrum,[1] which shows a temperature dependence similar to that of the analogous potassium trimer.[5] The ESR intensity of stationary Na_3 increases to a maximum at $T \sim 10$ K and then falls to zero without a noticeable change in linewidth. This behavior and the apparently anomalous coexistence of the two trimer spectra is surprising and potential explanations are currently being pursued. Also observed is atomic sodium in several matrix sites,[1,15] and an extensive, but well resolved, spectrum arising from a cluster other than Na_3.[16] Although the latter masks the $M=-3/2$ component of pseudorotating Na_3, the trimer contributes a noticeable intensity perturbation. Equation (9) predicts a total of 20 transitions for pseudorotating Na_3. However, even at elevated temperatures where spectral overlap is not severe, no hf components other than (± 3/2, ± 3/2, ± 3/2) and (± 1/2, ± 1/2, ± 1/2) were observed. This is not surprising. If the correlation times for pseudorotating K_3 and Na_3 are assumed comparable,[17] then Eq. (6), with $\tau_c \sim 2\times 10^{-10}$ s at 30 K from Ref. 6, predicts an exchange contribution to the linewidth of order 10 G. A broadening of this magnitude would probably make these transitions quite difficult to detect.

TABLE II. Magnetic parameters (hf constants in Gauss) for pseudorotating Na_3 in argon. Approximate errors (in parentheses) derive from uncertainties in Table I data.

Site	g_0	$\bar{a}$	$(\overline{a^2})^{1/2}$
A	2.0012(3)	93.2(2)	122.0(30)
B	2.0016(3)	95.6(2)	117.7(30)
C	2.0018(3)	94.7(2)	121.1(30)

TABLE III. Magnetic parameters (hf constants in Gauss) for stationary Na_3 in argon.[a] Experimental uncertainties are in parentheses.

Site	a_0	a_3	g_0	$\bar{a}$	$(\overline{a^2})^{1/2}$
I	149.5(15)	22.6(10)	2.0012(12)	92.1(8)	122.8(12)
II	153.0(15)	20.3(9)	2.0012(12)	95.2(8)	125.5(12)
III	151	21.2	2.0012	93.6	123.9

[a]For matrix sites I and II g_0, a_0, and a_3 are from Table 3 of Ref. 1. Parameters for site III (not reported in Table 3) are approximate. The average hf $\bar{a} = 1/3(2a_0 + a_3)$ assumes a_3 negative; $\overline{a^2} = 1/3(2a_0^2 + a_3^2)$.

Table II gives constants g_0, $\bar{a}$, and $(\overline{a^2})^{1/2}$ obtained by fitting the data of Table I to Eq. (9) with $H_e = 3312.2$ G. Since there are an equal number of data points and parameters, the error estimate derives from the uncertainty in the experimental line positions. The fit is particularly insensitive to the magnitude of $\overline{a^2}$, which enters Eq. (9) through the relatively small second order term.

A conceivable carrier other than pseudorotating Na_3 is a radical of the type NaX, where X is an impurity. Several examples of adduct formation by metal atoms have been documented.[18] For NaX (with $X = H_2O$, for example) a quartet hf pattern would also be expected. However, the data in Table I give a poor fit to the spin Hamiltonian for a radical containing a single ^{23}Na atom.

Table III reproduces[1] g_0, a_0, and a_3 for the stationary trimer in two matrix sites. Limited data for a third site, apparent in Fig. 3 of Ref. 1, were analyzed to give approximate a_0 and a_3 values assuming $g_0 = 2.0012$. A comparison of Tables II and III shows that the directly measured g_0 and $\bar{a}$ are remarkably close in magnitude to those predicted from the stationary spectrum, provided $a_3 < 0$. A similar correspondence of stationary and pseudorotating parameters has been demonstrated[2] for potassium trimers in argon. The agreement in $(\overline{a^2})^{1/2}$ is less satisfactory but, as noted above, the experimental uncertainty is large. Since this prevents a meaningful inversion of $\bar{a}$ and $\overline{a^2}$ to give a_0 and a_3, a

1-1 correspondence between stationary and pseudorotating matrix sites is not necessarily implied by these data.

In conclusion, several aspects deserve particular emphasis. The ESR analysis presented here provides additional evidence for pseudorotation in alkali trimer molecules and suggests that the dynamic behavior of Na_3 and K_3 may be comparable. Since the spin populations of the two stationary trimers are markedly similar,[1,2] this is not entirely suprising. Indeed a close correspondence between sodium and potassium parameters may be a general feature of these small cluster molecules.[15] In addition, the combination of stationary and pseudorotating spectra determine that $a_3 < 0$, as is the case for K_3.[2] A negative spin density at the apical atom is predicted by *ab initio* calculations,[3] but cannot be determined from the static spectra alone.[1,19] Finally, the ESR spectra for pseudorotating Na_3 provide a fairly stringent test for the relaxation matrix formulation itself. The measured dynamic frequency shifts [Eq. (8) of Sec. III] are $H_1 \sim -5$ and -10 G for $M = \pm 9/2$ and $\pm 3/2$, respectively. These values are approximately two orders of magnitude larger than the 10–100 mG shifts reported previously.[8–10]

ACKNOWLEDGMENTS

This research was supported in part by the City University of New York PSC-BHE Research Award Program and by the National Science Foundation under grant number CHE 79-13260. Acknowledgment is made to the Donors of the Petroleum Research Fund, administered by the American Chemical Society for partial support of this research.

[1] D. M. Lindsay, D. R. Herschbach, and A. L. Kwiram, Mol. Phys. 32, 1199 (1976).
[2] G. A. Thompson and D. M. Lindsay, J. Chem. Phys. 74, 959 (1981).
[3] R. L. Martin and E. R. Davidson, Mol. Phys. 36, 1713 (1978).
[4] W. H. Gerber and E. Schumacher, J. Chem. Phys. 69, 1692 (1978).
[5] G. A. Thompson, F. Tischler, D. Garland, and D. M. Lindsay, Surf. Sci. 106, 408 (1981).
[6] D. M. Lindsay, D. Garland, F. Tischler, and G. A. Thompson, Am. Chem. Soc. Symp. Ser. 179, Chap. 7 (1982).
[7] J. H. Freed and G. K. Fraenkel, J. Chem. Phys. 39, 326 (1963).
[8] G. K. Fraenkel, J. Chem. Phys. 42, 4275 (1965).
[9] R. J. Faber and G. K. Fraenkel, J. Chem. Phys. 47, 2462 (1967).
[10] G. K. Fraenkel, J. Phys. Chem. 71, 139 (1967).
[11] N. M. Atherton, *Electron Spin Resonance* (Wiley, New York, 1973).
[12] For a stationary trimer (Refs. 1 and 3) two nuclei are magnetically equivalent ($a_q = a_0$ for each) and the third is distinct ($a_q = a_3$). Beyond first order in a/H the Hamiltonian $\mathcal{H} = g_0\beta_e S_z H + a_0 \mathbf{S}\cdot(\mathbf{I}_1 + \mathbf{I}_2) + a_3 \mathbf{S}\cdot\mathbf{I}_3$ is not diagonal in the basis set (5). Good quantum numbers for the two indistinguishable nuclei are the magnitude (J) and projection (M) of $\mathbf{J} = \mathbf{I}_1 + \mathbf{I}_2$ and the correct eigenstates are $|m_S|J, M|m_3\rangle$. A similar difference in basis distinguishes the static spectrum Eq. (4) from the hf pattern arising from a single nucleus with $I = 9/2$ and hf constant $\bar{a}$.
[13] A. Abragam, *The Principles of Nuclear Magnetism* (Oxford University, London, 1961).
[14] C. P. Slichter, *Principles of Magnetic Resonance* (Springer, New York, 1980).
[15] C. K. Jen, V. A. Bowers, E. L. Cochran, and S. N. Foner, Phys. Rev. 126, 1749 (1962).
[16] G. A. Thompson, F. Tischler, and D. M. Lindsay (in preparation). ESR spectra have also been obtained for the analogous potassium cluster. The spectra show that the two molecules have very similar spin populations.
[17] A correlation time $\tau_c \sim 2\times10^{-10}$ s for pseudorotating Na_3 also justifies the two assumptions made previously, namely, $\omega_0^2\tau_c^2 \gg 1$ and $\langle\delta a^2\rangle^{1/2}\tau_c \ll 1$. For $\omega_0/2\pi = 9.3$ GHz and $\langle\delta a^2\rangle^{1/2} = 81$ G, $\omega_0^2\tau_c^2 \sim 40$ and $\langle\delta a^2\rangle^{1/2}\tau_c \sim 5\times10^{-2}$.
[18] For example: LiH_2O and $LiNH_3$, P. F. Meier, R. H. Hauge, and J. L. Margrave, J. Am. Chem. Soc. 100, 2108 (1978); $LiCO_2$, J. P. Borel, F. Faes, and A. Pittet, J. Chem. Phys. 74, 2120 (1981); AlC_2H_4, P. H. Kasai and D. McLeod, J. Am. Chem. Soc. 97, 5609 (1975).
[19] D. M. Lindsay, D. R. Herschbach, and A. L. Kwiram, Mol. Phys. 39, 529 (1980).

Appendix A.3

Matrix ESR spectra of polyatomic alkali metal clusters

G. A. Thompson, Frances Tischler, and D. M. Lindsay

Department of Chemistry, City University of New York, The City College, New York, New York 10031
(Received 9 December 1982; accepted 8 February 1983)

ESR spectra have been obtained for polyatomic sodium and potassium clusters in argon and nitrogen matrices. The spectra, tentatively assigned to alkali septemer molecules, show a large isotropic hf (a_1) from *two* equivalent alkali nuclei plus a much smaller splitting (a_2) from an additional (at least) *five* equivalent nuclei. For an argon matrix, the measured hf constants and g values are $a_1 = 118.16(4)$ G, $a_2 = 6.66(12)$, $g_0 = 1.9994$ (1) and $a_1 = 30.55(6)$ G, $a_2 = 1.79(2)$ G, $g_0 = 2.0017(1)$ for Na_7 and K_7, respectively. The ESR spin populations, $\rho_i = a_i/a$(atom), are compared with the orbital symmetries predicted by the simple Huckel approximation for a range of M_7, M_9, M_{11}, and M_{13} structures. Aside from the relatively unstable "T-shaped" arrangement, only a *few* three-dimensional structures give a satisfactory agreement with the ESR spectra. For M_7, a likely geometry is the pentagonal bipyramid. The ESR spin populations for Na_7 are almost identical in magnitude to those of K_7. If $a_2 < 0$, the total *isotropic* spin population is $\Sigma\rho_i \simeq 0.64$, which implies an ~ 36% p character for the unpaired electron.

I. INTRODUCTION

This paper reports on the electron spin resonance (ESR) spectra of matrix isolated sodium and potassium clusters, probably the alkali septemer molecules. Matrix samples were prepared by codepositing atomic alkali (2–5 mol%) with either argon or nitrogen on a liquid helium cooled sapphire surface. In addition to the features assigned to M_7, all matrices show the ESR spectra of both alkali atoms[1] and alkali trimer molecules.[2–4] No sample gave ESR spectra attributable to M_5. Septemer spectra are relatively more intense at the higher concentrations, but a further increase in alkali favors the formation of an unstructured resonance characteristic of large particles or the bulk metal phase.[5] The absence of additional ESR spectra supports a previous hypothesis[6] of a sharp, concentration dependent transition between molecular clusters and microcrystals.

The spectra attributed to Na_7 and K_7 show distinct "quantum size effects."[7] A single unpaired electron has an isotropic hyperfine (hf) interaction arising from an approximately 37% spin population on each of two equivalent alkali atoms, plus a much smaller (± 2%) spin population on each of (at least) five atoms. The ESR spin distribution was compared with the orbital symmetries predicted by the simple Huckel (SH) approximation for a range of 7, 9, 11, and 13 atom clusters. Although unsophisticated, the SH method gives a rapid overview of a large number of cluster sizes and geometries. Except through M_8, relatively few molecular structure calculations have been reported for *alkali* atom clusters.[8,9] In addition, SH calculations readily provide information on the molecular wave function, data which are most often omitted in reports on semiempirical and *ab initio* calculations. A qualitative agreement between experiment and SH theory is obtained for a few compact three dimensional structures, but not for straight chains or rings. For M_7 a likely geometry is the pentagonal bipyramid, the most compact packing arrangement for seven interacting spheres.[10]

II. EXPERIMENTAL

Alkali clusters were formed by codepositing atomic sodium or potassium (Gallery, 99.95%) with diluent argon (Airco, 99.9998%) or nitrogen (Airco, 99.9995%) on a sapphire plate mounted within an X-band ESR cavity. The cavity was attached to a variable temperature liquid helium dewar whose components have been described elsewhere.[2,3] The alkali was evaporated from a water shielded Knudsen effusion source, recently modified to include a quartz microbalanace (Veeco, QM-301). Matrices were grown at or slightly above 4.2 K, a 5 h deposition time being typical. The ratio of matrix gas: alkali varied from 20:1 to 70:1 corresponding to, respectively, 0.4 and 0.1 μmol h^{-1} of alkali incident on the sapphire plate. This range of concentration, two to five times greater than the 100:1 ratio used in the trimer experiments,[2,3] was found to give the optimum septemer intensity without causing excessive nucleation. At still greater concentrations, a broad resonance centered near the free electron g value was observed and this may be attributed to a conduction-electron spin resonance spectrum.[3] Annealing by warming the matrix to 30 K, gives a substantial improvement in spectral resolution and may also promote aggregation to Na_7. For argon, no further irreversible changes were observed, provided the matrix temperature (measured with a calibrated carbon resistor and accurate to ± 5%) did not exceed ~ 34 K. The ESR behavior of sodium in nitrogen was more complex. An additional, unassigned spectrum was observed during annealing at 25–26 K. This consists of ~ 16 groups of transitions separated by 45–50 G, but the spacing is irregular. On further warming to 29–30 K, these features were almost entirely replaced by the spectrum attributed to Na_7. At still higher temperatures, the latter spectrum abruptly disappears.

All spectra were recorded on a JEOL ME-3X ESR spectrometer (microwave power indicident on cavity ≃ 2 mW) using 100 kHz magnetic field modulation (peak-to-peak amplitude ≃ 1 G) and phase sensitive detection. The signal from the JEOL lock-in amplifier was further

 0021-9606/83/105946-08$02.10

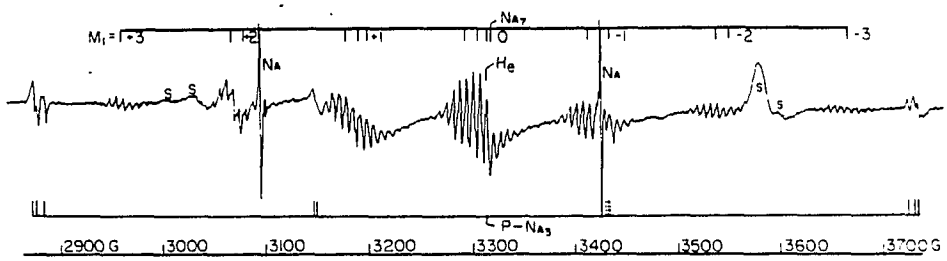

FIG. 1. ESR spectrum of Na_7 in an argon matrix at 33 K. The quantum number M_1 is the nuclear spin projection for 2 equivalent ^{23}Na nuclei. The further structure within $M_1 = \pm 2$, ± 1, and 0 arises from a second order splitting (see the text and Fig. 2). Also shown are atomic sodium, pseudorotating Na_3 and background sapphire signals labeled *S*. The resonance field of a free electron is $H_e = 3312.2$ G.

processed either with an active filter (typically a 1 s time constant for a scan rate of 2 G min^{-1}) or by averaging repetitive scans on a multichannel analyzer (Tracor Northern, TN 1710). Owing to a jitter of approximately ± 0.5 G in the JEOL field scan circuitry, the expected signal-to-noise enhancement of long acquisition times was never fully realized. The resonance frequency of the cavity plus sapphire plate and matrix sample was 9.2824(2) GHz over the temperature range 4.2–30 K. Individual spectra were calibrated with a proton magnetometer (Micronow, model 515). Relative and absolute magnetic field positions are judged accurate to ± 0.5% and ± 1 G, respectively.

III. SPECTRA AND ANALYSIS

A. Sodium

Figure 1 shows, for an argon matrix at 31 K, the ESR spectra of atomic sodium,[1] pseudorotating Na_3,[4] and the newly observed cluster species, most likely Na_7. The septemer spectrum consists of seven groups of first derivative transitions (isotropic hf splitting a_1) centered near the resonance field $H_e = 3312.2$ G of a free electron. Despite a careful search, features corresponding to a zero-field splitting or to changes of greater than unity in the electron spin projection were not observed, thus implying a cluster with an odd number of sodium atoms. Except, possibly, as transient events in nitrogen matrices, no phenomena characteristic of exchange or other dynamic process have been observed.

As shown in more detail in Fig. 2, the septet structure may be assigned to two magnetically equivalent $I = 3/2$ nuclei whose total nuclear spin angular momentum has magnitude J_1 and projection M_1, where $M_1 = +3, \ldots, -3$ and $3 \geq J_1 \geq |M_1|$.[2-4] Including terms up to third order in a_1/H,[11,12] the transition fields of each origin are [2,4]

$$H(J_1, M_1) = \frac{g_e}{g_0}(H_e - a_1 M_1) - \frac{1}{2}\left(\frac{g_e}{g_0}\right)^2 \frac{a_1^2}{H}\left[J_1(J_1+1) - M_1^2\right] - \frac{1}{2}\frac{a_1^3}{H^2} M_1\left[M_1^2 + \tfrac{1}{2} - J_1(J_1+1)\right], \quad (1)$$

where g_0 is the (isotropic) g value of the cluster and H is the magnetic field at a particular transition.

Each (J_1, M_1) origin in Fig. 2 corresponds to the center of a superhyperfine (shf) pattern of at least 16 equally spaced transitions. This further structure is described by adding to Eq. (1) a term

$$H(M_2) = -\frac{g_e}{g_0} a_2 M_2 , \quad (2)$$

where $a_2 \ll a_1$ is the shf splitting constant and $M_2 = \pm 1/2, \pm 3/2, \ldots$ is a nuclear spin projection quantum number[13] for this second group of magnetically equivalent $I = 3/2$ nuclei.[14]

Because of the marked decrease in intensity with increasing $|M_2|$, it has proved difficult to assign an upper bound to $|M_2|$ and thus to the number of equivalent sodium atoms responsible for the shf structure. Our original assessment[15] that we were observing Na_5 arose from an insufficient signal-to-noise (S/N) ratio leading to an assignment of $|M_2| \leq 9/2$, as would be expected of three equivalent $I = 3/2$ nuclei. That the spectral carrier is indeed larger than the pentamer is apparent from Fig. 3, which shows a detail (at $T = 4.2$ K) of the low field wing of $M_1 = +3$ and the high field wing of $M_1 = -3$. Although the ESR intensity at 4.2 K is significantly greater than at 30 K,[16] there is extensive overlap with the spectrum[2] of stationary Na_3 at lower temperatures. Clearly evident in Fig. 3 are transitions $M_2 = -15/2$ and $M_2 = -15/2$ for $M_1 = +3$ and -3, respectively. For $M_1 = -3$ [Fig. 3(b)], possible $M_2 = -17/2, -19/2, \ldots$ are obscured by the more intense features of pseudorotating Na_3.[4] As shown in Fig. 3(a), there is no overlap with the low field wing of $M_1 = +3$, even at 4.2 K. Here, however, the S/N ratio is still insufficient to rule out the presence of $M_2 = +17/2, +19/2, \ldots$.[17] Thus, for example, a cluster Na_9 with one set of two equivalent nuclei (the septet structure) and a second set of seven equivalent nuclei, contributing a 22 line shf ($M_2 = +21/2, \ldots, -21/2$), would also be consistent with the experimental spectra. As discussed in the following section, the number of seven (or greater) atom geometries having spin populations consistent with those measured is very limited.

For Na_7, the shf arising from five equivalent $I = 3/2$ nuclei should have relative intensities $1:5:15:\ldots:155:155:\ldots:1$ corresponding to $M_2 = -15/2, -13/2, -11/2, \ldots, -1/2, -1/2, \ldots, -15/2$. Measured intensities, while approximately in agreement with those ex-

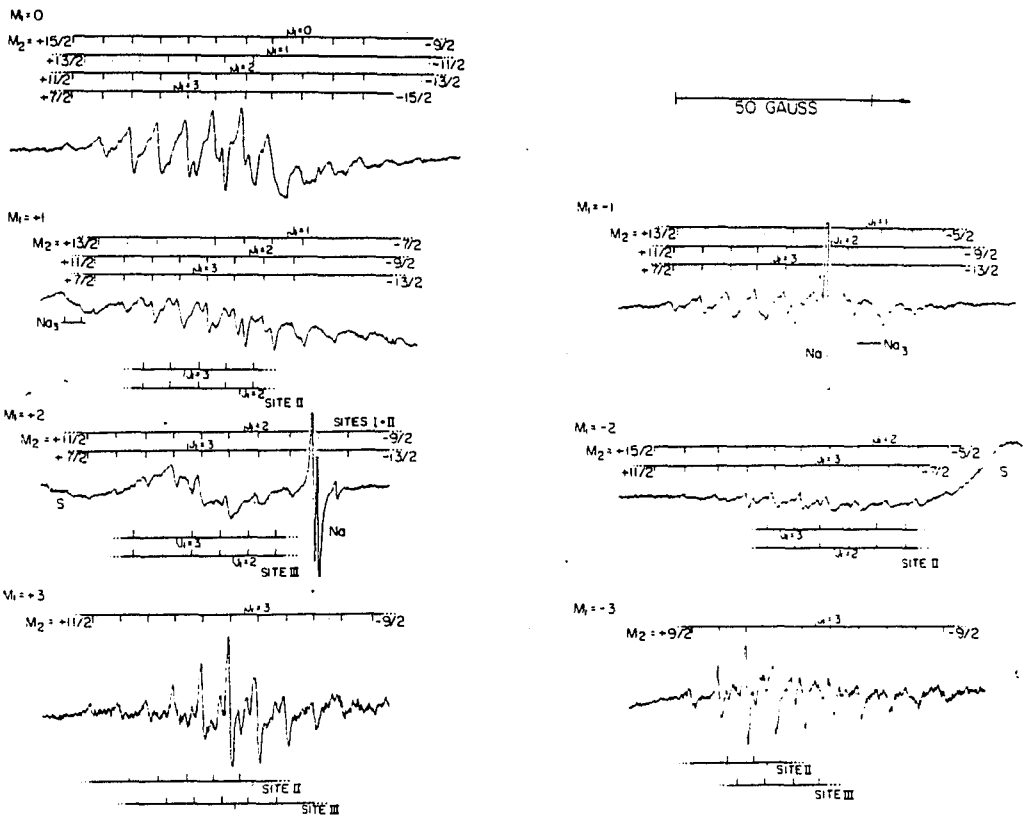

FIG. 2. Detail of Na_7 in argon at 32 K, showing matrix site effects. Full and broken lines denote, respectively, measured transition fields and those calculated using Eqs. (1) and (2) and the parameters of Tables I and II. Subscripts 1 and 2 designate different groups of equivalent nuclei with magnetic quantum numbers (J_1, M_1) and M_2, respectively. The gain for $M_1 = \pm 3$ is four times that of the other components. The remaining notation is the same as Fig. 1.

pected for Na_7, are sufficiently uncertain that Na_9 (or perhaps Na_{11}) is not precluded by these data. For example, the ratio of shf intensities is neither the same for each (J_1, M_1) component nor symmetric about its origin. These effects apparently arise from overlap of partially resolved (J_1, M_1) components, the presence of different matrix sites each with a slightly different g_0, a_1, a_2 and, possibly, a weak and unresolved anisotropic hf interaction.[18] Thus, while an assignment of our spectrum to Na_7 seems most likely, the possibility of a larger cluster species cannot be ruled out. It is hoped that experiments, currently in progress,[19] on the analogous lithium clusters ($^6Li_7$ and $^7Li_7$) will unambiguously resolve this question.

Table I compares the observed $H(J_1, M_1)$ with those calculated using Eq. (1) and the best fit parameters g_0 and a_1 given in Table II. Estimated errors, given in parentheses in Table II, are one standard deviation uncertainty in the fit to the experimental data. However, the calibration errors noted earlier, $\pm\frac{1}{2}\%$ and ± 1 G in the relative and absolute field positions, respectively, are larger. Also listed in Table I are average $\langle a_2 \rangle$ values determined for each (J_1, M_1) component; the mean of these values is given in Table II with an estimated error of one standard deviation. Labeled II and III in Fig. 2, several additional but weaker features can be assigned to clusters trapped in more than one distinct matrix site. These effects are well known for alkali atoms[1] and are also observed for Na_3[2,4] and Li_3[20] in argon matrices. The two minor sites shown in Fig. 2 were fit to Eqs. (1) and (2) with g_0, a_1, and a_2 values included in Table II. A spectrum almost identical to that shown in Fig. 1 was observed for sodium in a nitrogen matrix. Again, the assignment of seven groups of transitions to two equivalent $I = 3/2$ nuclei is excellent, with g_0, a_1, and a_2 (Table II) similar in magnitude to the corresponding parameters for an argon matrix.

Table II also includes isotropic spin populations ρ_1 and ρ_2 obtained by dividing a_1 and a_2 by the hf splitting constant of the gas-phase atom.[21] Because of their large

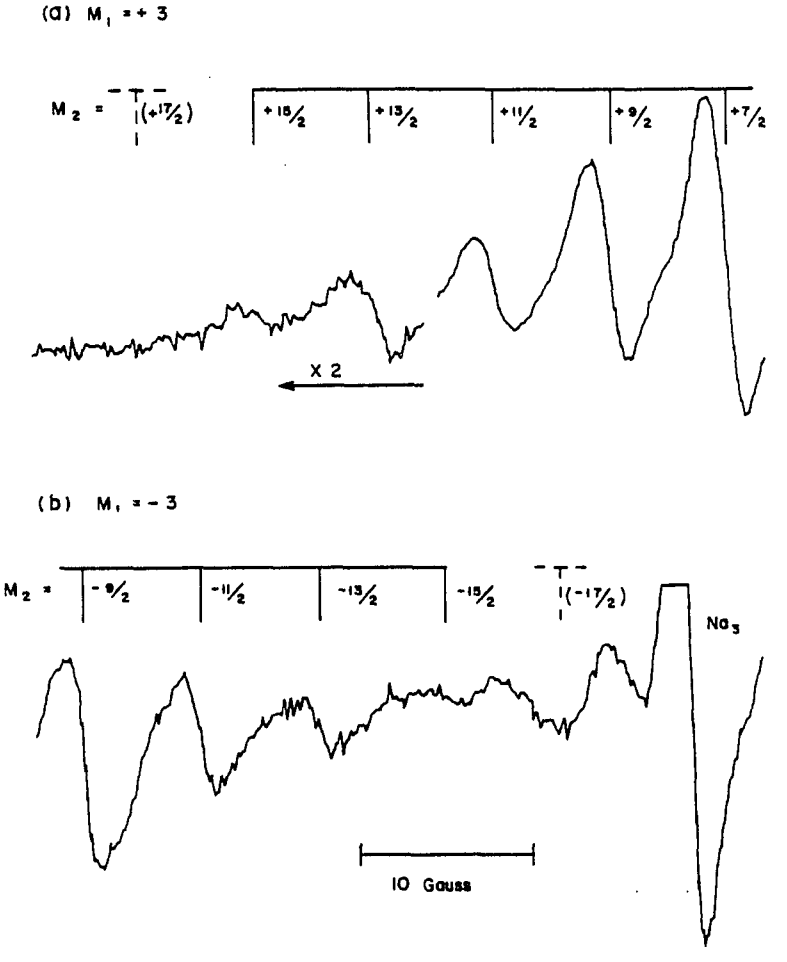

FIG. 3. Part of the spectrum of Na_7 in argon at 4.2 K with (a) low field wing of $M_1 = +3$ and (b) high field wing of $M_1 = -3$ obtained by signal averaging for 8 and 3 h, respectively. Transitions $M_2 = \mp 17/2$ denote estimated line positions for a hypothetical nine atom cluster having seven equivalent ^{23}Na nuclei.

magnitude both a_1 and ρ_1 are assumed to be positive. However, a_2 is small and may be either positive or negative.

B. Potassium

Figure 4 shows the ESR spectrum of $^{39}K_7$ in an argon matrix at 31 K. The spectral assignment closely follows that of the sodium cluster, except that third order corrections to the hf energy, the last term of Eq. (1), were ignored. Table III shows a comparison of measured transition fields (full lines in Fig. 4) with those calculated using Eqs. (1) and (2) and the best fit parameters of Table III.

Because of extensive overlap with the intense features of pseudorotating K_3,[3,22,23] a determination of the maximum $|M_2|$ value for these spectra is even more difficult than with sodium.[24] However, as shown in Table II, the experimental spin populations ρ_1 and ρ_2 of the potassium cluster are nearly identical to those of Na_7. Thus, it is reasonable to assume that the two spectra arise not only from clusters of the same size but also from molecules having a similar or identical structure and geometry. An analogous correspondence between the spin populations of Na_3 and K_3 (both stationary and pseudorotating) has been noted elsewhere.[3,4,20]

IV. DISCUSSION

The ESR spectra determine a characteristic symmetry for the wave function of the unpaired electron. Thus, regardless of stoichiometry, the nuclei of both the sodium and potassium cluster fall into two distinct groups: one set composed of two equivalent nuclei and a second of (at least) five equivalent nuclei. In addition, the hf data (Table II) show that the isotropic spin population on the two equivalent atoms (~ 37%) is large, while

TABLE I. Comparison of measured (matrix site I) and calculated transition fields, $H(J_1, M_1)$ defined in Eq. (1), for Na_7 in argon at 32 K. Experimental $\langle a_2 \rangle$ are average shf constants for individual (J_1, M_1) with uncertainties (see the text) in parentheses. Units are Gauss.

		$H(J_1, M_1)$			
M_1	J_1	Meas.	Calc.	Differences	$\langle a_2 \rangle$
+3	3	2956.6	2956.3	+0.3	6.80(6)
+2	2	3077.0	3076.6	+0.4	6.69(5)
	3	3063.6	3064.0	−0.4	6.63(4)
+1	1	3196.9	3196.8	+0.1	6.73(7)
	2	3188.4	3188.5	−0.1	6.54(5)
	3	3175.3	3175.8	−0.5	6.54(5)
0	0	3317.5	3317.1	+0.4	6.70(5)
	1	3312.5	3312.9	−0.4	6.58(7)
	2	3304.2	3304.5	−0.3	6.64(4)
	3	3290.8	3291.7	−0.9	6.60(3)
−1	1	3433.6	3433.3	+0.3	6.95(5)
	2	3424.9	3424.8	+0.1	6.58(9)
	3	3411.7	3412.2	−0.5	6.57(6)
−2	2	3549.6	3549.3	+0.3	6.59(6)
	3	3536.4	3536.7	−0.3	6.60(4)
−3	3	3665.6	3665.4	+0.2	6.85(5)

TABLE II. Magnetic parameters for sodium and potassium septemers with estimated errors (see the text) in parentheses. Also given are constants for the principal matrix site of the atom. Units of a_1, a_2 are Gauss.

Species[a]	g_0	a_1	$\pm a_2$	ρ_1[b]	$\pm\rho_2$[b]
Na	1.9995(4)	331.0(6)		1.047	
Na_7(I)	1.9994(1)	118.16(4)	6.66(12)	0.374	0.021
Na_7(II)	2.0023(1)	115.9(1)	6.3(2)	0.367	0.020
Na_7(III)	2.0027(1)	117.0(1)	6.5(2)	0.370	0.021
$Na_7(N_2)$	2.0023(3)	110.7(2)	6.8(1)	0.350	0.022
K	1.9990(1)	86.8(2)		1.053	
K_7	2.0017(1)	30.55(6)	1.79(2)	0.371	0.022

[a]Roman numerals in parentheses designate matrix sites. Except for $Na_7(N_2)$, data pertain to argon matrices at ~30–32 K.
[b]Isotropic spin populations ρ_1 and ρ_2 are ratios of a_1 and a_2 to hf constant of free atom, $a(^{23}Na) = 316.09$ G or $a(^{39}K) = 82.38$ G from Ref. 21.

that on each of the remaining atoms is only ± 2%. As for Na_9 and K_3,[2,3] this spin distribution is both qualitatively and quantitatively different from a simple combination of the spin populations of possible precursor molecules. At least in the case of sodium, spin populations are relatively unaffected by matrix site effects

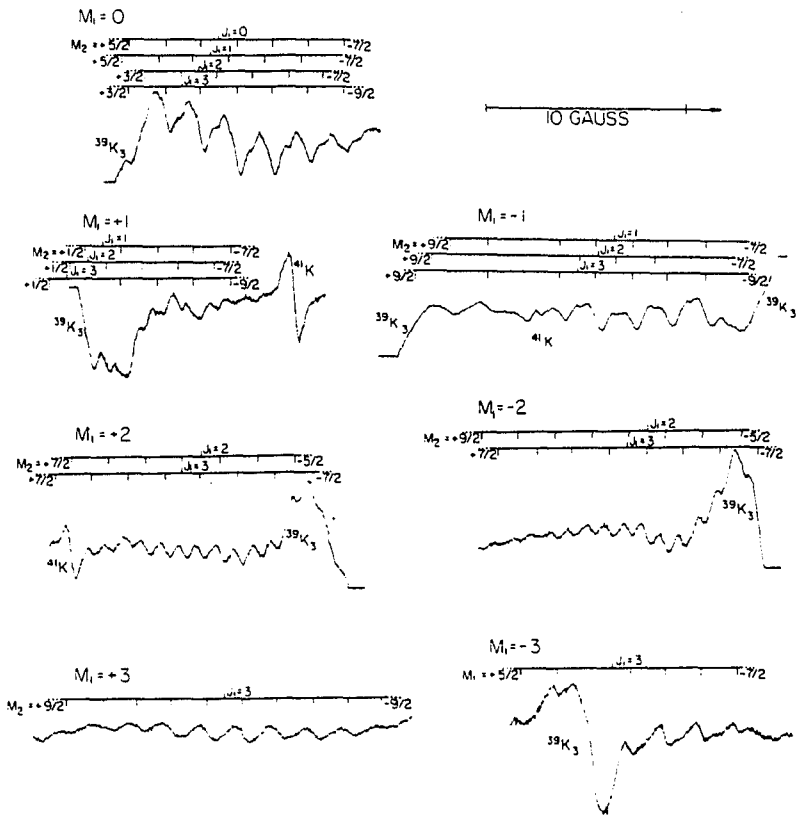

FIG. 4. ESR spectrum of $^{39}K_3$ in an argon matrix at 31 K with notation similar to that of Figs. 1 and 2. Also shown are weak ^{41}K transitions and intense spectra arising from pseudorotating $^{39}K_3$. $H_0 = 3312.2$ G.

TABLE III. Comparison of measured and calculated transition fields for K_7 in argon at 31 K. Notation is the same as Table I. Units are Gauss.

		$H(J_1, M_1)$			
M_1	J_1	Meas.	Calc.	Differences	$\langle a_2 \rangle$
+3	3	3221.3	3221.2	+0.1	1.79(1)
+2	2	3251.9	3251.9	0.0	1.82(1)
	3	3250.9	3251.0	−0.1	1.79(1)
+1	1	3282.7	3282.6	+0.1	1.80(3)
	2	3281.9	3282.0	−0.1	1.80(4)
	3	3280.9	3281.2	−0.3	1.80(1)
0	0	3313.6	3313.3	+0.3	1.80(1)
	1	3313.2	3313.0	+0.2	1.80(1)
	2	3312.6	3312.4	+0.2	1.79(1)
	3	3311.8	3311.6	+0.2	1.80(3)
−1	1	3343.8	3343.7	+0.1	1.75(3)
	2	3343.0	3343.1	−0.1	1.78(3)
	3	3342.1	3342.3	−0.2	1.75(3)
−2	2	3373.7	3374.1	−0.4	1.81(1)
	3	3372.7	3373.3	−0.6	1.80(1)
−3	3	3404.9	3404.5	+0.4	1.79(1)

or even by the matrix material (Ar or N_2) itself. Consequently, the ESR results imply that the new clusters should be viewed as chemically bound molecules having a preferred structure and geometry and not as an aggregation of smaller units (dimers, trimers, etc.) nor as entities which owe their properties to a stabilizing influence of the matrix host.

A large number of simple Huckel (SH) structures were examined in order to find cluster geometries with molecular orbitals, partially occupied or otherwise, of the same symmetry as the ESR spin distribution. In addition to the 15–20 arrangements assumed for M_7 molecules, SH calculations were also performed on M_9 (15 geometries), M_{11} (7 geometries), and M_{13} (17 geometries, including the icosahedron, cubo-octahedron, etc.). Since the ESR spectra imply $S = 1/2$, even numbered clusters were not considered. The total number of arrangements of n atoms increases very rapidly with cluster size and this limits the choice of geometries to those having a relatively high symmetry. For the large clusters, in particular, this selection was simplified by adopting, among others, the proposed or actual structures of bare transition metal clusters[25,26] and organometallic cluster compounds.[27] Because the calculations make no attempt to optimize bond lengths, bond angles, or energies, there is some ambiguity as to the details of a particular geometry. Thus, for example, the SH method does not distinguish between a linear chain with $D_{\infty h}$ symmetry and a "zig–zag" arrangement. Although the ESR spectra give indirect evidence for a significant s-p hybridization (see below), the SH basis set, a single function from each atom, does not allow the "subtlety" of including both s and p character. Even though no attempt was made to parametrize the calculations for Na or K, the *relative* stability of the different bonding arrangements does seem to be meaningful. Recent diatomics-in-molecules (DIM) calculations[28] have determined the binding energies for several alkali pentamer geometries. The structures considered were a trigonal bipyramid (point group D_{3h}), a square pyramid (C_{4v}), a ring (D_{5h}), a straight chain ($D_{\infty h}$), a branched chain (C_{2v}), and a tetrahedron (T_D). For M_5, the order of stability predicted by the SH method, $(D_{3h} \simeq C_{4v}) > D_{5h} > (D_{\infty h} \simeq C_{2v}) > T_D$, exactly follows the DIM results for Li_5, Na_5, and K_5.

Two general trends emerge from the SH calculations. First, except in the case of an "accidental equivalency,"[29] the only molecular orbitals with n-2 atoms equivalent and significantly different from the remaining pair of equivalent atoms are those in which the wave function has a node at all n-2 nuclei. As in the case of Na_3 and K_3,[2,3] spin polarization effects, not included in the SH model, would be expected to induce a small (most likely negative)[3,4,22,23] spin density at these nodal positions.

The second prediction (excepted by a few orbitally degenerate septemer geometries) of the SH calculations is that for *all cluster sizes* only *two arrangements* of atoms give rise to an orbital with symmetry to match the ESR spectra. These are T structures with nominally C_{2v} symmetry and bipyramidal geometries having a ring of n-2 equatorial atoms plus two apical atoms. For $n = 3$–13, the former have a nondegenerate half-filled orbital with $\rho_1 = 0.50$ for each of the "arm atoms" and a node at the remaining n-2 nuclei. For $n \geq 7$, however, this structure is 30%–35% less stable than the most strongly bound clusters of the same size. If relative Huckel energies have significance, as suggested by the data for M_5, then a T structure seems unlikely. Figure 5(a) shows the orbital scheme for M_7 with a pentagonal bipyramidal geometry (point group D_{5h}). The unpaired electron occupies a nondegenerate orbital with SH spin populations, $\rho_1 = 0.50$ on the two axial atoms and $\rho_2 = 0$ on each of the equatorial atoms. Although a realistic basis set and spin polarization effects will modify these values, the a_2' symmetry classification of this orbital will remain unchanged. For cluster sizes M_9–M_{13}, the ring bipyramidal structure is relatively stable and always has one (not always half-filled) orbital of the type shown in Fig. 5(a).

Figure 5 shows two further septemer geometries which, with appropriate Jahn–Teller distortions, might also give rise to the observed ESR spectrum.[30] The D_{3h} structure [Fig. 5(b)][31] has a doubly degenerate e' level with orbital composition (θ, ϵ) similar to that of the equilateral triangle.[2,3] Although unoccupied at the SH level, these orbitals might be more stable in the true septemer. If, in addition, the degeneracy of the e' orbital is lifted by a Jahn–Teller distortion, then the ϵ orbital would have $\rho_1 = 0.50$ on two atoms and $\rho_2 = 0$ on the remainder.[32] The octahedral structure [Fig. 5(c)] is threefold degenerate. Since each orbital has the sought after orbital composition, an elongation along any axis would give a singly occupied orbital of the correct symmetry. The degenerate structures would be expected to have rather flat potential surfaces with multiple energy minima. As in the case of the alkali trimer,[2,4] this situation would favor a relatively fluxional geometry. However, the ESR spectra are more characteristic of a static geometry and show no evidence of

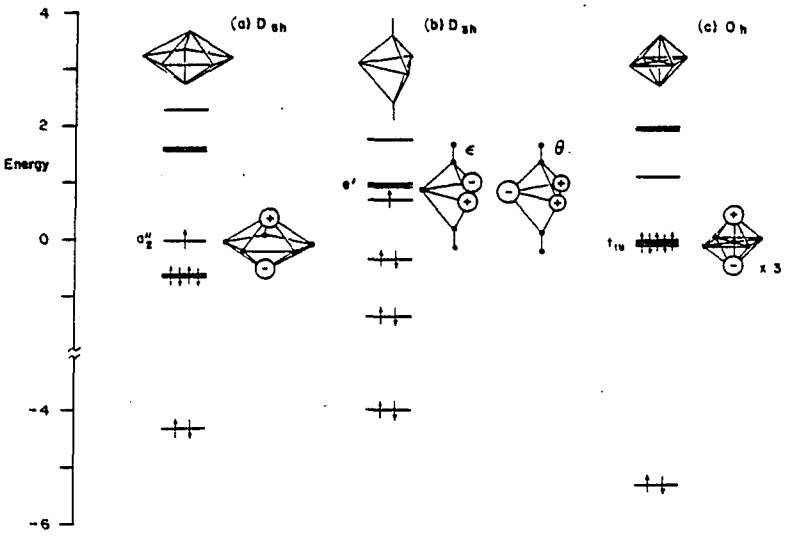

FIG. 5. Simple Huckel orbitals for alkali septemer molecules with (a) pentagonal bipyramidal, (b) D_{3h}, and (c) octahedral geometries. Energies are in units of the Huckel resonance integral β.

exchange effects. Thus, while comparable in energy to the D_{5h} arrangement, the degenerate structures seem less likely.

A further consequence of degenerate or near degenerate energy levels is the increasing likelihood of spin state $S > 1/2$. For high spin molecules the zero field splitting may cause absorption over a prohibitively large range of magnetic fields and so make the powder spectra of these species relatively difficult to detect. If sufficiently large, this interaction may even preclude the observation of all X-band transitions.[33] An additional consequence of degeneracies is the possibility of large and anisotropic g shifts which, analogous to the situation for matrix isolated $^2\pi$ molecules,[33] also makes detection difficult. In this context, it is interesting to note that the two most stable pentamer geometries (D_{3h} and C_{4v}) have, at the SH level, orbitally degenerate ground states and it may be for this reason that neither Na_5 nor K_5 were observed in our matrices.[34]

Although the SH method can give spin populations in qualitative agreement with those observed, an accurate prediction requires either configuration interaction or unrestricted spin orbitals and a more extended basis set, in particular the inclusion of p orbitals. Since the total isotropic spin populations ($\Sigma\rho$) of Table II do not sum to unity, the difference $1 - \Sigma\rho$ gives an approximate measure of the average p character of the unpaired electron. However, since the sign of ρ_2 is not determined by a single ESR spectrum, there is some ambiguity as to these values. If $\rho_2 > 0$ then, for an alkali septemer,[35] $\Sigma\rho \simeq 0.85$ for both sodium and potassium. Thus, the average p character is approximately 15% or very close in magnitude to the 11%–13% found for the corresponding trimers.[2–4] On the other hand, if $\rho_2 < 0$, as in the case of Na_3 and K_3, then $\Sigma\rho \simeq 0.64$ which implies a p character of 36%. For this situation, the mean hybridization of the septemer is close to the 30%–38% value of solid sodium and potassium.[20,36] For $\rho_2 < 0$, therefore, the ESR data suggest a tendency to greater hybridization with increasing cluster size and a close approach to the bulk metal value for the polyatomic clusters.

ACKNOWLEDGMENTS

This research was supported in part by the City University of New York Research Award Program and by the National Science Foundation under Grant No. CHE 79-13260.

[1] C. K. Jen, V. A. Bowers, E. L. Cochran, and S. N. Foner, Phys. Rev. 126, 1749 (1962).
[2] D. M. Lindsay, D. R. Herschbach, and A. L. Kwiram, Mol. Phys. 32, 1199 (1976).
[3] G. A. Thompson and D. M. Lindsay, J. Chem. Phys. 74, 959 (1981).
[4] D. M. Lindsay and G. A. Thompson, J. Chem. Phys. 77, 1114 (1982).
[5] See, for example, R. C. McMillan, J. Phys. Chem. Solids 25, 773 (1964); R. T. Schumacher and C. P. Slichter, Phys. Rev. 101, 58 (1956); D. A. Gordon, Phys. Rev. B 13, 3738 (1976).
[6] T. Welker and T. P. Martin, J. Chem. Phys. 70, 5683 (1979). Absorption spectra for small Na clusters have also been reported by G. A. Ozin and H. Huber, Inorg. Chem. 18, 1402 (1979); E. Schumacher, W. H. Gerber, H. P. Harri, M. Hofmann, and E. Scholl, Am. Chem. Soc. Symp. Ser. 179, 93 (1982); M. Hofmann, S. Leutwyler, and W. Schulze, Chem. Phys. 40, 145 (1979).
[7] R. Kubo, J. Phys. Soc. Jpn. 17, 975 (1962); J. Phys. (Paris) C 2, 69 (1977).
[8] Sodium clusters up to Na_8 have been studied using pseudopotential methods. See, J. Flad, H. Stoll, and H. Preuss, J. Chem. Phys. 71, 3042 (1979).
[9] Binding energies for Li_8, Li_9, and Li_{10} have been calculate

using the SCF $X\alpha$ technique. See, J. G. Fripiat, K. T. Chow, M. Boudart, J. B. Diamond, and K. H. Johnson, J. Mol. Catal. 1, 59 (1975).
[10]J. Friedel, J. Phys. (Paris) C 2, 1 (1977).
[11]R. W. Fessenden and R. H. Schuler, J. Chem. Phys. 43, 2704 (1965).
[12]N. M. Atherton, *Electron Spin Resonance* (Wiley, New York, 1973).
[13]Figure 2 assumes $a_2 < 0$. The ESR spectra do not distinguish the sign of this parameter, however.
[14]A bound on the possible inequivalency of these nuclei may be estimated from the ESR linewidth, approximately 1 G for sodium. For example, if four nuclei are equivalent and distinct from the fifth, then the hf constants of these two groups can differ by no more than ~5%.
[15]D. M. Lindsay, Bull. Am. Phys. Soc. 27, 303 (1982).
[16]Magnetic parameters show a small temperature dependence, with individual sites behaving slightly differently. For example, a_1 and a_2 for matrix site I decrease by approximately ½% and 2%, respectively, when the matrix temperature is raised from 4.2 to 32 K. As a consequence, the enhanced intensity at 4.2 K results primarily from a more exact overlap between the spectral features of several matrix sites. These phenomena are strikingly apparent for Li_7 in argon and will be discussed in detail in a forthcoming publication.
[17]Owing to the instrumental problems noted earlier, the approximately 8 h acquisition time of Fig. 3(a) is close to an upper limit for our current spectrometer. For a nine atom cluster, with a shf arising from seven equivalent nuclei, the relative intensities of $M_2 = \pm 15/2$ and $M_2 = \pm 17/2$ are expected to be 3:1. Thus, the predicted intensity of a hypothetical +17/2 component is comparable to the noise level of Fig. 3(a).
[18]The ESR spectra are characteristic of an isotropic g and A tensor and this might imply that the cluster is rotating. A small anisotropy in A would be expected, particularly if $a_2 < 0$. As discussed in Sec. IV, this implies a total p character of approximately 36%. If five atoms share this p character (a likely situation for a pentagonal bipyramid) then $|A_\perp - A_\parallel| \simeq 1$ G. This anisotropy would not be resolved for small $|M_2|$. For large $|M_2|$, the relatively weak parallel features might be obscured by the much stronger perpendicular transitions.
[19]D. A. Garland and D. M. Lindsay (to be published).
[20]D. A. Garland and D. M. Lindsay, J. Chem. Phys. 78, 2813 (1983).
[21]P. Kusch and V. W. Hughes, *Handbuch der Physik*, edited by S. Flügge (Springer, Berlin, 1959).
[22]G. A. Thompson, F. Tischler, D. Garland, and D. M. Lindsay, Surf. Sci. 106, 408 (1981).
[23]D. M. Lindsay, D. Garland, F. Tischler, and G. A. Thompson, Am. Chem. Soc. Symp. Ser. 179, 69 (1982).
[24]Consequently, unlike the case for sodium, the experimental g value for K_7 may be in error by ±1 shf splitting.
[25]R. P. Messmer, S. K. Knudson, K. H. Johnson, J. B. Diamond, and C. Y. Yang, Phys. Rev. B 13, 1396 (1976); C. Y. Yang, K. H. Johnson, D. R. Salahub, J. Kaspar, and R. P. Messmer, Phys. Rev. B 24, 5673 (1981).
[26]C. Bachmann, J. Demuynck, and R. Veillard, Faraday Symp. Chem. Soc. 14, 170 (1980); J. Demuynck, M-M. Rohmer, A. Strick, and A. Veillard, J. Chem. Phys. 75, 3443 (1981).
[27]Particularly helpful is, J. W. Lauher, J. Am. Chem. Soc. 100, 5305 (1978).
[28]S. C. Richtsmeir, D. A. Dixon, and J. L. Gole, J. Phys. Chem. 86, 3942 (1982). Previous, but less comprehensive, DIM calculations also show a similar trend in stability. See, B. T. Pickup, Proc. R. Soc. London Ser. A 333, 69 (1973); A. Gelb, K. D. Jordon, and R. Silbey, Chem. Phys. 9, 175 (1975).
[29]The one striking example of an accidental equivalency occurs for a nine atom cluster with a body centered cubic geometry. For this arrangement (the unit cell structure for the alkali metals), the SH spin populations are $\rho_1 = 0.37$ on two corner atoms, $\rho_2 = 0.04$ on six corner atoms, and $\rho_3 \simeq \rho_2 = 0.03$ on the body atoms. As noted earlier,[14] the ESR spectra might not distinguish an inequivalency of this magnitude.
[30]For M_9, M_{11}, and M_{13}, there appear to be on SH structures with degenerate orbitals (either occupied or vacant) which could give rise to a spin distribution analogous to that of the octahedral or D_{3h} arrangement for M_7.
[31]A distorted D_{3h} structure has been suggested by the authors of Ref. 8.
[32]A similar situation pertains to two triangular pyramids sharing a common apex. Here the partially occupied orbital is fourfold degenerate with a pair of (θ,ϵ) orbitals on each triangular base and nodes on the remaining four atoms.
[33]R. J. Van Zee, C. M. Brown, K. J. Zeringue, and W. Weltner, Jr., Acc. Chem. Res. 13, 237 (1980).
[34]An analogous gap in the ESR spectra of matrix isolated Sc clusters has been noted by L. B. Knight (private communication). Although spectra are assigned to Sc_3 and Sc_7, no Sc_5 was observed. Similarly, both Mn_3 and Mn_5 have ESR spectra but none is observed for Mn_3 or Mn_4. See, R. J. Van Zee, C. A. Bauman, S. V. Bhat, and W. Weltner, Jr., J. Chem. Phys. 76, 5636 (1982).
[35]A reassignment to M_9, say, makes little difference in the total spin populations.
[36]The bulk metal p character may be estimated from the Knight shift and Pauli spin susceptibility of the solid. See Ref. 3, in particular, footnote 64. A more complete discussion of the trend in p character is given in Ref. 20 which also includes data for lithium clusters.

Appendix A.4

Surface Science 106 (1981) 408–414
North-Holland Publishing Company

TEMPERATURE DEPENDENCE IN THE ESR INTENSITIES OF MATRIX ISOLATED POTASSIUM CLUSTERS

G.A. THOMPSON, Frances TISCHLER, Denise GARLAND and D.M. LINDSAY
Department of Chemistry, City University of New York, City College, New York, New York 10031, USA

Received 8 September 1980; accepted for publication 22 October 1980

Two distinct ESR spectra are observed when atomic potassium and argon are codeposited under conditions favorable to aggregation. A pattern of seven equally spaced quartets may be attributed to potassium trimer molecules with a symmetric linear or obtuse angled isosceles geometry. Trimer transitions show a pronounced peaking in intensity at $T \sim 17$ K. A second ESR spectrum consists of ten equally spaced hyperfine components, whose relative intensities approach the predicted distribution for three equivalent ^{39}K nuclei at high temperatures, but show a noticeable "alternating linewidth" effect at lower temperatures. These observations are interpreted in terms of a temperature dependent "pseudorotation" between three Jahn–Teller distortions of a D_{3h} molecule, most likely the trimer.

1. Introduction

In previous work [1, 2] by two of us (G.A.T. and D.M.L.), we reported magnetic parameters for two matrix isolated potassium clusters: The trimer, K_3, and a radical of distinctly different spectral character which we designated K_n. Magnetic parameters for K_3 were found to be markedly similar to those of the isovalent sodium trimer [3]. A spin population analysis for both Na_3 [3, 4] and K_3 [1, 2] shows that the unpaired electron resides almost entirely on two equivalent alkali atoms and has predominantly s- rather than p-character. Polarization effects induce a small spin density on the third atom. These data are consistent with both simple bonding ideas [2, 3] and recent ab initio calculations [5, 6], suggesting a linear or obtuse angled isosceles geometry of ground state symmetry $^2\Sigma_u^+$ or $^2B_2$, respectively. The ESR spectrum of K_n [1, 2] implies that the unpaired electron in this species is equally distributed over *three* ^{39}K nuclei. Suggested [1, 2] candidates for the carrier of this spectrum were the potassium pentamer with a chain structure, for which the unpaired electron would be expected to reside equally on three atoms, or a "pseudorotating" isomer of K_3. In the latter case, all three atoms are made equivalent by rapid exchange between the three obtuse angled geometries which arise from Jahn–Teller distortions from D_{3h} symmetry.

In this paper we present temperature dependent ESR intensities for potassium clusters in argon matrices and show evidence for an "alternating linewidth" effect [7, 8] in the ESR spectrum of K_n. This phenomenon is characteristic of dynamic processes in molecules and

0039-6028/81/0000-0000/$02.50

so provides additional evidence for a pseudorotation interpretation of K_n. A correlation diagram, which relates transition fields for the three obtuse angled trimer molecules, qualitatively explains the observed linewidth alternation in K_n.

2. Experimental

The experimental details have been reported elsewhere [2, 3]. Briefly, matrices are formed by codeposition of excess argon with atomic potassium on a sapphire plate mounted inside an ESR cavity which is itself attached to a variable temperature liquid helium dewar. Cluster formation occurs during deposition and is accomplished by warming the sapphire surface above a nominal deposition temperature of 4.2 K. For spectra shown here, temperature measurements were made with a calibrated carbon resistor and are judged accurate to within ±5%.

3. Hyperfine structure

A detailed discussion of ESR line positions is given in ref. [2]. As an aid to describing the intensity measurements which follow, this section summarizes certain features of the previous analysis. Both K_3 and K_n have doublet ground states ($S = 1/2$) and a well resolved hyperfine (hf) structure arising from the Fermi contact interaction of the electron spin with several $I = 3/2$ nuclei. All observed transitions have a first derivative lineshape as would be expected for powder spectra having an isotropic g tensor ($g = g_0 I$) and an isotropic hf interaction ($A_i = a_i I$).

Magnetic field positions for the trimer spectrum, seven groups of four transitions each, are described by

$$H(M, m_3) = (g_e/g_0)\left[H_e - \sum_{i=1}^{3} a_i m_i\right] = (g_e/g_0)\left[H_e - a_0 M - a_3 m_3\right], \tag{1}$$

where m_1 and m_2 are nuclear spin projection quantum numbers for two equivalent ^{39}K nuclei ($a_1 = a_2 = a_0$) and $M = m_1 + m_2$ is their sum. Since $I = 3/2$, $m_i = \pm 3/2$ or $\pm 1/2$ and M ranges in integral steps from +3 to −3. The quantum number m_3 and hf constant a_3 pertain to the third, non-equivalent nucleus. H_e and g_e denote, respectively, the resonance field and g value for a free electron. An expression similar to eq. (1), but with the added complication of a significant second order hf interaction, has been used to describe the ESR spectrum of Na_3 [3]. Since $a_3 \ll a_0$ [1, 2], eq. (1) gives rise to a septet of quartets as observed. For both K_3 and Na_3, a_0 arises from isotropic spin density on the trimer terminal atoms and is positive. However a_3 arises from spin polarization effects at the central or apical position and may be positive or negative.

Component transition fields for the ten line hf pattern observed for K_n were fit to,

$$H(M') = (g_e/g_0)[H_e - a_0 M'] \,. \tag{2}$$

Here $M' = m_1 + m_2 + m_3$ denotes the z-component of the total nuclear spin angular momentum of three magnetically equivalent ^{39}K nuclei ($a_1 = a_2 = a_3 = a_0$) and H_e, g_e have the same meaning as in eq. (1). For $I = 3/2$, M' ranges from +9/2 to −9/2 in integral steps.

4. Temperature dependence

Both K_3 and K_n are present in freshly deposited matrices at 4.2 K, but their spectra are difficult to deconvolute prior to an initial annealing of the matrix. Subsequently, the ESR intensities of both species are extremely reproducible, depending only upon the matrix temperature. It is these intensity data that we discuss in the present article. Transitions from atomic potassium, also observed in our matrices, show little intensity change with temperature.

Fig. 1 shows a plot of (first derivative) peak heights versus temperature for the $(M, m_3) = (+3, +1/2)$ component of the trimer spectrum and the $M' = -5/2$ component of K_n. The notation (M, m_3) and M' is the same as that introduced in connection with eqs. (1) and (2) of the preceding section. A marked peaking of intensity at $T \sim 17$ K is common to all unobscured (M, m_3) components of K_3 and is also apparent in spectra recorded during annealing. Within experimental error, trimer linewidths remain unchanged (after annealing) over the temperature range 4.2–25 K. This is somewhat surprising, since most mechanisms [2] for the intensity behavior in fig. 1 would be expected to give a broadening of ESR linewidths [9]. For K_n, there is a trend to smaller peak heights at lower temperatures, as shown for $M' = -5/2$ in fig. 2. This trend is common to all component transitions of K_n, but is reversed for $M' = \pm 9/2$ and $\pm 3/2$ below $T \sim 10$ K. Peak areas, approximated to the square of the linewidth times the (first derivative) peak height, show a less pronounced trend with temperature, but these data have a large experimental scatter.

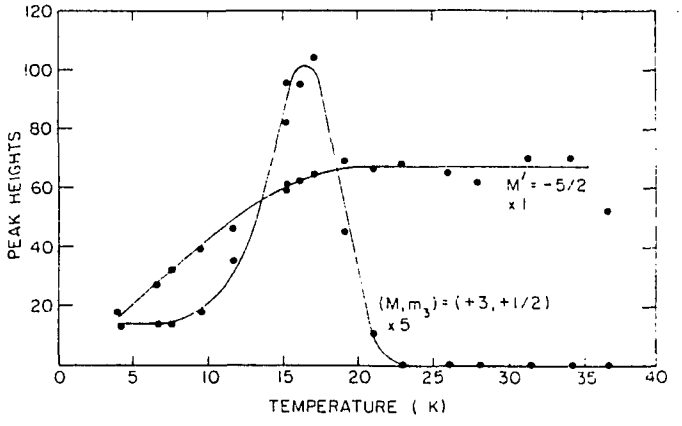

Fig. 1. Temperature dependence of ESR intensities for potassium clusters in argon matrices. $M' = -5/2$ and $(M, m_3) = (+3, +1/2)$ pertain to one component each of, respectively, the ESR spectrum shown in fig. 2 and the ESR spectrum of K_3, refs. [1, 2]. Relative to $M' = -5/2$, trimer intensities are 1/5 of those shown in the figure.

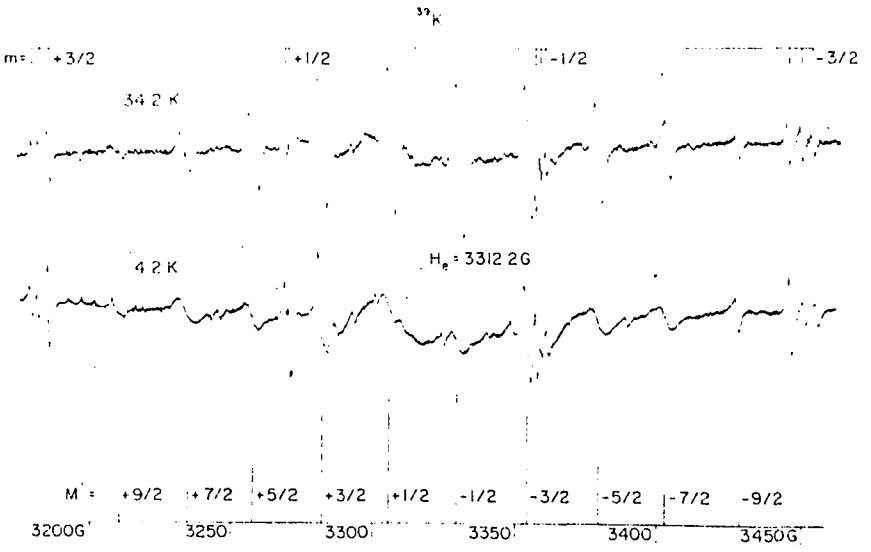

Fig. 2. Ten line spectrum of a radical $^{39}K_n$ in an argon matrix at 4.2 and 34.2 K. The "stick spectrum" shows the predicted intensity distribution for three equivalent ^{39}K nuclei. Also indicated are potassium atom resonances ($m = \pm 3/2, \pm 1/2$) for several matrix sites. $H_e = 3312.2$ G is the resonance field of a free electron for a cavity frequency of 9.2824(2) GHz.

In contrast to the trimer, however, K_n spectra show striking variations in linewidth with temperature, individual M' components being differently affected. Fig. 2 shows spectra recorded at two extreme values of temperature, 4.2 and 34.2 K. A broadening of the low field components, most pronounced for $M' = +9/2$, probably arises from two different matrix sites and gives an asymmetric appearance to the spectra at all temperatures. The "stick" diagram in fig. 2 was computed from eq. (2) and the best fit parameters of refs. [1, 2]. Component intensities, arising from the M' degeneracy of three equivalent ^{39}K nuclei in the high field limit [2, 10], are in the ratio 1:3:6:10:12:12:10:6:3:1. At high temperatures observed intensities do indeed approach the predicted ratio, but this is certainly not the case at $T = 4.2$ K. At low temperatures the $M' = \pm 7/2$, $\pm 5/2$ and $\pm 1/2$ components show pronounced line broadening, whereas $M' = \pm 9/2$ and $\pm 3/2$ are noticeably narrowed. A similar behavior in the ESR spectra of organic radicals in solution is generally termed the "alternating linewidth" effect [7, 8].

5. Discussion

Recent ab initio calculations on Li_3 [8] and Na_3 [9] emphasize the importance of dynamic Jahn–Teller effects in alkali trimer molecules. The principal features of the trimer potential surface are a central peak surrounded by a trough containing three potential wells. The three minima have obtuse isosceles geometry ($^2B_2$ symmetry) and are indis-

tinguishable except for a numbering of the nuclei. Adjacent wells are separated by saddle points which provide a relatively low energy path for intraconverting one obtuse form into another (pseudorotation).

In earlier work [2] it was pointed out that sufficiently fast pseudorotation would lead to an averaged trimer spectrum in which all three ^{39}K nuclei would appear equivalent. Moreover, the measured hyperfine splitting constant for K_n was almost exactly equal to the appropriate average of the measured hf splitting constants for the trimer, when a_3 was assumed to be negative.

Our observation of an alternating linewidth effect is likewise consistent with a pseudorotation mechanism. Fig. 3 shows a partial correlation diagram for the transition frequencies of the three obtuse angled forms of K_3. Each stick spectrum represents a different occupancy of the apical position as indicated at the top of the figure. Transition frequencies, plotted vertically, correspond to the spectral assignment of refs. [1, 2], eq. (1) with

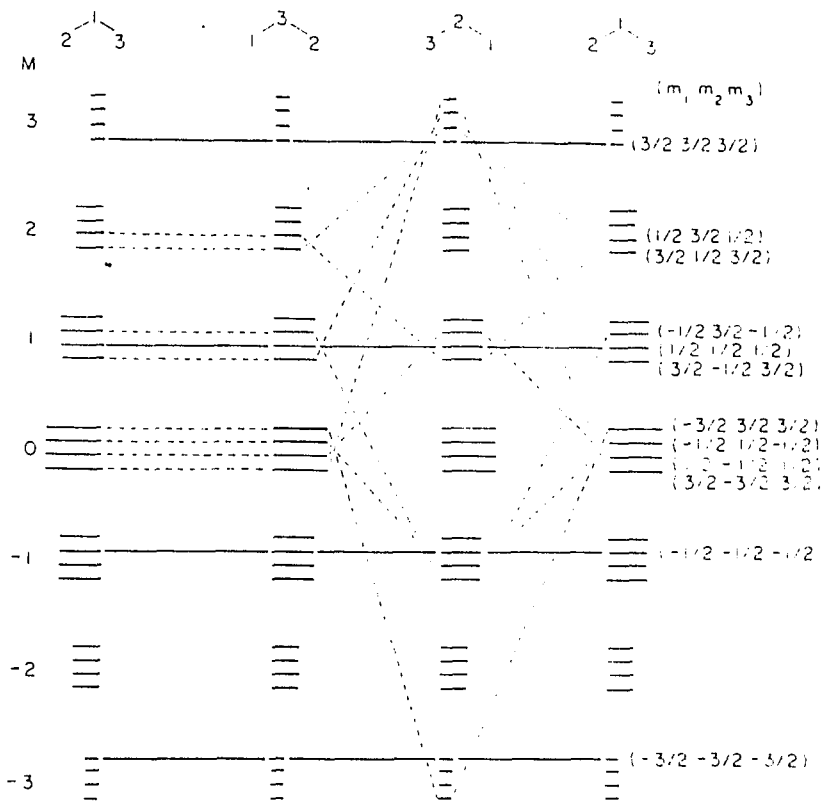

Fig. 3. Partial correlation diagram for the transition frequencies of three obtuse angled $^{39}K_3$ molecules. For an explanation, see text.

$a_1 < 0$. Relative intensities, plotted horizontally, denote the M-degeneracy associated with two equivalent $I = 3/2$ nuclei in the high field limit [3]. On the right hand side of fig. 3 several transitions have been labelled $(m_1 m_2 m_3)$, where $m_i = \pm 1/2, \pm 3/2$ is the magnetic quantum number for distinguishable nuclei $i = 1, 2$, or 3. Adjacent columns are correlated by joining just those transitions which have the same m-value for all three nuclei. Most correlations have been omitted for clarity. It is apparent that, while several transitions are unaffected by exchange between adjacent $^2B_2$ wells, in only four cases do frequencies remain constant when all three obtuse angled species are considered. These latter transitions have $(m_1 m_2 m_3) = (\pm 3/2 \pm 3/2 \pm 3/2)$ and $(\pm 1/2 \pm 1/2 \pm 1/2)$, corresponding to $M' = \pm 9/2$ and $\pm 3/2$, respectively. Thus the situation for K_n may be analogous to exchange effects in organic radicals in solution [7, 8]. At high temperatures, where exchange might be expected to be fast, all three nuclei become equivalent, giving an averaged ten line spectrum, as shown for $T = 34.2$ K in fig. 2. At low temperatures, however, pseudorotation rates may become comparable to the ESR timescale. In this regime $M' = \pm 9/2$ and $\pm 3/2$ are relatively unaffected by exchange and so remain narrow, but $M' = \pm 7/2, \pm 5/2$ and $\pm 1/2$ experience large frequency shifts and become broadened.

In conclusion, it should be pointed out that the pseudorotation mechanism outlined above need not imply that K_n is the potassium trimer. Any cluster for which the Jahn–Teller interaction might induce a similar three fold degenerate distortion is also plausible. For example, this situation also pertains to a potassium pentamer with a trigonal bipyramid structure (D_{3h} point group). For this geometry, simple Hückel calculations predict that the unpaired electron will occupy a doubly degenerate molecular orbital whose wavefunction has a node at both axial atoms. The spin distribution for the three equatorial atoms is identical to that in the equilateral triangle. Consequently a Jahn–Teller distortion to C_{2v} geometry would be expected to have consequences at least qualitatively similar to those in the trimer.

Acknowledgements

This work was supported by the City University of New York PSC-BHE Research Award Program and by the National Science Foundation under grant number CHE 79-13260. Acknowledgement is made to the Donors of The Petroleum Research Fund, administered by the American Chemical Society, for partial support of this research.

References

[1] D.M. Lindsay and G.A. Thompson, Bull. Am. Phys. Soc. 25 (1980) 244.
[2] G.A. Thompson and D.M. Lindsay, J. Chem. Phys. 74 (1981) 959.
[3] D.M. Lindsay, D.R. Herschbach and A.L. Kwiram, Mol. Phys. 32 (1976) 1199.
[4] D.M. Lindsay, D.R. Herschbach and A.L. Kwiram, Mol. Phys. 39 (1980) 529.
[5] W.H. Gerber and E. Schumacher, J. Chem. Phys. 69 (1978) 1692.

[6] R.L. Martin and E.R. Davidson, Mol. Phys. 36 (1978) 1713.
[7] N.M. Atherton, Electron Spin Resonance (Wiley, New York, 1973).
[8] J.H. Freed and G.K. Fraenkel, J. Chem. Phys. 39 (1963) 326;
G.K. Fraenkel, J. Phys. Chem. 71 (1967) 139;
P.D. Sullivan and J.R. Bolton, Advan. Magn. Reson. 4 (1970) 39.
[9] Not necessarily the case if matrix effects such as a phase transition are involved. While absent in pure argon, temperature dependent structural changes have been reported for doped matrices: B.I. Swanson and L.H. Jones, J. Chem. Phys. 73 (1980) 986.
[10] J.E. Harriman, Theoretical Foundations of Electron Spin Resonance (Academic Press, New York, 1978).

7

Appendix A.5

ESR of Stationary and Pseudorotating Alkali Trimer Molecules

D. M. LINDSAY, DENISE GARLAND, FRANCES TISCHLER, and G. A. THOMPSON

City University of New York, Department of Chemistry, City College, New York, NY 10031

The relaxation theory of ESR linewidths is specialized to the case of pseudorotating K_3. Trimer molecules are assumed to fluctuate randomly between the three stable configurations which correspond to static Jahn-Teller distortions from D_{3h} symmetry. A simulated ESR spectrum is shown to be in quite good agreement with the linewidth alternation observed for K_3 in argon at low temperatures. Measured linewidths give approximate correlation and transverse relaxation times, 10^{-8} sec $\lesssim \tau_c \lesssim 10^{-10}$ sec and 10^{-8} sec $\lesssim T_2 \lesssim 10^{-6}$ sec, for the temperature range 4.2 K $\lesssim T \lesssim 20$ K. The temperature dependence of τ_c is well represented by either exponential or power law behavior. Possible pseudorotation mechanisms, including a temperature dependent tunneling, are outlined.

Small metal clusters have received considerable attention because of their possible involvement as "active sites" in a variety of catalyzed reactions. Although not particularly noted for their catalytic activity, alkali clusters have a simple chemical composition and may, therefore, model the more complicated systems in a manner analogous to the role played by the hydrogen atom in atomic structure. Less emphasized is the fundamental nature of alkali clusters per se. Since the ground state of H_3 is not chemically bound, alkali trimers are the most elementary species which can exhibit a Jahn-Teller interaction.

In previous electron spin resonance (ESR) studies of matrix isolated Na_3 (1, 2) and K_3 (3, 4), alkali trimers have been shown to be chemically bound and well described both by simple bonding ideas (1, 3) and by the more sophisticated calculations recently employed for Li_3 (5), Na_3 (6) and K_3 (7). For the potassium trimer in argon, two distinct ESR spectra are observed (3). An obtuse angled isomer corresponds to one of three static Jahn-Teller distortions from D_{3h} symmetry, and is surprisingly similar to the

structure reported for Na_3 (1). A "pseudorotating" isomer is both qualitatively and quantitatively consistent with fast exchange between the three "stationary" trimer geometries. In a preliminary report on the trimer lineshape, the pseudorotating spectrum was shown to exhibit an "alternating linewidth" effect, as would be expected for an exchanging radical (4). In this paper, trimer linewidths are reported and discussed from the viewpoint of a purely phenomenological model involving a stochastic modulation of the trimer hyperfine splitting. Linewidth expressions, derived for the particular case of pseudorotating K_3, lead to a simulated ESR spectrum in quite good agreement with that observed. Approximate values for the trimer correlation and transverse relaxation times are computed. Possible exchange mechanisms are outlined in the last section.

Experimental

The experimental details have been reported elsewhere (1, 3). Briefly, matrices are formed by codeposition of excess argon with atomic potassium on a sapphire plate mounted inside an ESR cavity which is itself attached to a variable temperature liquid helium dewar. Cluster formation occurs during deposition and is accomplished by warming the sapphire surface above a nominal deposition temperature of 4.2 K. For spectra shown here, temperature measurements were made with a calibrated carbon resistor and are judged accurate to within ± 5%.

Trimer Spectra

Alkali trimer molecules have a relatively flat potential surface, whose principal features are a conical peak surrounded by a trough containing three potential wells (3, 5, 6). Figure 1 shows the trimer potential surface plotted as a function of Q_x and Q_y, the doubly degenerate pair of normal mode coordinates for D_{3h} symmetry (3). The central peak corresponds to a degenerate, $^2E'$ ground state of equilateral triangular geometry. The three potential minima have obtuse angled isosceles geometry ($^2B_2$ symmetry) and arise from three possible Jahn-Teller distortions from D_{3h} symmetry. Adjacent minima are separated by relatively low energy saddle points of acute isosceles geometry ($^2A_1$ symmetry). As shown by the broken line in Figure 1 this situation permits the intraconversion of obtuse triangular forms without passing through the energetically remote equilateral triangle ("pseudorotation").

In Reference 3, two distinct ESR spectra were identified for potassium clusters in argon matrices. Both spectra have doublet ground states ($S = \frac{1}{2}$) and a well resolved hyperfine (hf) structure arising from the Fermi contact interaction of the unpaired electron spin with three $I = \frac{3}{2}$ nuclei. Seven groups of four transitions each were assigned to a potassium trimer of $^2B_2$ symmetry whose apical and two equivalent terminal atoms have hf splitting

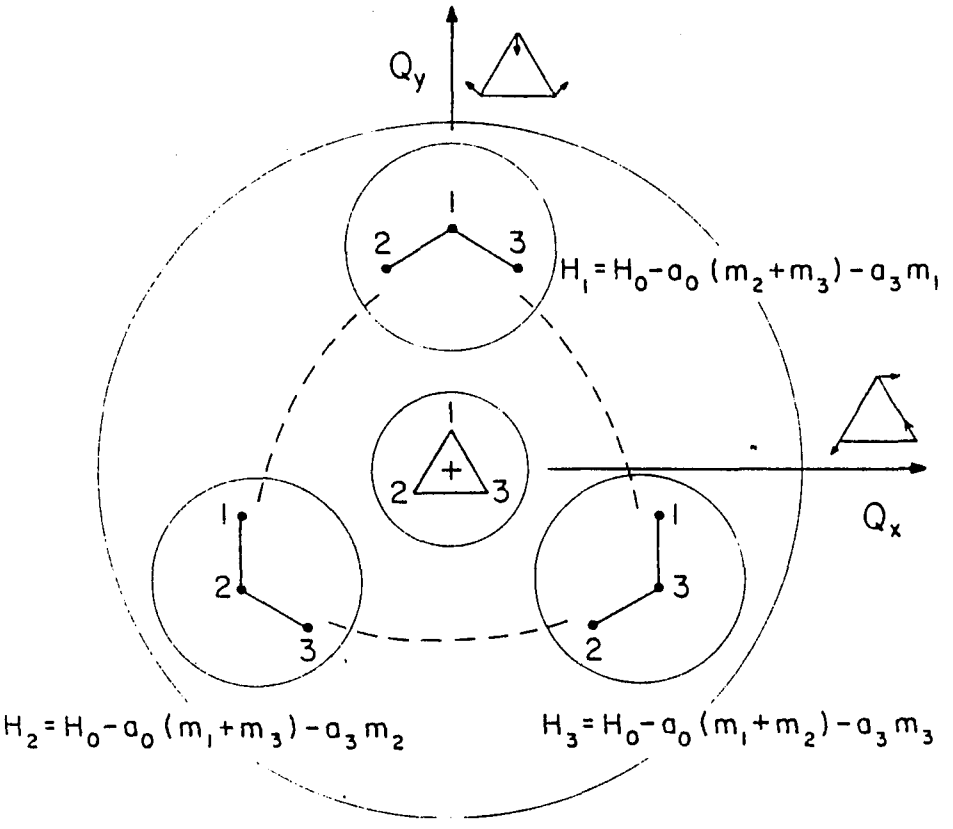

Figure 1. Normal coordinate and real space description of pseudorotating K_3. Circles represent energy contours for the trimer potential surface (3).

constants a_3 and a_0, respectively. Powder spectra were fit to

$$H_i = H_0 - a_0 M - a_3 m_i \qquad (1)$$

in which $m_i = m_1$, m_2 or m_3 is the spin projection quantum number for the apical nucleus and M is the sum of the corresponding quantities for the remaining two atoms. The term $H_0 = g_e/g_0 H_e$, where H_e and g_e denote the resonance field and g value for a free electron, describes the Zeeman interaction for an isotopic g tensor, $\underline{g} = g_0 \underline{1}$. For K_3 (estimated uncertainties in parentheses), $g_0 = 1.9985(5)$ with $a_0 = 39.0(3)$ gauss and $a_3 = \pm 4.7(2)$ gauss (3). The a_0 constant originates from bonding 4s orbitals on the terminal atoms and is positive; a_3, however, arises from spin polarization effects and may be either positive or negative (1, 2, 3).

Figure 1 gives magnetic field positions, derived from Equation (1) with i = 1, 2 or 3, for the three distorted trimer geometries. Since these differ only by a numbering of the nuclei, the ESR spectrum of "frozen" K_3 molecules will consist of a superimposition of indistinguishable obtuse angled trimer species. If, however, adjacent minima can exchange on a sufficiently fast time scale, then an average spectrum,

$$\langle H \rangle = \tfrac{1}{3} \sum_{i=1}^{3} H_i = H_0 - \tfrac{1}{3}(2a_0 + a_3)M' \qquad (2)$$

for which all three ^{39}K nuclei appear equivalent, will be observed. Since $M' = m_1 + m_2 + m_3$ ranges from $+\frac{9}{2}$ to $-\frac{9}{2}$ in integral steps, a ten line hf pattern having $\langle a \rangle = \frac{1}{3}(2a_0 + a_3)$ and a g value identical to that for the "frozen" trimer would be predicted. As discussed in Reference 3, the second ESR spectrum observed for argon matrices exactly fulfills these requirements. Previously denoted K_η, this spectrum was shown to have magnetic parameters $g_0 = 1.9990(5)$ and hf constant a = 24.5(7) gauss, in excellent agreement with the predictions of Equation (2), $g_0 = 1.9985(5)$ and a = 24.3(3) gauss, if a_3 is assumed to be negative.

Figure 2 shows the pseudorotating trimer spectrum at T = 34.2 K (4). Also shown in this figure is a "stick spectrum" in which component intensities, in the ratio 1:3:6:10:12:12:10:6:3:1, reflect the M' degeneracy of three equivalent $I = \frac{3}{2}$ nuclei in the high field limit (3, 4). Magnetic field positions for the simulated spectrum were computed using Equation (2) and the experimental parameters of Reference 3. A broadening of the low field transitions is observed at all temperatures and most likely arises from the trapping of radicals in more than one matrix site. Aside from this asymmetry in the linewidths, the agreement between computed and observed intensity ratios is quite good. At low temperatures, however, component intensities differ markedly from the expected 1:3:6:10:12:12:10:6:3:1 pattern. As shown for T = 4.2 K in Figure 3a the $M' = \pm \frac{7}{2}$, $\pm \frac{5}{2}$ and $\pm \frac{1}{2}$ components show a pronounced line broadening whereas $M' = \pm \frac{9}{2}$ and $\pm \frac{3}{2}$ remain narrow.

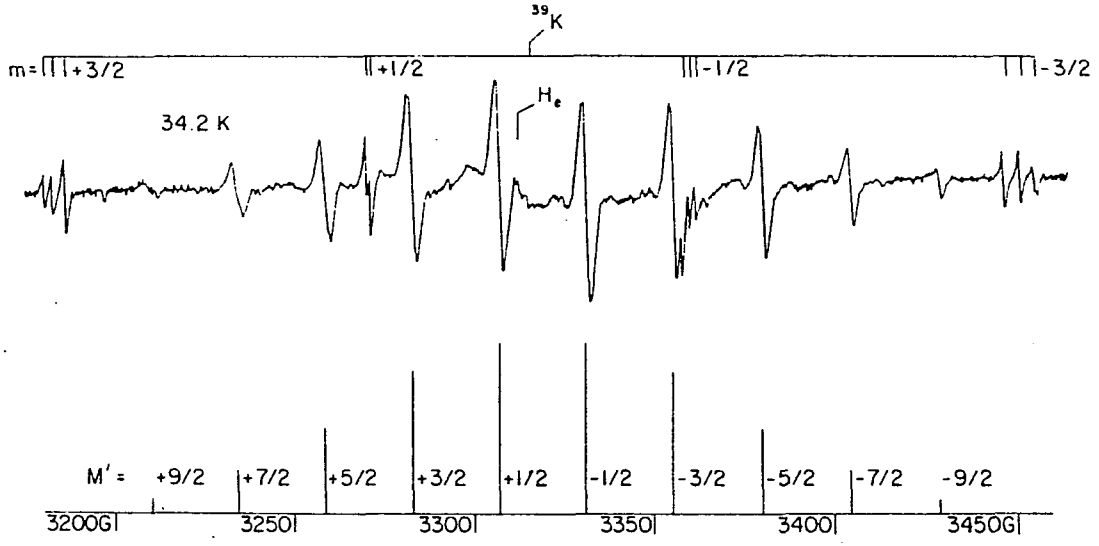

Figure 2. ESR spectrum of pseudorotating K_3 in an Ar matrix at 34.2 K. The "stick spectrum" shows the predicted intensity distribution for three equivalent ^{39}K nuclei. Also indicated are K atom resonances for several matrix sites. $H_e = 3312.3$ G is the resonance field of a free electron for a cavity frequency of 9.2824(2) GHz.

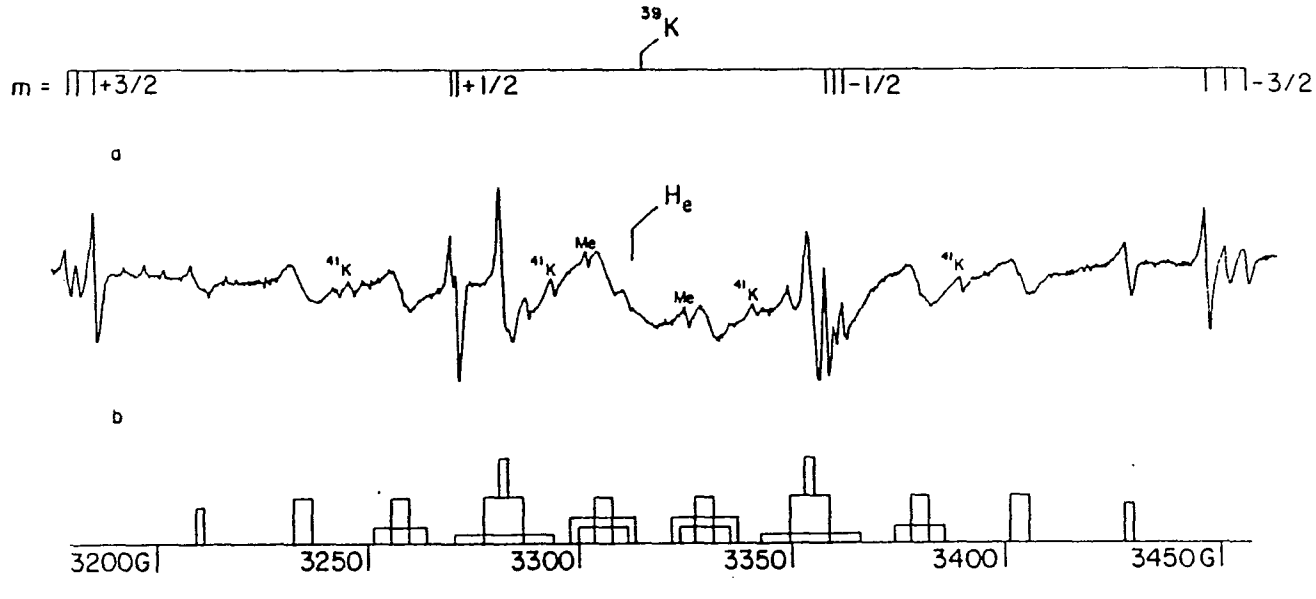

Figure 3. Comparison of observed (a) and simulated (b) spectra for pseudorotating K_3 in Ar matrices at 4.2 K. See also Fig. 2.

In Reference 4, this "alternating linewidth" effect (8) was shown to be consistent with a temperature dependent pseudorotation in K_3. A correlation diagram, which relates transition fields for the three obtuse angled trimer geometries, qualitatively predicts line broadening for $M' = \pm \frac{7}{2}, \pm \frac{5}{2}$ and $\pm \frac{1}{2}$ when pseudorotation is relatively slow. At high temperatures fast exchange leads to the motionally averaged spectrum shown in Figure 2.

Trimer Linewidths

The linewidth analysis for pseudorotating K_3 closely follows the more familiar treatment of relaxation mechanisms in both the NMR and ESR of chemically exchanging systems (8 - 12). Physically, the electron spin interacts with both the static, laboratory magnetic field and a random, fluctuating magnetic field arising from an isotropic hf coupling with the nuclear spins of the trimer. Hyperfine coupling constants are not explicitly time dependent. Rather they assume different values according as to possible occupancies of the three $^2B_2$ minima shown in Figure 1. Thus the hf interaction is time dependent only if the trimer is assumed to "jump" randomly from one well to another.

Two terms may contribute to the trimer linewidth. Diagonal elements of the hf interaction produce a secular modulation of the magnetic levels of both electron spin states without causing transitions. Off diagonal elements, which cause (lifetime broadening) transitions between Zeeman levels, give rise to a non-secular contribution. For either effect to be significant, the hf interaction must have "sufficient" magnitude. Non-secular terms face the additional requirement that the Fourier spectrum of the interaction be rich at the Larmor frequency, $\omega_0/2\pi = 9.3$ GHz. For K_3 in argon, the exchange rate for jumping between adjacent $^2B_2$ minima is never sufficiently fast for non-secular terms to make an appreciable contribution.

Several formalisms have been applied to relaxation in exchanging radicals. Principal among these are modifications of the classical Bloch equations (8, 12) and the more rigorous quantum mechanical theory of Redfield et al. (8 - 11). When applied in their simplest form, as in the present case for K_3, both approaches lead to the same result. Since the theory has been elegantly described by many authors (8 - 12), only those details which pertain to the particular example of K_3 will be presented here. Secular terms contribute to the ESR linewidth (Γ) and transverse relaxation time (T_2) by an amount

$$\Gamma = T_2^{-1} = \int_0^\infty G(\tau)\, d\tau \qquad (3)$$

where the correlation function $G(\tau) = \langle h_i h_j \rangle$ is the appropriate ensemble average for exchanging trimer species, and,

$$h_i = H_i - \langle H \rangle \qquad (4)$$

is defined, through Equations (1) and (2), in order to make $\langle h_i \rangle$ vanish. Although Equation (3) is strictly applicable to absorption spectra having Lorentzian lineshapes, its use in connection with a powder spectrum will have only a minor effect on the conclusions of this paper. The several approximations applied to deriving Equation (3) are well described in Reference 10. Most significant is the neglect of perturbation terms past second order. As a consequence, expressions derived in this section will be valid over most, but not all, of the temperature range employed in the ESR experiments.

Figure 4 shows the "three jump model" used in deriving $G(\tau)$ for pseudorotating K_3. Jumping between adjacent wells ($i = 1$, 2 or 3) is assumed to be a stationary, Markov process which may be characterized by a single, phenomenological rate constant λ. The three potential minima are assumed to be identical so that the probability of occupying any one well at a particular time τ is given by $P_i(\tau) = \frac{1}{3}$. Under these circumstances

$$G(\tau) = \sum_{i,j=1}^{3} h_i h_j P_i(o) P_{ij}(\tau) \tag{5}$$

where the $P_{ij}(\tau)$ are conditional probabilities relating the occupancies of wells i and j at the times $\tau = o$ and $\tau = \tau$, respectively. The $P_{ij}(\tau)$ may be formally derived by application of the Kolmogorov equations of probability theory (13). For the situation represented in Figure 4,

$$\begin{aligned} dP_{ii}/dt &= -2\lambda P_{ii} + 2\lambda P_{ij} \\ dP_{ij}/dt &= -\lambda P_{ij} + \lambda P_{ii} \end{aligned} \tag{6}$$

analogous to the more familiar expressions often encountered in the elementary theory of chemical reactions. For initial conditions $P_{ii}(o) = 1$ and $P_{ij}(o) = 0$, the simultaneous Equations (6) have a solution

$$\begin{aligned} P_{ii}(\tau) &= \tfrac{1}{3}[1 + 2e^{-\tau/\tau_c}] \\ P_{ij}(\tau) &= \tfrac{1}{3}[1 - e^{-\tau/\tau_c}] \end{aligned} \tag{7}$$

where $\tau_c = (3\lambda)^{-1}$ is a characteristic, correlation time for trimer exchange. Substitution of 4 and 7 in the expression 5 gives

$$G(\tau) = \tfrac{2}{9}(a_o - a_3)^2 f(M', k) e^{-\tau/\tau_c} \tag{8}$$

where

$$f(M', k) = M'^2 - 3(m_1 m_2 + m_1 m_3 + m_2 m_3) \tag{9}$$

with $k = m_1 m_2 m_3$. The function $f(M', k)$ is listed in Table I.

Table I. Parameters appearing in linewidth variation of pseudorotating K_3, Equation (10) of text.

M'	k	f(M', k)	D_k
±9/2	27/8	0	1
±7/2	9/8	1	3
±5/2	3/8	1	3
	-9/8	4	3
±3/2	1/8	0	1
	-3/8	3	6
	-27/8	9	3
±1/2	-1/8	1	3
	3/8	4	3
	-9/8	7	6

Also shown in this table are the number (D_k) of transitions (m_1, m_2, m_3) which contribute to a given k. Applying Equation (3) to individual hf components M' = $+\frac{9}{2},--,-\frac{9}{2}$ gives

$$\Gamma(M', k) = \tfrac{2}{9}(a_0 - a_3)^2 \cdot f(M', k) \cdot \tau_c \qquad (10)$$

where the last expression has been notated to show that exchange contributions to the trimer linewidth will, in general, be a sum of Lorentzian functions k. Equation (10) also shows that ESR linewidths are temperature dependent only through a corresponding variation in the correlation time τ_c.

Results for K_3

Table II shows the temperature variation in the peak-to-peak

Table II. Measured linewidth variation for pseudorotating K_3.

	Γ(gauss)			Γ(gauss)	
T(K)	M' = $-\frac{7}{2}$	M' = $-\frac{5}{2}$	T(K)	M' = $-\frac{7}{2}$	M' = $-\frac{5}{2}$
4.2	4.55	4.85	15.2	2.67	2.67
6.7	4.36	4.36	15.3	2.87	2.87
7.6	4.06	3.56	16.2	2.97	2.77
9.5	3.17	3.17	17.1	2.48	2.87
11.7	2.97	3.07	19.1	2.77	2.77
			20-35	2.18	2.57

linewidth for the M' = $-\frac{7}{2}$ and M' = $-\frac{5}{2}$ components for pseudorotating K_3. After an initial annealing of the matrix, measured linewidths (Γ) are independent of the sample history and, within

experimental error, depend only upon temperature. Above T ~ 20 K, ESR linewidths remain approximately constant and are represented by average values, Γ_0, as shown in the last entry of Table II. Γ_0 is taken to be a measure of temperature independent contributions to the ESR linewidth. Although powder spectra are most often inhomogeneously broadened, the exchange contribution to the trimer linewidth is assumed to be given by $\Gamma - \Gamma_0$. Owing to the 10-20% uncertainty in Γ, there is considerable scatter in these differences, particularly at higher temperatures. However, the linewidth data do give approximate values for τ_c and T_2 and allow an experimental test of the "three jump model" introduced in the preceding section.

Figures 3a and 3b show, respectively, observed and simulated spectra for the pseudorotating trimer at T = 4.2 K. Absorption linewidths for the "bar spectrum" were derived from Equation (10), with f(M', k) from Table I and $\frac{2}{9}(a_0 - a_3)^2 = 3.4 \times 10^{15}\ sec^{-2}$ from Reference 3. The correlation time, $\tau_c = 3.8 \times 10^{-9}$ sec, was chosen to give the measured linewidth for M' = $-\frac{7}{2}$, $\Gamma = \Gamma_0 + \Gamma(M', k)$ = 4.6 G from Table II. Relative areas in Figure 3b reflect the D_k degeneracy given in Table I. For ESR transitions, (m_1, m_2, m_3) = $(\pm\frac{7}{2}, \pm\frac{3}{2}, \pm\frac{3}{2})$ and $(\pm\frac{1}{2}, \pm\frac{1}{2}, \pm\frac{1}{2})$, f(M', k) = 0 and trimer exchange is not predicted to contribute to the linewidth. Accordingly, bar spectra for these transitions correspond to $\Gamma = \Gamma_0$ = 2.2 G with ESR intensities equal to that measured for M' = $-\frac{1}{2}$. Aside from the matrix site effects noted earlier, the general features of the observed spectrum are quite well represented in Figure 3b.

Trimer linewidths were compared with both an exponential, $\tau_c = \tau_0 e^{\delta/T}$, and a power law, $\tau_c = \tau_0 T^{-n}$, temperature dependence in the correlation time τ_c. Figure 5 shows the least squares fit for M' = $-\frac{7}{2}$. Both plots represent the experimental linewidth equally well (correlation coefficient, r = 0.90) and the present data are not sufficiently accurate to distinguish between the two interpretations. For reasons given below, the data point at T = 4.2 K was not included in this fit. Similar results (but with r = 0.98) pertain to M' = $-\frac{5}{2}$. Although, as shown in Figure 3b, two k components contribute to this transition, it is most likely that the broad, f(M', k) = 4 and narrow, f(M', k) = 1, features are sufficiently well separated for the latter to dominate the observed M' = $-\frac{5}{2}$ linewidths.

Table III gives the computed parameters for both M' = $-\frac{7}{2}$ and

Table III. Least squares parameters (defined in text) for trimer correlation times (τ_c). Estimated errors are given in parentheses.

	$\tau_c = \tau_0 e^{\delta/T}$		$\tau_c = \tau_c T^{-n}$	
M'	$\tau_0 \times 10^{11}$(sec)	δ(K)	$\tau_0 \times 10^{8}$(sec K^n)	n
$-\frac{7}{2}$	17(5)	16(3)	3.4(21)	1.5(3)
$-\frac{5}{2}$	5.8(11)	21(2)	18(11)	1.9(2)

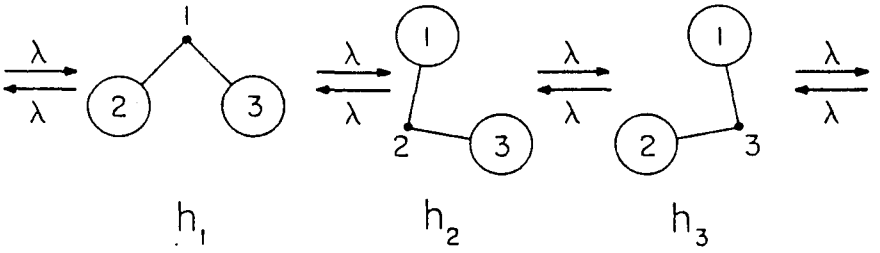

Figure 4. Three-jump model for pseudorotating K_3. See Eq. 4 for definition of h_i.

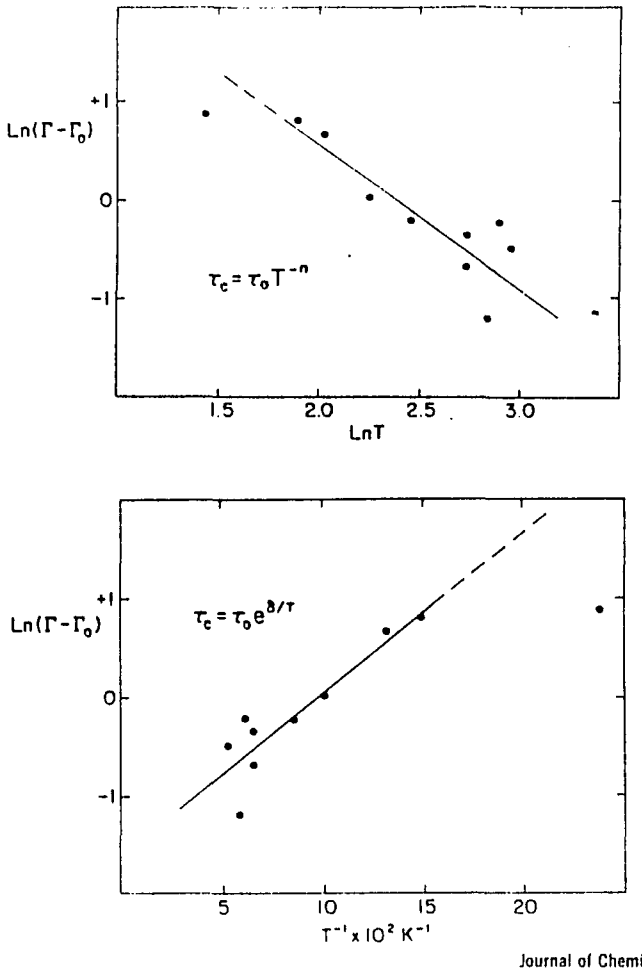

Journal of Chemical Physics

Figure 5. Comparison of measured ESR linewidths (Γ) with assumed temperature dependence in trimer correlation times (τ_c) a, $\tau_c = \tau_0 T^{-n}$ b, $\tau_c = \tau_0 e^{\delta/T}$.

$M' = -5/2$. Estimated uncertainties, in parentheses, represent one standard deviation in the least squares fit to the experimental data. Table IV summarizes several parameters of interest for

Table IV. Temperature variation in correlation time (τ_c), secular linewidth, $\Gamma(M', k)$, and transverse relaxation time (T_2) for $M' = -7/2$. The Larmor frequency $\omega_0/2\pi$ = 9.3 GHz. For an explanation, see text.

T (K)	$\tau_c \times 10^{10}$ (sec)	$\Gamma(M', k)$ (gauss)	$T_2 \times 10^8$ (sec)	$(\tau_c/T_2)^{1/2}$	$\omega_0\tau_c$
4	93	11	3.2	0.54	540
6	24	2.9	12	0.14	140
8	13	1.6	23	0.08	76
10	8.4	1.0	35	0.05	49
15	4.9	0.6	60	0.03	29
20	3.8	0.5	77	0.02	22

pseudorotating K_3. These data were calculated from Equation (10), with $f(M', k) = 1$ and $\frac{2}{3}(a_0 - a_3)^2 = 3.4 \times 10^{15}$ sec^{-2} from Reference 3, together with the least squares τ_0 and δ from Table III. These example results permit a check on several of the approximations alluded to earlier. A necessary condition for second order perturbation theory to be valid is $(\tau_c/T_2)^{1/2} << 1$ (10). As shown by the data in column 5 of Table IV, this approximation breaks down at low temperatures and predicted linewidths become much larger than those actually observed. The ratio of the non-secular to the secular contribution to the trimer linewidth is of order $(1 + \omega_0^2\tau_c^2)^{-1}$ (8 - 12). As shown by the last entry in Table IV line. broadening by non-secular terms is quite negligible over the temperature range T = 4-20 K.

Discussion

Contingent upon the details of the potential surface for K_3, several mechanisms may give rise to the observed temperature dependence in τ_c. If the ground vibronic state for the trimer is of order kT below the energy barrier to pseudorotation, then the correlation time (inversely proportional to the rate constant for exchange) would be expected to show Arrhenius type behavior. Alternatively, the trimer ground state might lie above the pseudorotation barrier, as has been suggested for Li_3 (5). In this situation a fast, but temperature independent, exchange would be predicted. However, since the trimer potential surface is markedly flat, matrix effects may play a particularly important role. Thus the matrix might "lock" the trimer into an obtuse angled geometry at some temperatures but be sufficiently fluid to allow pseudorotation at others.

For Na_3, which is expected to be more closely analogous to

the potassium trimer than Li_3, Martin and Davidson (6) estimate a zero point vibrational energy $\omega \sim 85$ cm^{-1} with a barrier to pseudorotation, $2\beta \sim 200$ cm^{-1}. Particularly critical for Jahn-Teller systems (14), is the distortion parameter ρ_0 (Δ in the notation of (6)). Referring to Figure 1, ρ_0 is the radial distance from the conical peak to the average energy minimum in the trough region of the trimer potential surface. For Na_3, $\rho_0 \sim 0.5$ Å (6). If vibrational frequencies, potential parameters, and bond distances scale according to, respectively, the force constant, bond energy, and internuclear distance of the corresponding alkali dimers, then, very approximately, $\omega \sim 65$ cm^{-1} with $2\beta \sim 150$ cm^{-1} and $\rho_0 \sim 0.6$ Å for K_3. Consequently the ground vibronic level of K_3 is some 85 cm^{-1} below the pseudorotation barrier and, for $4 \lesssim T \lesssim 35$ K, exchange can only occur by quantum mechanical tunneling. This rate may be approximately calculated using a WKB method similar to that applied to the more familiar case of ammonia inversion (15). Using the previously estimated parameters for K_3 (reduced mass, $\mu = \frac{2}{3}m$ = 26 amu) and numerical integration of an assumed cosine potential we find a tunneling frequency of order 1 GHz.

Although temperature dependent tunneling is not, of course, to be expected for gas-phase molecules, its occurence for transition metal complexes in the solid phase has been well documented (14, 16, 17). Even in carefully prepared crystals, random strains are of sufficient magnitude to make the previously assumed equivalence of potential minima no longer valid. If, for K_3 in argon, matrix effects contribute a similar blurring of the trimer energy levels, then tunneling between adjacent wells no longer conserves energy. Transitions from the vibronic ground state of one well to the corresponding level of its inequivalent neighbor must now be stimulated by phonon absorption or emission. As given elsewhere (14, 16, 17), the several possible mechanisms correspond to the direct Raman or Orbach processes more familiarily applied to spin lattice relaxation. In all three cases this situation leads to an attenuation of the gas-phase tunneling frequency and complex, generally hyperbolic, temperature behavior for τ_c. In certain limiting situations either an exponential or power law temperature dependence is predicted. Consequently our results for K_3 in argon are also consistent with a trimer zero point energy well below the pseudorotation barrier.

Acknowledgments

This work was supported by the City University of New York PSC-BHE Research Award Program and by the National Science Foundation under grant number CHE 79-13260. Acknowledgment is made to the Donors of The Petroleum Research Fund, administered by the American Chemical Society, for partial support of this research.

Literature Cited

1. Lindsay, D. M.; Herschbach, D. R.; Kwiram, A. L. Mol. Phys. 1976, 32, 1199.
2. Lindsay, D. M.; Herschbach, D. R.; Kwiram, A. L. Mol. Phys. 1980, 39, 529.
3. Thompson, G. A.; Lindsay, D. M. J. Chem. Phys. 1981, 74, 959.
4. Thompson, G. A.; Tischler, F.; Garland, D.; Lindsay, D. M. Surf. Sci. 1981, in press.
5. Gerber, W. H.; Schumacher, E. J. Chem. Phys. 1978, 69, 1692.
6. Martin, R. L.; Davidson, E. R. Mol. Phys. 1978, 36, 1713.
7. Dietz, E. R. Phys. Rev. 1981, A23, 751.
8. Atherton, N. M. "Electron Spin Resonance"; Wiley: New York, 1973.
9. Freed, J. H.; Fraenkel, G. K. J. Chem. Phys. 1963, 39, 326.
10. Abragam, A. "The Principles of Nuclear Magnetism"; Oxford: London, 1961.
11. Slichter, C. P. "Principles of Magnetic Resonance"; Harper and Row: New York, 1963.
12. Carrington, A.; McLachlan, A. D. "Introduction to Magnetic Resonance"; Harper and Row: New York, 1967.
13. Feller, W. "An Introduction to Probability Theory and Its Applications", Wiley: New York, 1967; Volume I.
14. Englman, R. "The Jahn-Teller Effects in Molecules and Crystals"; Wiley: New York, 1972.
15. Townes, C. H.; Schawlow, A. I. "Microwave Spectroscopy"; McGraw-Hill: New York, 1955.
16. Ham, F. S. in "Electron Paramagnetic Resonance", edited by Geschwind, S.; Plenum: New York, 1972.
17. Williams, F. I. B.; Krupka, D. C.; Breen, D. P. Phys. Rev. 1969, 179, 255.

RECEIVED September 18, 1981.

Reprinted from ACS SYMPOSIUM SERIES, No. 179
METAL BONDING AND INTERACTIONS IN HIGH TEMPERATURE SYSTEMS
James L. Gole and William C. Stwalley, Editors

REFERENCES

1. P. J. Foster, R. E. Leckenby and E. J. Robbins, J. Phys. B 2, 478 (1969). See also, E. J. Robbins, R. E. Leckenby, and D. Willis, Adv. Phys. 16, 739 (1967).

2. K. A. Gingerrich, D. L. Cocke, and F. Miller, J. Chem. Phys. 64, 4027 (1976).

3. C. H. Wu, J. Chem. Phys. 65, 3181 (1976).

4. Notable is the work of Ozin et al. See, for example, G. A. Ozin, Catal. Rev.-Sci. Eng. 16, 191 (1977), and references therein.

5. See, for example, M. Moskovits and D. P. DiLella, J. Chem. Phys. 72, 2267 (1980); V. E. Bondybey and J. H. English, J. Chem. Phys. 73, 42 (1980).

6. A. Herrmann, E. Schumacher, and L. Woste, J. Chem. Phys. 68, 2327 (1978).

7. A. Herrmann, S. Leutwyler, and E. Schumacher, Helv. Chim. Acta 61, 453 (1978).

8. A. Herrmann, M. Hofmann, S. Leutwyler, E. Schumacher, and L. Woste, Chem. Phys. Lett. 62, 216 (1979).

9. D. M. Lindsay, D. R. Herschbach, and A. L. Kwiram, Mol. Phys. 32, 1199 (1976).

10. R. L. Martin and E. R. Davidson, Mol. Phys. 36, 1713 (1978).

11. W. H. Gerber and E. Schumacher, J. Chem. Phys. 69, 1692 (1978).

12. J. L. Gole, R. H. Childs, D. A. Dixon, and R. A. Eades, J. Chem. Phys. 72, 6368 (1980).

13. E. R. Dietz, Phys. Rev. A23, 751 (1981).

14. G. A. Ozin and S. A. Mitchell, Angew. Chemie Int. Ed. Eng. 22, 674 (1983).

15. T. H. Maugh II, Science 219, 474 (1983).

16. T. H. Maugh II, Science 219, 944 (1983).

17. T. H. Maugh II, Science 220, 592 (1983).

18. G. Delacretaz, J. D. Goniere, R. Monet, and L. Woste, Appl. Phys. B29, 55 (1982).

19. G. Ozin, M. Backer, S. Mitchell, and D. McIntosh, Angew. Chem. Int. Ed. Eng. 22, 166 (1983).

20. JES-ME-3X Electron Spin Resonance Instrument Instruction Manual, Japan Electron Optics Laboratory Co., Ltd., Tokyo, Japan.

21. ER Series Users Manual (1982), IBM Instruments Inc., Danbury, CT.

22. C. P. Poole, Jr., Electron Spin Resonance, 2nd Ed. (Wiley, New York, 1983).

23. D. M. Lindsay, 1974, Ph.D. Thesis, Harvard University.

24. H. V. Malmstadt, C. G. Enke, S. R. Crouch, and G. Horlick, Optimization of Electronic Measurements (W. A. Benjamin, Reading, MA, 1974).

25. J. P. Goldsborough and T. R. Koehler, Phys. Rec. 133, A 135 (1964).

26. C. K. Jen, V. A. Bowers, E. L. Cochran, and S. N. Foner, Phys. Rec. 126, 1749 (1962).

27. D. M. Lindsay, D. R. Herschbach, and A. L. Kwiram, Chem. Phys. Lett. 35, 175 (1974).

28. A. N. Nesmeyanov, Vapour Pressure of the Chemical Elements, Elsevier, New York, 1963); also see J. L. Margrave, The Characterization of High-Temperature Vapors (Wiley, New York, 1967).

29. R. C. Weast (Ed.), CRC Handbook of Chemistry and Physics, 62nd Ed. (CRC Press, Inc., Boca Raton, FL, 1981).

30. A. Carrington and A. D. McLachlan, Introduction to Magnetic Resonance (Haper and Row, New York, 1967).

31. J. E. Wertz and J. R. Bolton, Electron Spin Resonance (McGraw-Hill, New York, 1972).

32. N. M. Atherton, Electron Spin Resonance (Wiley, New York, 1973).

33. P. B. Ayscough, "Electron Spin Resonance in Chemistry" (Methuen, London, 1967).

34. C. P. Slichler, Principles of Magnetic Resonance (Harper and Row, New York, 1963).

35. A. Abragam and B. Bleaney, Electron Paramagnetic Resonance of Transition Metal Ions (Oxford, New York, 1970).

36. G. Breit and I. I. Rabi, Phys. Rev. 38, 2082 (1931).

37. P. H. Kasai and D. McLeod Jr., J. Chem. Phys. 55, 1566 (1971).

38. J. A. Weil, J. Mag. Res. 4, 394 (1971).

39. W. Weltner, Jr., D. McLeod, Jr., and P. H. Kasai, J. Chem. Phys. 46, 3172 (1967).

40. A. R. Boate, J. R. Morton, and K. F. Preston, J. Mag. Res. 24, 259 (1976).

41. D. M. Lindsay and G. A. Thompson, J. Chem. Phys. 77,1114 (1982).

42. J. H. Freed and G. K. Fraenkal, J. Chem. Phys. 34, 326 (1963).

43. G. K. Fraenkal, J. Chem. Phys. 42, 4275 (1965).

44. A. Hudson and G. R. Luckhurst, Chem. Rev. 69, 191 (1969).

45. A. G. Redfield, Adv. Mag. Res. 1, 1, (1965).

46. G. A. Thompson and D. M. Lindsay, J. Chem. Phys. 74, 959 (1981).

47. G. A. Thompson, F. Tischler, D. Garland, and D. M. Lindsay, Sur. Sci. 106, 408 (1981).

48. D. M. Lindsay, D. Garland, F. Tischler, and G. A. Thompson, Am. Chem. Soc. Symp. Soc. 179, Chap. 7 (1982).

49. G. A. Thompson, F. Tischler, and D. M. Lindsay, J. Chem. Phys. 678, 5946 (1983).

50. J. A. Howard, K. F. Preson and B. Mile, J. Am. Chem. Soc., 6226 (1981).

51. S. C. Richtsmier, R. A. Eades, D. A. Dixon, and J. L. Gole, Am. Chem. Soc. Symp. Soc. 179, Chap. 12 (1982).

52. W. H. Gerber, 1980, Ph.D. Thesis, University of Bern, Switzerland.

53. D. A. Garland and D. M. Lindsay, J. Chem. Phys. 74, 959 (1983).